

**Response of the coccolithophore  
*Emiliana huxleyi* to increased CO<sub>2</sub> and Fe  
availability within the plankton food web**

**Doctoral Thesis**

*Maria del Rosario Lorenzo Garrido*



UNIVERSIDAD  
DE MÁLAGA

**UNIVERSITY OF MALAGA  
FACULTY OF SCIENCES**

PhD Programme in  
Cell and Molecular Biology

Department of Ecology 2016

**Supervisor: María Segovia**



UNIVERSIDAD  
DE MÁLAGA

AUTOR: María del Rosario Lorenzo Garrido

 <http://orcid.org/0000-0003-2927-2184>

EDITA: Publicaciones y Divulgación Científica. Universidad de Málaga



Esta obra está bajo una licencia de Creative Commons Reconocimiento-NoComercial-SinObraDerivada 4.0 Internacional:

<http://creativecommons.org/licenses/by-nc-nd/4.0/legalcode>

Cualquier parte de esta obra se puede reproducir sin autorización pero con el reconocimiento y atribución de los autores.

No se puede hacer uso comercial de la obra y no se puede alterar, transformar o hacer obras derivadas.

Esta Tesis Doctoral está depositada en el Repositorio Institucional de la Universidad de Málaga (RIUMA): [riuma.uma.es](http://riuma.uma.es)



**Response of the coccolithophore *Emiliana huxleyi* to  
increased CO<sub>2</sub> and Fe availability within the plankton  
food web**

UNIVERSIDAD  
DE MÁLAGA



Doctoral Thesis

María del Rosario Lorenzo Garrido



UNIVERSIDAD  
DE MÁLAGA

**UNIVERSIDAD DE MÁLAGA**

FACULTAD DE CIENCIAS  
DEPARTAMENTO DE ECOLOGÍA Y GEOLOGÍA  
Área de Ecología

**Response of the coccolithophore *Emiliana huxleyi* to  
increased CO<sub>2</sub> and Fe availability within the plankton  
food web**

Memoria presentada para optar al  
grado de Doctor en Ciencias Ambientales  
por María del Rosario Lorenzo Garrido

Dirigida por María Segovia Azcorra





UNIVERSIDAD  
DE MÁLAGA

**UNIVERSIDAD DE MÁLAGA**

FACULTAD DE CIENCIAS  
DEPARTAMENTO DE ECOLOGÍA Y GEOLOGÍA  
Área de Ecología

Visado en Málaga a 30 de Septiembre de 2016

La directora

Fdo. María Segovia Azcorra  
Prof. Titular del Área de Ecología  
Universidad de Málaga

Memoria presentada para optar al Grado de Doctor en Ciencias Ambientales

Fdo. María del Rosario Lorenzo Garrido



UNIVERSIDAD  
DE MÁLAGA

**UNIVERSIDAD DE MÁLAGA**

FACULTAD DE CIENCIAS  
DEPARTAMENTO DE ECOLOGÍA Y GEOLOGÍA  
Área de Ecología

D<sup>a</sup> MARÍA SEGOVIA AZCORRA, Profesora Titular del Departamento de Ecología y Geología (Área de Ecología) de la Facultad de Ciencias de la Universidad de Málaga,

**CERTIFICA:**

Que la presente memoria titulada "Response of the coccolithophore *Emiliania huxleyi* to increased CO<sub>2</sub> and iron availability within the plankton food web" presentada por la Licenciada en Ciencias Ambientales María del Rosario Lorenzo Garrido, ha sido realizada bajo mi dirección y el trabajo presentado no ha sido utilizado en tesis anteriores. Y considerando que representa trabajo de Tesis Doctoral, autorizo su presentación y defensa para optar al Grado de Doctor en Ciencias Ambientales.

Y para que así conste, a los efectos oportunos, firma el presente en Málaga a 30 de Septiembre de 2016.

D<sup>a</sup> María Segovia Azcorra  
Prof. Titular del Área de Ecología  
Universidad de Málaga

Esta Tesis doctoral ha sido subvencionada por el Ministerio de Educación mediante una beca de Formación de Profesorado Universitario (AP2010-5565) y por el Ministerio de Ciencia e Innovación Consejería de Innovación, Ciencia y Empresa, (MICINN) mediante el proyecto de investigación **“Interferencia de la disponibilidad de hierro sobre el aumento de CO<sub>2</sub> y radiación UV en procesos de estrés oxidativo y muerte celular en fitoplancton marino: consecuencias en la modificación de la diversidad”** (CTM/MAR2010-17216) cuya investigadora principal es la Dra. María Segovia Azcorra.



## Contents

Chapter 1	General Introduction Thesis outline	1
Chapter 2	Iron availability modulates the effects of future CO <sub>2</sub> levels within the marine planktonic food web	17
Chapter 3	Effects of increased CO <sub>2</sub> and iron availability on the carbon assimilation and calcification during an <i>Emiliana huxleyi</i> bloom	53
Chapter 4	Physiological stress response associated to elevated CO <sub>2</sub> and dissolved iron in a phytoplankton community dominated by the coccolithophore <i>Emiliana huxleyi</i>	85
Chapter 5	Particulate trace metal dynamics in response to increased CO <sub>2</sub> and iron availability in a coastal mesocosm experiment	121
Chapter 6	Interactive effects of CO <sub>2</sub> , Fe, and UV radiation on primary production and calcification of the coccolithophore <i>Emiliana huxleyi</i> : <i>In vitro</i> physiological response	153
	6.1 Effects of elevated CO <sub>2</sub> in the coccolithophore <i>Emiliana huxleyi</i> : Effects on growth, photosynthesis, calcification and spectral sensitivity of photoinhibition	183
	6.2 Short-term response to the effects of Fe availability, increased CO <sub>2</sub> and UV radiation of <i>Emiliana huxleyi</i>	211
Chapter 7	General discussion and conclusions	211
References		221
List of Figures and Tables		243
Resumen		247

## *Abbreviations*

A: Anteraxanthin

Al: Aluminium

BED: Biological effective dose

BEI: Biological effective irradiance

BER: Base excision repair

BUTA: 19' butanoyloxyfucoxanthin

BWF: Biological weighting function

CAL: Central area length

CAW: Central area width

CCM: Carbon concentration mechanism

Cd: Cadmium

CFC: Chlorofluorocarbon

Chl-*a*: Chlorophyll a

C<sub>i</sub>: Inorganic carbon

CL-FIA: Flow injection analysis chemiluminescence detection system

Co: Cobalt

CO<sub>2</sub>: Carbon dioxide

CO<sub>3</sub><sup>2-</sup>: Carbonate ion

CPD: Cyclobutane pyrimidine dimmer

Cu: Copper

DD: Diadinoxanthin (DD)

dFe: Dissolved iron

DBS: Dextran-bound sulphanilamide

DFB: Desferrioxamine B

DIC: Dissolved inorganic carbon

DOC: Dissolved organic carbon

DSA: Distal shield area

DL: Distal shield length

DW: Distal shield width

DT: Diatoxanthin

eCA: External carbonic anhydrase

$E_k$ : Light saturation parameter

ERC: Exposure response curve

Fe: Iron

$f\text{HCO}_3^-$ : Fraction of  $\text{HCO}_3^-$  uptake

Fuco: Fucoxanthin

$F_v/F_m$ : Optimal quantum yield

$\text{H}^+$ : Hydrogen ion

$\text{H}_2\text{CO}_3$ : Carbonic acid

$\text{HCO}_3^-$ : Hydrogen carbonate

HEXA: 19'-hexanoyloxyfucoxanthin

HR-ICPMS: High-resolution inductively coupled plasma mass spectrometry

ID: Isotope disequilibrium

Lut: Lutein

Mn: Manganese

Mo: Molybdenum

Neo: Neoxanthin

NER: Nucleotide excision repair

NPQ: Non-photochemical quenching

OA: Ocean Acidification

## *Abbreviations*

OH<sup>-</sup>: Hydroxide ion

OL: Organic ligand

OSL: Outer shield length

PAR: Photosynthetically active radiation

Pb: Lead

pCO<sub>2</sub>: Partial pressure of carbon dioxide

Peri: Peridinin

pFe: Particulate iron

PIC: Particulate inorganic carbon

PL: Photolyase

POC: Particulate organic carbon

PON: Particulate organic nitrogen

ppmV: Parts per million by volume

Pras: Prasinolanthin

PSI: Photosystem I

PSII: Photosystem II

rETR<sub>max</sub>: Maximal electron relative transport rate

RLC: Rapid light curve

ROS: Reactive oxygen species

RR: Rain ratio

Rubisco: Ribulose-1,5-bisphosphate carboxylase/oxygenase

SEM: Scanning electron microscope

SOW: Synthetic oceanic water

TA: Total alkalinity

tFe: Total iron

Ti: Titanium

TPC: Total particulate carbon

UVR: Ultraviolet radiation

V: Violaxanthin

Z: Zeaxanthin

Zn: Zinc



Chapter 1

# General Introduction



## Ocean Acidification

Anthropogenic CO<sub>2</sub> emissions from fossil fuels burning and land use change have caused a considerable increase in atmospheric CO<sub>2</sub> concentrations from 280 to 400 µatm since the industrial revolution (Tans 2014). Oceans have absorbed about 30% of the anthropogenic carbon emissions over the past 200 years (Solomon et al. 2007). The predictions state that the current partial pressure of CO<sub>2</sub> (pCO<sub>2</sub>) will be exceeded more than twice in the worst-case scenario by the year 2100 (Figure 1.1, IPCC 2013).

The changes that seawater chemistry occurs as a consequence of CO<sub>2</sub> uptake lowering the pH, are termed ocean acidification. When CO<sub>2</sub> dissolves in seawater, it reacts with water and forms carbonic acid (H<sub>2</sub>CO<sub>3</sub>) that dissociates into bicarbonate (HCO<sub>3</sub><sup>-</sup>) and hydrogen ions (H<sup>+</sup>), leading to a decrease of pH. Earth system models project a global additional decrease in pH by 2100 ranging from 0.06 to 0.32 units, on top of the already decreased 0.1 units since the beginning of the industrial era, depending on our future emissions (Ciais et al. 2013). The oceanic uptake of CO<sub>2</sub> further heads to diminished carbonate ion, CO<sub>3</sub><sup>-2</sup>, concentrations and thus to a decrease in the saturation levels of the CaCO<sub>3</sub> minerals calcite and aragonite (Doney et al. 2009). Ocean acidification has the potential to affect the performance of marine organisms. Marine phytoplankton contribute to half of the world's total primary productivity, sustaining marine food webs and driving the biogeochemical cycles of carbon and nutrients (Field et al. 1998). Furthermore, phytoplankton incorporates annually approximately 45 to 50 billion metric tons of inorganic carbon (Field et al. 1998), removing a quarter of CO<sub>2</sub> emitted to the atmosphere by anthropogenic activities (Canadell et al. 2007). Thus, the response of phytoplankton to ocean acidification is key for understanding future changes in marine ecosystems (Doney et al. 2009).



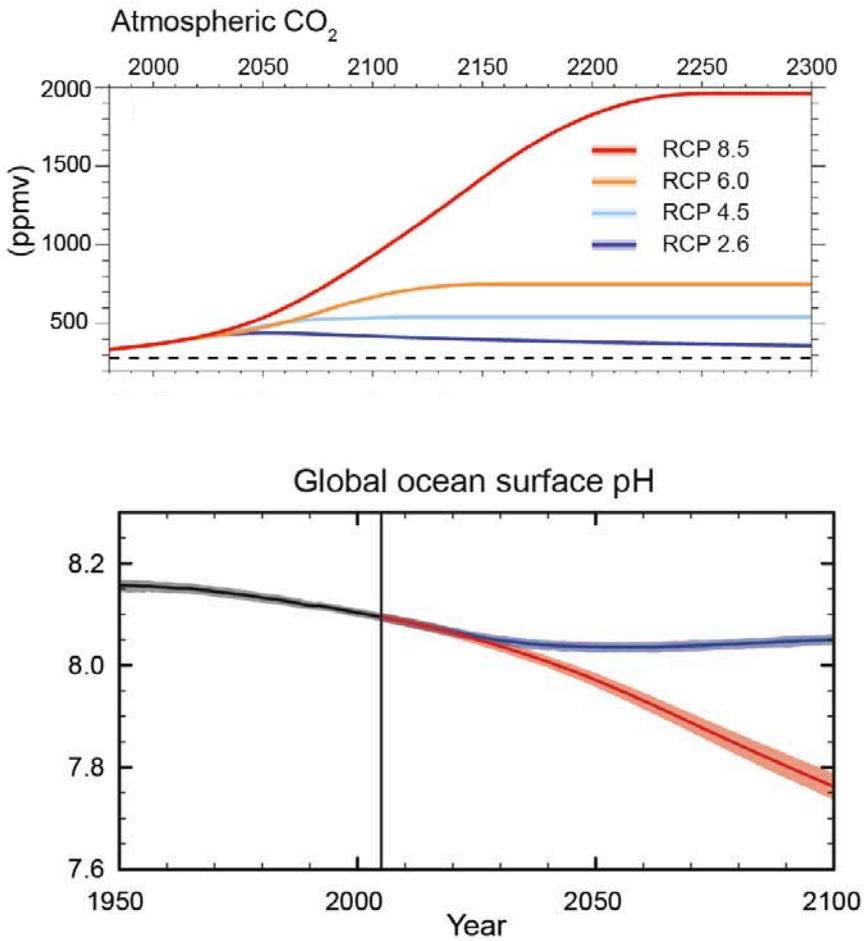


**Figure 1.1.** (a) Atmospheric CO<sub>2</sub> as simulated by Earth System Models of Intermediate Complexity (EMICs) for the four Representative Concentration Pathways (RCP) up to year 2300 (Zickfeld et al. 2013). The dashed line indicates the pre-industrial CO<sub>2</sub> concentration. (b) Coupled Model Intercomparison Project Phase 5 (CMIP5) multi-model simulated time series from 1950 to 2100 for global mean ocean surface pH. Taken from the IPCC Fifth Assessment Report (2013) and Summary for Policymakers (2014).



## Effects of ocean acidification on phytoplankton

The extent to which phytoplankton may respond to increased  $\text{CO}_2$  (decreased pH) is likely to depend on the physiological mechanisms of inorganic carbon uptake and intracellular assimilation. During photosynthesis,  $\text{CO}_2$  is fixed in phytoplankton by the carboxylating enzyme Rubisco (ribulose-1, 5-biphosphate carboxylase/oxygenase). However, for most species, Rubisco is less than half saturated under current  $\text{CO}_2$  levels (Riebesell 2004). Furthermore, the dual role of the Rubisco as oxygenase produces a significant inhibition of  $\text{CO}_2$  fixation. This limited  $\text{CO}_2$  fixation together with Rubisco's low affinity for  $\text{CO}_2$  is counterbalanced by the operation of carbon concentrating mechanisms (CCMs) that provide a  $\text{CO}_2$ -rich environment around the enzyme, suppressing the oxygenase and saturating the carboxylase activity (Beardall & Raven 2004). Most marine phytoplankton species show little effect on their photosynthetic rates because their photosynthesis is already saturated by carbon, due to the presence of CCMs that actively take up inorganic carbon, either as  $\text{CO}_2$  or  $\text{HCO}_3^-$  or both (Giordano et al. 2005). Increased  $\text{CO}_2$  might directly benefit biomass production either by enhancing the carboxylation reaction at Rubisco (Raven et al. 2005), by reducing  $\text{CO}_2$  leakage (Rost et al. 2006), or by allowing a down-regulation of activity of the energy-consuming CCMs (Kranz et al. 2010). Raven (1991) proposed that a downregulation of the photosynthetic machinery in phytoplankton could increase the resource use efficiency. On the other hand, the predicted pH drop represents an increase in the  $\text{H}^+$  concentrations, which may affect intracellular pH, membrane potential, energy partitioning and, enzyme activity (Flynn et al. 2012, Taylor et al. 2012). Ocean acidification may reduce phytoplankton growth rates through direct pH effects (Berge et al. 2010). Thus, ocean acidification may potentially both stimulate and reduce, due to the increase in  $\text{CO}_2$  concentration and through direct pH effects by marine phytoplankton, respectively.

The decrease in oceanic pH caused by elevated  $\text{CO}_2$  will impact calcification rates.  $\text{CaCO}_3$  is one of the most common building materials used in the formation



of skeletons, shells, and other protective structures in the marine biota. Calcification is facilitated by high pH and high  $\text{CO}_3^{2-}$  concentration. These conditions are achieved at the site of calcification through energy-consuming ion transport processes such as for instance phosphate uptake (Paasche 2002). The energetic cost of calcification is thought to increase with ocean acidification causing a decrease in pH and in the carbonate ( $\text{CO}_3^{2-}$ ) concentration. This extra energy needed to compensate for the changes in seawater carbonate chemistry depends on the specific pathways employed in  $\text{CaCO}_3$  precipitation, specific for each taxonomic group. A case in point is coccolithophores (Prymnesiophyceae), a group of unicellular microalgae growing in the surface layer of the ocean and the most productive calcifying organisms in the sea (Paasche 2002). It is known that intracellular pH in coccolithophores is particularly sensitive to changes in external pH (Suffrian et al. 2011, Flynn et al. 2012, Taylor et al. 2012). This indicates that the direct negative effect of high  $\text{H}^+$  concentration on calcification rates may at some point be overcome by increasing availability of  $\text{HCO}_3^-$  substrate of calcification (Bach et al. 2013). Therefore, the majority of coccolithophores reduce their level of calcification when growing at elevated  $\text{CO}_2$  (Langer et al. 2009, De Bodt et al. 2010, Langer 2011, Richier et al. 2011, Lefebvre et al. 2012, Rokitta & Rost 2012) and the fossil record suggests that eras with reduced  $\text{CO}_2$  levels (e.g. glacial era) have favoured more heavily calcified cells (Beaufort et al. 2011).

Increased  $\text{CO}_2$  will alter competitive relationships and can result in shifts of plankton species composition due to the sensitivity to carbon enrichment that widely differs among taxa (Riebesell & Tortell 2011, Mackey et al. 2015). Such changes have important implications for marine organisms, affecting physiological processes (Figure 1.2). In turn, changes in the physiology of individuals alter the dynamics of their populations and ultimately may affect the entire ecosystem.

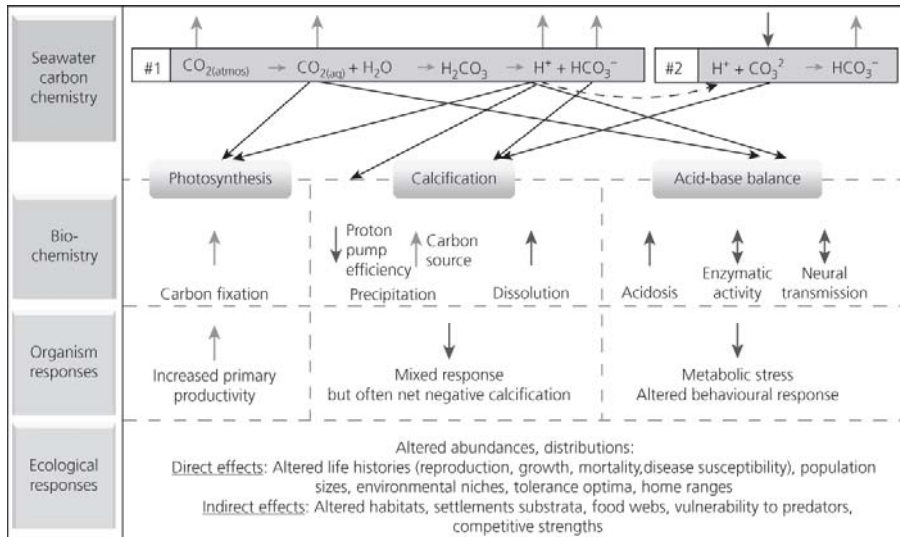


**Figure 1.2.** Diagram about the effects of ocean acidification on changes in seawater carbon chemistry, biochemistry, the response of the organism and the ecological responses. Diagram taken from Iglesias-Rodriguez et al. 2016.

Based on the biological processes responsible for carbon fixation, two biological carbon pumps can be distinguished: (1) the organic carbon pump, driven by photosynthesis, and (2) the carbonate counter pump, generated by the formation of calcium carbonate ( $\text{CaCO}_3$ ) shell material by calcifying plankton, calcification. While photosynthesis fixes  $\text{CO}_2$  into organic carbon, acting as a net sink of atmospheric  $\text{CO}_2$ , calcification converts two  $\text{HCO}_3^-$  anions into one molecule of  $\text{CaCO}_3$  and one molecule of  $\text{CO}_2$ , acting as a net source of  $\text{CO}_2$  in the surface ocean. Hence, the two carbon pumps reinforce each other in terms of maintaining a vertical dissolved inorganic carbon (DIC) gradient, whereas they counteract each other with respect to their impact on air–sea  $\text{CO}_2$  exchange, this process is called “carbonate counter pump” (Rost & Riebesell 2004). The relative strength of the two biological carbon pumps, represented by the so-called rain ratio (the ratio of particulate inorganic to organic carbon in exported biogenic matter), determines

the flux of CO<sub>2</sub> between the surface ocean and the overlying atmosphere. Attending to global organic carbon vertical fluxes studied, the organic carbon pump clearly dominates over the carbonate counter pump (Rost & Riebesell 2004).

Consequently, the effect of elevated CO<sub>2</sub> on calcification and photosynthesis could affect carbon export by altering the “rain ratio”. A reduced calcification provides a negative feedback to rising atmospheric CO<sub>2</sub> levels, contributing to the stabilization of the Earth’s climate (Hoffman & Schellnhuber 2009). However, strong correlations between the export fluxes of POC and mineral particles, especially with CaCO<sub>3</sub>, have been found, the so-called “ballast effect” (Klaas & Archer 2002, Sanders et al. 2010). Mineral ballast, especially CaCO<sub>3</sub>, plays a dominant role in carrying matter through the water column. If the flux of mineral ballast declines, there will be less transport of POC into the deep ocean and a reduction of its export fluxes weakens the strength of the biological carbon pump. As a result, the mentioned above “negative calcification feedback” on rising atmospheric CO<sub>2</sub> levels is counteracted by the reduced mineral ballast transport (“ballast feedback”). Furthermore, there is another consequence: the organic matter is oxidized in shallow waters when mineral-ballast fluxes weaken, hypoxic zones start to expand considerably in the oceans in our model world—with potentially harmful impacts on a variety of marine ecosystems (Hoffman & Schellnhuber 2009).

Changing the pH of seawater is also expected to affect the efficiency of the enzymatic processes involved in acquiring organic forms of nitrogen and phosphorus. Ocean acidification can also inhibit organic nitrogen and phosphorus acquisition in marine organisms (Hutchins et al. 2009). Thus, the biogeochemical cycling of macronutrients is predicted to be greatly affected by ocean acidification (Hutchins et al. 2009). Concomitantly, the distribution and speciation of trace metals in the ocean is also affected by the variations in pH due to OA (Millero et al. 2009). Because most organic particles in seawater are negatively charged, their surface sites will become less available to adsorb metals as pH decreases. These



changes are expected to alter the availability and toxicity of metals for marine organisms.

## Trace metals

Trace metals (Mn, Fe, Co, Cu, Zn, and Cd) are required for numerous processes in phytoplankton and can influence phytoplankton growth and community structure (Morel & Price 2003). Trace metals are necessary for the growth and survival of photosynthetic organisms (Price & Morel 1990, Morel & Price 2003) and the metal contents of phytoplankton (metal quotas) reflect biochemical demands as well as environmental availability, influencing the distribution of metals in the ocean (Sunda 2012).

Among all the trace metals, iron (Fe) is the most important, required for essential physiological and molecular processes in phytoplankton. Iron is cofactor of metalloenzymes and proteins, which are vital to metabolic processes such as photosynthesis, respiration, electron transport, nitrate metabolism, detoxification of reactive oxygen species (ROS) and DNA repair (Behrenfeld & Milligan 2013). For example, most of the cell's Fe requirement (up to 80 %) is associated with photosynthesis (Raven 1999), since nearly every aspect of thylakoid electron transport is Fe dependent. Iron is required in both photosystems (2–3 atoms for PSII; 12 atoms for PSI): the cytochrome  $b_6f$  complex (5 atoms), which links the two photosystems, and the ferredoxin molecule (2 atoms; Raven 1999). This strong Fe contingent deeply influences electron transport kinetics.

Iron is the fourth most abundant element on Earth but its solubility is extremely low in contemporary well-oxygenated waters resulting in low Fe concentrations in many natural aquatic systems (Norman et al. 2014). In today's oxygenated world, surface ocean iron concentrations may be as low as 20 pM (Rue & Bruland 1995), and phytoplankton have responded to these conditions with a diversity of mechanisms for acquiring iron and economizing its cellular demand. Iron exists in seawater in two oxidation states: soluble Fe (II) and low soluble Fe



(III). Generally, the predominant form of Fe in seawater is the more thermodynamically stable Fe (III). The chemical form of iron is defined by physical size fractions separated on the basis of filtration methods (Bruland 2001); hence these forms are operationally defined. The size fractions comprise particulate ( $>0.2 \mu\text{m}$ ) and dissolved fraction ( $<0.2 \mu\text{m}$ ). The dissolved fraction is divided in colloidal and soluble. Several studies have demonstrated that the majority of the dissolved concentration (mostly  $>99\%$ ) is in the form of metal organic complexes (Gledhill & van den Berg 1994, Rue & Bruland 1995). Fe binds to organic molecules called organic ligands (OLs) that can be weak or strong depending on the stability constant (i.e. association constant for the equilibrium that exists between the metal and the organic ligand). This organic complexation is extremely important for maintaining solubility and controlling the bioavailability of Fe to phytoplankton. The complexation and speciation of Fe can result in Fe limitation conditions, because the Fe bioavailable concentration is below than the requirements of phytoplankton (Marchetti & Maldonado 2016). The bioavailability may be defined as the degree to which a certain compound can be accessed and utilized by an organism. Thus, Fe stress due to low Fe concentration is widespread in open waters and in some coastal areas (Behrenfeld & Milligan 2009), affecting phytoplankton growth, physiology and production of organic matter and biogenic minerals.

Ocean acidification will have an impact on the thermodynamics and kinetics of metals in seawater. The changes in the speciation of metals due to the lower pH will result in changes in the behaviour of metals in seawater. The decrease in concentration of  $\text{OH}^-$  (due to the decrease in pH) and  $\text{CO}_3^{2-}$  (due to changes in carbonate chemistry) can affect the solubility, adsorption, toxicity and the rates of redox processes (Millero et al. 2009). All these changes could possibly affect the concentrations and chemical speciation of iron, and hence on iron availability to phytoplankton. The decrease in pH will promote rates of reduction of Fe (III) to soluble Fe (II), and retard the oxidation of Fe (II) to Fe (III) (Millero et al. 2009).





Moreover, many organic complexation reactions are sensitive to changes in pH (Shi et al. 2010). The effects of ocean acidification in Fe could enhance the solubility leading to increased iron concentration but as mentioned above more than 99% of dissolved Fe is bound to strong organic ligand. Shi et al. (2010) reported that the conditional stability constant of iron-organic ligand complexes increased as pH decreased when the ligand was an acidic binding group. Thus, the changes in Fe availability will depend on the nature of the organic ligands (Shi et al. 2010).

### **Interactive effects between Fe and increased CO<sub>2</sub>**

Only a few studies have been focused on the interactive effects between ocean acidification and Fe concentrations. The responses obtained were different depending on the features of the natural phytoplankton community. Additionally, the Fe requirement is generally higher in coastal phytoplankton species than in oceanic species, probably reflecting the environmental conditions of their habitats (Sunda & Huntsman 1995a). As a result, the effects of changes in iron availability due to changes in CO<sub>2</sub> conditions could differ depending on the nature of the iron demand of each phytoplankton species.

The interactive effects of ocean acidification and Fe have been shown to influence the phytoplankton physiology and the changes in the community. It has been shown that under increased CO<sub>2</sub> concentration in different regions dominated by diatoms and in cultures of *Thalassiosira weissflogii* there were no effects in primary production with conditions of Fe limitation (Hoppe et al. 2013, Yoshimura et al. 2013, 2014, Sugie & Yoshimura 2016). Furthermore, a negative (Shi et al. 2010, Sugie et al. 2013, Yoshimura et al. 2013, 2014) or positive response (Hopkinson et al. 2010) have also been observed under elevated CO<sub>2</sub> and iron-limitation during different experiments in natural assemblages and in laboratory conditions. The discrepancies observed can be due to a number of factors,



including differences in the Fe concentrations, Fe speciation and the phytoplankton community composition.

It is widely recognised that the lack of knowledge on the interplay of the different environmental factors is one of the main constraints in our ability to predict the functioning and composition of the future ocean. Therefore, further studies are essential to unravel the effects of ocean acidification on trace metal bioavailability and the synergistic effects to assess their impacts on phytoplankton within the food web.

## Thesis outline

Within the future predicted scenario, different stressors of global change will vary simultaneously (Boyd & Doney 2002). These changes will affect phytoplankton, leading to shifts in community composition and biomass and it is known that the responses obtained are in some cases specie-specific. Due to the importance of phytoplankton in sustaining marine food webs and driving the biogeochemical cycles of carbon and nutrients, it is key to understand all the possible responses from the different species as a consequence of the different changes in global change driven factors.

The most important biogeochemical cycle is the global carbon cycle and coccolithophores play a major role contributing with ca. 1–10% to total organic carbon fixation and with approximately 50% to pelagic deep ocean CaCO<sub>3</sub> sediments. In particular, *Emiliana huxleyi* is the most abundant and widespread coccolithophore in the world's ocean with a global distribution from the tropics to subarctic waters accounting for 20%–50% of the total coccolithophore community in most areas and close to 100% in subpolar waters (Mohan et al. 2008). Coccolithophores in general are known to follow a haplo-diplontic life cycle, with individuals of both stages being able to propagate independently by mitosis (Billard 1994). *Emiliana huxleyi* can exist as calcified, non-motile, diploid (2N) cells and non-calcified, motile, haploid (1N) cells, with the capability of unlimited





asexual cell division (Green et al. 1996). A third form, known to be diploid, nonmotile, and uncalcified, may be a culture artifact (Klaveness 1972, Green et al. 1996).

Furthermore, *E. huxleyi* produces extensive blooms in temperate latitudes and subpolar regions such as the Northern Atlantic (Holligan et al. 1993). The blooms generally coincide with a combination of thermal stratification and high irradiance in phosphate-poor environment (Nanning & Tyrrell 1996, Tyrrell & Taylor 1996). However, the temperature is not an overriding environmental factor and the temperature range of maximum growth rates can oscillate between 10-26 °C (Paasche 2002). Precisely due to the high growth rates achieved under high N:P ratios, its capacity to grow under elevated irradiances, its ability to use organic compounds and the fact that it can release allelochemicals to the surrounding medium, this species can outcompete others from the same niche where it inhabits, thriving along vast ocean regions.

*Emiliana huxleyi* is the keystone of the coccolithophores and it has been widely studied in many different works, with one or more global change stressors either in laboratory or in natural conditions. The results obtained varied depending on the differences between natural assemblages (where interactions with other plankton groups exist) or controlled laboratory experiments (where there can be disparities due to culture conditions). The main general response observed is that ocean acidification will affect *E. huxleyi*. However, there is a lack of knowledge on the response to interactive effects of ocean acidification and dissolved Fe at different levels in this species.

The aim of this thesis is to gain deeper insight in the physiological response of *E. huxleyi* to increased CO<sub>2</sub> and Fe availability within the food web using mesocosms and also under controlled laboratory experiments. Mesocosms allow the use of perturbation studies in natural communities analysing the interactive effects of multiple stressors across multiple trophic levels. On the other hand, the effect of increased CO<sub>2</sub> and/or Fe levels modulating the response to ultraviolet



radiation (UVR) exposure were assessed under culture conditions. Therefore, this thesis addresses the following major questions:

1. What is the growth response of *E. huxleyi* to elevated pCO<sub>2</sub> and changes in Fe availability? How the response of *E. huxleyi* to the different pCO<sub>2</sub> and Fe levels leads to cascading effects on other members of the plankton community? What is the impact of *E. huxleyi* behaviour in the global C-cycle under the above-mentioned circumstances?
2. Are carbon assimilation and calcification processes affected by increased CO<sub>2</sub> and Fe availability in *E. huxleyi*? Are the variations in carbon assimilation and calcification explained by the changes observed in the phytoplankton community?
3. Does the phytoplankton community overcome the stress induced by increased CO<sub>2</sub> and Fe levels? Are there protective, and/or defense mechanisms involved in the response of *E. huxleyi*?
4. How the particulate trace metals change during the bloom of *E. huxleyi* due to CO<sub>2</sub> and Fe levels? Are the particulate trace metals related to *E. huxleyi*?
5. Does the effect of increased CO<sub>2</sub> and/or Fe levels modulate the response to UVR exposure in *E. huxleyi* in culture conditions?

To tackle these questions, a mesocosm experiment was carried out in the Raunefjord (Bergen, Norway) and manipulated to achieve combinations of ambient and increased pCO<sub>2</sub> and dFe to investigate the interactive effects of both stressors on functional plankton groups. In **Chapter 2**, the increased CO<sub>2</sub> concentrations as well as the addition of the siderophore desferrioxamine B (DFB) promoted the enhancement of dissolved Fe. The response to both factors (CO<sub>2</sub> and Fe) was assessed for the whole food web. A bloom of the coccolithophore *E. huxleyi* was developed under ambient CO<sub>2</sub> conditions and increased dissolved Fe,



indicating *in situ* Fe limitation. Furthermore, ocean acidification negatively affected *E. huxleyi* and *Synechococcus*, while the rest of the plankton community was unaffected.

**Chapter 3** refers to the assessment of carbon assimilation processes including acquisition and accumulation, and calcification, to study the effects of increased CO<sub>2</sub> and Fe in the plankton community. Furthermore, the phytoplankton cellular stoichiometry was also studied because it is a key factor in biogeochemical cycling of nutrients. Carbon acquisition remained invariable with the different treatments and changes in the community. However, carbon assimilation and calcification were enhanced under ambient CO<sub>2</sub> conditions and increased dissolved Fe, showing the same trend as the phytoplankton community.

In **Chapter 4**, the stress response of the different phytoplankton groups was studied to unravel the effects of increased CO<sub>2</sub> and Fe levels. For this purpose, the photosynthetic response and the protective mechanisms (accessory pigments) were assessed, in combination with the determination of the impact of the response by means of cell viability, oxidative stress and DNA damage analyses. The results obtained showed that Fe is needed for DNA repair and to overcome oxidative stress in *E. huxleyi*.

**Chapter 5** analysed the changes in particulate trace metals (Fe, Cu, Mn, Co, Cd, Zn, Mo and Ti) during the bloom of *E. huxleyi* to decipher their impact on phytoplankton under the two factors (CO<sub>2</sub> and Fe) already mentioned. Whether the source of the trace metals was biotic or lithogenic was also analysed, revealing that Fe and Ti were from lithogenic origin and the rest of the metals showed a strong biogenic component. Ocean acidification changed the relative concentrations of particulate metals; a result mainly driven by the effects of ocean acidification on the growth of different phytoplankton phyla, but modulated by dissolved Fe concentrations.



As future perspectives and in addition to the mesocosm study with a natural plankton community, experimental work was performed to elucidate the interactive effect of the exposure to UV radiation (UVR) with increased CO<sub>2</sub> and/or different Fe levels. In **Chapter 6**, *E. huxleyi* was grown at ambient and predicted future CO<sub>2</sub> conditions to analyse the susceptibility of this species to UVR, by using biological weighting functions (BWFs) for the inhibition of photosynthesis. Data revealed that the sensibility was the same under both ambient and high CO<sub>2</sub> conditions. On the other hand, *E. huxleyi* was also grown at two different Fe levels simultaneously exposed to different irradiance treatments (only photosynthetically active radiation (PAR) and PAR with UVR) under present and future CO<sub>2</sub> conditions. The objective of this experiment was to study the interactive effects of Fe, CO<sub>2</sub> and UVR on the ecophysiological response of *E. huxleyi*. The results showed that Fe played the major role in controlling the response of the coccolithophore and the inhibition by UVR was diminished under high CO<sub>2</sub>. This could suggest a possible signalling role of CO<sub>2</sub> in photoprotective mechanisms.

## Chapter 2

# **Iron availability modulates the effects of future CO<sub>2</sub> levels within the marine planktonic food web**

María Segovia, M Rosario Lorenzo\*, Maria T Maldonado, Aud Larsen, Stella A. Berger, Tatiana M. Tsagaraki, Francisco J. Lázaro, Concepción Iñiguez, Candela García-Gómez, Armando Palma, Michaela A. Mausz, Francisco J.L. Gordillo, Jose A. Fernández, Jessica L. Ray, Jorun K. Egge

*Manuscript accepted in Marine Ecological Progress Series  
pending revision*

## Abstract

Ocean acidification (OA) due to increased CO<sub>2</sub> emissions derived from anthropogenic activities is affecting marine ecosystems at an unprecedented rate altering biogeochemical cycles. Therefore, direct empirical studies on natural communities are required to analyse the interactive effects of multiple stressors while spanning multiple trophic levels. Here, we investigate the interactive effects of CO<sub>2</sub> and iron availability on functional plankton groups according to predicted future scenarios using mesocosms and employing a full-factorial design, comprising all combinations of ambient and increased pCO<sub>2</sub> and dissolved iron (dFe). Manipulation of both factors increased dFe compared to the control. During the 22 experimental days, the plankton community structure showed two distinct phases. In phase 1 (days 1-10), only bacterioplankton abundances increased at elevated pCO<sub>2</sub> regardless of Fe manipulation. In contrast, a strong community response was evident in phase 2 (days 11-22) where the coccolithophore *Emiliana huxleyi* biomass massively increased at ambient CO<sub>2</sub> and increased dFe, unexpectedly indicating *in situ* iron limitation. *Emiliana huxleyi* plays a major role in the global carbon cycle by regulating the exchange of CO<sub>2</sub> across the ocean-atmosphere interface through photosynthesis and calcium carbonate precipitation. Ocean acidification negatively affected *E. huxleyi* and cyanobacterium *Synechococcus* sp., while the rest of the plankton community was unaffected. Surprisingly, increased dFe partially mitigated the negative effect of elevated pCO<sub>2</sub> imposed on the coccolithophores, indicating that physiological Fe-mediated-acclimation of *E. huxleyi* to ocean acidification might have effects on food web dynamics, influencing carbon export, and the rain ratio, affecting future ecosystem functioning.

**Key words:** Global change, iron, CO<sub>2</sub>, mesocosms, plankton food web, *Emiliana huxleyi*, *Synechococcus* sp.



## Introduction

In the geological past, planet Earth has experienced significant changes in natural climate driven factors. However, at present, the main drivers, such as carbon dioxide (CO<sub>2</sub>) concentration, eutrophication and ultraviolet radiation, are increasing at an unprecedented rate (Hoegh-Guldberg & Bruno 2010). CO<sub>2</sub> concentration is projected to reach 900  $\mu\text{atm}$  (or ppmv) by the end of this century (IPCC 2013), altering seawater chemistry by lowering its pH (ocean acidification, OA) and the saturation state of calcium carbonate (Doney et al. 2009). Within plankton, phytoplankton play key roles in biogeochemical cycles, in marine food web dynamics and productivity, as well as in the consumption and production of climate forcing gases. In turn, changes in climate are likely to affect phytoplankton productivity and species composition. Some phytoplankton species may benefit from increased CO<sub>2</sub> levels within future scenarios while it may be detrimental to others (Riebesell & Tortell 2011). Haptophyta (e.g. coccolithophorids), which are of global importance in the carbon cycle, is one of the phytoplankton phylum most affected by elevated CO<sub>2</sub> concentration (Paasche 2002). Additionally, high latitude areas where coccolithophores typically bloom might experience stronger changes in carbonate chemistry due to the higher solubility of CO<sub>2</sub> in colder waters (Riebesell et al. 2013). However, experimental work on the effects of high pCO<sub>2</sub> on coccolithophores has revealed contradictory results depending on the species and strain used, the physicochemical conditions, and whether the studies were carried out in natural communities or in laboratory cultures (Langer et al. 2006, Hutchings 2011, Riebesell & Tortell 2011, Mackey et al. 2015). Furthermore, the impact of elevated pCO<sub>2</sub> on organisms in other trophic levels is not well understood; studies focusing on micro- and mesozooplankton, bacterioplankton or viruses have given results that are often contradicting and/or inconclusive (Larsen et al. 2008, Caron et al. 2013, Niehoff et al. 2013, Endres et al. 2014).



OA affects marine nutrient biogeochemistry and, in particular, has a profound impact on trace metal solubility and speciation. Among metals, Fe is the most essential micronutrient controlling phytoplankton growth mainly, but not exclusively, through nitrate assimilation and photosynthesis (Behrenfeld & Milligan 2013). Fe bioavailability (i.e. iron available for uptake and thus, growth) is controlled by many factors including: a) dissolved Fe concentrations; b) the concentration and strength of iron binding organic ligands (OLs) which modulates Fe speciation; c) irradiance effects on iron redox chemistry and ligand binding strength and d) pH (Sunda & Huntsman 1995a, Maldonado & Price 2001, Barbeau et al. 2003, Shi et al. 2010). The chemistry of metals in seawater is greatly affected by pH. Low pH increases Fe solubility thus, dFe concentrations (Millero et al. 2009). Likewise, elevated CO<sub>2</sub> enhanced dFe levels during a mesocosm experiment in a Norwegian fjord (Breithbarth et al. 2010) and in subarctic waters (Yoshimura et al. 2013). The effects of OA on organically bound iron are more complex and affect Fe bioavailability. Organic ligands solubilize particulate iron and increase the residence time of dFe in the ocean. Depending on the Fe ligand type (carboxylates, hydroxymates or catecholates) the bioavailability of Fe can either decrease or remain unaffected under OA (Shi et al. 2010). Thus, the net effect of OA on phytoplankton iron nutrition is dependent on the balance between increases in iron solubility and changes in iron bioavailability mediated by organic ligand complexation.

In a rapidly changing environment, it is critical to gain adequate understanding of the vulnerability of ecosystems to global driven perturbations. However, predictions for whole ecosystems are challenging because of synergistic and antagonistic effects of multiple stressors (Crain et al. 2008). Perturbation studies in natural communities using *in situ* mesocosms are necessary to address such challenges, because of their high degree of realism compared to microcosms, and the impracticability to perform large-scale OA experiments in the open ocean (in which mechanistic relationships are not always identified) (Stewart et al.



2013). Specifically, mesocosm experiments allow directly analysis of the interactive effects of multiple stressors across multiple trophic levels (Riebesell et al. 2010, Stewart et al. 2013, Riebesell & Gattuso 2015).

Here we present the main results from a mesocosm experiment that aimed to investigate the effects of future changes in pCO<sub>2</sub> and Fe availability during a bloom of the coccolithophore *Emiliana huxleyi* within a natural plankton community. *Emiliana huxleyi* is a major primary producer in the world's oceans and a sensitive phytoplankton to elevated pCO<sub>2</sub>. This species is of paramount significance in the global carbon cycle since it is responsible for a large fraction of the ocean calcium carbonate production and export to the deep ocean contributing to the regulation of the exchange of CO<sub>2</sub> across the ocean-atmosphere interface (Rost & Riebesell 2004). To our knowledge this mesocosm experiment is the first to manipulate pCO<sub>2</sub> and iron concentrations simultaneously, and examine their combined effects and interactions on planktonic organisms in multiple trophic levels.

We investigated (a) the effects of elevated pCO<sub>2</sub> levels on dissolved Fe; (b) the extent to which changes in Fe availability affect the growth of *E. huxleyi* and other autotrophs and, (c) whether different pCO<sub>2</sub> and Fe levels, and their interaction, lead to cascading effects on other members of the plankton community.

## Materials and methods

### Experimental design

A mesocosm experiment was carried out in the Raunefjord (60.39 °N, 5.32 °E), off Bergen, Norway, June 5-27, 2012. Twelve mesocosms (11 m<sup>3</sup> each) were set-up in a full-factorial design with all combinations of ambient and high pCO<sub>2</sub> and two treatments of dFe in three independent replicate mesocosms per treatment. High-density polyethylene (HDPE) mesocosms were filled with fjord water



pumped from 8 m depth. They were covered with low-density polyethylene (LDPE) lids in order to avoid  $p\text{CO}_2$  losses and contamination. Mesocosms and their lids were transparent to photosynthetically active radiation (PAR) and ultraviolet radiation (UVR). After the first sampling day (0), the seawater of half of the mesocosms was enriched with  $\text{CO}_2$  (Schulz et al. 2009) to achieve  $p\text{CO}_2$  concentrations corresponding to levels predicted for the year 2100 (900  $\mu\text{atm}$ , HC), (IPCC 2013) and the other half were not manipulated (ca. 390  $\mu\text{atm}$ , LC). All mesocosms were continuously and gently mixed by using an airlift system (Egge & Heimdal 1994). For the  $\text{CO}_2$  enrichment, 150 L of fjord water was aerated with pure  $\text{CO}_2$  at a flow rate of 1.5 L  $\text{min}^{-1}$  overnight and added to each of the high  $p\text{CO}_2$  (HC) mesocosms. To maintain the  $p\text{CO}_2$  in the HC treatments, ambient air was mixed with pure  $\text{CO}_2$  at a flow rate of 200 mL  $\text{min}^{-1}$  and the enriched mixture (900  $\mu\text{atm}$   $\text{CO}_2$ ) was pumped directly to the airlift system. LC treatment consisted of only-ambient air similarly connected. HEPA filters were placed between the air pumps and the airlift system to avoid particulate contamination. Mesocosms were fertilised after initial sampling (day 0) by addition of 10  $\mu\text{M}$  nitrate and 0.3  $\mu\text{M}$  phosphate to induce a bloom of the coccolithophorid *E. huxleyi* (Egge & Heimdal 1994). On day 7, half of the mesocosms (3LC and 3 HC) were amended with 70 nM (final concentration) of the siderophore desferrioxamine B (DFB) to promote changes in iron availability. The treatments were named LC-DFB (control), LC+DFB, HC+DFB and HC-DFB. Water samples from each mesocosm were taken from 2 m depth by gentle vacuum pumping of 25 L volume into acid-washed carboys that were quickly transported to the onshore laboratory. All variables were analysed on a daily basis and/or every other day, except otherwise stated.

### **$p\text{CO}_2$ , DIC, $\Omega_{\text{calcite}}$ , pH, alkalinity and rain ratio**

$p\text{CO}_2$  inlet flows in all the mesocosms were measured by non-dispersive infrared analysis by using a  $\text{CO}_2$  gas analyser (LI-820, Li-COR).  $p\text{CO}_2$ , dissolved inorganic



carbon (DIC) and the calcite saturation state ( $\Omega_{\text{calcite}}$ ) were calculated from daily measurements of pH, temperature, salinity and total alkalinity (TA) using the CO<sub>2</sub>Calc software (Robbins et al. 2010). pH was measured in all mesocosms using a pH-meter (CRISON Basic 20+) calibrated daily using NBS (National Bureau of Standards) scale. Salinity was measured with a conductivity-meter (CRISON 524). The accuracy of the pH meter and conductivity meter was  $\pm 0.01$  pH units and  $\pm 1.5$  % respectively. TA was measured using the classical Gran's potentiometric method (Gran 1952). The rain ratio (RR) was calculated applying the models of Ridgwell et al. (2007) and Hoffmann & Schellnhuber (2009).

### **Dissolved iron (dFe)**

Dissolved Fe (dFe) samples were obtained from each mesocosm every 4<sup>th</sup> day, filtered through 0.2  $\mu\text{M}$  AcroPak supor membrane capsule filters (Pall, USA) into LDPE bottles, and immediately acidified with ultra-clean HCl (Seastar) in a Class 100 laminar flow hood. Total dFe measurements were conducted by chemiluminescence flow injection analysis (CL-FIA, Waterville Analytical, USA) as described in de Baar et al. (2008) and de Jong et al. (1998). All filters, sampling and filtration equipment were trace metal cleaned using HCl and subsequent high purity water (MilliQ) rinses and protected with double bags for storage and transport. Trace metal clean techniques were used throughout all the process when collecting and manipulating samples for both dissolved and particulate metals analyses.

### **Chlorophyll *a* (Chl *a*) concentration and in vivo Chl *a* fluorescence**

Water samples (750 mL) were collected every other day from each mesocosm to determine total Chlorophyll *a* (Chl *a*) concentration. Samples were filtered onto 0.7  $\mu\text{m}$  GF/F filters (Millipore) and kept at -80°C until analyses. Chl *a* was extracted in N,N-dimethylformamide overnight at 4°C in the dark. Chl *a* content was determined spectrophotometrically and the concentrations were calculated



by using Wellburn (1994) equations. Optimal quantum yield ( $F_v/F_m$ ) of PSII charge separation was measured in 10 min dark-adapted samples by pulse amplitude modulated fluorometry (Water-PAM, Waltz, Effeltrich, Germany) as described by Schreiber et al. (1986). After initial dark measurement and a saturation pulse to determine minimum fluorescence ( $F_0$ ) and maximum fluorescence ( $F_m$ ), respectively,  $F_v/F_m$  was obtained, considering  $F_v/F_m$  as  $(F_m - F_0)/F_m$ . Thus,  $F_v$  is the maximal variable fluorescence of a dark-adapted sample,  $F_m$  is the maximal fluorescence intensity with all PSII reaction centres closed,  $F_0$  the basal fluorescence. High  $F_v/F_m$  values indicate that cells are in healthy physiological condition, whereas a decrease in  $F_v/F_m$  indicates stress of any kind (Foyer et al. 1994, Behrenfeld & Milligan 2013).

### **Plankton analyses**

*Phytoplankton <20 µm and bacterioplankton:* Phytoplankton cells smaller than 20 µm from each mesocosm were analysed using a FACSCalibur flow cytometer (Becton Dickinson, USA) equipped with an air-cooled laser providing 15 mW at 488 nm and with a standard filter set-up. The trigger was set on red fluorescence and samples were analysed for 300 s at an average flow rate of 56 µL min<sup>-1</sup>. Autotrophic groups were discriminated on the basis of the side-scatter signal (SSC) versus pigment autofluorescence (chlorophyll and phycoerythrin) according to Marie et al. (1999) and Larsen et al. (2001), and biovolumes converted into carbon-biomass according to Kana & Glibert (1987), Menden-Deuer & Lessard (2000) and Olenina et al. (2006).

Enumeration of bacterioplankton was performed according to Marie et al. (1999). The samples were fixed with glutaraldehyde (0.5% final concentration) for 30 min at 4°C, snap frozen in liquid nitrogen, stored at -80°C and stained with SYBR Gold Nucleic Acid Stain (Invitrogen) for 10 min at 80°C in the dark after thawing before counting using a Cytomics FC 500 flow cytometer (Beckman Coulter) equipped with a 20 mW 488 nm air-cooled argon-ion laser and standard filters. The



discriminator was set to green fluorescence and the samples were analysed for 60 s at a flow rate of 30  $\mu\text{L min}^{-1}$ . Data were calibrated by measuring latex fluorospheres (1.0  $\mu\text{m}$  in diameter; Polysciences Inc.) at 525 nm using CXP analysis software. Bacterial abundances were transformed into carbon-biomass according to Lee & Fuhrman (1987) and Vrede et al. (2002).

*Phytoplankton >20  $\mu\text{m}$  and microzooplankton*- Live samples were immediately analysed with a FlowCAM (Fluid Imaging Technologies, Scarborough, Maine, USA) using a 4x objective and a 300  $\mu\text{m}$  flowcell to analyse particles ranging from 18 to 1000  $\mu\text{m}$  equivalent spherical diameter (ESD) and run in automatic imaging mode (Jakobsen et al. 2011). 6.3 mL of each sample were analysed at flow rates adjusted to guarantee that no more than 1 particle appeared in each frame. All the image collages were post analysed to separate the main taxonomic groups (diatoms, dinoflagellates and ciliates). Abundances and particle sizes of these groups (Jakobsen & Carstensen 2011) were then converted into carbon-biomass using the equations provided in Menden-Deuer & Lessard (2000).

*Mesozooplankton* was sampled at the beginning and at the end of the experiment. At the beginning, samples were collected by filtering 2.2  $\text{m}^3$  water pumped through a 90  $\mu\text{m}$  Apstein plankton net (Hydrobios, Kiel, Germany) as described in Nejstgaard et al. (2006). At the end of the experiment, the whole water column of the mesocosms were mixed with a 45 cm disc (Striebel et al. 2013), immediately sampled by two vertical 90  $\mu\text{m}$  net tows and preserved in 4% borax-buffered formaldehyde solution. Species composition and abundance was determined using a dissecting microscope and the total mesozooplankton biomass was calculated according to Nejstgaard et al. (2006).

### **Net growth rates**

Apparent net growth rates for phytoplankton and bacterioplankton were calculated according to the logistic model:



$$\ln [(K-N)/N] = \ln [(K-N_0) - 1] - \mu t$$

where K refers to the loading capacity of the mesocosms, N is the cell density at any given time,  $N_0$  is the cell density at time 0,  $\mu$  is the intrinsic growth rate, and t is the time (in days).

### Iron requirements

Fe demand (mol Fe per L of seawater) for each phytoplankton group was calculated using published Fe:C ratios ( $\mu\text{mol Fe per mol C}$ ) and the maximum C biomass achieved by each phytoplankton group during the experiment. The estimates of C biomass were calculated as described above. We assumed Fe:C ratios ( $\mu\text{mol:mol}$ ) published for *E. huxleyi* (Muggli & Harrison 1996), diatoms (Sarhou et al. 2005), *Synechococcus* sp. and Prasinophytes (Quigg et al. 2010), picoeukaryotes (Timmermans et al. 2005) and dinoflagellates (Marchetti & Maldonado 2016).

### Irradiance and temperature

Solar spectral irradiance comprising photosynthetically active radiation wavelengths (PAR, 400-700 nm) ultraviolet radiation A (UVA, 320-400 nm) and ultraviolet radiation B (UVB, 280-320 nm) was recorded at 2 m depth in one mesocosm (5 min. intervals) using a spectroradiometer TRIOS RAMSES (Ramses, TrioS GmbH, Germany). Because the spectroradiometer developed a crust of ferric material that interfered with all the analyses this mesocosm was excluded as a replicate and was only used for irradiance measurements. HOBO Pendant Temperature/Light loggers (Onset Computer Corporation, Massachusetts, USA) were attached to the airlift system in one of each treatments at the depths 0 m, 1 m, 2 m, and 3 m to check that mesocosms received the same irradiance as well as to monitor water temperature.



## Statistical analyses

Statistical significance of treatment effects on variables measured was analysed by performing Split-Plot ANOVAs (also called SPANOVA or mixed-model ANOVA) followed by post-hoc Sidak or Tukey and Bonferroni tests, respectively (considering  $p < 0.05$  and/or  $p < 0.01$  as significant). When appropriate, data were specifically tested for significant differences ( $p < 0.05$ ) induced by the treatments by using 1 or 2 Way ANOVAs and/or Student's t-tests, as well as Pearson's product-moment correlations. All analyses were performed using the GLM (general linear model) procedure with main effects (CO<sub>2</sub>, dFe), time (repeated measure) and all interactions. Data were previously checked for normality (by Saphiro-Wilks' test), homoscedasticity (by Cochran's and Levene's tests) and sphericity (by Mauchly's and/or Bartlett's tests). Variables met all the criteria above mentioned. Statistical analyses were performed by using the software Statistica v12 (Statsoft, Inc.) and SPSS v22 (IBM statistics).

## Results

### Experimentally induced stressors (carbonate system and dissolved iron)

The experimental set-up was successful in that pCO<sub>2</sub> reflected the target concentration of 900  $\mu\text{atm}$  in the high CO<sub>2</sub> treatment (HC) *versus* 390  $\mu\text{atm}$  in the ambient CO<sub>2</sub> treatment (LC) (Figure 2.1a). pCO<sub>2</sub> dropped significantly about 2-fold between day 3 and 10 (Bonferroni,  $p < 0.001$ ) as a consequence of biological activity in both HC and LC treatments, but re-addition of CO<sub>2</sub>-enriched fjord water on days 3, 7 and 10 (in HC) re-established pCO<sub>2</sub> to 1100  $\mu\text{atm}$ . pH stabilised at around 7.8 in HC and 8.1-8.3 in LC treatments (Table 2.1). Average alkalinity was 2029 ( $\pm 60$ )  $\mu\text{mol L}^{-1}$  for all mesocosms and DIC remained stable after day 5 at 1953 ( $\pm 36$ )  $\mu\text{mol L}^{-1}$  in HC and 1795 ( $\pm 61$ )  $\mu\text{mol L}^{-1}$  in LC (Table 2.1).  $\Omega_{\text{calcite}}$  was significantly higher in LC than in HC (t-test  $p < 0.05$ ; Table 2.1).

To induce changes in Fe availability, 70 nM of the siderophore DFB was added to half of the mesocosms. Even though DFB is a strong Fe binding organic



ligand often used to induce iron limitation in phytoplankton (Wells 1999), DFB additions may also increase the dissolved Fe pool in environments with high concentrations of colloidal and/or particulate Fe, such as fjords (Kuma et al. 1995, Öztürk et al. 2002). In this experiment, the DFB addition increased dissolved iron. Before DFB was added on day 7, the initial dFe concentration was 5 nM (mean of all mesocosms), without significant differences between LC and HC treatments (Figure 2.1b, SPANOVA,  $p=0.069$ ). Dissolved Fe concentrations in the control (LC-DFB) remained at this level throughout the experiment (SPANOVA  $p=0.399$ , post-hoc Bonferroni  $p<0.001$ ). The DFB amendment on day 7, resulted in a significant ca. 3-fold increase in dFe in both HC and LC treatments by day 17 (post-hoc Sidak  $p=0.003$  and  $p=0.0004$ , respectively) relative to the initial levels (post-hoc Bonferroni  $p=0.002$ ). On day 17, the only treatment significantly different from the rest in terms of dFe was the control (LC-DFB, post-hoc Sidak  $p=0.0004$ ), which showed the lowest dFe levels. At high  $p\text{CO}_2$  without DFB addition (i.e. HC-DFB treatment) dFe also increased ca.3-fold by day 17, confirming the expected increase in iron solubility due to lowering pH (Millero et al. 2009). Surprisingly, dFe decreased sharply between days 17 and 21. In contrast, the +DFB treatments sustained high dFe throughout day 21, regardless of the  $p\text{CO}_2$  level (post-hoc Sidak,  $p\leq 0.025$ ). These results suggest that Fe solubility was enhanced by either the addition of DFB and/or  $\text{CO}_2$ . Furthermore, significant effects of  $p\text{CO}_2$ , DFB, and their interaction were observed on the availability of dFe during the experiment.

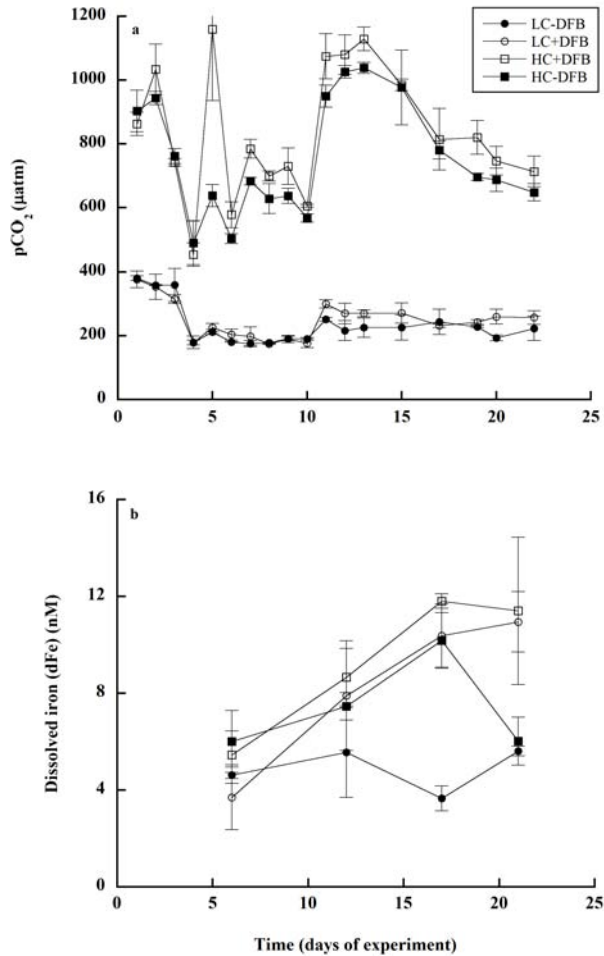


**Figure 2.1.** Temporal development of CO<sub>2</sub> partial pressures (pCO<sub>2</sub>) (a) and dissolved iron (dFe) (b) within the mesocosms. Ambient pCO<sub>2</sub> and ambient dFe (black filled circle); ambient pCO<sub>2</sub> and increased dFe (LC+DFB, open circle); increased pCO<sub>2</sub> and increased dFe (HC+DFB, open square), increased pCO<sub>2</sub> and ambient dFe (HC-DFB, black filled square). Symbols indicate means of measurements in three independent mesocosms (n=3) except for LC-DFB where n=2. Error bars indicate standard deviations.

**Table 2.1.** Measured pH, total alkalinity (TA,  $\mu\text{mol L}^{-1}$ ) and calculated dissolved inorganic carbon (DIC,  $\mu\text{mol L}^{-1}$ ) and calcite saturation estate ( $\Omega_{\text{calcite}}$ ) under the different treatments; LC: ambient  $\text{CO}_2$  (390  $\mu\text{atm}$ ); HC: increased  $\text{CO}_2$  (900  $\mu\text{atm}$ ); -DFB (ambient dFe); +DFB (increased dFe). Note that DFB was added on day 7. Data are means of three independent mesocosm bags  $\pm$  standard deviation (in brackets), except for LC-DFB treatment in which  $n=2$ . Significant differences between treatments within each day are represented by different letters (2-Way ANOVA followed by post-hoc Tukey tests, considering  $p<0.05$  as significant). The rain ratio (RR) was calculated applying the models from Ridgwell et al. (2007) and Hoffmann & Schellnhuber (2009). The calculated RR represents the average between the 2 models, and standard deviation between brackets.

	pH				Total Alkalinity				DIC				$\Omega_{\text{calcite}}$				Rain ratio			
	LC-DFB	LC+DFB	HC+DFB	HC-DFB	LC-DFB	LC+DFB	HC+DFB	HC-DFB	LC-DFB	LC+DFB	HC+DFB	HC-DFB	LC-DFB	LC+DFB	HC+DFB	HC-DFB	LC-DFB	LC+DFB	HC+DFB	HC-DFB
Day 1	8.04 (0.01) <sup>a</sup>	8.05 (0.02) <sup>a</sup>	7.71 (0.02) <sup>b</sup>	7.70 (0.04) <sup>b</sup>	2100 (20) <sup>a</sup>	2176 (40) <sup>a</sup>	2096 (25) <sup>a</sup>	2140 (34) <sup>a</sup>	1933 (6) <sup>a</sup>	2002 (44) <sup>ab</sup>	2041 (20) <sup>bc</sup>	2086 (25) <sup>c</sup>	2.98 (0.04) <sup>a</sup>	3.15 (0.10) <sup>a</sup>	1.5 (0.08) <sup>b</sup>	1.53 (0.14) <sup>b</sup>	0.75 (0.06) <sup>a</sup>	0.80 (0.08) <sup>a</sup>	0.41 (0.11) <sup>b</sup>	0.41 (0.10) <sup>b</sup>
Day 3	8.06 (0.05) <sup>a</sup>	8.10 (0.02) <sup>a</sup>	7.77 (0.01) <sup>b</sup>	7.75 (0.01) <sup>b</sup>	2086 (23) <sup>a</sup>	2046 (6) <sup>a</sup>	2060 (35) <sup>a</sup>	2046 (15) <sup>a</sup>	1910 (33) <sup>a</sup>	1861 (11) <sup>a</sup>	1989 (33) <sup>b</sup>	1980 (16) <sup>b</sup>	3.07 (0.25) <sup>a</sup>	3.28 (0.09) <sup>a</sup>	1.68 (0.04) <sup>b</sup>	1.63 (0.04) <sup>b</sup>	0.77 (0.07) <sup>a</sup>	0.82 (0.08) <sup>a</sup>	0.45 (0.09) <sup>b</sup>	0.44 (0.09) <sup>b</sup>
Day 5	8.24 (0.02) <sup>a</sup>	8.22 (0.02) <sup>a</sup>	7.66 (0.15) <sup>b</sup>	7.81 (0.02) <sup>b</sup>	2027 (40) <sup>a</sup>	2032 (8) <sup>a</sup>	1956 (108) <sup>a</sup>	1975 (67) <sup>a</sup>	1775 (27) <sup>a</sup>	1793 (14) <sup>a</sup>	1917 (143) <sup>a</sup>	1894 (66) <sup>a</sup>	4.16 (0.5) <sup>a</sup>	4.22 (0.15) <sup>a</sup>	1.30 (0.6) <sup>b</sup>	1.77 (0.09) <sup>b</sup>	1.06 (0.19) <sup>a</sup>	1.03 (0.18) <sup>a</sup>	0.38 (0.10) <sup>b</sup>	0.47 (0.08) <sup>b</sup>
Day 10	8.28 (0.01) <sup>a</sup>	8.3 (0.03) <sup>a</sup>	7.84 (0.00) <sup>b</sup>	7.86 (0.01) <sup>b</sup>	2045 (48) <sup>a</sup>	2006 (5) <sup>a</sup>	2021 (14) <sup>a</sup>	2013 (15) <sup>a</sup>	1769 (34) <sup>a</sup>	1727 (17) <sup>a</sup>	1915 (16) <sup>b</sup>	1930 (14) <sup>b</sup>	4.49 (0.03) <sup>a</sup>	4.85 (0.21) <sup>a</sup>	1.93 (0.01) <sup>b</sup>	2.01 (0.02) <sup>b</sup>	1.15 (0.25) <sup>a</sup>	1.21 (0.29) <sup>a</sup>	0.51 (0.07) <sup>b</sup>	0.53 (0.06) <sup>b</sup>
Day 22	8.22 (0.06) <sup>a</sup>	8.16 (0.03) <sup>a</sup>	7.77 (0.03) <sup>b</sup>	7.81 (0.02) <sup>b</sup>	2003 (35) <sup>a</sup>	1983 (38) <sup>a</sup>	1996 (15) <sup>a</sup>	2006 (12) <sup>a</sup>	1777 (38) <sup>a</sup>	1773 (28) <sup>a</sup>	1926 (7) <sup>b</sup>	1924 (10) <sup>b</sup>	4.08 (0.3) <sup>a</sup>	3.59 (0.29) <sup>a</sup>	1.64 (0.1) <sup>b</sup>	1.80 (0.07) <sup>b</sup>	1.03 (0.18) <sup>a</sup>	0.90 (0.11) <sup>a</sup>	0.44 (0.09) <sup>b</sup>	0.48 (0.08) <sup>b</sup>



### Plankton community structure and dynamics

The experiment was divided in two clearly different phases, with significant changes in chlorophyll *a* (Chl *a*) and the carbon-based biomass of plankton groups (Figure 2.2, Figure 2.3). Phase 1 comprised days 0 to 10, and phase 2 days 11 to 22.

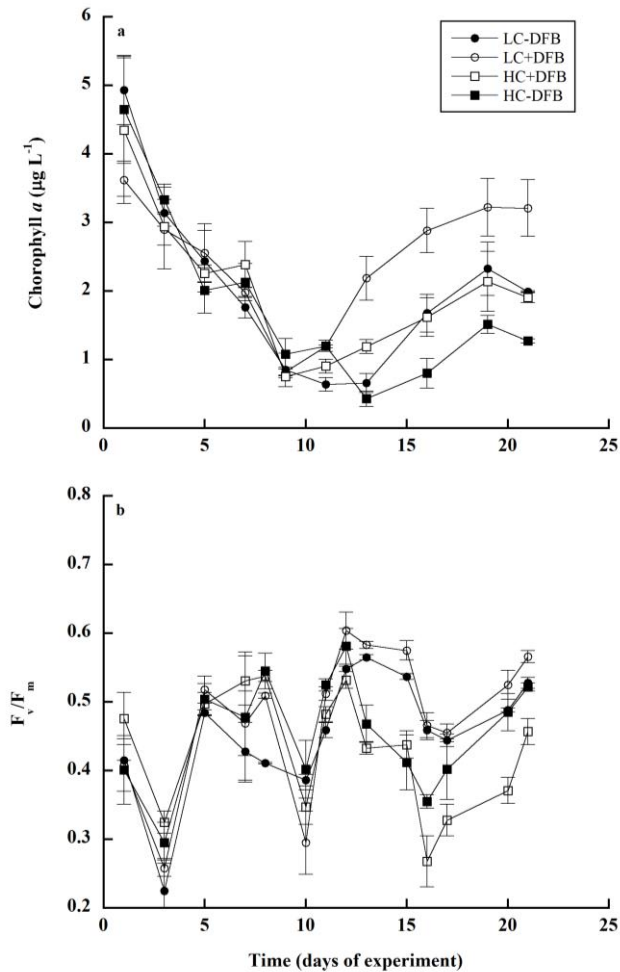


**Figure 2.2.** Temporal development of total Chl *a* concentration (a) and optimal quantum yield of Chl *a* associated to photosystem II ( $F_v/F_m$ ) (b) within the mesocosms in the different treatments. Symbols (as in Figure 2.1) indicate means of measurements in three independent mesocosms ( $n=3$ ) except for LC-DFB where  $n=2$ . Error bars correspond to standard deviations.

In phase 1, Chl *a* decreased from 4.34 to 0.87  $\mu\text{g L}^{-1}$  in all mesocosms (Figure 2.2a) due to the rapid break-down of a diatom bloom (also in the fjord) which was dominated by chain forming *Skeletonema costatum*. (Figure 2.3f, Supplemental Figure 2.2S). Picoeukaryotes (0.1-2  $\mu\text{m}$ ), small nanoeukaryotes (2-7  $\mu\text{m}$ ), big nanoeukaryotes (6-20  $\mu\text{m}$ ), and dinoflagellates (20-200  $\mu\text{m}$ ) showed comparable peak dynamics and declined towards the end of phase 1 (Figure 2.3c-e,g). This decline was followed by similar dynamics in the ciliate community (post-hoc Bonferroni  $p < 0.001$ ) (Figure 2.3h, Supplemental Figure 2.1S). There were no significant differences between treatments in Chl *a* and  $F_v/F_m$  (Figure 2.2) nor for any of the planktonic groups (Figure 2.3, all SPANOVA,  $p > 0.05$ ) during phase 1. Only heterotrophic bacterioplankton biomass (Figure 2.3i) and its net growth rate were significantly higher in the HC treatment than in the LC treatment by days 9-10 ( $\sim 64 \mu\text{g C L}^{-1}$ , post-hoc Sidak  $p = 0.026$  and  $p = 0.016$ , days 9 and day 10 respectively). However, biomass and net growth rates of bacterioplankton reversed and were higher in the LC than HC treatments during phase 2 (Table 2.2).

During phase 2, Chl *a* concentration increased in all treatments (Figure 2.2a) due to elevated biomass of *E. huxleyi* (5-10  $\mu\text{m}$ ), *Synechococcus* sp. (0.6-2  $\mu\text{m}$ ), small and big nanoeukaryotes, and to a lower extent, dinoflagellates (20-200  $\mu\text{m}$ ) (Figure 2.3 a-e, g). Chl *a* remained below 2  $\mu\text{g L}^{-1}$  in the HC treatments, while it culminated at  $\sim 3.5 \mu\text{g L}^{-1}$  on day 19 under LC conditions (Figure 2.2a). Significant differences in Chl *a* concentration between HC and LC were observed independent of DFB addition (Figure 2.2a) (post-hoc Tukey  $p < 0.0001$ ). However, DFB addition (on day 7) had a delayed positive effect on Chl *a* in phase 2 (post-hoc Tukey  $p < 0.0001$  and Bonferroni,  $p \leq 0.001$ ).  $F_v/F_m$  (Figure 2.2b) was significantly higher in LC than in HC treatments in this period ( $p < 0.05$ ). Under LC conditions +DFB promoted a significant increase in  $F_v/F_m$  with respect to the control (LC-DFB) (post-hoc Sidak  $p < 0.05$ ) (Figure 2.2b). In contrast, in the HC treatments  $F_v/F_m$  was higher in the absence of DFB. The coccolithophore *E.*

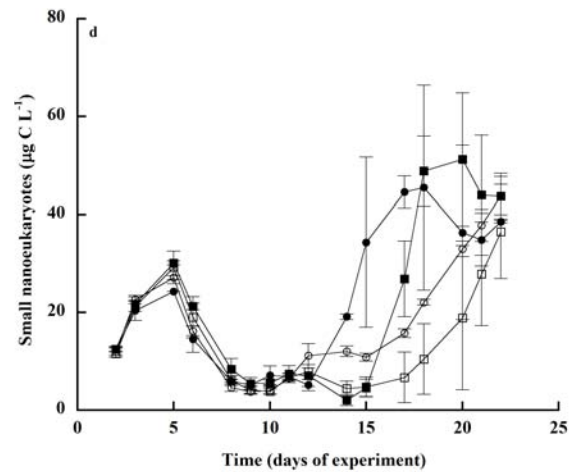
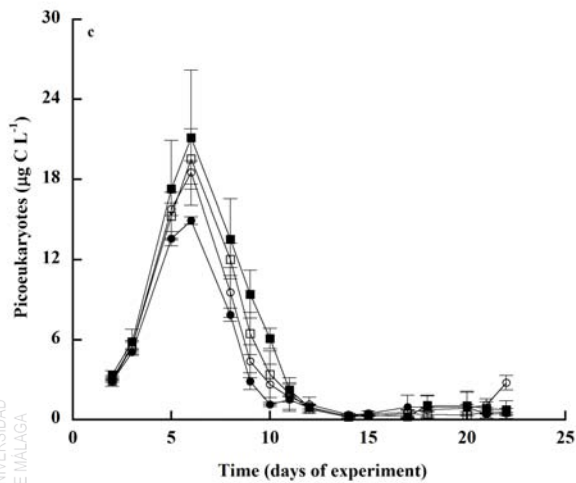
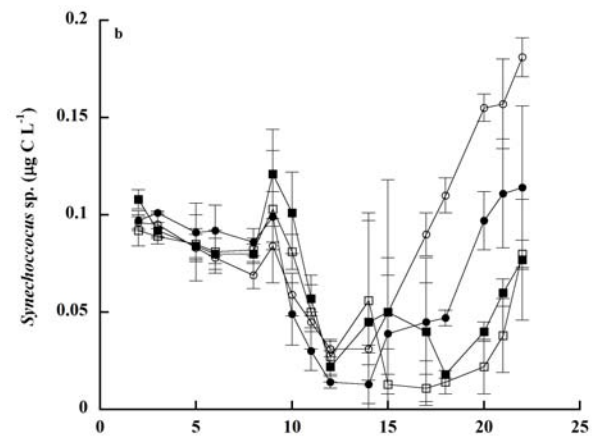
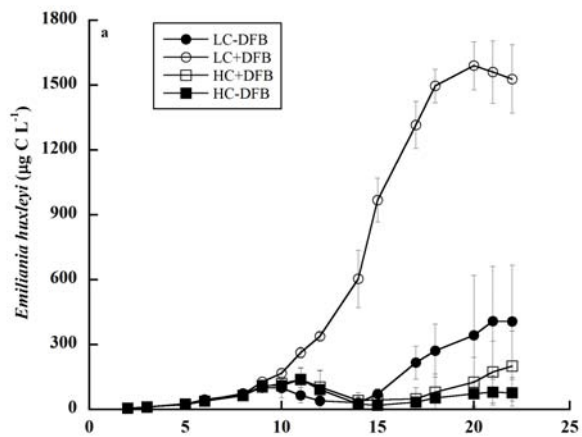


*huxleyi* and the cyanobacterium *Synechococcus* sp. were affected by both pCO<sub>2</sub> and Fe conditions.

A massive increase in *E. huxleyi* biomass was evident in the LC+DFB treatment reaching 1600 µg C L<sup>-1</sup> corresponding to 60 000 cells mL<sup>-1</sup> (Figure 2.3a and Supplemental Figure 2.15a, respectively) in phase 2. In contrast, *E. huxleyi* biomass was much lower in the HC treatments (200 µg C L<sup>-1</sup> in HC+DFB and 78 µg C L<sup>-1</sup> in HC-DFB) and remained at levels below than those in the control mesocosms LC-DFB (400 µg C L<sup>-1</sup>) (Figure 2.3a). Thus, the biomass of *E. huxleyi* was significantly negatively affected by pCO<sub>2</sub> (post-hoc Sidak p<0.0001), positively by iron (post-hoc Sidak p<0.0001) and by the interactive effects of both factors (post-hoc Sidak p<0.0001). In mesocosms treated with DFB, *E. huxleyi* clearly dominated the phytoplankton biomass under low pCO<sub>2</sub> and high dFe conditions with up to 9000 times higher biomass than the other groups (Figure 2.3a) and faster net growth rates (up to 0.61 d<sup>-1</sup>, Table 2.2). The 3-fold increase in dFe as a result of DFB addition produced a significant 4-fold increase in *E. huxleyi* biomass at ambient pCO<sub>2</sub> with respect to the control (LC-DFB) and 8 and 20-fold higher *E. huxleyi* biomasses with respect to HC+DFB and HC-DFB, respectively. In contrast, elevated pCO<sub>2</sub> had a negative effect on *E. huxleyi* net growth rates, inhibiting growth by 50% relative to the LC treatments (Table 2.2).

**Figure 2.3.** Temporal development of phytoplankton, microzooplankton and heterotrophic bacterioplankton biomasses (µgC L<sup>-1</sup>) in the mesocosms exposed to different CO<sub>2</sub> and dFe treatments. (a) *Emiliania huxleyi* (5-10 µm); (b) *Synechococcus* sp., (0.6-2 µm); (c) picoeukaryotes (0.1-2 µm); (d) small nanoeukaryotes (Prasinophytes, small Haptophytes, 2-7 µm); (e) big nanoeukaryotes (small single celled diatoms and flagellated forms, 6-20 µm); (f) Diatoms (chain forming *Skeletonema costatum*, 20->500µm); (g) Dinoflagellates (20-200 µm); (h) Ciliates (20-200 µm); (i) heterotrophic bacterioplankton (0.2-0.7 µm). Symbols (as in Figure 2.1) indicate means of measurements in three independent mesocosms (n=3) except for LC-DFB where n=2. Error bars indicate standard deviations.





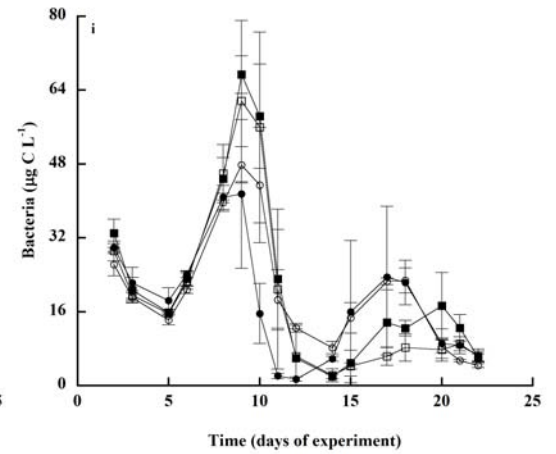
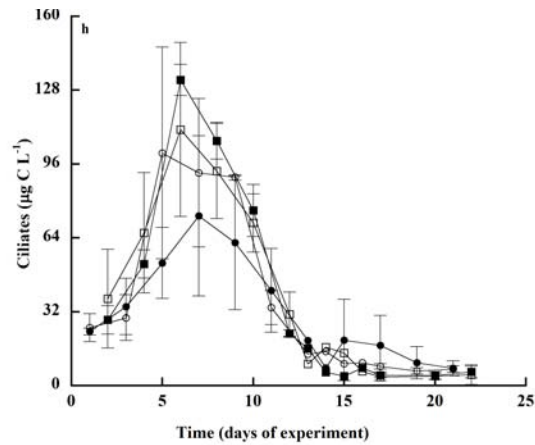
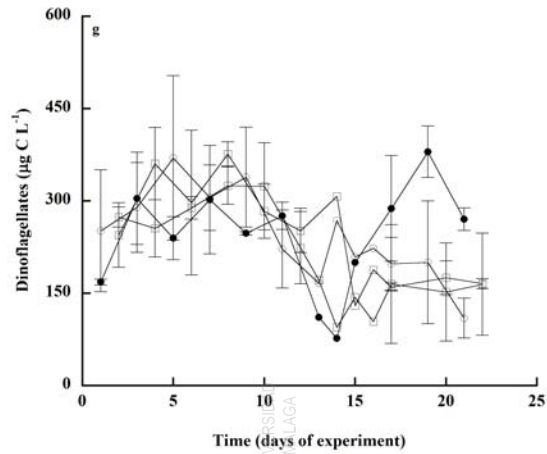
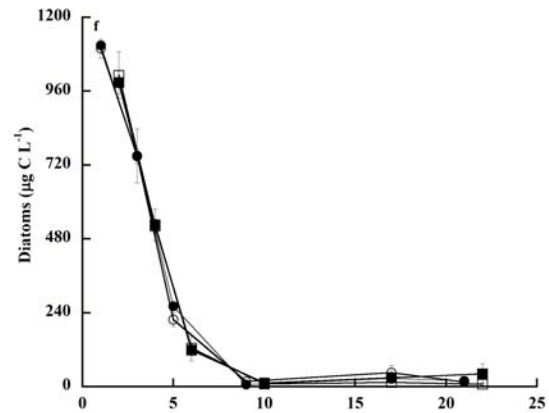
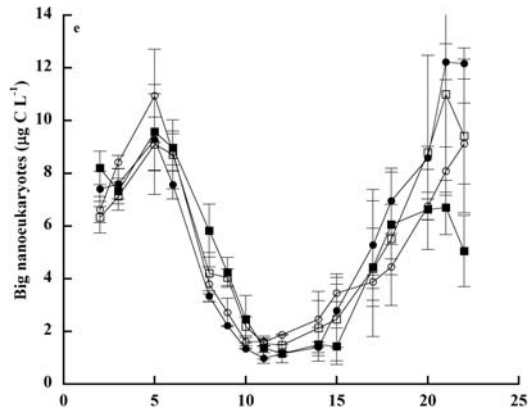


**Table 2.2.** Net growth rates ( $\mu$  in  $d^{-1}$ ) of the different groups calculated with the logistic model under the different treatments; LC: ambient  $CO_2$  (390  $\mu atm$ ); HC: increased  $CO_2$  (900  $\mu atm$ ); -DFB (ambient dFe); +DFB (increased dFe). In the logistic model  $LN((K-N)/N)$ . K is the carrying capacity, N corresponds to cells numbers at a given time and the growth rate ( $\mu$ ) is the slope from the linear regression. Data are means of three independent mesocosm bags  $\pm$  standard deviation (in brackets) except for LC-DFB treatment in which n=2. Significant differences between treatments within the same time period (i.e. 0d to 10d or 11d to 22d) are represented by different letters (2-Way ANOVA followed by post-hoc Tukey tests considering  $p < 0.05$  as significant). Significant differences between the two time periods mentioned within the same treatment are represented by an asterisk (t-test, considering  $p < 0.05$  as significant). Blank spaces mean that net growth rates have non-significant determination coefficients ( $R^2$ ). Note that DFB was added on day 7.

Growth rates	$\mu_{LC-DFB}$		$\mu_{LC+DFB}$		$\mu_{HC+DFB}$		$\mu_{HC-DFB}$	
	0-10	11-22	0-10	11 to 22	0-10	11-22	0-10	11-22
<i>Emiliana huxleyi</i> (5-10 $\mu m$ )	0.38(0.02) <sup>a*</sup>	0.52(0.06) <sup>a*</sup>	0.41(0.01) <sup>a*</sup>	0.61(0.00) <sup>b*</sup>	0.50(0.06) <sup>a*</sup>	0.42(0.06) <sup>c*</sup>	0.54(0.09) <sup>a*</sup>	0.33(0.01) <sup>d*</sup>
<i>Synechococcus</i> sp (0.6-2 $\mu m$ )	-	0.04(0.06) <sup>a*</sup>	-	0.59(0.07) <sup>b*</sup>	-	0.43(0.06) <sup>a*</sup>	-	0.36(0.10) <sup>a*</sup>
Picoeukaryotes (0.1-2 $\mu m$ )	1.28(0.04) <sup>a*</sup>	0.34(0.21) <sup>a*</sup>	1.18(0.18) <sup>a*</sup>	0.14(0.02) <sup>a*</sup>	1.02(0.04) <sup>a*</sup>	0.11(0.05) <sup>a*</sup>	1.16(0.10) <sup>a*</sup>	0.09(0.05) <sup>a*</sup>
Small nanoeukaryotes (2-7 $\mu m$ )	0.20(0.02) <sup>a</sup>	0.31(0.04) <sup>a</sup>	0.30(0.02) <sup>a</sup>	0.32(0.03) <sup>a</sup>	0.30(0.01) <sup>a</sup>	0.21(0.14) <sup>a</sup>	0.30(0.11) <sup>a</sup>	0.40(0.12) <sup>a</sup>
Big nanoeukaryotes (6-20 $\mu m$ )	0.32(0.21) <sup>a</sup>	0.40(0.01) <sup>a</sup>	0.42(0.03) <sup>a*</sup>	0.35(0.06) <sup>a*</sup>	0.28(0.08) <sup>a*</sup>	0.36(0.05) <sup>a*</sup>	0.32(0.05) <sup>a</sup>	0.47(0.09) <sup>a</sup>
Dinoflagellates (30-75 $\mu m$ )	0.26(0.02) <sup>a*</sup>	-	0.34(0.02) <sup>a*</sup>	-	0.35(0.26) <sup>a*</sup>	-	0.25(0.08) <sup>a*</sup>	-
Bacterioplankton (0.2-0.7 $\mu m$ )	0.55(0.08) <sup>a*</sup>	0.77(0.03) <sup>a*</sup>	0.55(0.10) <sup>a*</sup>	0.72(0.04) <sup>a*</sup>	0.86(0.07) <sup>b*</sup>	0.51(0.12) <sup>a*</sup>	0.997(0.12) <sup>b*</sup>	0.72(0.28) <sup>a*</sup>



After an initial decrease during phase 1, *Synechococcus* sp. recovered during phase 2 (Figure 2.3b and Supplementary Figure 2.1Sb). The fastest recovery was observed in the LC treatments, with net growth rates of 0.58 d<sup>-1</sup> and biomasses of 0.18 µg C L<sup>-1</sup> in the LC+DFB mesocosms (Table 2.2, Figure 2.3b). Elevated pCO<sub>2</sub> had significant negative effects on *Synechococcus* sp. from day 12 onwards (post-hoc Sidak p=0.018 and Bonferroni p<0.001) while dFe had no effect (p=0.785). In general, biomass values and/or net growth rates of other microorganisms were not significantly affected by changes in pCO<sub>2</sub>, and/or dFe levels or their interaction during phase 2 (all SPANOVAs, p>0.05). Mesozooplankton was dominated by calanoid copepods and reached high biomass in all treatments from initially 16.5 µg C L<sup>-1</sup> to 159-223 µg C L<sup>-1</sup> at the end of the experiment (Figure 2.4), but there were no significant differences on total mesozooplankton due to treatments (SPANOVA, p>0.05).

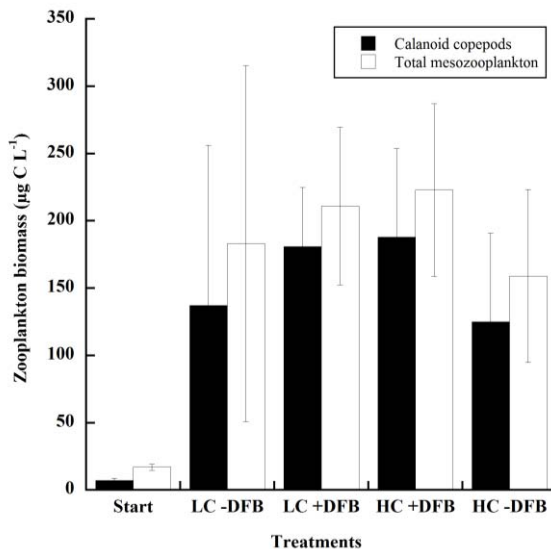


**Figure 2.4.** Total mesozooplankton biomass (white bars) and calanoid copepods (black bars) at the beginning and at the end of the experiment. Bars indicate means of measurements in three independent mesocosms (n=3) except for LC-DFB where n=2. Error bars indicate standard deviations.



## Discussion

The target CO<sub>2</sub> concentrations were achieved in the twelve mesocosms. The reproducibility between the triplicates of each treatment was high, allowing us to isolate and identify single and interactive effects on the variables measured. Instead of our intention to induce Fe limitation with the DFB addition on day 7, we found that DFB enhanced dFe levels, likely due to an increase in Fe solubility. Similar results have also been found in other fjord environments (Öztürk et al. 2002). Indeed, a decrease in particulate iron concomitant to an increase in dissolved iron, up to a significant 12-fold change from particulate iron to dissolved iron in the LC+DFB treatment (Supplemental Figure 2.2S, Supplemental Table 2.2S), indicates that DFB mediated the transfer of Fe from the particulate to the soluble pool. In addition, Fe solubility is enhanced at pH lower than 7.8 (Kuma et al. 1996). Hence, high CO<sub>2</sub> also increased dissolved Fe levels in our experiment, as previously observed in a mesocosm experiment in the same fjord (Breithbarth et al. 2010). In conclusion, in fjord environments dissolved Fe levels increased similarly by either the addition of CO<sub>2</sub> and/or DFB. In the high CO<sub>2</sub> treatment (HC), the presence of the siderophore prevented the re-precipitation of dFe (Figure 2.1b) implying that either increasing pCO<sub>2</sub> or DFB may result in high dissolved Fe levels, therefore maintaining Fe in the dissolved pool.

These distinct chemical conditions steered the mesocosms performance into two clearly differentiated phases. In phase 1 (day 0-10) ambient dFe conditions in the mesocosms were sufficient for all planktonic groups to meet their iron demand (in the range of pM, Supplemental Table 2.1S) and nutrients were sufficient to sustain growth (Supplemental Figure 2.3S). Phase 1 thus consisted of a phytoplankton bloom succession similar to what has previously been reported (Paulino et al. 2008) with small autotrophs being grazed by microzooplankton (data not shown), which in turn were probably preyed upon by copepods (Nejstgaard et al. 2001). However, no pCO<sub>2</sub> effects were observed in phase 1 in any of the functional groups, except for bacterioplankton.





Heterotrophic bacteria reacted positively to HC treatments in phase 1 and had higher net growth rates at increased pCO<sub>2</sub> levels, possibly due to enhanced available DOM, in agreement with previous studies (Endres et al. 2014) (Supplemental Figure 2.3S). The reverse situation in phase 2 (days 12-18) may reflect changes in bacterial community composition, but further studies are needed.

In phase 2 (day 11-22), the coccolithophore *E. huxleyi*, and the cyanobacterium *Synechococcus* sp. were both affected by the different pCO<sub>2</sub> and Fe conditions. The effects of increased pCO<sub>2</sub> on *E. huxleyi* are in agreement with previous mesocosms studies (Riebesell et al. 2007), showing that elevated pCO<sub>2</sub> had a detrimental impact on the net growth of *E. huxleyi*, while at ambient pCO<sub>2</sub> and high N:P ratios, *E. huxleyi* dominates the phytoplankton communities (Paasche 2002).

The most remarkable results in our experiment were the massive increase in *E. huxleyi* biomass and its growth rate in the LC+DFB treatment (up to 20-fold higher biomass and 2-fold faster growth rate, Figure 2.3a, Table 2.2) (cell numbers also increased several orders of magnitude relative to other autotrophic groups). It is not surprising that under ambient CO<sub>2</sub> *E. huxleyi* flourished due to its ability to exploit efficiently organic nutrients, use ammonium instead of nitrate and have an efficient alkaline phosphatase (shown in Supplemental Figure 2.3S, and reflected in Paasche (2002)). However, the beneficial effect of DFB is more cryptic. Our results point to that the DFB addition actually increased dFe, resulting in higher biomass. The insufficiency of the ambient dFe to support the *E. huxleyi* biomass can be demonstrated by calculating the iron demand of the bloom relative to the concentration of dFe in the control (LC-FB). Our estimated Fe demand to sustain *E. huxleyi* abundance in LC+DFB was ~6-10 nM (Supplementary Table 2.2S), a dFe concentration measured in all treatments except in the control mesocosms with ambient pCO<sub>2</sub> and no DFB (LC-DFB, dFe concentration of 4.5 nM). Therefore in the control treatment, the cells were most



likely experiencing Fe limitation (i.e. the rate of dFe supply is slower than that of iron demand by the coccolithophore), which was affecting their growth rates (Table 2.2). The faster growth rates observed in the presence of DFB imply that Fe bound to DFB is bioavailable to *E. huxleyi*, as previously demonstrated by Lis et al. (2015).

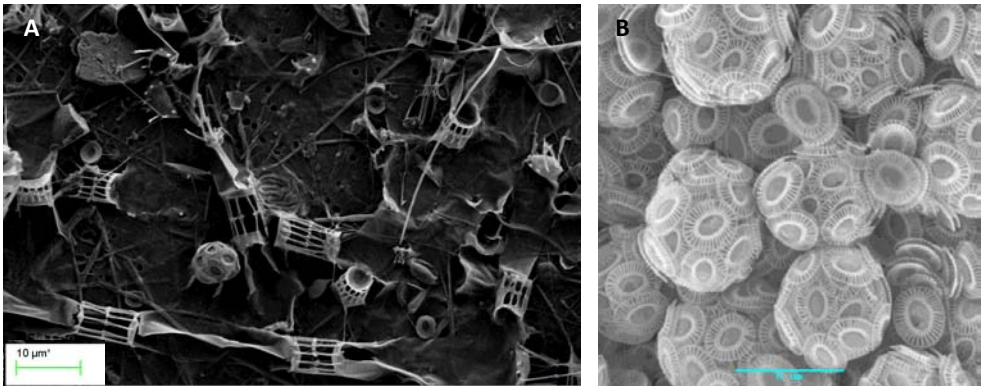


**Figure 2.5.** SEM photographs from treatment LC+DFB (A) with the decline of *Skeletonema* sp and before the bloom of *Emiliana huxleyi* (day 4) and (B) during the bloom of *Emiliana huxleyi* (day 18).

In addition to slower net growth rates and reduced Chl *a*, significant lower  $F_v/F_m$  values were observed in the LC-DFB with respect to the LC+DFB treatment from days 11-22 (Figure 2.2b), in accordance with values observed in *E. huxleyi* under Fe limitation at the same light conditions than in our experiment (Honey et al. 2013). This combination of symptoms is typical of Fe deficient algae (Behrenfeld & Milligan 2013), offering further support for the Fe limited condition of *E. huxleyi* in the control. The observed *E. huxleyi* biomass as well as Chl *a* do however increase slightly in the control (LC-DFB) in spite of assumed iron limitation. It can be considered that dFe should decrease under these circumstances. However, Fe demand estimated for the control is 0.8 to 1nM (data not shown). The drawdown of such iron concentration by *E. huxleyi* in the control



is within the error range of our dFe measurement, thus dFe uptake by the cells, might not have been evident. On the other hand, biomass can increase, and cells can still be iron limited. In this case, limited cells show slower net growth rates than Fe-replete cells (Sunda & Huntsman 1995), in full agreement with our results.

Fe availability often limits primary productivity in open-ocean waters and in some coastal upwelling regions (de Baar & Boyd 2000), but Fe limitation in fjord environments is less common (Öztürk et al. 2002). Fe bioavailability depends not only on dissolved Fe concentrations, but also on Fe speciation. Although *E. huxleyi* net growth rates were higher in the LC than in the HC treatments, high biomass values in LC were not sustained at *in situ* dFe concentrations (i.e. -DFB treatment). It could be argued that the positive effect of the DFB addition on the biomass of *E. huxleyi* is due to DFB's ability to buffer high concentrations of toxic metals in the fjord. A previous study in the Raunefjord documented the production of strong organic ligands for copper (Cu) by *Synechococcus* sp. after a rain event that resulted in significant input of dissolved Cu (dCu) levels from ~7 nM to 16 nM (Muller et al. 2005). During our experiment, dCu concentrations were typical of this fjord, not excessively high, and did not change throughout the experiment (~7-9 nM, Chapter 5). Given the low affinity of DFB for divalent metals, it is unlikely that the DFB addition affected Cu speciation or any other divalent metal, such as Zn.

The only mesocosm treatment where *E. huxleyi* did not dominate the phytoplankton community was in the HC-DFB treatment. DFB was added in 17.5-fold excess to the fjord dFe concentration, therefore we assume that all dFe was complexed to DFB. Our results suggest that *E. huxleyi* is able to utilise DFB-bound Fe (FeDFB). Indeed, *E. huxleyi* has been shown to produce organic complexes with high affinity for Fe (Boye & Van den Berg 2000) and to be able to acquire Fe from organic Fe complexes (Hartnett et al. 2012), including Fe-DFB (Shaked & Lis 2012, Lis et al. 2015). Most likely, *E. huxleyi* was able to access Fe bound to DFB by



means of a reductive pathway (Maldonado & Price 2001), one of the most prevalent Fe acquisition mechanisms in phytoplankton. The fact that *E. huxleyi* biomass in the HC treatments was significantly higher in presence than in the absence of DFB further suggests that the cells were able to cope better with the unfavourable effects of ocean acidification when they were not simultaneously Fe limited. The negative effects OA has on calcifying algae is caused by external acidification reducing the  $[H^+]$  electrochemical gradient, impairing the cellular passive  $[H^+]$  outflow that is a by-product of the calcification process (Taylor et al. 2012). In addition, maintaining a constant intracellular pH is energetically costly and OA likely affect the cellular energy demands (Taylor et al. 2012). Metabolism drives traits that determine fitness, growth and survival of populations (Dell et al. 2011), thus increased dFe during our experiment may have helped the cells to meet the extra metabolic demands imposed by the decrease in pH, allowing them to sustain growth.

*Synechococcus* sp. was also negatively affected by increased pCO<sub>2</sub> leading to reduced net growth and biomass in the HC treatment during phase 2 of this experiment in agreement with Paulino et al. (2008), but in contrast to another study from the Raunefjord locality (Larsen pers. comm.). The estimated Fe demand for *Synechococcus* sp. net growth was ~2 pM, well below the dFe concentrations in the control (LC-DFB). This suggests that Fe concentration did not influence the net growth of *Synechococcus* sp. and niche differences in *Cyanobacteria* Fe-metabolism are well documented (Desai et al. 2015). The harmful pCO<sub>2</sub> effects on this species are not well understood; though it has been hypothesised that high pCO<sub>2</sub> might decrease photosynthetic efficiency and light saturation constants or affect nutrient availability or competition with other taxa (Mackey et al. 2015), being perhaps more sensitive to grazing pressure. Therefore, we do not know at present whether the increased pCO<sub>2</sub> effects on *Synechococcus* sp. are indirect.





The consequences of the interactive effects of pCO<sub>2</sub> and Fe availability on *E. huxleyi* can be critical to C-cycling and marine ecosystems. Within the future predicted climate scenario for coastal ecosystems, particulate and/or colloidal iron might become more solubilized by lower pH (Sunda & Huntsman 1995, Breithbarth et al. 2010), by natural organic ligands, and/or by increased ultraviolet radiation, which mediates photo-solubilisation (Kuma et al. 1996, Hassler & Schoeman 2009). Given the variability of responses to increased pCO<sub>2</sub> observed in *E. huxleyi* (Hutchings 2011, Riebesell & Tortell 2011, Meyer & Riebesell 2015) some strains that are held-back by iron limitation might become more abundant, gaining a competitive advantage through their low stringent requirements for nutrients and high growth under photoinhibitory conditions (Paasche 2002) at increased Fe availability. According to the results shown here, the deleterious effect of OA on the development of *E. huxleyi* blooms will be more relevant in high Fe environments than in Fe-limited ones. The loss of C production of *E. huxleyi* (estimated as the areas below the curves in Figure 2.3a) due to OA was ~92 % in enhanced Fe availability conditions, and ~70 % in ambient Fe conditions. The potential benefit of higher Fe availability in an acidified ocean will be overridden by the decrease in pH itself. However, increased dFe by DFB in high-pCO<sub>2</sub>-seawater enhanced *E. huxleyi* C production by ~60%. Fe-favoured strains of *E. huxleyi* could outcompete other phytoplankton and influence the counterbalance between the carbonate pump and the organic carbon pump (i.e. the rain ratio, RR) (Rost & Riebesell 2004). RR is the ratio of particulate inorganic to organic carbon in exported biogenic matter (calcite:POC or PIC:POC), which is used as a proxy for calcification vs. photosynthesis (Hutchings 2011). In our experiment, RRs were significantly higher in LC than in HC treatments (average 0.9 vs. 0.4 respectively, Table 2.1) in close agreement with a wide number of experiments (Meyer & Riebesell 2015). Furthermore, Fe limitation has been shown to decrease PIC:POC ratios (Muggli & Harrison 1996) and CaCO<sub>3</sub> production rates (Schulz et al. 2004) in cultures of *E. huxleyi*, while the opposite



has been shown under P and N limitation (Paasche 2002). PIC: POC in our study increased significantly (c.a. 4-fold) during phase 2 in LC+DFB relative to all other treatments (Chapter 3), implying that the increase in dFe enhanced calcification, in agreement with a former study (Muggli & Harrison 1996). Sustained growth and possibly calcification under future increased pCO<sub>2</sub> levels might be mediated by strains that are favoured by high-dFe. If so, the PIC ballast effect in surface oceans (Sanders et al. 2010) would not be affected (calcite saturation state above 1, as shown in Table 2.1) and the downward POC flux would continue and directly influence the RR.

In summary, this study demonstrates that Fe concentrations may control phytoplankton community structure in coastal ecosystems and that ocean acidification can enhance Fe bioavailability. This is contrary to the idea that Fe is rarely limiting in fjord and/or estuarine environments, and that OA might decrease or does not change Fe availability depending on the organic ligands present. Moreover, as previously reported, *E. huxleyi* might be negatively affected in a near future scenario by increased pCO<sub>2</sub> levels. However, our study indicates that some *E. huxleyi* strains might have higher Fe requirements than initially thought. Thus, in areas with high total Fe concentrations (particulate and dissolved Fe), the detrimental effects of increased pCO<sub>2</sub> on these strains can be partially mitigated by enhanced dFe, possibly inducing cascading effects on food web dynamics, carbon export, and the rain ratio, finally affecting the exchange of CO<sub>2</sub> across the ocean-atmosphere interface. The interactive effects of pCO<sub>2</sub> and Fe observed in our mesocosm study highlight the importance of examining multiple stressors simultaneously combined in natural communities. Investigating how multiple drivers, competition, acclimation and adaptation interact at longer experimental times and affect natural plankton communities is essential to better predict how marine ecosystems will respond to future changes.





### Acknowledgements

This work was funded by CTM/MAR 2010-17216 research grant from the Spanish Ministry for Science and Innovation (Spain) to MS. MRL and CI were funded by FPU grants from the Ministry for Education (Spain). MAM and JAF were supported by Grant no. 228224, Transnational Access, from the EU FP7-INFRA-2008-1 MESOAQUA (Network of leading MESOCosm facilities to advance the studies of future AQUATIC ecosystems from the Arctic to the Mediterranean). AL was supported by the EU-ERC grant 250254 (MINOS) and the RCN project no. 225956/E10 (MicroPolar: Processes and Players in Arctic Marine Pelagic Food Webs – Biogeochemistry, Environment and Climate Change). We thank Jay T Cullen for hosting MRL to analyse dFe at his laboratory, Iole di Capua for counting mesozooplankton, and the Spanish Institute for Oceanography (IEO-Fuengirola, Málaga) for silicic acid analyses. We also thank Jens C Nejtgaard and Hans H Jakobsen for discussions and suggestions, and the MBS staff for logistic support.



## Supplemental Information

### Methods

#### Total iron analyses (tFe)

Total iron concentration consists of both dissolved and particulate iron pools (dFe and PFe). Methodology for dFe analyses is described in M&M section in the main document. For particulate iron analyses (PFe) seawater samples (1-3.5 L) were gently filtered onto 0.45  $\mu\text{m}$  Supor<sup>®</sup>-450 filters. Filters were precleaned with 10% trace metal hydrochloric acid (Fisher, trace metal grade) at 60°C overnight, rinsed with Milli-Q water, dried and stored until further analysis. Filters were digested in 7 mL acid-washed Teflon vials (Teflon, Rochester, NY, USA) (pre-cleaned with 10% trace metal hydrochloric acid and nitric acid -trace metal grade- at 70 °C during 2-3 days each step). Samples were digested in 3 mL of HNO<sub>3</sub> and 0.5 mL of HF (Fisher, trace metal grade) for 1 h at 200 °C in closed vials and HF was evaporated afterwards at the same conditions. One-and-a-half mL of HNO<sub>3</sub> was to the samples and incubated at 150 °C overnight. Samples were then mixed with 2.25 mL of HClO<sub>4</sub> (Fisher, Optima grade) and heated for 4 h at 200 °C. After complete digestion, samples were evaporated at 200°C until dry, dissolved in 1% HNO<sub>3</sub> with 1 ppb indium as internal standard, and analyzed by using a high-resolution inductively coupled plasma-mass spectrometer (HR-ICPMS, Element XR, Thermo Scientific). Filter blanks were subjected to the same process than samples and blank values were subtracted from sample measurements. Trace metal clean techniques were used throughout all the process when collecting and manipulating samples for both dissolved and particulate metals analyses.

#### Inorganic and organic nutrients

Inorganic nutrient concentrations were analysed in a QuAatro AQ2 AACE autoanalyser (Seal Analytical Ltd, Fareham, UK) following the methods described by Grashoff et al. (1983). Fifty ml water samples from each mesocosm were





collected every other day, filtered through 0.7 µm GF filters (Millipore) and immediately frozen at - 20°C until analysis. The detection limits of the inorganic nutrients were 0.03 µM for nitrates, 0.01 µM for nitrites, 0.02 µM for phosphates, 0.05 µM for silicic acid and 0.06 µM for ammonia. Dissolved organic carbon (DOC) and nitrogen (DON) were analysed from 50 ml water samples, collected every other day, filtered through 0.2 µm cellulose acetate filters (Whatman) and stored in acid washed and precombusted glass bottles at 4°C in darkness until analysis. DOC and total dissolved nitrogen (TDN) were measured in a Shimadzu TOC-L analyser equipped with a total nitrogen module (TNM-1) coupled to it. Dissolved organic nitrogen (DON) was calculated by subtracting the total inorganic nitrogen fraction from the TDN.

## Supplementary Tables

**Table 2.1S.** Fe demand was calculated for each group to meet their Fe quotas at the highest cell numbers reached during the experiment and transformed into biomass. We assumed Fe: C ratios (µmol:mol) published for *E. huxleyi* grown at the same irradiance at that of the mesocosms sampling depth (150-200 µmol m<sup>-2</sup> s<sup>-1</sup>) (Muggli & Harrison 1996), diatoms (Sarhou et al. 2005), *Synechococcus* sp. and Prasinophytes (Quigg et al. 2010), picoeukaryotes (Timmermans et al. 2005), dinoflagellates and Haptophytes (Marchetti & Maldonado 2016). Data are averages of replicate mesocosms and standard deviations are shown in brackets.

Iron demand (nM)	
<i>Emiliana huxleyi</i> (5-10 µm)	10.14 (1.7)
<i>Synechococcus</i> sp. (0.6-2 µm)	2.40 x 10 <sup>-03</sup> (1.58 x 10 <sup>-10</sup> )
Picoeukaryotes (0.1-2 µm)	1.47 x 10 <sup>-03</sup> (4.7 x 10 <sup>-07</sup> )
Dinoflagellates (30-75µm)	9.60 x 10 <sup>-07</sup> (7.33 x 10 <sup>-11</sup> )
Small nanoeukaryotes (2-7 µm)	2.74 x 10 <sup>-02</sup> (8.6 x 10 <sup>-03</sup> )
Big nanoeukaryotes (6-20 µm)	2.13 x 10 <sup>-02</sup> (6.4 x 10 <sup>-03</sup> )
Long chain diatoms (>30 µm)	1.80 x 10 <sup>-06</sup> (2.5 x 10 <sup>-07</sup> )

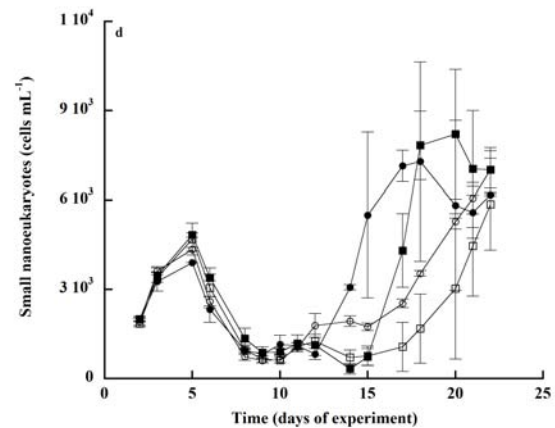
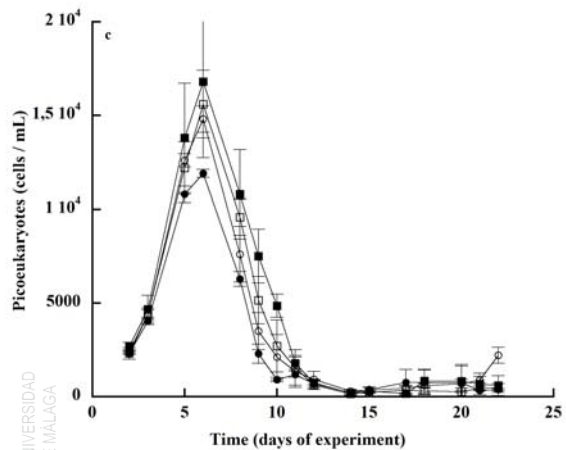
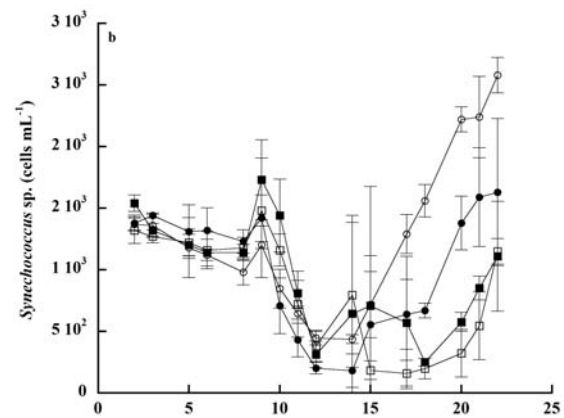
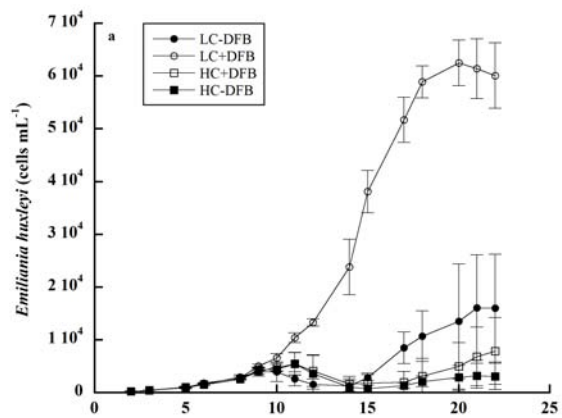


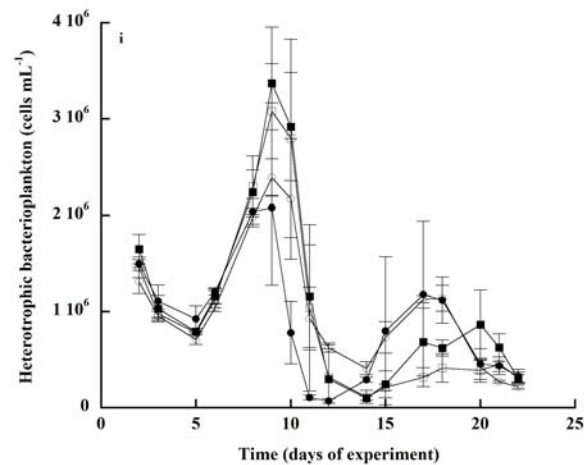
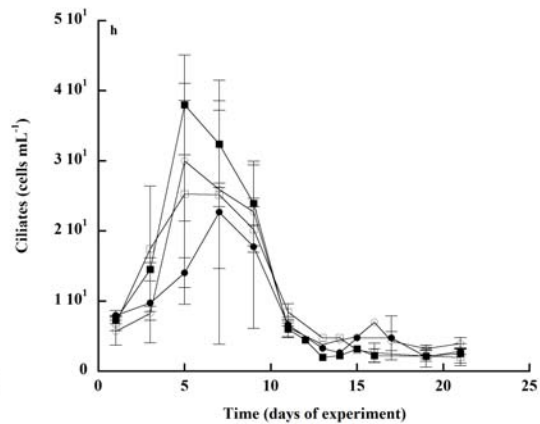
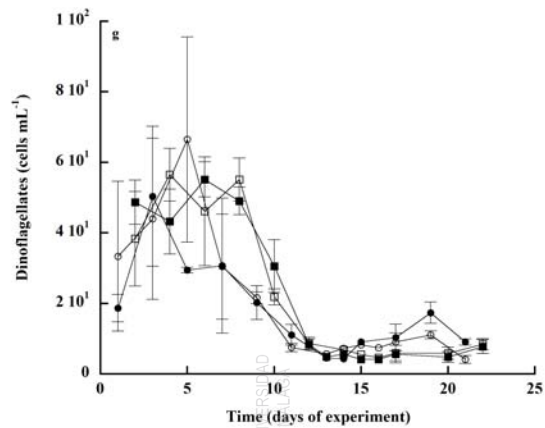
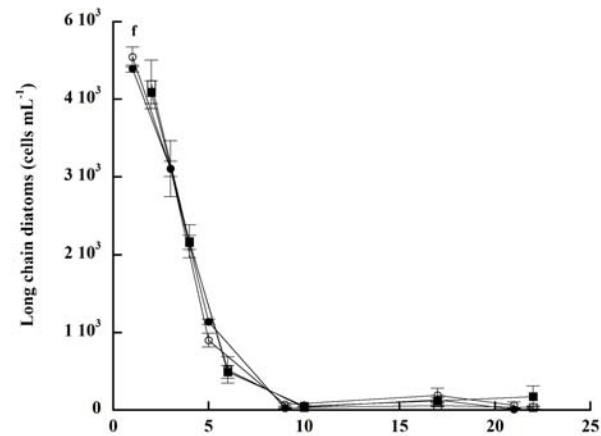
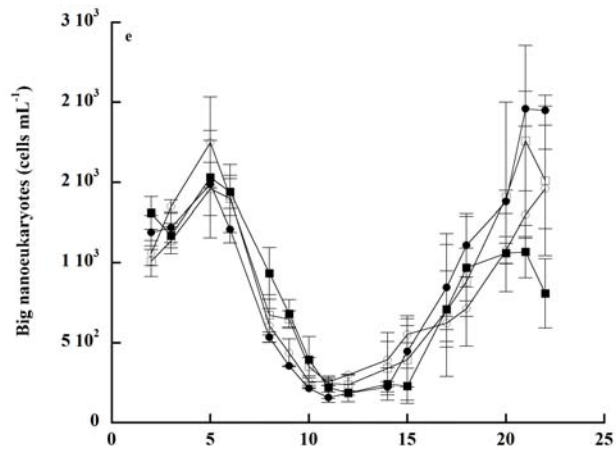
**Table 2.2S.** Fold change in particulate and dissolved iron between days 12 and 21 under the different treatments; LC: ambient CO<sub>2</sub> (390 μatm); HC: increased CO<sub>2</sub> (900 μatm); -DFB (ambient dFe); +DFB (increased dFe). Note that DFB was added on day 7. Data are means of three independent mesocosm bags ± standard deviation (in brackets), except for LC-DFB treatment in which n=2.

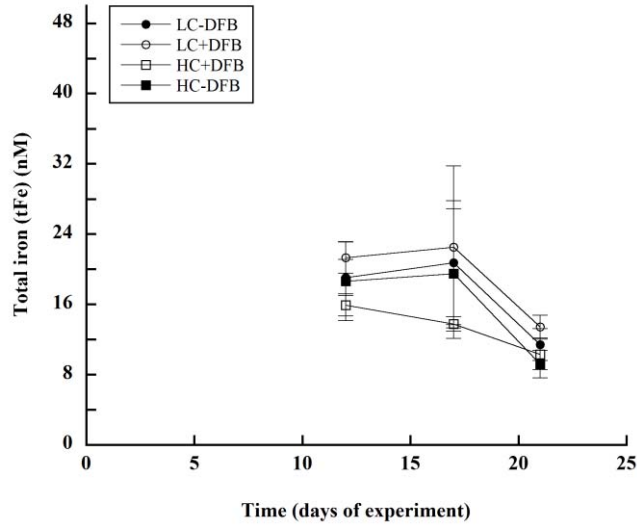
Treatment	Particulate Fe (PFe)	Dissolved Fe (dFe)
LC-DFB	-7.69 (2.01)	0.06 (1.87)
LC+DFB	-12.23 (1.81)	4.35 (1.28)
HC+DFB	-6.76 (0.52)	1.13 (2.07)
HC-DFB	-7.98 (4.59)	2.71 (0.58)

## Supplementary Figures

**Supplementary Figure 2.1S.** Temporal development of phytoplankton, microzooplankton and heterotrophic bacterioplankton (cells mL<sup>-1</sup>) within the mesocosms in the different treatments. Ambient pCO<sub>2</sub> and ambient dFe (LC-DFB, black filled circle); ambient pCO<sub>2</sub> and increased dFe (LC+DFB, open circle); increased pCO<sub>2</sub> and increased dFe (HC+DFB, open square), increased pCO<sub>2</sub> and ambient dFe (HC-DFB, black filled square). Symbols indicate means of measurements in three independent mesocosms (n=3) except for LC-DFB where n=2. Error bars indicate standard deviations. (a) *Emiliania huxleyi* (5-10 μm); (b) *Synechococcus* sp., (0.6-2 μm); (c) picoeukaryotes (0.1-2 μm); (d) small nanoeukaryotes (Prasinophytes, small Haptophytes, 2-7 μm); (e) big nanoeukaryotes (small single celled diatoms and flagellated forms, 6-20 μm); (f) Diatoms (chain forming *Skeletonema*, 20->500 μm); (g) Dinoflagellates (20-200 μm); (h) Ciliates (20-200 μm); (i) heterotrophic bacterioplankton (0.2-0.7 μm).

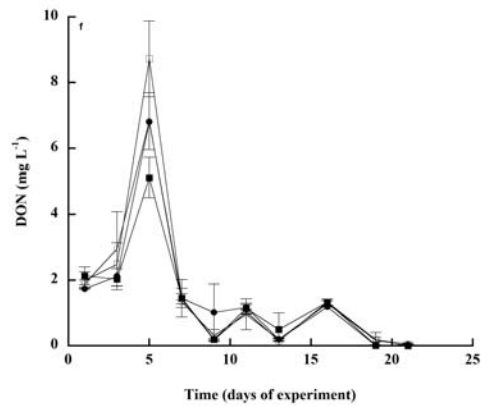
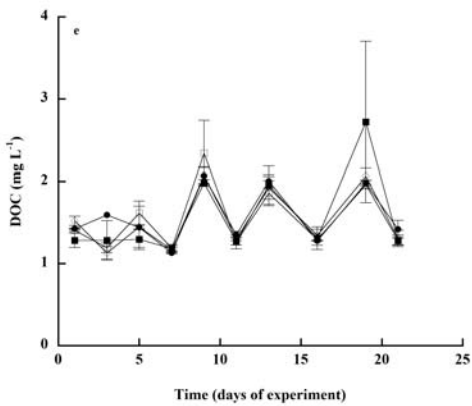
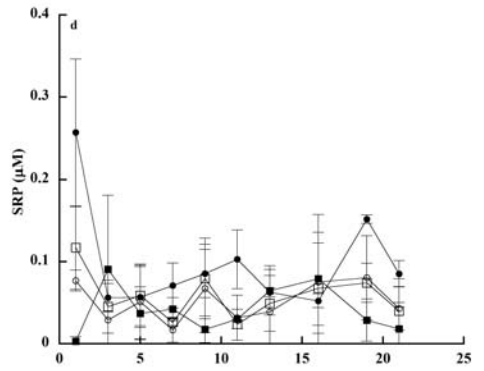
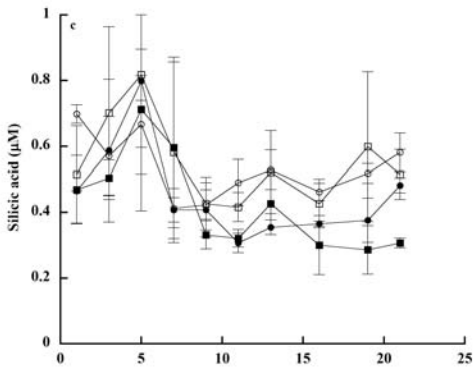
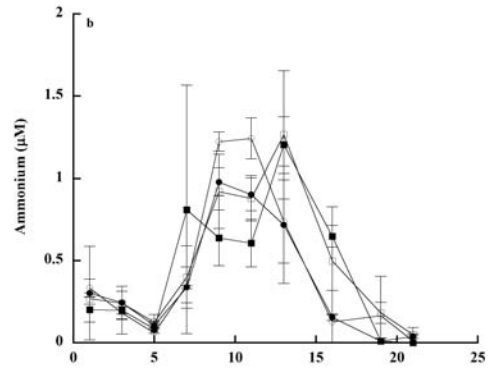
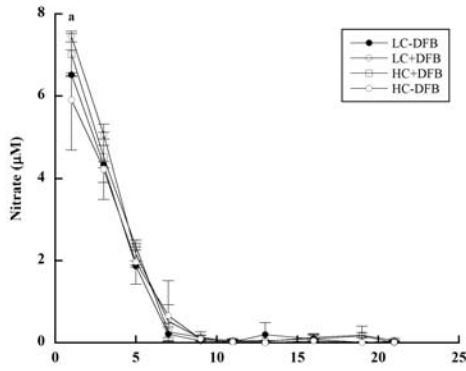






**Supplementary Figure 2.2S.** Temporal development of total iron (tFe) concentrations within the mesocosms in the different treatments. Ambient pCO<sub>2</sub> and ambient dFe (LC-DFB, black filled circle); ambient pCO<sub>2</sub> and increased dFe (LC+DFB, open circle); increased pCO<sub>2</sub> and increased dFe (HC+DFB, open square), increased pCO<sub>2</sub> and ambient dFe (HC-DFB, black filled square). Symbols indicate means of measurements in three independent mesocosms (n=3) except for LC-DFB where n=2. Error bars indicate standard deviations.

**Supplementary Figure 2.3S.** Temporal development of major nutrient concentrations within the mesocosms in the different treatments. Ambient pCO<sub>2</sub> and ambient dFe (LC-DFB, black filled circle); ambient pCO<sub>2</sub> and increased dFe (LC+DFB, open circle); increased pCO<sub>2</sub> and increased dFe (HC+DFB, open square), increased pCO<sub>2</sub> and ambient dFe (HC-DFB, black filled square). Symbols indicate means of measurements in three independent mesocosms (n=3) except for LC-DFB where n=2. Error bars indicate standard deviations.



## Chapter 3

# **Effects of increased CO<sub>2</sub> and iron availability on the carbon assimilation and calcification during an *Emiliana huxleyi* bloom**

M Rosario Lorenzo\*, Concepción Iñiguez, Jorun K Egge, Aud Larsen,  
Stella A Berger, Candela García-Gómez, María Segovia

*Manuscript for submission*

## Abstract

The potential interactive effects of ocean acidification and iron availability on phytoplankton ecophysiological processes are still unknown. We conducted an *in situ* mesocosm experiment to investigate the single and combined effects of increased CO<sub>2</sub> and iron availability on photosynthetic carbon assimilation processes including acquisition and fixation, and calcification during a bloom of the coccolithophore *Emiliana huxleyi*. Phytoplankton cellular stoichiometry (C:N ratio), a key factor in biogeochemical cycling of nutrients, was also included in our study. We observed that inorganic carbon (C<sub>i</sub>) acquisition was unaffected by CO<sub>2</sub> and iron availability and that the main inorganic carbon source used was HCO<sub>3</sub><sup>-</sup>. Carbon fixation instead was negatively affected by high CO<sub>2</sub> levels whereas increased iron availability promoted highest values of carbon fixation and calcification under present CO<sub>2</sub> conditions. Although C<sub>i</sub> acquisition was unaffected by CO<sub>2</sub> and iron, the different treatments had an effect on C<sub>i</sub> accumulation as shown by particulate organic matter (POM) concentrations showing the same response as carbon fixation rates. The accumulation ratio of POC to PON was significantly different between treatments showing an imbalance between CO<sub>2</sub> assimilation caused by the nutrient depletion. The differences observed in carbon fixation were due to the negative impact of increased CO<sub>2</sub> in *E. huxleyi*. Such main effect was more significant than positive effects of increased Fe availability. Thus, our results suggest that ocean acidification might decrease inorganic carbon mineralisation and organic carbon production under iron-replete conditions affecting the biological carbon pump and biogeochemical processes in coastal ecosystems.

**Key words:** Ocean acidification, dissolved iron, desferoxamine-B, calcification, carbon concentrating mechanisms, carbon fixation, primary productivity, elemental composition, stoichiometry, mesocosm experiment, *Emiliana huxleyi*





## Introduction

Oceans have absorbed one-third of the CO<sub>2</sub> released into the atmosphere as a result of anthropogenic activities, producing a decrease in pH of 0.1 since preindustrial times and changes in the dissolved inorganic carbon (C<sub>i</sub>) equilibrium due to CO<sub>2</sub> dissolution in seawater (ocean acidification, OA) (IPCC 2013). Additionally, the atmospheric CO<sub>2</sub> concentration is expected to reach more than 900 μatm by 2100 and pH to decrease from 8.1 to 7.8 (IPCC 2013). Thus, HCO<sub>3</sub><sup>-</sup> concentrations will increase by 17% and CO<sub>3</sub><sup>2-</sup> concentrations will be reduced by 50%, altering the calcium carbonate saturation state (Doney et al. 2009). OA is then expected to have direct impacts on photosynthesis, calcification and elemental composition of marine phytoplankton, leading to changes in phytoplankton communities (Riebesell & Tortell 2011, Mackey et al. 2015).

Marine phytoplankton contributes to half of the world's total primary productivity, sustaining marine food webs and driving the biogeochemical cycles of carbon (C) and nutrients (Field 1998). The responses of phytoplankton to a changing environment are essential to understand future variations in marine ecosystems. The effect of elevated pCO<sub>2</sub> levels on photosynthesis and growth is species-specific; some species benefit, while others show no response or even inhibition within future scenarios (reviewed in Riebesell & Tortell 2011, Mackey et al. 2015). The sensitivity of phytoplankton to increased pCO<sub>2</sub> seems to be related to the mode of C<sub>i</sub> acquisition and most species are able to regulate such carbon acquisition by means of CO<sub>2</sub> concentrating mechanisms (CCMs) (Beardall & Giordano 2002, Rost et al. 2003, Giordano et al. 2005). CCMs act increasing the efficiency of net C fixation by concentrating CO<sub>2</sub> in the vicinity of Rubisco, suppressing the oxygenase activity and saturating the carboxylase activity (Beardall & Raven 2004). The efficiency and regulation of CCM differs among phytoplankton species and functional groups (Colman et al. 2002, Giordano et al. 2005).



Changing carbonate chemistry in seawater due to decrease in pH is likely to affect calcification rates of calcifying organisms. Coccolithophores are one of the most important groups of calcifiers in today's oceans producing calcium carbonate plates (coccoliths), and accounting for 1–10% to marine primary production. Furthermore, coccolithophores contribute with ~50% to the pelagic  $\text{CaCO}_3$  deposition in sediments in parallel with particulate organic carbon (POC) export to the deep ocean (called the ballast effect) (Paasche 2002). The best-studied coccolithophorid is *Emiliana huxleyi*, which plays a fundamental role in the dynamics of marine food webs and  $\text{CO}_2$  sequestration. Marine biogenic calcification ( $\text{CaCO}_3$  formation) is known to decay with decreasing seawater pH in different strains of coccolithophores (Riebesell & Tortell 2011; Rokitta & Rost 2012). However, no changes in calcification or in the ratio of  $\text{CaCO}_3$  to organic matter production (PIC:POC) at elevated  $p\text{CO}_2$ , as well as stimulating effects of OA on calcification have also been reported (Iglesias-Rodriguez et al. 2008, Langer et al. 2009, Rickaby et al. 2010); possibly due to differences in experimental design or data normalization (Riebesell et al. 2008, Field et al. 2011).

The elemental composition of phytoplankton could be affected by future high  $\text{CO}_2$  conditions, because the increase in  $\text{CO}_2$  levels has the potential to change the cycling of important elements (Hutchins et al. 2009). The interaction between changes in  $\text{CO}_2$  and other physicochemical factors could influence the biological effects of ocean acidification (Boyd & Hutchins 2012, Boyd et al. 2015). The bioavailability of trace metals is affected by changing carbonate chemistry, which affects pH-sensitive coordination chemistry with the trace metals (Millero et al. 2009). Among them, Fe is an essential trace element for phytoplankton growth due to its key role in metabolic processes such as photosynthesis, respiration and N-assimilation (Behrenfeld & Milligan 2013). Importantly, its availability is regulated by changes in pH (Millero et al. 2009, Shi et al. 2010). At elevated  $\text{CO}_2$  conditions, the Fe-availability depends on many factors including dissolved Fe concentrations, Fe speciation, organic ligands and their interactions (Sunda 2010,





Shaked & Lis 2012, Chapter 2). Despite that phytoplankton production in the oceans is often limited by nitrogen and/or Fe (Saito et al. 2008); little is known concerning the effect of CO<sub>2</sub> on phytoplankton ecophysiology under changes in Fe availability. The response to increased CO<sub>2</sub> in the elemental composition and primary production obtained depended on the sensitivity of each phytoplankton community to changes in Fe availability (Hoppe et al. 2013, Sugie et al. 2013, Yoshimura et al. 2013, 2014).

To unravel the single and interactive effects of increased pCO<sub>2</sub> and Fe availability on the mechanisms of carbon assimilation and calcification, an *Emiliania huxleyi* bloom was induced in a mesocosm experiment. The aim of the present study was to analyse (i) whether increased CO<sub>2</sub> and Fe availability changes the preference of the C<sub>i</sub> source and the mechanisms involved in inorganic carbon acquisition within the phytoplankton community; (ii) whether carbon fixation and calcification are affected under different Fe and CO<sub>2</sub> levels; and (iii) whether variations in carbon assimilation and /or calcification explains the shifts observed in the phytoplankton community during the experiment. This experimental study provides new insights on the knowledge of carbon metabolism within a coastal phytoplankton community exposed to future environmental scenarios.



## Materials and methods

### Experimental set-up

The experimental work was carried out in June 2012 in the Raunefjord, off Bergen, Norway, as described in detail in Chapter 2. Briefly, 12 polyethylene mesocosms ( $\sim 11 \text{ m}^3$ ) covered by lids (both transparent to PAR and UVR) were filled with fjord water from 8 m depth and manipulated to achieve two different  $\text{CO}_2$  levels corresponding to the present (390 ppm, LC) and to levels predicted for year 2100 (900 ppm, HC). Specific  $\text{CO}_2$  concentrations, as well as  $\text{CO}_2$  inlet flows in all the mesocosms, were measured by non-dispersive infrared analysis by using a Li-Cor (LI-820)  $\text{CO}_2$  gas analyser (Li-COR, Nebraska, USA) and  $\text{CO}_2$  AirSense-310 sensors (Digital Control Systems, Inc, USA).  $\text{CO}_2$  concentration in the mesocosms was calculated from pH and total alkalinity measurements using the  $\text{CO}_2$  SYS software (Robbins et al. 2010). Iron was manipulated by addition of the siderophore desferrioxamine B (DFB) on day 7 to promote two different Fe conditions (+DFB, high dissolved iron; and -DFB, ambient dissolved Fe). Dissolved Fe concentration increased  $\sim 3$ -fold with respect to the control as a result of both factors manipulation. The multifactorial, experimental design comprised triplicate mesocosms per treatment and the combinations of high and ambient  $\text{pCO}_2$  and dFe levels resulting in a total of 12 mesocosms: 3x LC-DFB (control), 3x LC+DFB, 3x HC+DFB and 3x HC-DFB. Nitrate ( $10 \mu\text{M}$ ) and phosphate ( $0.3 \mu\text{M}$  final concentrations) were added once at the beginning of the experiment to induce a bloom of the coccolithophorid *Emiliana huxleyi*.

### Isotope disequilibrium

The isotope disequilibrium assay (ID) was used to determine the relative fraction of  $\text{HCO}_3^-$  and  $\text{CO}_2$  uptake in concentrated cell suspensions of the phytoplankton community according to the method described in detail in Elzenga et al. (2000); Martin & Tortell (2006) and Tortell et al. (2008). Briefly, short-term cellular  $^{14}\text{C}$  accumulation was monitored during a transient disequilibrium between  $^{14}\text{CO}_2$  and





H<sup>14</sup>CO<sub>3</sub><sup>-</sup> in solution. Following the addition of a <sup>14</sup>CO<sub>2</sub>-rich spike (pH 7) to cell suspensions at pH 8.5, the specific activity of CO<sub>2</sub> is initially high, decaying exponentially to an equilibrium value, whereas the specific activity of H<sup>14</sup>CO<sub>3</sub><sup>-</sup> / <sup>14</sup>CO<sub>3</sub><sup>-2</sup> remains nearly constant during the experiment. Therefore, the time course of <sup>14</sup>C accumulation reflects the specific activity of CO<sub>2</sub> and HCO<sub>3</sub><sup>-</sup>. Cells that transport only HCO<sub>3</sub><sup>-</sup> should exhibit a linear time course of <sup>14</sup>C accumulation, assuming a constant rate of <sup>14</sup>C fixation. Contrary, cells that transport only CO<sub>2</sub> should exhibit a negative slope curve, because rates of <sup>14</sup>C uptake will be high initially and decrease over time.

Samples (0.5-3 L) were concentrated by gentle filtration under low pressure on 0.8 μm, 47-mm polycarbonate membranes to a final volume of 20-30 mL at the same fjord temperature in a temperature controlled room. Chlorophyll *a* (Chl *a*) content in the concentrates was measured by extraction in 90% acetone overnight and determined fluorometrically using a Turner fluorometer 10-AU (Turner BioSystems, CA, USA). Final Chl *a* concentration in cell concentrates ranged from 0.2 to 400 μg L<sup>-1</sup>. During the filtration procedure, cells were kept in suspension, while the medium was gradually exchanged with pH 8.5 fjord water buffered with 20 mM Bicine. Concentrated cell suspensions (4 mL sub-sample) were transferred into a 20-mL glass cuvette, acclimated for 15 min to 150-μmol photons m<sup>-2</sup> s<sup>-1</sup> at 11 °C in a custom-made transparent Plexiglas® container, and 20 μCi <sup>14</sup>C spike pH 7.0 in 50 mM HEPES was injected. Two hundred μL subsamples were withdrawn at short intervals (between 5 s and 10 min) and dispensed into 1 mL of 50% HCl to stop C fixation and remove unassimilated inorganic carbon. Experiments were carried out in the presence and absence of the membrane-impermeable carbon anhydrase (CA) inhibitor dextra-bound sulphanilamide (DBS, Ramidus AB, Sweden) to examine the role of extracellular CA (eCA). The inhibitor was added to a final concentration of 100 μM at least 15 min prior to the assays.

For quantitative interpretation, <sup>14</sup>C disequilibrium data were fitted according to the equations presented in Martin & Tortell (2006) using a Marqand-

Levenberg non-linear regression algorithm in SigmaPlot 11 (Systat Software, Chicago, USA). Two physiological parameters were obtained: the fraction of  $\text{HCO}_3^-$  uptake ( $f$   $\text{HCO}_3^-$ ) and the rate of extracellular  $\text{CO}_2$ : $\text{HCO}_3^-$  interconversion ( $\alpha'$ ). The fraction of  $\text{HCO}_3^-$  uptake,  $f$ , is the fraction of photosynthetically fixed C derived from  $\text{HCO}_3^-$  and the relative eCA activity is estimated by a catalytic enhancement factor, which is defined as  $(\alpha':\alpha)$ , where  $\alpha'$  is obtained in control experiments and  $\alpha$  is the uncatalyzed thermodynamic rate (obtained in the inhibitor treatment). The results are expressed as catalytic enhancement factors (in the inhibitor treatment). Thus, a catalytic enhancement factor of 1 indicates no detectable eCA activity.

### Carbon fixation rates

Carbon fixation rates were estimated by using *in-vitro* short-term  $^{14}\text{C}$  uptake assays of concentrated cell suspensions according to Steemann-Nielsen (1952). 0.5–3 L of seawater were pre-concentrated in 20–30 ml as mentioned above. All incubations were carried out in 20-ml glass vials in a custom-made transparent plexiglas container, continuously homogenized by a magnetic stirrer at ambient fjord conditions (10–11 °C and 150  $\mu\text{mol photons m}^{-2} \text{ s}^{-1}$  provided by white light LED-lamps). Prior to the addition of  $\text{H}^{14}\text{CO}_3^-$ , samples were pre-acclimated for 15 min to the above-mentioned conditions, thereafter inoculated with 10  $\mu\text{Ci H}^{14}\text{CO}_3^-$  (final concentration) and incubated for 30 min. Dark controls were run under the same conditions. After incubation, 4N HCl was added to stop the reaction and to remove excess  $\text{DI}^{14}\text{C}$ . Samples were transferred to 20 ml scintillation vials and left open in the fume hood over night to remove excess  $\text{DI}^{14}\text{C}$ . The scintillation cocktail (Ultima Gold, Perkin Elmer, USA) was added and the radioactivity of each sample was measured using a Packard Tri Carb Liquid Scintillation Analyser, model 1900 A (Perkin Elmer, USA).



### **Particulate Matter**

Total particulate carbon (TPC) and particulate organic nitrogen (PON) were measured on a C:H:N elemental analyser (Perkin-Elmer 2400 CHN) from 0.5-1 L samples gently filtered onto pre-combusted (12 h, 500 °C) and dried at 65 °C GF/F filters (Whatman). For determination of particulate organic carbon (POC), filters were fumed with saturated HCl. Particulate inorganic carbon (PIC) was assessed as the difference between TPC and POC. Water samples (0.15-0.5 L) were filtered gently onto 0.8µm polycarbonate filters, in triplicates, for analysis of particulate Ca. Dry filters was measured by wavelength dispersive X-ray fluorescence (WDXRF) (S4 Pioneer, Bruker-AXS, Karlsruhe, Germany) according to Paulino et al. (2013).

### **Statistical analyses**

Data were checked for normality (by Shapiro-Wilks' test), homoscedasticity (by Levene's test) and sphericity (by Mauchly's test). All data met the requirements to perform parametric tests. Statistical significance of treatment effects was carried out using Split-Plot ANOVA followed by post-hoc Sidak and Bonferroni tests (considering  $p < 0.05$  as significant). All analyses were performed using the General Linear Model (GLM) procedure with main effects, time (repeated measure) and interaction terms. Some of the data were specifically tested for significance of differences ( $p < 0.05$ ) promoted by the treatments using ANCOVA. Statistical analyses were carried out using SPSS v22 (IBM statistics) and the Systat statistical package included in Sigmaplot 12 (Systat Software, Chicago, USA).



## Results

Most of the variables analysed in this study followed a general trend that showed no effects of treatments (CO<sub>2</sub> and DFB) during the first 10 days (phase 1) of the experiment, but that responded to the treatments during the last 12 days (phase 2) (see Chapter 2 for details on the plankton community behaviour).

### HCO<sub>3</sub><sup>-</sup> was the main C<sub>i</sub> source and was not affected by Fe and pCO<sub>2</sub>

The fraction of HCO<sub>3</sub><sup>-</sup> uptake ( $f\text{HCO}_3^-$ ) derived from <sup>14</sup>C accumulation curves is presented in Table 3.1 for control experiments without DBS addition (a), and for the DBS treated experiments (b). The results point out that HCO<sub>3</sub><sup>-</sup> was the major source of inorganic C uptake for photosynthesis in all treatments over time as indicated by  $f\text{HCO}_3^-$  values obtained for the control. The average  $f\text{HCO}_3^-$  was  $0.88 \pm 0.03$  suggesting that ~90% of fixed C was derived from extracellular HCO<sub>3</sub><sup>-</sup>. The values of  $f\text{HCO}_3^-$  in DBS-treated cells were slightly lower and ranged from 0.81 to 0.91 with an average of  $0.85 \pm 0.03$ . Neither in the control nor the DBS treated assays did we observe significant differences in  $f\text{HCO}_3^-$  between treatments (Table 3.1). There were no significant differences between treatments during the experiment in  $f\text{HCO}_3^-$  of the control or the DBS treated assays (Table 3.1). Model fits to the time course of <sup>14</sup>C accumulation showed slight differences between the control and DBS-treated samples in the HC treatments, presented as increased curvature in the presence of the eCA inhibitor. Both curves (with and without DBS) were clearly significantly different from the theoretical uptake curve based only on CO<sub>2</sub> incorporation. This difference between curves supported that direct HCO<sub>3</sub><sup>-</sup> transport accounted for the majority of C uptake by the phytoplankton assemblage for all treatments (Figure 3.1).



**Table 3.1.** Carbon uptake parameters derived from isotope disequilibrium (ID) results in all treatments: Ambient pCO<sub>2</sub> and ambient dFe (LC-DFB); ambient pCO<sub>2</sub> and increased dFe (LC+DFB); increased pCO<sub>2</sub> and increased dFe (HC+DFB), increased pCO<sub>2</sub> and ambient dFe (HC-DFB).  $f\text{HCO}_3^-$  is the fraction of total C uptake attributable to uptake HCO<sub>3</sub><sup>-</sup> in the presence of the membrane-impermeable carbon anhydrase (CA) inhibitor dextran-bound sulphanilamide (DBS) (a) and in the control without DBS (b), while  $\alpha' : \alpha$  is the relative external carbonic anhydrase (eCA) activity estimated by a catalytic enhancement factor (c), where  $\alpha'$  is obtained in control experiments (without the inhibitor treatment) and  $\alpha$  is the uncatalyzed thermodynamic rate ( $\alpha=0.0019$ ). Values are the mean of three independent mesocosms  $\pm$  standard deviation (SD), except for LC-DFB treatment in which n=2.

**a)  $f\text{HCO}_3^-$  (control)**

Days	LC-DFB	LC+DFB	HC+DFB	HC-DFB
3	0.86 (0.02)	0.88 (0.05)	0.86 (0.00)	0.87 (0.02)
9	0.91 (0.02)	0.94 (0.03)	0.91 (0.04)	0.91 (0.02)
14	0.88 (0.00)	0.87 (0.01)	0.89 (0.02)	0.86 (0.05)
19	0.84 (0.00)	0.86 (0.00)	0.91 (0.04)	0.85 (0.01)

**b)  $f\text{HCO}_3^-$  (DBS-treatment)**

Days	LC-DFB	LC+DFB	HC+DFB	HC-DFB
3	0.91 (0.00)	0.87 (0.04)	0.85 (0.02)	0.84 (0.005)
9	0.91 (0.02)	0.87 (0.04)	0.88 (0.04)	0.85 (0.05)
14	0.84 (0.07)	0.83 (0.01)	0.87 (0.02)	0.82 (0.00)
19	0.85 (0.00)	0.83 (0.01)	0.88 (0.02)	0.81 (0.00)

**c) eCA catalytic enhancement ( $\alpha' : \alpha$ )**

Days	LC-DFB	LC+DFB	HC+DFB	HC-DFB
3	3.82 (0.46)	5.62 (1.55)	3.99 (2.15)	1.91 (0.47)
9	1.00 (0.00)	1.00 (0.00)	1.00 (0.00)	2.11 (0.41)
14	1.15 (0.21)	1.00 (0.00)	1.60 (0.28)	1.88 (0.38)
19	1.33 (0.36)	1.65 (0.48)	1.42 (0.07)	1.76 (0.10)



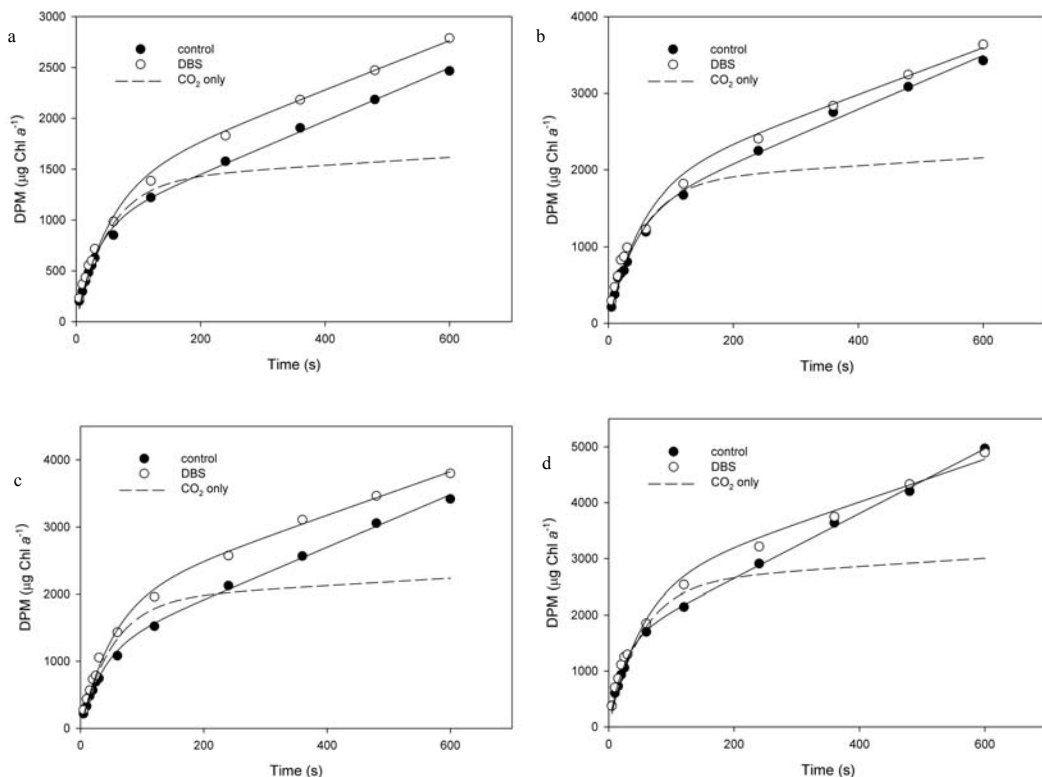


**Figure 3.1.** Results of isotope disequilibrium experiments from the different treatments at the end of the experiment. a) Ambient  $p\text{CO}_2$  and ambient dFe (LC-DFB); b) ambient  $p\text{CO}_2$  and increased dFe (LC+DFB); c) increased  $p\text{CO}_2$  and increased dFe (HC+DFB); d) increased  $p\text{CO}_2$  and ambient dFe (HC-DFB). Open symbols represent samples treated with the membrane-impermeable carbon anhydrase (CA) inhibitor dextran-bound sulphanilamide (DBS), and closed symbols represent the control without DBS. The dashed line indicates the theoretical uptake curve for phytoplankton that only incorporates  $\text{CO}_2$  (i.e.  $f=0$ ). DPM corresponds to disintegrations per minute.

### eCA activity shifted with the bloom

$^{14}\text{C}$  fixation data were also used to estimate extracellular carbonic anhydrase activity. The estimations of eCA activity derived from curve fits of the  $^{14}\text{C}$  time course data are presented in Table 3.2. The highest eCA activity was obtained at the beginning of the experiment (4-fold higher than uncatalyzed rates of  $\text{HCO}_3^-/\text{CO}_2$  interconversion,  $\alpha'$ ). In contrast, the lowest  $\alpha'$  values were obtained at the end of the experiment (similar to uncatalyzed rates of  $\text{HCO}_3^-/\text{CO}_2$  interconversion,



thus giving a catalytic enhancement factor of 1), indicating a very low or even non-existent eCA activity (Table 3.2). These differences of eCA values varied significantly different over time. Figure 3.2 shows how the presence of eCA activity could change the <sup>14</sup>C time course accumulation transforming <sup>14</sup>C accumulation data from LC+DFB treatment at the beginning of the experiment. The <sup>14</sup>C time course curves were transformed into instantaneous rates (DPM s<sup>-1</sup>) by calculating the slope of <sup>14</sup>C activity between successive measurement time points as explained in Tortell & Morel (2002) and Tortell et al. (2008). In the control experiment, <sup>14</sup>C accumulation rates decreased more rapidly to a steady state value than in the DBS treatment, suggesting increased expression of extracellular carbonic anhydrase (eCA).

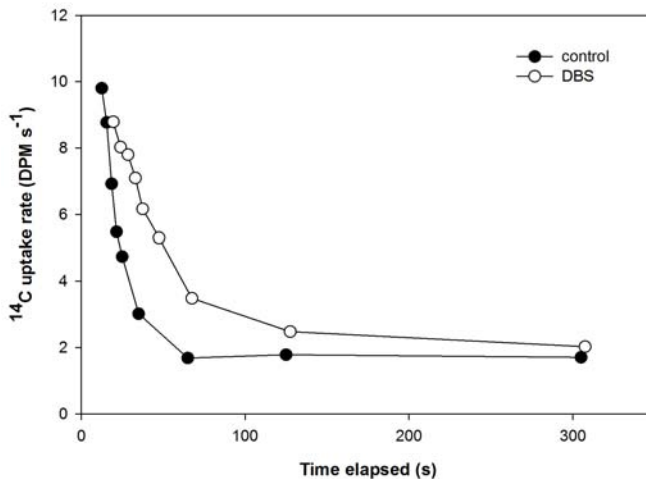


**Figure 3.2.** Instantaneous <sup>14</sup>C uptake curves for phytoplankton in LC+DFB treatment on day 3, showing an enhancement of <sup>14</sup>C equilibration in control experiments compared to DBS-treated experiments. Open symbols represent samples treated with the membrane-impermeable carbon anhydrase (CA) inhibitor dextran-bound sulphanilamide (DBS), and closed symbols represent the control without DBS.

### Increased Fe concentrations enhanced carbon fixation rates in ambient pCO<sub>2</sub>

Carbon fixation rates as measured per volume ( $\mu\text{g C L}^{-1} \text{h}^{-1}$ ) decreased to low levels in all treatments during phase 1 (Figure 3.3a). In phase 2, carbon fixation increased significantly 8-fold in LC+DFB treatments until day 16 (compared to the rest of the treatments) before decreasing by approximately 50%. Carbon fixation rate remained low in all other treatments, with the exception of the control (LC-DFB) in which a temporary peak in carbon fixation was observed on day 19. We observed significant differences during the entire time course due to changes in CO<sub>2</sub>, dFe and the interaction of both factors. Carbon fixation rates measured per Chl *a* ( $\mu\text{g C } \mu\text{g Chl } a^{-1} \text{h}^{-1}$ ) showed a tendency of higher production in LC+DFB during the second half of the experiment (Figure 3.3b). This trend is visible from day 14 with significant differences between LC-DFB vs. LC+DFB and LC+DFB vs. HC+DFB from day 16 onward (Figure 3.3b).

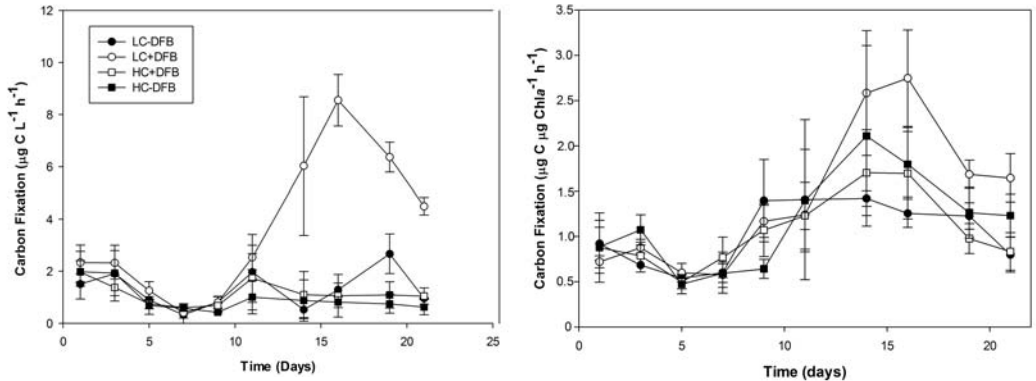


**Figure 3.3.** Temporal development of (a) carbon fixation per volume ( $\mu\text{g C } \mu\text{g Chl } a^{-1} \text{h}^{-1}$ ) and (b) carbon fixation per Chl *a* ( $\mu\text{g C } \mu\text{g Chl } a^{-1} \text{h}^{-1}$ ) in the different treatments. Ambient pCO<sub>2</sub> and ambient dFe (LC-DFB, ●); ambient pCO<sub>2</sub> and increased dFe (LC+DFB, ○); increased pCO<sub>2</sub> and increased dFe (HC+DFB, □), increased pCO<sub>2</sub> and ambient dFe (HC-DFB, ■). Symbols indicate the mean of measurements in three independent mesocosms (n=3) except for LC-DFB where n=2. Error bars indicate standard deviations.



### Organic and inorganic carbon production decreased in high pCO<sub>2</sub>

Particulate matter (PON, POC, PIC, and Ca) concentrations showed no differences during phase 1. In the second phase, we observed a significant negative effect of CO<sub>2</sub>- on PON and POC concentrations (Figure 3.4, Table 3.3). PON concentrations were significant higher in LC than in HC treatments. POC responded significantly positive to DFB addition in LC treatments but not in HC treatments (Figure 3.4, Table 3.3). Thus, there was a significant interactive effect of the CO<sub>2</sub>- and DFB-treatments on the variables. Initial PIC concentrations were undetectable in all treatments. At the end of the experiment, PIC showed an increase of 4-fold in LC+DFB vs. LC-DFB, 20-fold vs. HC+DFB, and 35-fold increase with respect to HC-DFB. PIC was 7-fold higher in the control (LC-DFB) than in the HC treatments and showed significant differences due to both factors and their interaction (Figure 3.4).

**Table 3.2.** Elemental ratio of particulate organic carbon to nitrogen (POC:PON in mol:mol) in all treatments: Ambient pCO<sub>2</sub> and ambient dFe (LC-DFB); ambient pCO<sub>2</sub> and increased dFe (LC+DFB); increased pCO<sub>2</sub> and increased dFe (HC+DFB), increased pCO<sub>2</sub> and ambient dFe (HC-DFB). Values are the mean of three independent mesocosms ± standard deviation (SD), except for LC-DFB treatment in which n=2. Different letters represent significant differences between treatments within each day (2-Way ANOVA followed by post-hoc Tukey test, considering p<0.05 as significant).

Days	LC-DFB	LC+DFB	HC+DFB	HC-DFB
3	8.69 (0.44) <sup>a</sup>	8.36 (0.26) <sup>a</sup>	7.73 (0.11) <sup>b</sup>	7.68 (0.27) <sup>b</sup>
7	7.85 (0.62) <sup>a</sup>	7.45 (0.11) <sup>a</sup>	7.84 (0.48) <sup>a</sup>	7.54 (0.06) <sup>a</sup>
11	8.63 (0.76) <sup>a</sup>	8.72 (0.25) <sup>ab</sup>	8.25 (0.22) <sup>b</sup>	8.49 (0.31) <sup>b</sup>
16	9.95 (0.35) <sup>a</sup>	11.82 (0.26) <sup>b</sup>	9.73 (0.96) <sup>a</sup>	8.51 (0.73) <sup>a</sup>
21	13.75 (0.79) <sup>a</sup>	16.13 (0.36) <sup>b</sup>	11.26 (0.48) <sup>c</sup>	12.18 (0.30) <sup>c</sup>

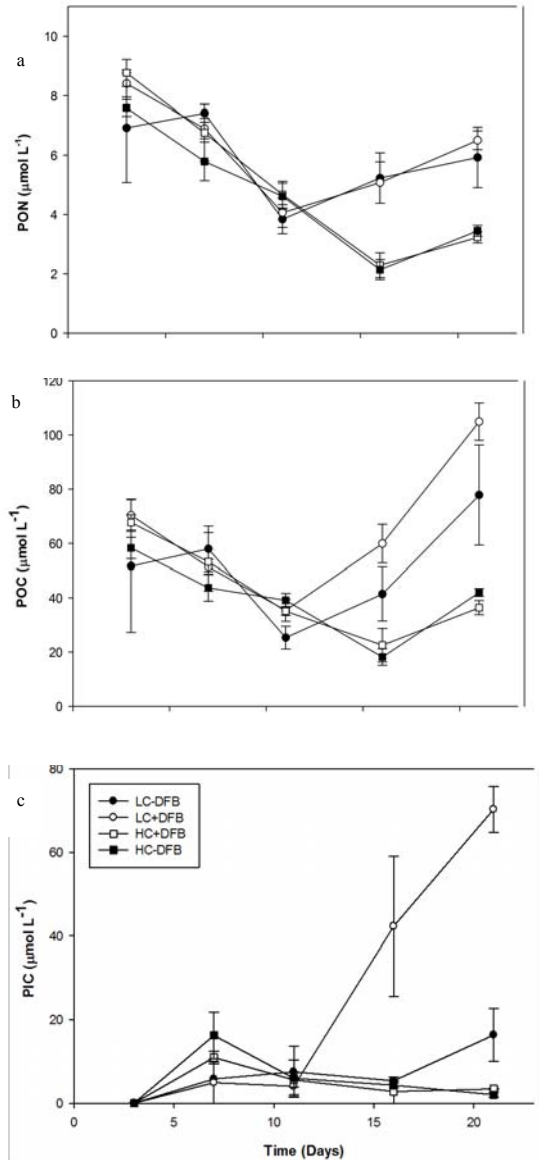


**Figure 3.4.** Temporal development of particulate organic nitrogen (a), particulate organic carbon (b) and inorganic carbon (c) concentrations ( $\mu\text{mol L}^{-1}$ ) during the experiment in the different treatments: ambient  $\text{pCO}_2$  and ambient dFe (LC-DFB, ●); ambient  $\text{pCO}_2$  and increased dFe (LC+DFB, ○); increased  $\text{pCO}_2$  and increased dFe (HC+DFB, □), increased  $\text{pCO}_2$  and ambient dFe (HC-DFB, ■). Symbols indicate means of measurements in three independent mesocosms ( $n=3$ ) except for LC-DFB where  $n=2$ . Error bars indicate standard deviations.



The POC:PON ratio significantly decreased with increasing pCO<sub>2</sub> (independent of DFB addition) and was positively affected by dFe (Table 3.2). In order to determine the effect of the treatments on POM net production during phase 2, ΔPOC and ΔPON were calculated for each treatment by subtracting the concentrations on day 11 from the result obtained at the end of the experiment. Calculated ΔPOC and ΔPON in phase 2 were significantly higher in LC than in HC treatments (p<0.001). Similarly, the ratio ΔPOC:ΔPON was significantly affected by CO<sub>2</sub> (p<0.001) and the slopes of regressions for HC and LC were significantly different (ANCOVA, p=0.037, data not shown).

Changes in PIC/POC ratios (indicators for calcification) were driven by changes in POC values in all treatments (Figure 3.5). However, there were also changes due to variations in PIC in LC+DFB for which the highest values were obtained (average PIC/POC was 0.7). Thus PIC/POC was affected by both CO<sub>2</sub>, DFB, their interaction and over time. When calcification was assessed as particulate Ca per POC (comprising the particulate calcium in attached and detached coccoliths and based on day-to-day pairs of Ca and C determinations), the Ca/POC ratio showed differences due to the treatments during phase 2 with highest values (an increase of 5~folds per day) measured in LC+DFB treatment (Figure 3.5). In agreement with particulate Ca concentration (Supplemental Figure 3.S2), Ca/POC ratio was higher in LC+DFB treatment and showed a linear increase over time. At the end of the experiment, HC treatments resulted in the lowest ratios (~0.06) compared to the control (~4-fold higher) and LC+DFB (~10-fold higher) with the same significant differences as PIC/POC ratio (Table 3.3).

Furthermore, changes in TPC, POC and Ca concentration were assessed as POM net production during the dominance of *Emiliana huxleyi* in each treatment considering for the LC+DFB treatment the period between day 11 and 21 and for the other treatments the period between day 16 and 21 (when *E. huxleyi* dominates or presented higher cell concentration).



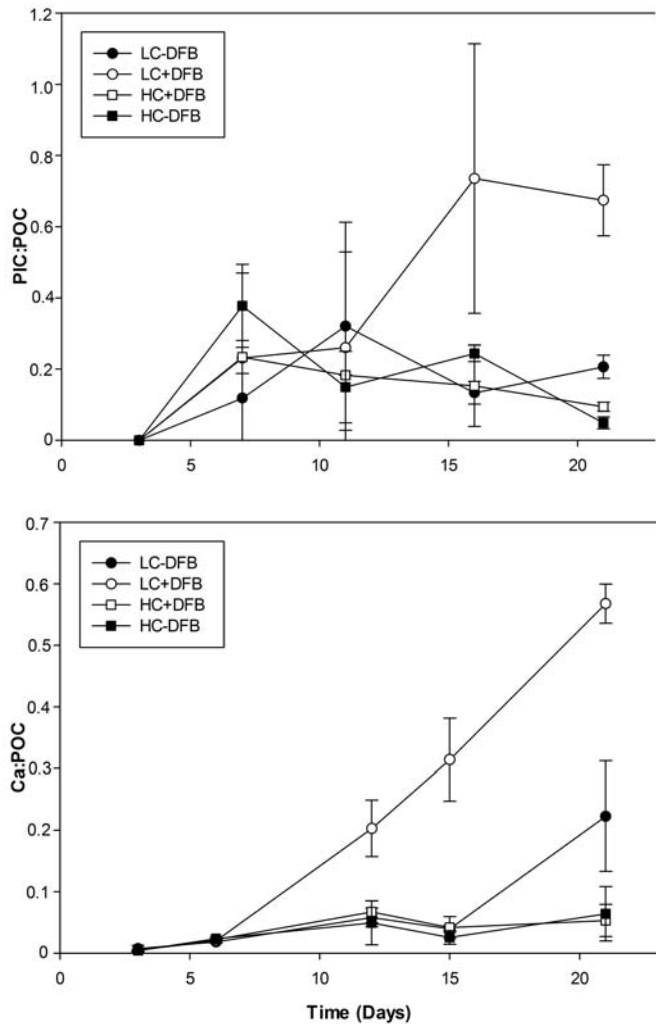


**Figure 3.5.** Temporal development of molar inorganic C:organic C (a) and molar Ca:organic C ratios (b) in all the treatments during the experiment. Ambient  $pCO_2$  and ambient dFe (LC-DFB, ●); ambient  $pCO_2$  and increased dFe (LC+DFB, ○); increased  $pCO_2$  and increased dFe (HC+DFB, □), increased  $pCO_2$  and ambient dFe (HC-DFB, ■). Symbols indicate means of measurements in three independent mesocosms ( $n=3$ ) except for LC-DFB where  $n=2$ . Error bars indicate standard deviations.



TPC production showed significant differences due to carbon, DFB and the interaction of both factors. The lowest values were observed for HC treatments. For the LC treatments, the mean rate of the control (LC-DFB) was  $9.43 \pm 5.26 \mu\text{mol L}^{-1} \text{d}^{-1}$  and for the LC+DFB treatment  $13.22 \pm 0.71 \mu\text{mol L}^{-1} \text{d}^{-1}$ . The mean of Ca production was similar in HC conditions, but increased in LC +DFB and control conditions, respectively. Ca production presented significant difference due to both factors and the interaction. POC production only showed differences due to CO<sub>2</sub> main factor ( $p < 0.05$ ).

**Table 3.3.** Statistical analyses (Split-Plot ANOVA followed by post-hoc Sidak) of the effects of CO<sub>2</sub>, DFB, and their interaction, on the variables analysed during the development of a bloom of the coccolithophore *Emiliana huxleyi* in the different treatments.

	CO <sub>2</sub>	DFB	Interaction	Time
<i>f</i> HCO <sub>3</sub> <sup>-</sup> (control)	0.827	0.08	0.953	0.310
<i>f</i> HCO <sub>3</sub> <sup>-</sup> (DBS-treatment)	0.246	0.635	0.026	0.078
eCA catalytic enhancement	0.659	0.282	0.435	<0.001
Carbon fixation- per Volume	<0.001	<0.001	0.001	<0.001
Carbon fixation- per Chl <i>a</i> content	0.298	0.255	0.053	<0.001
PON concentration	0.007	0.006	0.262	<0.001
POC concentration	<0.001	0.001	0.002	0.039
PIC concentration	<0.001	<0.001	<0.001	<0.001
POC:PON ratio	<0.001	0.182	0.012	0.001
PIC:POC ratio	<0.001	<0.001	<0.001	<0.001
Ca:POC ratio	<0.001	0.001	0.001	<0.001

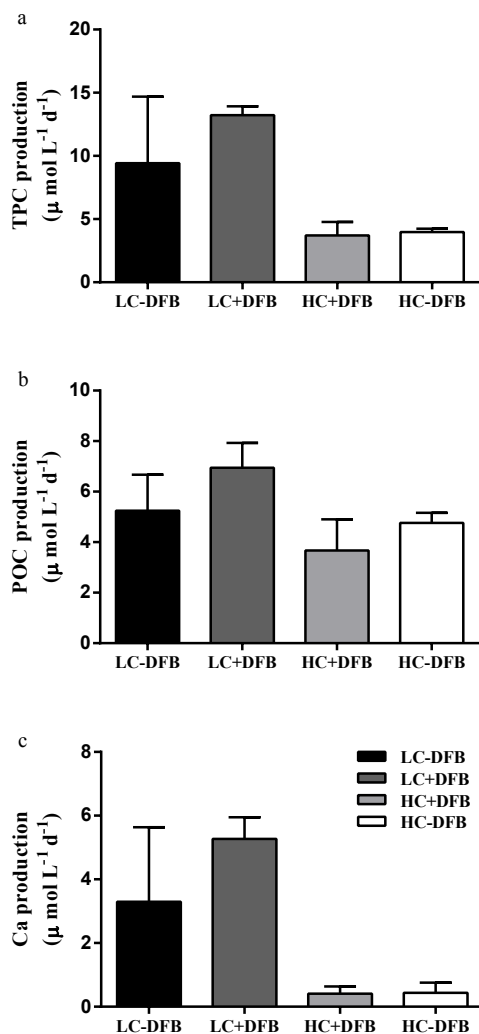


**Figure 3.6.** Total particulate carbon (TPC) production during *E. huxleyi* dominance between d16 and d21, except for LC+DFB treatment from d11 until d21 (a); organic carbon (POC) production (b); and particulate calcium (Ca) production (c) for the different treatments: ambient  $\text{pCO}_2$  and ambient dFe (LC-DFB, black); ambient  $\text{pCO}_2$  and increased dFe (LC+DFB, dark gray); increased  $\text{pCO}_2$  and increased dFe (HC+DFB, light shading), increased  $\text{pCO}_2$  and ambient dFe (HC-DFB, white). Data correspond to means of measurements in three independent mesocosms ( $n=3$ ) except for LC-DFB where  $n=2$ . Error bars indicate standard deviations.



## Discussion

Our mesocosm experiment demonstrated that carbon cycling processes are affected by changes in Fe availability and CO<sub>2</sub> concentration during a mesocosm experiment. During this experiment, a phytoplankton bloom dominated by the coccolithophorid *Emiliana huxleyi* occurred in the treatment with ambient CO<sub>2</sub> and increased dFe (LC+DFB). In addition to the CO<sub>2</sub> and Fe manipulation, nutrients (nitrate and phosphate) were added to the mesocosms at the beginning of the experiment to promote the growth of *Emiliana huxleyi*. The increased Fe availability showed a positive effect on carbon assimilation, incorporation and fixation, and calcification processes. This is in agreement with the results obtained in Chapter 2, suggesting that the cells were Fe-limited in the control (LC-DFB).

Rising global CO<sub>2</sub> is changing the carbonate chemistry of seawater (IPCC 2013). Since increased CO<sub>2</sub> concentrations are known to affect several carbon assimilation processes (Mackey et al. 2015) it can be expected that the photosynthetic inorganic carbon uptake and the membrane-bound extracellular CA (eCA) activity from phytoplankton will also be influenced. The major source of inorganic carbon uptake by photosynthetic C fixation in the present experiment was HCO<sub>3</sub><sup>-</sup>, which is the common carbon source in many phytoplankton communities in a variety of oceanic regions (Tortell et al. 2010). Our data are in agreement with previous studies showing that *E. huxleyi* had moderate affinities for C<sub>i</sub> and that HCO<sub>3</sub><sup>-</sup> appeared as the primary C<sub>i</sub> source (Herfort et al. 2003, Rokitta & Rost 2012, Stojkovic et al. 2013). Changes in Fe availability and primary productivity in natural phytoplankton assemblages do not seem to influence HCO<sub>3</sub><sup>-</sup> utilisation nor do changes in pCO<sub>2</sub> in laboratory cultures or natural communities (Cassar et al. 2004, Martin & Tortell 2006, Tortell et al. 2010, 2013). Our results congruently show that the different communities that developed during the experiment constitutively expressed HCO<sub>3</sub><sup>-</sup> transporters without differences between treatments (Table 3.2). This apparent insensitivity to increased CO<sub>2</sub> of HCO<sub>3</sub><sup>-</sup> uptake affinity obtained may derive from instantaneous pH effects



(Kottmeier et al. 2014), because of the measurements are performed under stabilized pH conditions that often do not mimic environmental situations but constitutively express  $\text{HCO}_3^-$  transporters. The presence of  $\text{HCO}_3^-$  transporters can indicate the capacity of phytoplankton to directly use  $\text{HCO}_3^-$  when  $\text{CO}_2$  becomes limiting under blooming conditions, when pH values increase up to 8.5 or higher than natural levels (Kottmeier et al. 2014).

The isotope disequilibrium results also allowed us to estimate the eCA-catalyzed enhancement of  $\text{HCO}_3^-$ - $\text{CO}_2$ . Highest levels of eCA activity were found when long chain-forming diatoms were most abundant (days 0 to 10, phase 1), contributing to elevated biomasses at the beginning of the experiment (Supplemental Figure 3.S1). However, there was low or inexistent eCA activity when *E. huxleyi* dominated the community at the end of the experiment (days 11-22, phase 2). The low eCA levels indicate the dominance of direct  $\text{HCO}_3^-$  transport as a mode of inorganic C uptake (accounting for ~85% of total inorganic C uptake). The low eCA activity showed by *E. huxleyi* and the  $\text{HCO}_3^-$  utilisation suggest an important role of bicarbonate transporters that could be strain-specific. The discovery of *E. huxleyi* pangenome (Read et al. 2013) explains the different metabolic-response repertoires observed depending on the environmental conditions (e.g.  $\text{CO}_2$  and Fe). Even though the genome analysis shows that *E. huxleyi* has nine putative CAs, none of them have been identified as external ones and, gene expression data indicate that the up-regulation of these genes occur at  $\text{CO}_2$  concentrations below those currently experienced (380 and 900 ppm) (Bach et al. 2013). Yet, the core genome of *E. huxleyi* contains low-affinity DIC transporters (Read et al. 2013). Comparing the molecular data with the high  $\text{HCO}_3^-$  uptake capacity and eCA expression observed in our physiological assays, our results indicate the physiological potential of this *E. huxleyi* strain to maintain efficient inorganic C acquisition under blooming conditions.

Neither  $\text{HCO}_3^-$  transport nor eCA activity was related to the partial pressure of  $\text{CO}_2$  ( $p\text{CO}_2$ ) as shown previously (Tortell et al. 2010). Tortell et al. (2013) suggest





a higher and potentially CO<sub>2</sub>-dependent activity for intracellular CA, which acts dehydrating HCO<sub>3</sub><sup>-</sup> to deliver CO<sub>2</sub> at the site of C fixation by Rubisco. In addition, the observed lack of CO<sub>2</sub>-dependent regulation of eCA during phase 1 could be explained by interspecific differences in the CO<sub>2</sub>-dependent regulation of inorganic C uptake in diatoms (Rost et al. 2003, Trimborn et al. 2009). High eCA activity has been reported for diatoms compared to other groups of phytoplankton (nanoflagellates and haptophytes) in natural assemblages (Martin & Tortell 2006, Tortell et al. 2010). The differences in eCA activity observed during our experiment could be attributed to the differences in the taxonomic composition of the treatments (Table 3.2, Supplemental Figure 3S.1).

Although C<sub>i</sub> acquisition was unaffected by CO<sub>2</sub> and Fe, the different treatments did effect on C<sub>i</sub> accumulation as shown by particulate organic matter (POM) concentrations (Figure 3.4, Table 3.1) and carbon fixation rates (Table 3.3) showing the same trend that the development of the bloom (Figure 3.2, Supplemental Figure 3S.1). Increased Fe availability at ambient CO<sub>2</sub> concentration (LC+DFB) enhanced carbon fixation and promoted the *E. huxleyi* bloom. In contrast, the carbon fixation rates were similar and lower in HC treatments and in the control (LC-DFB) (Figure 3.4). In accordance, elevated CO<sub>2</sub> did not have any effect on carbon fixation rates in previous mesocosm experiments carried out in the same fjord (Delille et al. 2005, Egge et al. 2009). However, other studies presented different responses of primary production to high CO<sub>2</sub> such as an increase, a decrease or no response (Riebesell & Tortell 2011, Mackey et al. 2015). This chapter and chapter 2 suggested that the results obtained under ambient conditions (control) are due to *E. huxleyi* cells experiencing a constrained metabolism because Fe was limiting net growth rates and biomass increases. In such nutrient-limiting scenario, cells may down-regulate their maximum C fixation capacity. Thereby, there are no differences between control (LC-DFB) and HC treatments during the experiment until day 19 when the carbon fixation rate increase as well as POC concentrations (Figure 3.3 & 3.4) and the growth rate of *E.*



*huxleyi* (Chapter 2), following the trend of the treatment LC+DFB treatment. The carbon fixation rates obtained should approach to gross primary production since short incubations reflect the total cellular capacity for C fixation (gross primary production), while longer-term rates include a significant contribution of respiration and other C-loss processes (Tortell et al. 2010). Thus, the gross carbon fixation rates could not reflect the differences observed in POC concentrations between HC treatments and the control (LC-DFB treatment).

Organic matter (OM) dynamics are mainly driven by biological processes and ultimately reflected the dynamics of phytoplankton photosynthesis. Both POC and PON productions were significantly lower at high CO<sub>2</sub> levels compared to the ambient CO<sub>2</sub> conditions and the highest values were obtained in treatments with increased dFe (Figure 3.4 & 3.5). These changes in OM production were most likely related to shifts within the phytoplankton community (Supplemental Figure 3S.1) responding to diverse environmental conditions. On the other hand, an alternative and/or concomitant explanation for the differences observed in POC production between LC and HC treatments could be that the phytoplankton physiology is affected. Cytoplasmic pH changes produced by perturbations in the cells' microenvironment by high pCO<sub>2</sub> (Suffrian et al. 2011, Flynn et al. 2012, Taylor et al. 2012) can alter key physiological processes in coccolithophores (Rokitta et al. 2012, Muller & Nisbet 2014, Holtz et al. 2015). While possible positive effects of increased Fe availability on aiding cells physiology in HC treatments were observed in *E. huxleyi* (Chapter 2), the negative impact of high pCO<sub>2</sub> might become more significant in organic carbon production (Figure 3.4). Moreover, organic carbon production has been shown to differ depending on Fe availability under high CO<sub>2</sub> conditions, e.g. increased CO<sub>2</sub> concentration had no influence on C production under Fe limiting conditions, whereas C production reached at high CO<sub>2</sub> levels with Fe enrichment (Feng et al. 2010, Hoppe et al. 2013). The difference in such responses could be attributed to environmental conditions, which strongly affect



phytoplankton community composition and metabolism (Richier et al. 2014, Yoshimura et al. 2014b).

In this study, the accumulation ratio of POC to PON was significantly different between treatments (Table 3.1) with differences also due to the interaction with Fe availability as previously shown (Yoshimura et al. 2014b) when the nutrients (nitrate, phosphate, silicic acid) were exhausted or at low concentrations. Nutrient depletion can cause an imbalance between CO<sub>2</sub> assimilation, changes in the stoichiometric composition and altered biogeochemical pathways through the microbial food web (Bellerby et al. 2008). The comparison between C assimilation relative to N uptake and the Redfield C:N ratio can indicate carbon overconsumption (Toggweiler 1993) and this imbalance in carbon and nitrogen assimilation has been related to nutrient limitation of the cell (Schartau et al. 2007). Elevated C:N of accumulated POM in N-limited conditions was also observed in response to high CO<sub>2</sub> in natural communities (Losh et al. 2012). In contrast, constant C:N of net produced POM among the different CO<sub>2</sub> conditions has been reported (Kim et al. 2006, Riebesell et al. 2007, Engel et al. 2008, Feng et al. 2010, Czerny et al. 2013), suggesting that phytoplankton communities presented constant C:N under nutrient-replete conditions and this ratio did not change significantly due to pCO<sub>2</sub> variations and Fe additions when the nutrients were not exhausted (Sugie et al. 2013a, Yoshimura et al. 2014). It has been attributed that increases in POC:PON ratios under nutrient deficiency is due to preferential PON degradation, intracellular increase of the C:N ratio or an excess of carbon fixation (Engel 2002, Taucher et al. 2012). Therefore, the ratios obtained could be due to excess in carbon fixation.

In accordance with the model proposed for *E. huxleyi* by Muller & Nisbet (2014) both net inorganic carbon and organic carbon productions were affected by ocean acidification (Figure 3.5). Coccolithophores are potentially affected by pH through effects on calcification and the physiological effects due to elevated CO<sub>2</sub> concentration (Bach et al. 2011). Additionally, we demonstrated that interactive



effects between  $\text{CO}_2$  and Fe directly affected calcification in *E. huxleyi* during the bloom development. It is important to consider the different phytoplankton groups and their biomass contribution present in each treatment with respect to *E. huxleyi* (Supplemental Figure 3S.1). The PIC:POC ratio reflected the ratio of carbon deposited in coccoliths to carbon converted to organic form by photosynthesis as Ca:POC ratio. Schulz et al. (2004) demonstrated that the growth and calcification rate of *E. huxleyi* were reduced under low Fe conditions. Comparing the results obtained in LC treatments between ambient (-DFB) and increased Fe concentrations (+DFB), a decrease in the growth rates was observed in -DFB in this experiment (Chapter 2). Such a decay also occurred in the PIC:POC and Ca:POC ratios, and Ca production (Figure 3.4 & 3.5). On the other hand, high  $\text{CO}_2$  affected calcification negatively by reducing the overall production of  $\text{CaCO}_3$  during the *E. huxleyi* bloom (Figure 3.5). The decrease in PIC:POC and Ca:POC ratios are attributed to a decrease in calcification, as well as an increase in organic carbon production but could also be due to the net specific growth rate of *E. huxleyi*. The growth rate dropped off with increased  $\text{CO}_2$  and increased in  $\text{CO}_2$  conditions and increased Fe and this decrease might have influenced differences in net PIC accumulation (Figure 3.4). Despite intraspecific variability, negative effects of OA on calcification and on the cellular ratios were observed for the dominant bloomer in our system, *E. huxleyi*, supportive of previous studies (Riebesell & Tortell 2011, Meyer & Riebesell 2015), even though some strains of *E. huxleyi* appear to be less sensitive to ocean acidification (Langer et al. 2009, Beaufort et al. 2011). Diminished calcification, and a decreased PIC/POC ratio, could lead to a negative feedback in atmospheric  $\text{CO}_2$  concentration (Zondervan et al. 2001). But it could affect the ballast effect (i.e. the strong correlations between the export fluxes of POC and mineral particles), affecting the transport of POC into the deep ocean and contributing with an increase of  $\text{CO}_2$  concentration counterbalancing the possible negative feedback. Therefore, our results are thus highly ecologically relevant in view of the current global changes.





### Concluding remarks

The results obtained in this study provide evidences that changes in CO<sub>2</sub> concentration and Fe availability affect carbon assimilation processes during an *Emiliania huxleyi* bloom. The low eCA activity showed by *E. huxleyi* and the HCO<sub>3</sub><sup>-</sup> utilisation (unaffected by CO<sub>2</sub> and Fe availability) suggest an important role of bicarbonate transporters, indicating the physiological potential of this *E. huxleyi* strain to maintain efficient carbon acquisition under blooming conditions. Thus, whereas carbon production was enhanced with the high Fe availability in ambient CO<sub>2</sub> (LC+DFB treatment) and however, the carbon accumulation was negatively affected by increased CO<sub>2</sub> either as inorganic or organic carbon production. Our study shows that CO<sub>2</sub> play a primary role controlling the net carbon production but the positive effect of increased Fe availability in increased CO<sub>2</sub> in a system dominated by *E. huxleyi*. The possible Fe positive effect was not fully determined because the community was not dominated by *E. huxleyi* in the HC-DFB treatment, and so the other species present (mainly big nanoeukaryotes, unaffected by high CO<sub>2</sub>) masked this effect. We suggest that the modulation of Fe availability under future CO<sub>2</sub> conditions could be relevant for different phytoplankton groups and influence biogeochemical cycles. In future global change scenarios, Fe supply and CO<sub>2</sub> concentration might change simultaneously (Boyd et al. 2015) thus, our results underline that the effects of ocean acidification on cell stoichiometry and carbon assimilation might differ when other stressors are included. Nevertheless, more studies are required to analyse responses of coccolithophores to multiple stressors within the marine ecosystem to be able to have a better understanding of the full consequences of global change.



### **Acknowledgments**

This work was funded by CTM/MAR 2010-17216 (PHYTOSTRESS) research grant from the Spanish Ministry for Science and Innovation (Spain) to MS. MRL and CI were funded by FPU grants from the Ministry for Education (Spain). SAB was supported by Grant no. 228224 from the EU FP7-INFRA-2008-1 MESOAQUA (Network of leading MESOcosm facilities to advance the studies of future AQUAtic ecosystems from the Arctic to the Mediterranean). We thank all the rest of the Phytostress team for collaboration and help. We thank Philippe Tortell for advice with the isotope disequilibrium technique and data processing. We also thank the Marine Biologic Station (MBS) staff for logistic support.

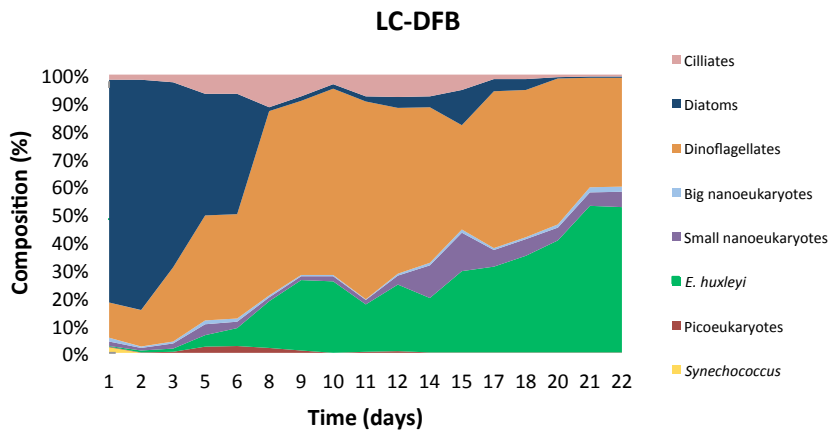


## Supplemental Material

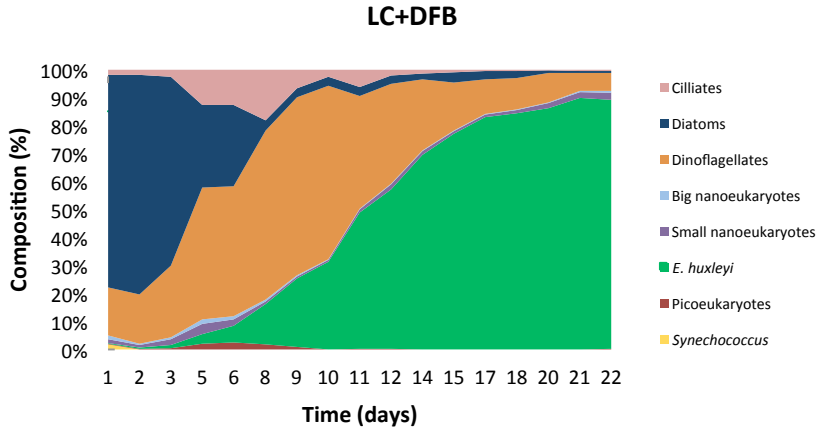
The seawater carbonate system in the mesocosms was manipulated to achieve two different CO<sub>2</sub> levels, corresponding to the present (390 μatm, LC) and to levels predicted for year 2100 (900 μatm, HC). The siderophore desferoxamine B (DFB) was added to half of the mesocosms (70 nM final concentration) to promote two different Fe conditions (+DFB and -DFB). Dissolved Fe (dFe) concentration increased ~3-fold with respect to the control as a result of both factors manipulation.

**Figure 3.1S.** Temporal development of phytoplankton and microplankton abundances (cells mL<sup>-1</sup>) in the different treatments during the experiment. Ambient pCO<sub>2</sub> and ambient dFe (LC-DFB); ambient pCO<sub>2</sub> and increased dFe (LC+DFB); increased pCO<sub>2</sub> and increased dFe (HC+DFB), increased pCO<sub>2</sub> and ambient dFe (HC-DFB).

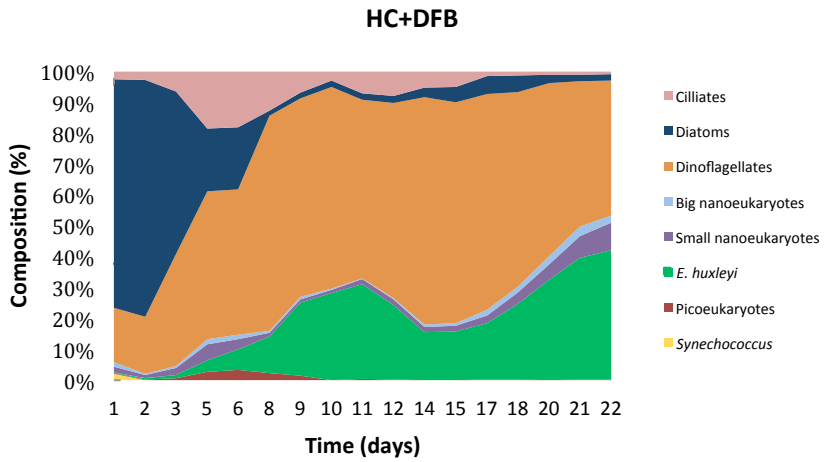
□



□



□





□

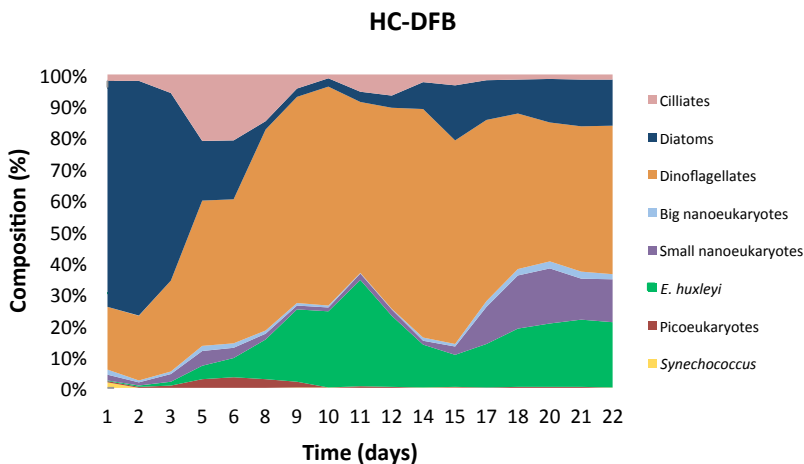
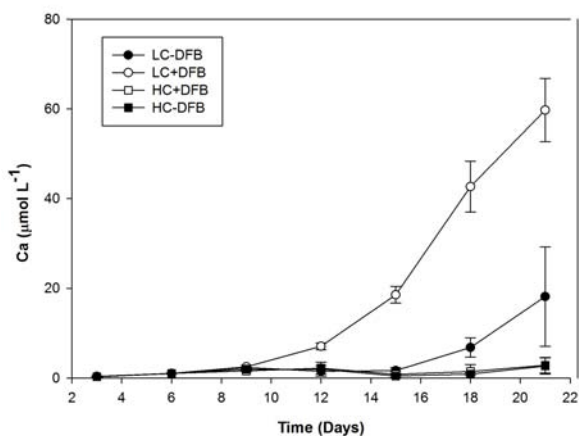


**Figure 3.25.** Temporal development of molar Ca in all the treatments during the experiment. Ambient pCO<sub>2</sub> and ambient dFe (LC-DFB, ●); ambient pCO<sub>2</sub> and increased dFe (LC+DFB, ○); increased pCO<sub>2</sub> and increased dFe (HC+DFB, □), increased pCO<sub>2</sub> and ambient dFe (HC-DFB, ■). Values are the mean of three independent mesocosm bags ± standard deviation (SD), except for LC-DFB treatment in which n=2.





## Chapter 4

# **Physiological stress response associated to elevated CO<sub>2</sub> and dissolved iron in a phytoplankton community dominated by the coccolithophore *Emiliana huxleyi*.**

María Segovia, M Rosario Lorenzo\*, Candela García-Gómez,  
Concepción Íñiguez

*Manuscript for submission*

## Abstract

In the present work we investigated the physiological response of the phytoplankton community and in particular, the response of the coccolithophore *Emiliana huxleyi* to combined effects of increased and ambient CO<sub>2</sub> and iron concentrations, during a mesocosm experiment. Changes in both factors promoted a shift in the phytoplankton community structure by day 10 of the experiment, leading to 2 well distinct phases (phase 1 and 2, before and after day 10, respectively). We report on the main physiological responses occurring in phase 2, when a massive bloom of the coccolithophore *Emiliana huxleyi* developed. Pigments performance was higher under increased iron levels, leading to a better functioning of the electron transport chain that was modulated by CO<sub>2</sub> levels. Thus, high Fe also promoted a significant increase in  $F_v/F_m$  and in the photosynthetic efficiency with respect to the control treatment (ambient CO<sub>2</sub> and ambient Fe). Strikingly, cell death was only detected during the community shift (between days 10-12) and was mostly affected by high CO<sub>2</sub> levels. The accumulation of reactive oxygen species (ROS) decreased under elevated Fe, thus, the general oxidative stress was very low in general, pointing to a more active metabolism rather than to a stressed metabolism. DNA lesions, caused by ultraviolet radiation (UVR) and excess irradiance, were minimised by high Fe levels. *Emiliana huxleyi* has been reported not to have high Fe requirements for growth. However, we demonstrate in this experiment that Fe is essential for DNA repair, to overcome oxidative stress and to keep the photosynthetic machinery functional in the studied *E. huxleyi* strain.

## Key words

CO<sub>2</sub>, iron, stress response, phytoplankton community, *Emiliana huxleyi*, photosynthesis, thylakoidal electron transport chain, pigments, cell death, oxidative stress, DNA damage/repair.





## Introduction

Anthropogenic activities are resulting in a progressive enhancement of atmospheric CO<sub>2</sub> towards levels predicted to reach around 900  $\mu\text{atm}$  by the year 2100 (IPCC 2013), are decreasing ocean pH (ocean acidification, OA) and also the calcium carbonate saturation state (Doney et al. 2009, Beardall et al. 2009) at an unprecedented rate. In addition, concomitant global warming may enhance stratification reducing nutrient availability and irradiance will be increased due to a narrower thermocline (Boyd & Doney 2002). A quarter of the CO<sub>2</sub> emitted to the atmosphere by anthropogenic activities since the beginning of the industrial era has been absorbed by the oceans. However, most of the anthropogenic CO<sub>2</sub> remains above the permanent thermocline and up to 30% remains in the upper 200 metres of the water column unequivocally affecting physiological processes (Sabine et al. 2004).

OA also affects biogeochemical processes and highly impacts trace metal solubility and speciation. Trace metals are required for numerous physiological processes in phytoplankton. Among them, Fe is the most essential trace metal for phytoplankton for crucial physiological processes controlling phytoplankton growth by means of nitrate assimilation and increased photosynthesis (Behrenfeld & Milligan 2013). Therefore, changes in Fe bioavailability have profound consequences in biologically mediated responses, ultimately affecting carbon fluxes in marine systems (Marchetti & Maldonado 2016). Iron is usually complexed to hydroxides and so the decrease in pH will change Fe speciation, increasing the solubility of Fe (III) and preventing Fe (II) from binding to carbonate (Millero et al. 2009) due to the carbonate ion will be reduced by 54% at low pH (Beardall et al. 2009). Additionally, the increased CO<sub>2</sub> concentration in seawater and thus, the decrease in seawater pH, increase Fe solubility (Millero et al. 2009), but such increase depends on the nature of strong organic Fe ligands (Shi et al. 2010). It is widely known that elevated CO<sub>2</sub> also affects phytoplankton (Mackey et al. 2015). Field experiments have shown mixed responses to alteration in CO<sub>2</sub> and



Fe concentrations within natural phytoplankton assemblages from HNLC regions. Fe availability increased as a result of CO<sub>2</sub> enrichment in a mesocosm experiment in the same fjord where this experiment was carried out (Breithbart et al. 2010). In contrast, decreases in Fe uptake rates, Fe availability and growth of phytoplankton with increasing CO<sub>2</sub> levels were observed in the North Atlantic and the Bering Sea (reviewed in Marchetti & Maldonado 2016).

Coccolithophores is one of the taxa most affected by CO<sub>2</sub> (Riebesell & Tortell 2011). The majority of coccolithophores reduce their level of calcification when growing at increased CO<sub>2</sub> and the fossil record suggests that eras with reduced CO<sub>2</sub> levels (e.g. glacial maxima) have favoured more heavily calcified cells (Beaufort et al. 2011). Elevated CO<sub>2</sub> may act as stressor in coccolithophores due to problems related to calcification (Mackey et al. 2015), leading to subsequent adding effects of other stressors, such as excess of PAR and UVR irradiances, that are able to exert harming effects in cells with insufficient calcium carbonate (Gao et al. 2009, Xu et al. 2011). In Chapter 2, we showed in this very experiment that the coccolithophore *Emiliana huxleyi* was negatively affected by increased CO<sub>2</sub> and ambient iron conditions, but its biomass massively increased at ambient CO<sub>2</sub> and increased dFe, suggesting *in situ* iron limitation. However, increased dissolved Fe partially mitigated the negative effect of elevated pCO<sub>2</sub> indicating that *E. huxleyi* was able to acclimate better to ocean acidification when Fe was high. Therefore, the underlying physiological response to acclimation to stress must be very tightly regulated by iron in the studied natural strain. Fe is required for many processes; hence it is involved in a plethora of cell functions including carbon (C) and nitrogen (N) fixation, nitrate and nitrite reduction, chlorophyll synthesis, and the electron transport chains of respiration and photosynthesis. Fe is also incorporated into several enzymes used by cells to deal with reactive oxygen species (ROS) (Twining & Baines 2013), and in some of the enzymes that participate in DNA repair (Lukianova & Davis 2005, Morita et al. 2010).



Despite the considerable contribution of marine phytoplankton to global climate and biogeochemical cycles, many aspects of the physiology of these organisms in future global change-ocean biology relationships are poorly understood. Thus, experimental designs aiming to unravel the relevance of the interactive effects of global change drivers, contribute to reduce the lack of knowledge on the interplay of the different environmental factors, which is one of the main constraints in our ability to predict the functioning and composition of the future ocean.

Here we present the results from a mesocosm experiment that aimed to investigate the effects of future changes in pCO<sub>2</sub> and Fe availability on the physiological stress response during a bloom of the coccolithophore *Emiliana huxleyi* within a natural plankton community. *Emiliana huxleyi* is the keystone species of the coccolithophores (Paasche 2002). It is a globally relevant species, playing a major role in the global carbon cycle by regulating the exchange of CO<sub>2</sub> across the ocean-atmosphere interface through photosynthesis and calcium carbonate precipitation (Rost & Riebesell 2004) and, it has also been demonstrated that it is a sensitive phytoplankton to elevated pCO<sub>2</sub> (Riebesell & Tortell 2011). The objective of this work was: i) examine the effects of increased CO<sub>2</sub> and iron levels in the stress response of the different phytoplankton groups; ii) analyse the effect of increased CO<sub>2</sub> and dissolved Fe in the thylakoidal transport chain and accessory pigments; iii) to determine the impact of the response by means of cell viability, oxidative stress and DNA damage analyses. This study is the first to analyse the stress physiological response of different phytoplankton species in a mesocosm experiment where CO<sub>2</sub> and Fe concentrations were simultaneously manipulated.



## Material and methods

### Experimental design

A mesocosm experiment was carried out in the Raunefjord (60.39 °N, 5.32 °E), off Bergen, Norway. Twelve mesocosms (11 m<sup>3</sup> each) were set-up in a full-factorial design with all combinations of ambient and high pCO<sub>2</sub> and two treatments of dFe in three independent replicate mesocosms per treatment. High-density polyethylene (HDPE) mesocosms were filled with fjord water pumped from 8 m depth. They were covered with low-density polyethylene (LDPE) lids in order to avoid pCO<sub>2</sub> losses and contamination. Mesocosms and their lids were transparent to PAR and UVR. After the first sampling day (0), the seawater of half of the mesocosms was enriched with CO<sub>2</sub> (Schulz et al. 2009) to achieve pCO<sub>2</sub> concentrations corresponding to levels predicted for the year 2100 (900 µatm, HC), (IPCC 2013) and the other half were not manipulated (ca. 390 µatm, LC). All mesocosms were continuously and gently mixed by using an airlift system (Egge & Heimdal 1994). For the CO<sub>2</sub> enrichment, 150 L of fjord water was aerated with pure CO<sub>2</sub> at a flow rate of 1.5 L min<sup>-1</sup> overnight and added to each of the high pCO<sub>2</sub> (HC) mesocosms. To maintain the pCO<sub>2</sub> in the HC treatments, ambient air was mixed with pure CO<sub>2</sub> at a flow rate of 200 mL min<sup>-1</sup> and the enriched mixture (900 µatm CO<sub>2</sub>) was pumped directly to the airlift system. LC treatment consisted of only-ambient air similarly connected. HEPA filters were placed between the air pumps and the airlift system to avoid particulate contamination. Mesocosms were fertilised after the initial sampling (day 0) by addition of 10 µM nitrate and 0.3 µM phosphate to induce a bloom of the coccolithophorid *Emiliania huxleyi* (Egge & Heimdal 1994). On day 7, half of the mesocosms (3LC and 3 HC) were amended with 70 nM (final concentration) of the siderophore desferrioxamine B (DFB) to promote changes in iron availability. Dissolved iron (dFe) concentration increased ~3-fold with respect to the control as a result of both factors manipulation. The treatments were named LC-DFB (control), LC+DFB, HC+DFB and HC-DFB. Water samples from each mesocosm were taken from 2 m depth by gentle vacuum



pumping of 25 L volume into acid-washed carboys that were quickly transported to the onshore laboratory. All variables were analysed on a daily basis and/or every other day, except otherwise stated.

### **Irradiance and temperature**

Solar spectral irradiance comprising photosynthetically active radiation wavelengths (PAR, 400-700 nm) ultraviolet A (UVA, 320-400nm) and ultraviolet B (UVB, 280-320 nm) was recorded at 2 m depth in M3 (LC-DFB), every 1 h every day, by using a TRIOS RAMSES (Ramses, TrioS GmbH, Germany) spectroradiometer that was deployed in the M3 mesocosm. For a basic control of all of the mesocosms receiving the same irradiance at the surface and monitoring of temperature, HOBO Pendant Temperature/Light loggers (Onset Computer Corporation, Massachusetts, USA) were attached to the airlift system at 0, 1, 2 and 3 m depth and also at surface in air. The equivalent biologically effective irradiances were calculated using the biological weighting functions (BWFs) for chloroplast inhibition (Jones & Kok 1966), general plant damage (Caldwell 1971), DNA damage (Setlow 1974), inhibition of phytoplankton photosynthesis (Cullen et al. 1992) and inhibition of photosynthesis in Antarctic phytoplankton (Cullen & Neale 1997). These data are summarized in Table 4.1.

### **Pigments concentration**

For this purpose, samples (1 to 2 L) were collected from each mesocosm and gently filtered through GF/F filters. Samples were snap frozen in liquid nitrogen and kept at -80°C until analysis. Pigments were extracted using N,N-dimethylformamide (DMF) overnight at 4 ° C. Chlorophyll *a* (Chl *a*) concentration was determined spectrophotometrically and the concentration was calculated according to Wellburn (1994). Lutein (Lut), neoxanthin (Neo), violaxanthin (V), anteraxanthin (A), zeaxanthin (Z), chlorophyll *c*<sub>2</sub> (Chl *c*<sub>2</sub>), chlorophyll *c*<sub>3</sub> (Chl *c*<sub>3</sub>), peridinin (PERI), fucoxanthin (FUCO), 19'-butanoyloxyfucoxanthin (BUTA), 19'-



hexanoyloxyfucoxanthin (HEXA), diadinoxanthin (DD), diatoxanthin (DT), prasinoxanthin (PRAS), Pheophorbide (Pheo) and chlorophyllide a (Chlide) were determined by HPLC as described in Lubian & Montero (1998).

### ***In vivo* chlorophyll a (Chl *a*) fluorescence**

Optimal quantum yield ( $F_v/F_m$ ) of PSII was measured in 20 min dark-adapted samples by pulse amplitude modulated fluorometry (Water-PAM, Waltz, Effeltrich, Germany). Rapid light curves (RLCs) were constructed according to Figueroa et al. (2009) and fitted to the model of Eilers & Peters (1986) to obtain the initial slope ( $\alpha_{ETR}$ ) and maximal electron relative transport rate ( $rETR_{max}$ ). The light saturation parameter ( $E_k$ ) was derived from  $rETR_{max}$  and  $\alpha$ .

### **Cell viability**

Cell viability was assessed using the nucleic acid stain SYTOX Green (Invitrogen, Oregon, USA) according to Segovia & Berges (2009). SYTOX Green only stains the nucleic acid of cells that have compromised plasma membranes. Green staining of the cell nucleus indicates a dead cell, before the cell loses its integrity and lyses (Veldhuis et al. 2001) while viable cells are not stained and fluoresce in red. Samples from each mesocosm (1-2 L) were concentrated by gentle filtration under low pressure on 0.8  $\mu$ m, 47-mm polycarbonate membranes to a final volume of 15 mL at 10°C. Chlorophyll *a* (Chl *a*) content in the concentrates was measured by extraction in 90% acetone overnight and determined fluorometrically using a Turner fluorometer 10-AU (Turner BioSystems, CA, USA). Final Chl *a* concentration in cell concentrates ranged from 0.2 to 400  $\mu$ g L<sup>-1</sup>. SYTOX-Green (5  $\mu$ M final concentration) was added to 1 mL of the concentrated cell suspensions from the natural phytoplankton community. Samples were incubated at 10 °C (natural temperature condition in the fjord) in darkness for 60 min. Fluorescence was quantified in a NIKON epifluorescence microscope at an excitation of 490 nm and an emission of 525 nm. Between 30-50 fields of view (FOVs) were analysed per



sample (N≥600). Positive controls consisting of 100% killed cells were run in parallel and obtained by pre-treating the samples with 1% glutaraldehyde (final concentration) for 2 h at 4 °C.

### **General oxidative stress**

The intracellular accumulation of reactive oxygen species (ROS) was assayed in concentrated cell suspensions from the natural phytoplankton community (as above) by using a modification of the method used by Segovia & Berges (2009) described in Bouchard et al. (2013). Shortly, cells were incubated with 10µM carboxy-H<sub>2</sub>DFFDA (Invitrogen, Oregon, USA) (final concentration) at 10 °C for 90 min in darkness. Fluorescence was quantified in a NIKON epifluorescence microscope at an excitation of 490 nm and an emission of 525 nm. Between 30-50 fields of view (FOVs) were analysed per sample (N≥600).

### **DNA Damage**

DNA damage was assessed according to García-Gómez et al. (2012). For this purpose, samples (1 to 2 L) were collected from each mesocosm and gently filtered through 0.8 µm polycarbonate filters. Samples were snap frozen in liquid nitrogen and kept at -80°C until analysis. For analysis, DNA was extracted and quantified from the filters; 15 ng of DNA were used from each sample for immunodetection of CPDs with a monoclonal anti-CPD antibody (H3, Affitech). Positive controls consisted of UVR-radiated DNA from lambda phage and *Dunaliella tertiolecta* (García-Gomez et al. 2014). Negative controls consisted of the same former DNA sample species without radiation. Unspecific cross-reactivity controls were carried out by incubating the membranes with only the secondary antibody in the absence of the primary antibody. The signal was detected by chemiluminescence (ECL, GE healthcare, Buckinghamshire, UK) and the intensity of cross-reactions quantified in a Gel Logic Image Analyser (Eastman-Kodak, Rochester, NY, USA).



### Statistical analyses

Data were checked for normality (by Saphiro-Wilks' test), homoscedasticity (by Cochran's and Levene's tests) and sphericity (by Mauchly's and/or Bartlett's tests). Variables met all criteria to perform parametric tests. Statistical significance of treatment effects on variables was performed by using Split-Plot ANOVA (also called SPANOVA or mixed-model ANOVA) followed by post-hoc Sidak or Tukey and Bonferroni tests, respectively (considering  $p < 0.05$  and/or  $p < 0.01$  as significant). When appropriate, data were specifically tested for significant differences ( $p < 0.05$ ) induced by the treatments by using 1 or 2 Way ANOVAs and/or Student's t-tests, as well as Pearson's product-moment correlations. All analyses were performed using the GLM (general linear model) procedure with main effects ( $\text{CO}_2$ , dFe), time (repeated measure) and all interactions. Statistical analyses were performed by using the software Statistica v12 (Statsoft, Inc.) and SPSS v22 (IBM statistics).

## Results

### Irradiance and Temperature

Meteorological conditions during the experiment were stable with 75% clear sky days and 25% partly cloud covered days. Average midday range (solar noon  $\pm$  2 h) irradiance in the mesocosms at 2 m depth was  $276.2 (\pm 45) \mu\text{mol photons m}^{-2} \text{s}^{-1}$  PAR;  $1.61 (\pm 0.98) \text{ W m}^{-2}$  UVA; and  $0.01 (\pm 0.01) \text{ W m}^{-2}$  UVB. The midday average irradiance varied around this mean on days with cloud cover. Experimental irradiances and corresponding weighted irradiances (i.e. biological effective irradiance, BEI), as well as the biological effective dose (BED) calculated for the control mesocosms are shown in Figure 4.1 and Table 4.1. Irradiance and transmittance through polyethylene mesocosms and lids are shown in Supplemental Table-4.2S. The water temperature in the mesocosms during the experiment varied between 10-11°C corresponding to the surrounding fjord temperature.



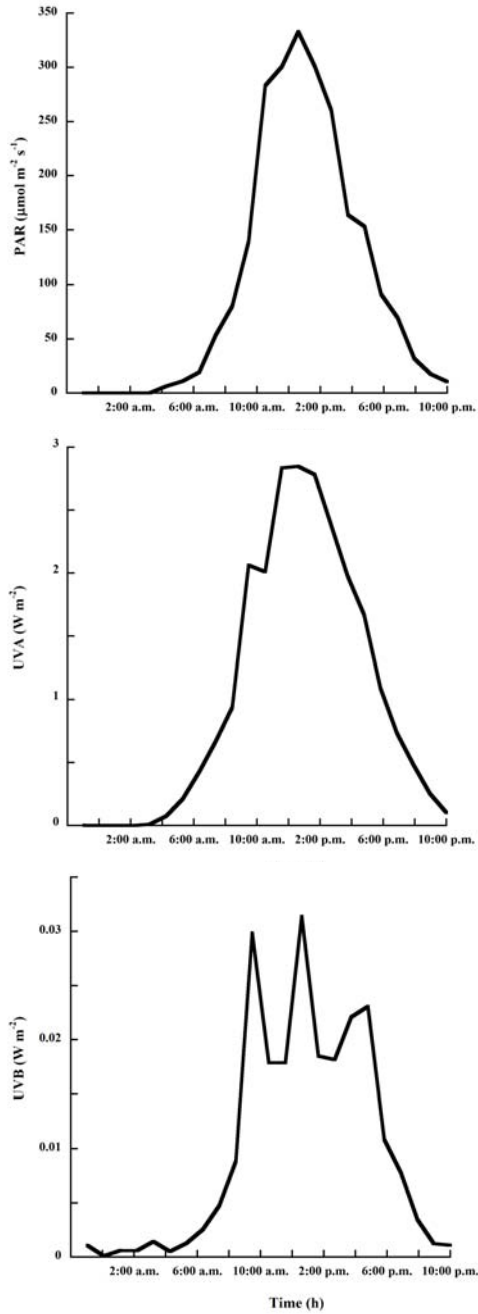


**Figure 4.1.** Experimental irradiances (PAR, UVA and UVB radiation) in the control mesocosms in day 6 (just before the addition of DFB on day 7).



**Table 4.1.** Experimental irradiances, corresponding weighted irradiances (BEI) and the biological effective dose (BED) were estimated in the control mesocosms in day 6 (just before the addition of DFB on day 7) by using the biologically effective 300 nm normalised weighting function for DNA damage (Setlow 1974), general plant damage (Caldwell 1971), inhibition of phytoplankton photosynthesis (Cullen et al. 1992), inhibition of photosynthesis in Antarctic phytoplankton (Cullen & Neale 1997) and chloroplast inhibition (Jones & Kok 1966).

<b>Experimental Irradiance</b>	
UVB (280-320 nm, $W m^{-2}$ )	0.015
UVA (320-400 nm, $W m^{-2}$ )	2.057
PAR (400-700 nm, $\mu mol\ quanta\ m^{-2}\ s^{-1}$ )	180.97
<b>Weighted Irradiance (BEI (<math>W m^{-2}</math>)/BED (<math>KJ m^{-2}</math>))</b>	
DNA damage	0.0042/2.18
Generalised plant response	0.0039/2.05
Inhibition of phytoplankton photosynthesis of <i>Phaeodactylum</i>	0.052/27.29
Inhibition of photosynthesis in Antarctic phytoplankton	0.09/49.49
Photosynthesis of Chloroplasts	0.37/191.68

### **Phytoplankton biomass and pigments: Increased CO<sub>2</sub> and iron availability promoted a shift in the phytoplankton community structure**

Pigment composition was dependent on the shifts in the phytoplankton community that took place during the mesocosm experiment reported in Chapter 2. Two phases were observed during the experimental course: phase 1 comprised days 0-10, and phase 2 days 11-22 (Supplemental Figure 4.1S).

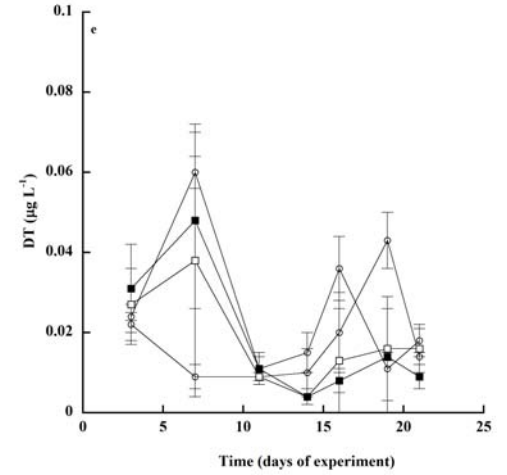
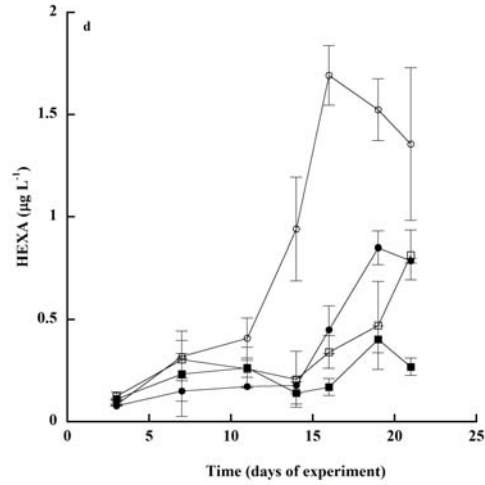
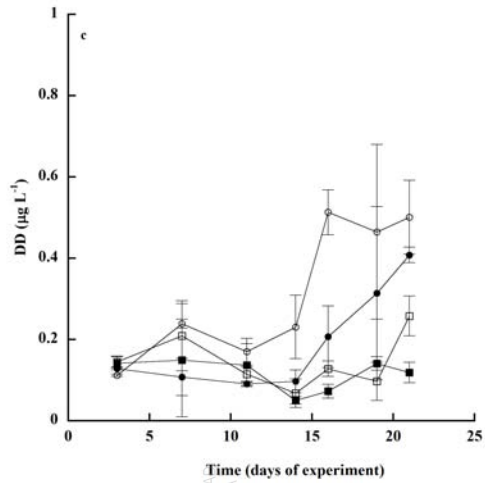
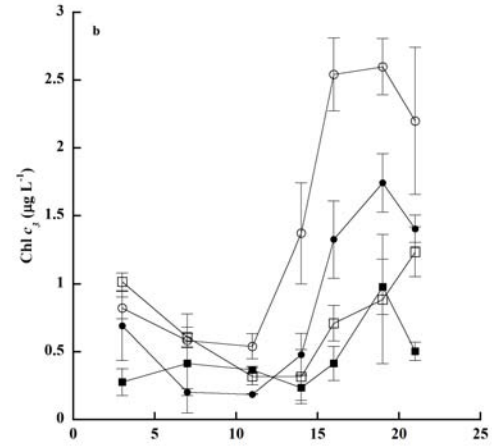
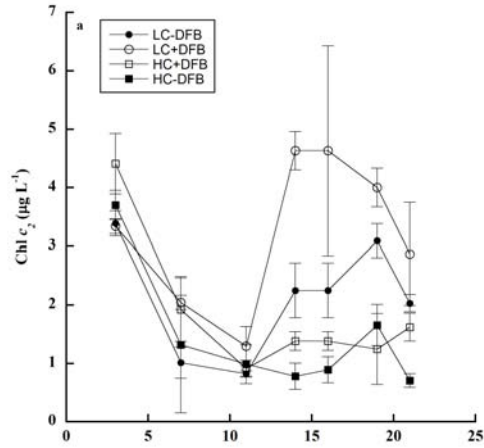
*Phase 1-* Mesocosms were filled at the time of an intense diatom bloom in the fjord, constituted by long chain forming diatoms (*Skeletonema costatum*, *Thalassiosira* spp., *Chaetoceros* spp. and other diatoms, Supplemental Figure 4.1S), which declined by day 7. Other phytoplankton groups peaked between days 3 and 5, to decline sharply after day 5. Namely, picoeukaryotes (Supplemental Figure 4.1SC), small nanoeukaryotes likely constituted by small Prasinophytes and small Haptophytes (Supplemental Figure 4.1Sd) and big nanoeukaryotes formed

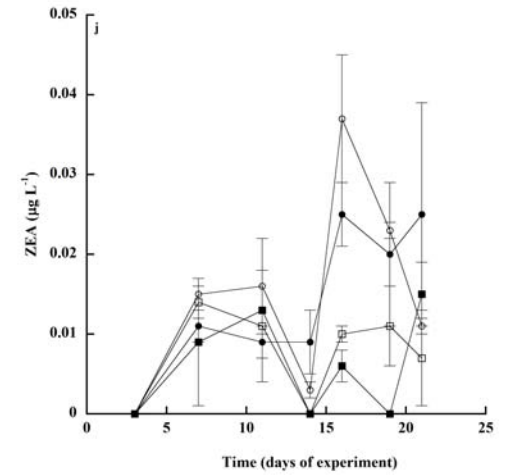
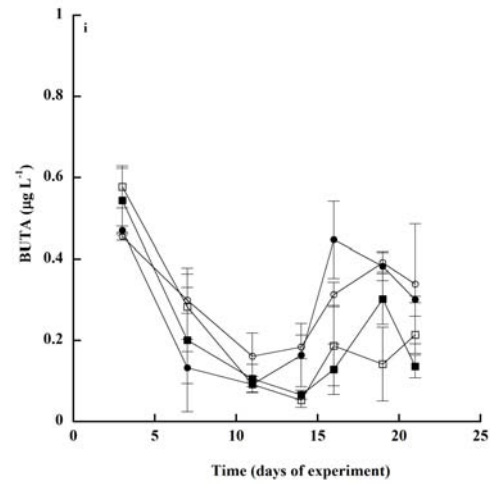
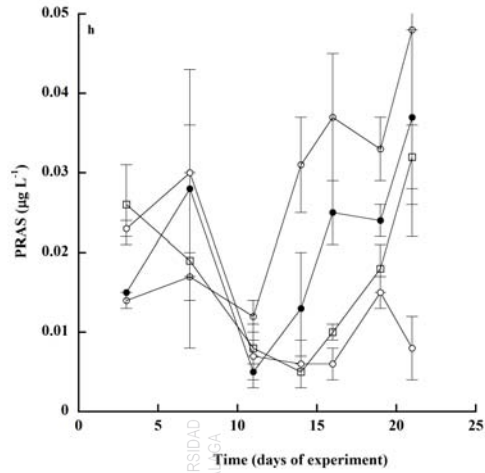
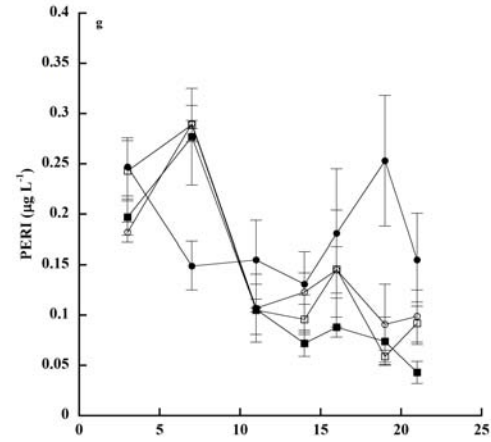
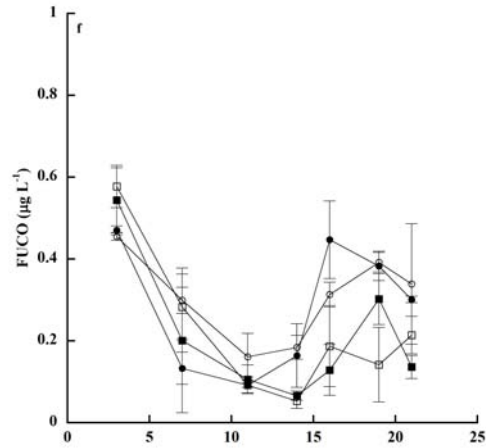


by single celled diatoms and flagellated forms (Supplemental Figure 4.1Se). Microplankton such as dinoflagellates (dominated by *Gyrodinium* spp. and *Ceratium* sp. and less abundant species such as *Protoperidinium* spp., *Dinophysis* spp., *Prorocentrum* spp.) (Supplemental Figure 4.1Sg), were also present, contributing with significant biomass. *Synechococcus* sp. and *E. huxleyi* also contributed with Chl *a* but did not grow significantly in this phase (Supplemental Figure 4.2Sa,b). Thus, the increase in Chl *a* experienced due to these organisms' growth was masked by the declining microphytoplanktonic diatoms. During phase 1 neither there were significant differences due to treatments on changes in species composition/ proportions, nor in any of the pigments concentration (Table 4.2).

*Phase 2* - A bloom of the coccolithophore *E. huxleyi* was observed under LC +DFB conditions outcompeting the rest of the groups. This bloom was not observed neither in the control treatment (LC-DFB) nor in the HC treatments (Supplemental Figure 4.1Sa). *Synechococcus* sp. showed a similar pattern than *E. huxleyi* abundance but it contributed to the total Chl *a* with very low biomass (Supplemental Figure 4.1Sa). Picoeukaryotes, small and big nanoeukaryotes and microphytoplankton were not affected either by changes in CO<sub>2</sub>, dFe levels or their interaction.

**Figure 4.2.** Temporal development of pigments concentrations ( $\mu\text{g L}^{-1}$ ) within the mesocosms: (a) chlorophyll *c*<sub>2</sub>, (b) chlorophyll *c*<sub>3</sub>, (c) diadinoxanthin, (d) 19'-hexanoyloxyfucoxanthin, (e) diatoxanthin, (f) fucoxanthin, (g) peridinin, (h) prasinoxanthin, (i) 19'-butanoyloxyfucoxanthin and (j) zeaxanthin. Ambient pCO<sub>2</sub> and ambient dFe (black filled circle); ambient pCO<sub>2</sub> and increased dFe (LC+DFB, open circle); increased pCO<sub>2</sub> and increased dFe (HC+DFB, open square), increased pCO<sub>2</sub> and ambient dFe (HC-DFB, black filled square). Symbols indicate means of measurements in three independent mesocosms (n=3) except for LC-DFB where n=2. Error bars indicate standard deviations.





### **Increased dFe favoured the accumulation of pigments independent on the pCO<sub>2</sub> levels**

Chlorophylls  $c_2$  and  $c_3$ , diadinoxanthin (DD), and hexanoyloxyfucoxanthin (HEXA) presented a similar pattern. High pCO<sub>2</sub> negatively affected the pigments concentration in phase 2, while increased dFe (+DFB) had a general positive effect on increasing their levels. Therefore, the effect was not so evident in HC conditions when compared to LC (Figure 4.2a-d, Table 4.2). Diatoxanthin (DT) did not exhibit differences between treatments during the experiment (Figure 4.2e, Table 4.2) except for day 19 where the control was significantly higher than the rest of treatments (post-hoc Sidak,  $p < 0.05$ ). Fucoxanthin (FUCO) and peridinin (PERI) concentrations increased from day 14 onwards in the control (LC-DFB) and were significantly different from all of the other treatments (Figure 4.2f,g Table 4.2). Prasinoxanthin (PRAS) and butanoyloxyfucoxanthin (BUTA) constantly augmented in LC during this period, while HC lowered its content. However, although a positive effect of high dFe seemed to be observed in the LC+DFB condition (Figure 4.2h,i Table 4.2) it was not significant. Zeaxanthin (Z) was significantly higher in LC vs HC from day 14 onwards regardless of iron levels (Figure 4.2j, Table 4.2); thus, its concentration was affected by pCO<sub>2</sub> main effects but not by DFB or the interaction of both factors. Lutein (Lut), neoxanthin (Neo), violaxanthin (V), anteraxanthin (A), pheophorbide (Pheo) and chlorophyllide *a* (Chlide) were not detected. The pigmentary ratios HEXA/FUCO and DT+DD/FUCO drastically changed in phase 2 and were strongly affected by dFe and modulated by CO<sub>2</sub> (Figure 4.3, Table 4.2).

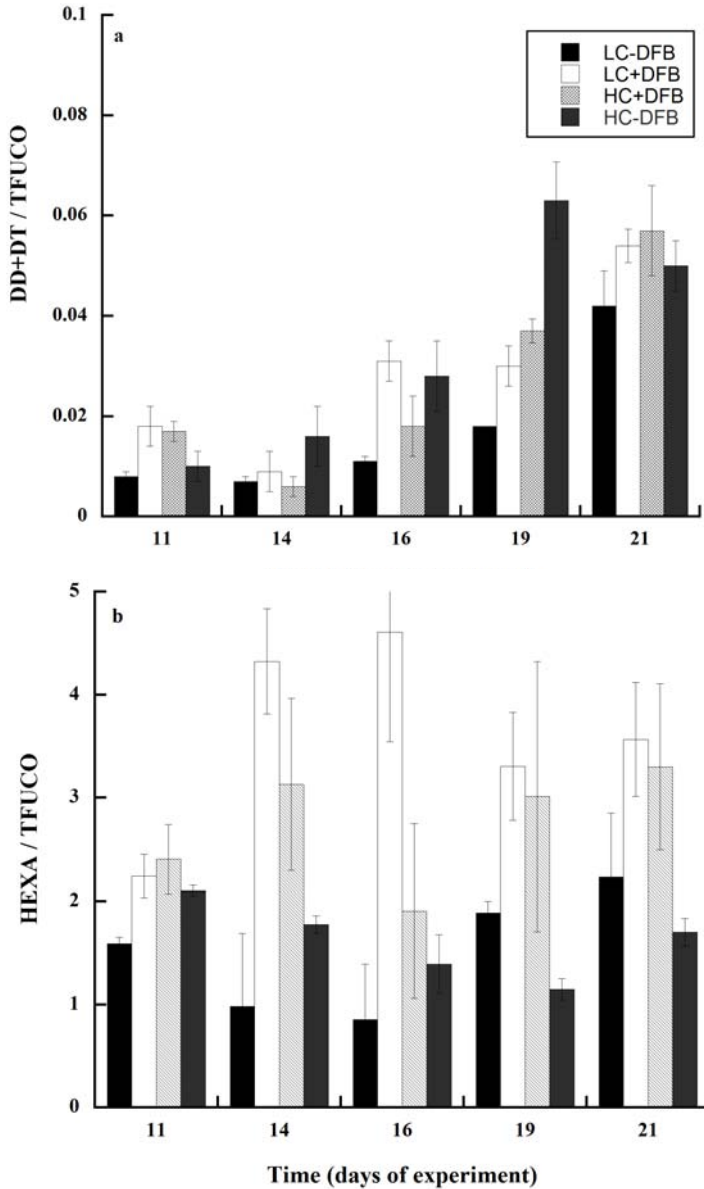


**Figure 4.3.** Ratios of (a) diatoxanthin and diadinoxantin to total fucoxanthins (DT+DD/TFUCO) and (b) 19'-hexanoyloxyfucoxanthin to total fucoxanthins (HEXA/TFUCO). Ambient pCO<sub>2</sub> and ambient dFe (LC-DFB, black); ambient pCO<sub>2</sub> and increased dFe (LC+DFB, white); increased pCO<sub>2</sub> and increased dFe (HC+DFB, striped), increased pCO<sub>2</sub> and ambient dFe (HC-DFB, grey). Data are means of measurements in three independent mesocosms (n=3) except for LC-DFB where n=2. Error bars indicate standard deviations.

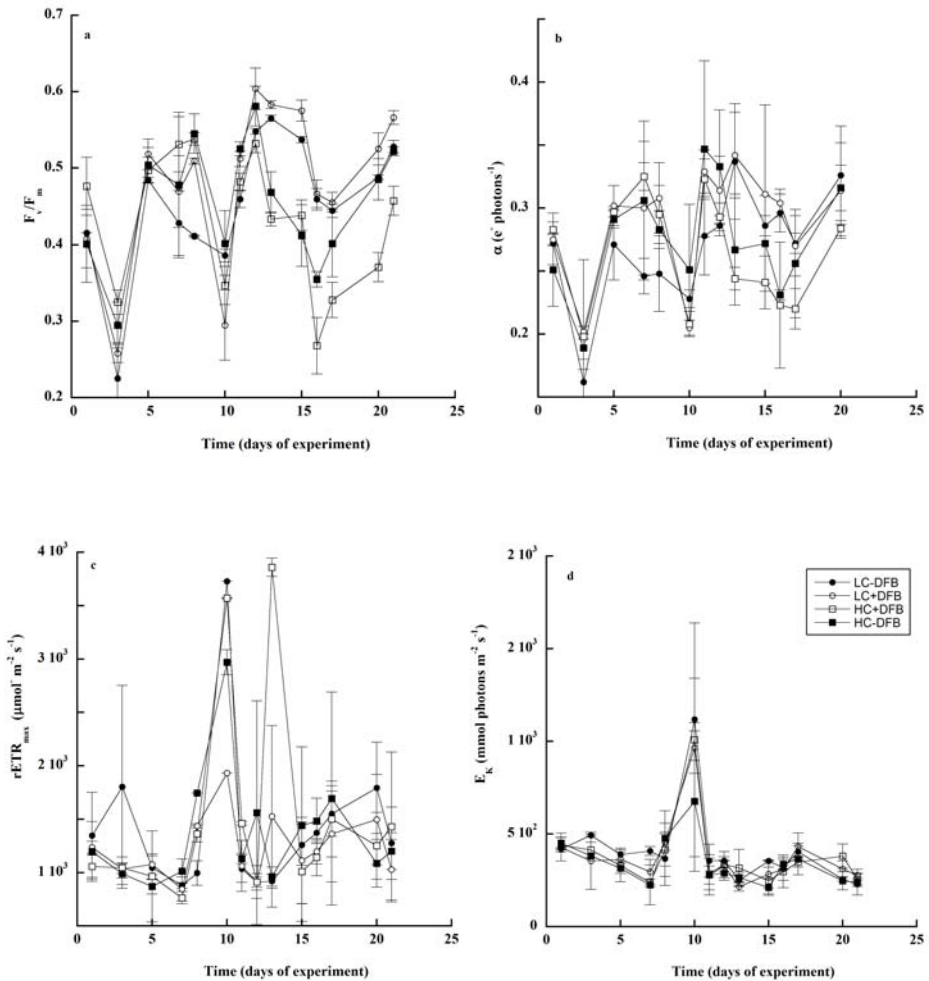


**Figure 4.4.** Temporal development of the photosynthetic parameters: (a)  $F_v/F_m$ , (b)  $\alpha$ , (c)  $rETR_{max}$  and  $E_k$ . Ambient  $pCO_2$  and ambient dFe (black filled circle); ambient  $pCO_2$  and increased dFe (LC+DFB, open circle); increased  $pCO_2$  and increased dFe (HC+DFB, open square), increased  $pCO_2$  and ambient dFe (HC-DFB, black filled square). Symbols indicate means of measurements in three independent mesocosms (n=3) except for LC-DFB where n=2. Error bars indicate standard deviations.



### **Photosynthetic parameters were dependent on pCO<sub>2</sub> and dFe concentration**

During phase 1 (days 1-10) there were no significant differences between treatments in any of the photosynthetic parameters (Figure 4.4). However, in day 10, a transitory decrease in  $F_v/F_m$  (Figure 4.4a) and in the photosynthetic efficiency ( $\alpha$ ) (Figure 4.4b) were observed, in parallel with an increase in  $rETR_{max}$  (Figure 4.4c) and  $E_k$  (Figure 4.4d) in all the treatments. Between days 11-22 (phase 2),  $F_v/F_m$  was significantly higher in LC than in HC treatments. In LC, high dFe (+DFB) promoted a significant increase in  $F_v/F_m$  with respect to the control (LC-DFB) (Table 4.2). In contrast, in the HC treatments  $F_v/F_m$  was higher in the absence of DFB. Both pCO<sub>2</sub> and DFB factors, and their interaction had significant effects on  $F_v/F_m$  during all this period. The photosynthetic efficiency ( $\alpha$ ) matched the  $F_v/F_m$  trend and LC showed higher values than in HC. DFB addition had a significant positive effect on LC treatments promoting a higher efficiency, while it did not exert any potential benefit in HC (Table 4.2).  $P_{max}$  and  $E_k$  did not present significant differences between treatments in phase 2.

### **Cell death was affected by high CO<sub>2</sub> and general oxidative stress decreased under high dFe**

Cell death was not detected during the whole experiment except for days 11 and 14 (Figure 4.5a). On day 11, 20 % cells showed SYTOX-positive green fluorescence, therefore pointing to the complete lost of viability under increased pCO<sub>2</sub>. In LC, there were 4-fold less green fluorescent-labelled cells indicating that indeed HC had a significant negative effect on part of the phytoplankton population when compared to LC (Table 4.2). The percentage of SYTOX-positive cells decreased 10-fold to threshold levels by day 14. Green fluorescence emitted by the cells due to general oxidative stress was significantly higher in HC than in LC at the beginning of the experiment, declining by 60% between days 3 and 7. As it was observed for cell death, ca. 20% of the cells showed symptoms of oxidative stress on day 11 (Figure 4.5b). However, in this case, the percentage of green fluorescent labelled



cells was significantly higher at ambient dFe (-DFB treatments) than in high-dFe grown cells (+DFB), and independent on the pCO<sub>2</sub> levels (Table 4.2).

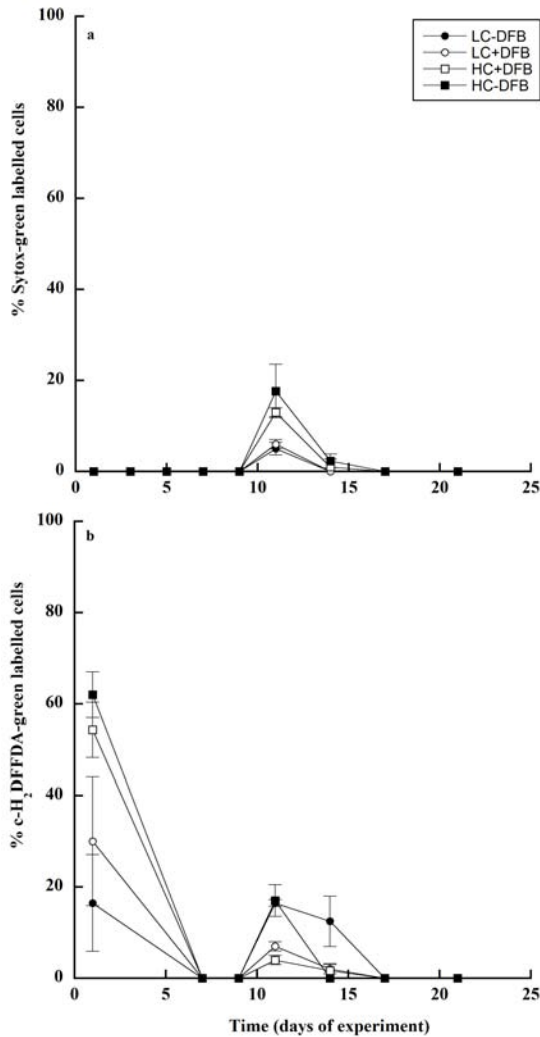


**Figure 4.5.** Temporal development of percentage of cells SYTOX-Green labelled (a) and percentage of cells c-H<sub>2</sub>DFFDA-green labelled (b). Ambient pCO<sub>2</sub> and ambient dFe (black filled circle); ambient pCO<sub>2</sub> and increased dFe (LC+DFB, open circle); increased pCO<sub>2</sub> and increased dFe (HC+DFB, open square), increased pCO<sub>2</sub> and ambient dFe (HC-DFB, black filled square). Symbols indicate means of measurements in three independent mesocosms (n=3) except for LC-DFB where n=2. Error bars indicate standard deviations.



### DNA damage was minimised by increased dFe in *Emiliana huxleyi*

In phase 1, cyclobutane pyrimidine dimers (CPDs) formation significantly increased 4-fold between days 1 and 3 (Figure 4.6), to remain steady and with no differences between treatments up to day 9 (Table 4.2). CPDs sharply increased in those cells subjected to high dFe (+DFB) in day 9, while the treatment showing less DNA damage was HC-DFB. CPDs content was drastically reduced between days 9 and 11. As phase 2 progressed, the treatments that exhibited significant increased levels of accumulated DNA damage were those at ambient dFe (-DFB) (Table 4.2). By contrast, the treatments with +DFB presented significant lower CPDs concentration than the control, regardless of pCO<sub>2</sub>.

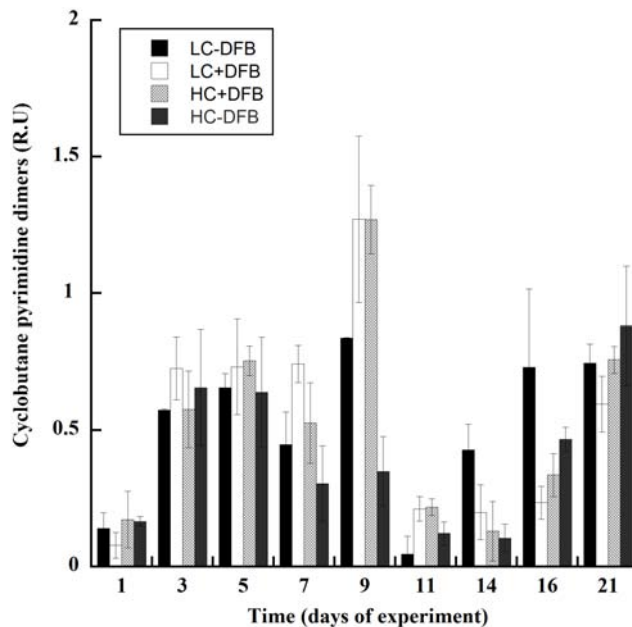


**Figure 4.6.** Temporal development of cyclobutane pyrimidine dimers (CPDs) within the mesocosms. Ambient pCO<sub>2</sub> and ambient dFe (LC-DFB, black); ambient pCO<sub>2</sub> and increased dFe (LC+DFB, white); increased pCO<sub>2</sub> and increased dFe (HC+DFB, striped), increased pCO<sub>2</sub> and ambient dFe (HC-DFB, grey). Data are means of measurements in three independent mesocosms (n=3) except for LC-DFB where n=2. Error bars indicate standard deviations.



**Table 4.2.** Statistical analyses (Split-plot ANOVA) of the effects of CO<sub>2</sub>, DFB, and their interaction, as well as the effect of time, on the variables analysed in the different treatments: LC, ambient CO<sub>2</sub> (390 µatm); HC, increased CO<sub>2</sub> (900 µatm); -DFB, (ambient dFe); +DFB, (increased dFe) considering p<0.05 as significant.

Factor	CO <sub>2</sub>	DFB	Time	CO <sub>2</sub> xDFB	CO <sub>2</sub> xDFBxTime
F <sub>v</sub> /F <sub>m</sub>	<0.001	<0.001	<0.001	<0.05	<0.001
α	<0.01	ns	<0.005	<0.05	ns
E <sub>k</sub>	ns	ns	ns	ns	ns
rETR <sub>max</sub>	<0.05	ns	ns	ns	ns
Chl c <sub>3</sub>	<0.001	<0.001	<0.05	<0.05	<0.05
Chl c <sub>2</sub>	<0.01	ns	<0.001	ns	ns
PERI	<0.05	ns	<0.001	ns	ns
BUTA	<0.01	ns	<0.01	ns	ns
FUCO	<0.001	ns	<0.01	ns	ns
HEXA	<0.001	<0.001	<0.001	<0.001	<0.001
DD	<0.001	<0.001	<0.01	<0.01	ns
DT	<0.05	ns	<0.001	<0.05	<0.01
Zea	<0.001	ns	<0.05	ns	ns
PRAS	<0.01	ns	<0.001	ns	ns
HEXA/FUCO	ns	<0.001	<0.001	<0.05	<0.001
DT+DD/TFUCO	ns	ns	<0.05	<0.001	<0.001
Cell death	<0.01	ns	<0.001	ns	ns
Oxidative stress	<0.01	ns	ns	ns	<0.05
DNA damage	ns	<0.001	<0.001	<0.05	<0.05



## Discussion

In the present work we studied the physiological processes that interact from the molecular to the organism level, in order to understand the final response of the phytoplankton community and in particular, the response of the coccolithophore *Emiliania huxleyi* to the interactive manipulation of CO<sub>2</sub> levels and iron bioavailability. The reproducibility between the triplicates of each treatment was high, allowing us to isolate and identify single and interactive effects on the variables measured. We assessed the behaviour of the variables in relationship to the different functional phytoplankton groups during three important time periods along the experiment (for details see Chapter 2): i) phase 1 (days 0-10), characterised by the absence of factors effects on the phytoplankton community and consequently the lack of response, ii) shift-point (day 10-11), when the phytoplankton community shifted due to mid-term effects of increased CO<sub>2</sub> and dissolved iron (dFe) levels, and iii) phase 2 (days 11-22), distinguished by an evident response of the community to treatment effects in the long-term. A bloom of the coccolithophore *E. huxleyi* was developed in this phase under ambient CO<sub>2</sub> and increased dFe (LC +DFB), outcompeting the rest of the groups. This bloom was not observed neither in the control at ambient CO<sub>2</sub> and dFe (LC-DFB) nor in the high CO<sub>2</sub> conditions, although *E. huxleyi* was the most abundant species in all treatments except in HC-DFB (Supplemental Figure 4.2S). In Chapter 2, we demonstrated that Fe concentrations may control phytoplankton community structure in coastal ecosystems, that ocean acidification can enhance Fe bioavailability and, that in areas with high total Fe concentrations (particulate and dissolved Fe), the detrimental effects of increased pCO<sub>2</sub> on *E. huxleyi* can be partially mitigated by enhanced dFe depending on the cellular strain. Therefore, consequences of the interactive effects of pCO<sub>2</sub> and Fe availability on *E. huxleyi* can be critical to C-cycling and marine ecosystems.

From the physiological point of view, Fe plays a basic major role in plankton ecology since every aspect of thylakoid electron transport and accessory pigments



is Fe dependent. A decline in cellular pigment content seems a general response to Fe stress (Beherenfeld & Milligan 2009). The response showed by the community when dFe concentration increased demonstrated that *E. huxleyi* was experiencing Fe limitation (the highest growth rates were presented by cells in the LC+DFB treatment whilst the lowest Chl *a* values were shown in those treatments with ambient iron and high HC) (Chapter 2; Supplemental Figure 4.1S). The concentration of pigments occurred during phytoplankton community succession (Figure 4.2) as widely reported in other experiments (Suffrian et al. 2008, Polimene 2012). Pigment signatures are used to determine the contribution of the distinct taxonomic groups in natural assemblages. Accordingly, the distribution of pigments in our experiment is in agreement with the flow cytometry analysis performed in this experiment (Supplemental Figure 4.1S). Pigments changed specifically in days 10-11, in parallel with a community shift that was observed in phase 2 (Supplemental Figure 4.1S). Xanthophylls, fucoxanthins and chlorophylls corresponding to Cyanophyta, Heterokontophyta, Haptophyta, Dinophyta and Chlorophyta (Takaichi 2011) were present in the mesocosms (Figure 4.2).

However, what determines phytoplankton species fitness, succession and distribution are the physiological trade-offs between light harvesting, photoacclimation or photoprotection and dissipation of excess energy, in which all pigments participate. In phase 2, chlorophylls  $c_2$  and  $c_3$  were the two pigments that showed the highest concentrations and closely followed the same trend than *E. huxleyi* biomass (Supplemental Figure 4.1S). They are considered secondary chlorophylls especially found in light-harvesting complexes (LHCs). Due to the distribution in LHCs, the function of Chl *c* in photosynthesis has been described as an enhancement of light absorption, particularly in the blue wavelength (Mizoguchi et al. 2011). The DD-DT cycle was probably active, playing a key role being the main driver for non-photochemical quenching (NPQ) (i.e. the non-radiative dissipation of excess of energy reaching the photosynthetic apparatus, Demmig-Adams et al. 1996). However, the VAZ cycle was most likely not active,





because neither violaxanthin, nor anteraxanthin were detected, and only zeaxanthin accumulated in phase 2 (Figure 4.2). HEXA, PRAS, and PERI peaked in phase 2 in the treatments with highest biomass accumulation (LC+DFB). These pigments possess light-harvesting functions and have been shown to be highly efficient transferring energy to chlorophylls, which is an essential step to ensure an efficient utilization of the available light by absorbing photons at wavelengths not “covered” by chlorophyll. All the pigments were significantly negatively affected by CO<sub>2</sub> levels and most of them positively by dFe (Table 4.2).

In multispecific bloom situations, the ratio of DT+DD to total fucoxanthins (DT+DD/TFUCO) can be used as an indicator of the cellular physiological status of *E. huxleyi* (Stolte et al. 2000), instead of using the ratio DT+DD/CHLA that also accounts for other taxonomic groups present. Increased HEXA/TFUCO rates have been observed in nutrient-limited *E. huxleyi* as a consequence of reduced growth (a similar nutrient scenario than in this experiment, see Chapter 2). We observed the highest HEXA/TFUCO ratios (mol:mol) under LC+DFB, followed by HC+DFB treatments (Figure 4.3), always well above the control (LC-DFB) and HC-DFB treatment. HEXA has been shown to also have light-harvesting functions in *E. huxleyi* (Stolte et al. 2000); hence, HEXA is most likely increasing the antenna, and possibly the number of reaction centres. This points out to a constrained physiological status of the cells at ambient dFe concentration (LC-DFB), and to a benefit of high dFe effects for the cell under HC (Chapter 2). In agreement, the (DT+DD)/TFUCO ratios were higher in the +DFB condition respect to the control (Figure 4.3) and regardless pCO<sub>2</sub>. Under this condition, a lower (DT+DD)/TFUCO (mol:mol) ratio implies a dilution of the DD-DT cycle, meaning that the cells’ capacity for non-photochemical quenching (NPQ) is decreased, thus being prone to photodamage. Indeed, it is known that Fe-limited cells show a high susceptibility to photooxidation (Behrenfeld & Milligan 2009).

The above-mentioned pigments performance was higher under increased iron levels, leading to a better functioning of the electron transport chain although



CO<sub>2</sub> could modulate this effect (Table 4.2). Photosynthetic parameters were significantly affected by both CO<sub>2</sub> and iron levels in phase 2. It is worth mention that in day 10, a transitory decrease was observed in both  $F_v/F_m$  and photosynthetic efficiency ( $\alpha$ ). At the same time,  $rETR_{max}$  ( $P_{max}$ ) and  $E_k$  increased (due to a lowered  $\alpha$ ) (Figure 4.4). This corresponded to the community shift in which some groups completely declined, while others' growth rates increased. During days 11-22 high dFe (+DFB) promoted a significant increase in  $F_v/F_m$  with respect to the control (LC-DFB) and  $\alpha$  at the expense of a constant  $rETR_{max}$ .  $F_v/F_m$  values and growth rates are in agreement with those observed for *E. huxleyi* cultures grown under different Fe conditions at ambient CO<sub>2</sub> (Honey et al. 2013). The  $F_v/F_m$  decay under iron stress is a widely observed response (Behrenfeld & Milligan 2013) and so the electron transport chains are the primary control on cell growth under low iron conditions. This explains that under elevated dFe levels, the increases in pigments ratios and photosynthetic parameters values lead to higher *E. huxleyi* growth rates (Chapter 2).  $F_v/F_m$  and  $\alpha$  were significantly lower in HC than in LC treatments affecting the growth rates. The inability to sustain high operative electron transport rates and cell division at increased CO<sub>2</sub>, is most likely due the inability of the cells to regulate the internal pH. Maintaining a constant intracellular pH is energetically costly and OA likely affect the cellular energy demands (Taylor et al. 2012).

It is expected that a stressed cell metabolism (by both the lack of iron needed to meet the cell quotas or by an excess of CO<sub>2</sub> i.e. lower pH) will produce reactive oxygen species (ROS: singlet oxygen, hydroxyl and peroxy radicals among others), directly by the harming effects of excess light reaching the cell due to affected pigments (by decreasing the size of the sink for electrons produced in the light reactions of photosynthesis), or indirectly, due to chemical, physical, or photosensitized reactions inside and outside the cells (Lesser 2006). This can finally lead into cell death (Segovia et al. 2009, Bouchard et al. 2013, Sobrino et al. 2014). Strikingly, cell death was only detected during the shift in the community



between days 10-12 (Figure 4.5a) and not when the bloom of large chain diatoms was crashing in phase 1, or, when some of the phytoplankton groups declined in phase 2. A possible explanation is that a dead cell lasts very little time in a natural plankton community where there is high grazing pressure and recycling is fast, hence, dead cells cannot simply be detected because they are not there. Indeed, Chapter 2 reported that small autotrophs could have been grazed by microzooplankton, which in turn were probably preyed upon by copepods in this experiment. Other possibility is that cellular ROS-detoxification and repair processes were highly effective, and ROS production also correlated with growth metabolism, similarly to other metabolic and enzymatic activities under non-stressing conditions (Sobrinho et al. 2014). ROS signal was also detected on days 10-16 in parallel with cell death (Figure 4.5b). A higher oxidative stress was observed in -DFB treatments, that was buffered when dFe increased. The fact that LC+DFB treatments showed significantly higher ROS fluorescent signal than HC+DFB, also points towards a more active metabolism. Furthermore, ca. 20% of stained cells mean that around 80% were not ROS stained, indicating that oxidative stress was very low, or basal in the treatments. This seems to be in agreement with the lack of other symptoms of stress such as the production of dimethylsulfoniopropionate (DMSP) by the coccolithophore during the experiment, which did not follow a pattern, throwing inconclusive results (Michaela Mausz *pers.comm.*).

Cellular repair processes depend on energy supply (ATP and NADPH), nitrogen and phosphorus for proteins and nucleic acids synthesis, thus, final responses showing the balance between cellular damage and repair depend on nutrient availability (Litchman et al. 2002). *Emiliania huxleyi* outcompetes other phytoplankton at high N:P rather than low N:P, it exploits organic nutrients successfully, it is not photoinhibited at high irradiances and it presents high growth rates (Paasche 2000), thriving under ambient CO<sub>2</sub> scenarios. Macronutrient concentrations in the present study were low but enough to support cell's growth along the experiment, meeting the cell's stoichiometric



requirements (Chapter 2). However, Fe was insufficient for *E. huxleyi* at ambient conditions (LC-DFB) (Chapter 2), leading to held-back cells and impairing growth because the cell's stoichiometric quotas were not fulfilled. This trace metal is not only essential in photosynthesis and respiration, it is also the co-factor of many proteins that participate in other cellular processes which are key to ensure cellular viability and growth, among them, the proteins involved in DNA repair and ROS scavenging.

Ocean acidification is known to decrease calcification (Riebesell & Tortell 2011), producing malformed coccoliths, therefore increasing the impact of high PAR irradiance and short wavelengths corresponding to the UVA and UVB bands of the solar spectra in the cell (Gao et al. 2009). Under these circumstances, higher DNA damage by means of cyclobutane pyrimidine dimers (CPDs) accumulation would be expected in the HC treatments, as a consequence of a higher UVR dose (Table 4.1). Remarkably, once that phase 2 was well established (days 12-22), the concentration of CPDs was significantly higher in the control (LC-DFB) than in any of the other treatments (Figure 4.5, Table 4.2). DNA lesions were minimised by high dFe, either promoted by the addition of DFB alone (LC+DFB), by increased CO<sub>2</sub>, (HC-DFB), or by both (HC+DFB). In any case, LC+DFB was the treatment that presented the lowest CPDs concentration (Figure 4.6). Photolyase (PL) is the enzyme that cleaves the cyclobutane ring of the pyrimidine dimer in a process called "photoreactivation" (Sancar 1994). While most DNA damage products are repaired via a variety of "remove and replace" (nucleotide excision and base excision repair (NER and BER)) mechanisms, pyrimidines are repaired directly photolyases (Britt 2004). The PL-mediated photoreactivation process has been already demonstrated in several species of phytoplankton (Buma et al. 2000, Boelen et al. 2001, Yi et al. 2006, Heijde et al. 2010, Brazard et al. 2012, García-Gómez et al. 2014). However, this is the first time that CPDs accumulation subjected to multiple stressors different than UVR is reported in *E. huxleyi*. This indicates that the response of *E. huxleyi* to ambient UVR is modulated by both Fe





and CO<sub>2</sub> and that natural levels of UVR are able to cause harmful effects in this species. CPDs bring both, DNA and RNA polymerases, to a standstill and may result in mutations or cell death. If DNA repair is effective, then cell survival is high and cell stress due to the oxidative burst decreases due to genes encoding for enzymes involved in ROS scavenging (superoxide dismutase, catalases, ascorbate peroxidases, glutathione reductase) being transcribed, as well as other genes necessary for the cell functioning (García-Gómez et al. 2016). The conclusion is that Fe is needed for DNA repair and to overcome oxidative stress in *E. huxleyi*.

Thus, Fe might also be directly required, because there are a large number of proteins that have this metal as a cofactor, being a compulsory requisite for catalyses. Indeed, the presence of genes encoding for Fe-metalloproteins in the *E. huxleyi* genome (Read et al. 2013) provide further evidence for the importance of Fe in the stress response of this coccolithophore (see Supplemental Table 4.1S for genes ID). For example, we have found genes encoding for DNA repair processes such as photolyases (CRY 1, 2, 3 and 4) and endonucleases, which participate in CPDs excision and BER respectively. Genes encoding for enzymes related to ROS detoxification such as a Fe-Mn superoxide dismutase, catalase, ascorbate peroxidase, glutathione reductase, ascorbate oxidase, NAD(P)H dehydrogenase (containing a flavodoxin-like domain), peroxiredoxins, thioredoxins and a thioredoxin reductase are also present. A gene encoding for a *mrp* protein related to cell cycle control and cell division, was also found. Genes encoding for protein disulfide oxidoreductases such as putative glutathione-S-transferase and ferredoxin-sulfite reductase required in assimilatory sulfate reduction pathway are present as well. Ferric reductase genes are essential components of the iron assimilatory pathway that were also detected in the genome. Genes encoding for ferredoxin-nitrite reductase precursor (enzyme that participates in nitrogen metabolism and nitrogen assimilation) and ferredoxin-dependent glutamate synthase (catalysis of the formation of L-glutamine and 2-oxoglutarate from L-glutamate, using NADH, NADPH or ferredoxin as hydrogen acceptors) also came



across. Last but not least, a number of genes encoding for iron-dependent proteins related to electron transport were encountered, such as photosystems I and II subunits, cytochrome oxidase assembly factor COX15 (catalyses the final step of heme a synthesis of the Cyt C oxidase complex), several cytochromes and their complexes (involved in the electron transport chains), a putative mitochondrial J-type chaperone (required for the assembly of iron-sulfur (Fe/S) clusters in mitochondria), NADPH-cytochrome P450 reductase (serves as the electron donor to almost all eukaryotic cytochromes P450, and has a flavodoxin domain), cytochrome *b<sub>5</sub>* reductase (participates in the electron transport chain), ferredoxin (is the last electron acceptor in the electron transport chain thus reducing the enzyme NADP+ reductase) .

### **Concluding remarks**

*Emiliania huxleyi* experienced Fe limitation under ambient dFe conditions in the fjord and increased dFe partially mitigated the negative effect of elevated pCO<sub>2</sub> inflicted on the coccolithophores. This indicates a physiological Fe-mediated-acclimation of this species to ocean acidification (Chapter 2). The stress response showed in this study further supports this, adding evidence about Fe being directly needed for essential physiological processes: i) increased dFe favoured the accumulation of pigments and it was modulated pCO<sub>2</sub> levels; ii) photosynthetic parameters behaviour was directly related to the accessory pigments trend; iii) the threshold reactive oxygen species (ROS) levels corresponded to normal metabolism, most likely suggesting an efficient detoxifying mechanism; and iv) DNA damage was minimised by increased dFe. However, Fe might also be indirectly needed to fulfil the energy requirements imposed by the proteins involved in such processes, and that is not supplied under ambient dFe due to limitation, or that is diminished due to the negative effect of OA on cell's physiology. All this results taken together evidence that the study of the



interactive effects between different global change driven factors is crucial to be able to understand and predict how the future ocean can be effected.

### **Acknowledgements**

This work was funded by CTM/MAR 2010-17216 (PHYTOSTRESS) research grant from the Spanish Ministry for Science and Innovation (Spain) to MS. MRL and CI were funded by FPU grants from the Ministry for Education (Spain). We thank the rest of the PHYTOSTRESS team for collaboration, and the Marin Biology Station (MBS) staff for logistic support.



## Supplemental Material

**Supplemental Table 4.1S.** Identified Fe-Metalloproteins genes in the genome of *Emiliania huxleyi* (Read et al. 2013), encoding for the corresponding following proteins.

Gene list	ID
A/G-specific adenine DNA glycosylase, mutY	17282666
Acyl-CoA synthetase	17287093
Ascorbate oxidase	17268477
Cytochrome B561	17266481
Cytochrome b6/f complex SU VII	3562427
Cytochrome oxidase assembly factor COX15	17282119
Deoxyribodipyrimidine photolyase/cryptochrome	17270234
Deoxyribodipyrimidine photolyase/cryptochrome	17277048
Deoxyribodipyrimidine photolyase/cryptochrome	17262103
Deoxyribodipyrimidine photolyase/cryptochrome	17264089
Endonuclease III	17262368
Fatty acid synthase	17283081
Ferredoxin	17250658
Ferredoxin	17285904
Ferredoxin, 2Fe-2S	17259948
Ferredoxin-dependent glutamate synthase	17280450
Ferredoxin-nitrite reductase precursor	17283887
Ferredoxin-sulfite reductase	17256250
Ferredoxin-sulfite reductase	17282643
Ferredoxin-sulfite reductase	17259035
Ferric reductase	17268462
Ferric reductase	17272735
Glutathione S-transferase	19046419
Glutathione S-transferase P	17280036
Hypothetical protein	17263548
Hypothetical protein	



Hypothetical proteins	
Mitochondrial manganese superoxide dismutase	17267818
MRP protein	17269531
NAD(P)H dehydrogenase	19046606
NAD(P)H dehydrogenase	19046606
NADH-cytochrome B5 reductase	17284685
NADPH-cytochrome P450 reductase	17280251
NADPH-cytochrome P450 reductase	17280251
N-glycosylase/DNA lyase	17277269
Peroxiredoxin	19046203
Peroxiredoxin	17264933
Photosystem I subunit III	3562420
Photosystem I subunit III	3562420
Polyketide synthase	17257969
Putative ABC transporter	17280191
Putative Cry-DASH cryptochrome	17261457
Putative Cry-DASH cryptochrome	17257259
Putative cytochrome b5 reductase	17286410
Putative glutathione-S-transferase	17287011
Putative mitochondrial J-type chaperone	17263969
Putative mitochondrial J-type chaperone	17259500
Putative mitochondrial J-type chaperone	17263969
Putative mitochondrial J-type chaperone	17259500
Superoxide dismutase, Cu-Zn	17260763
Superoxide dismutase, manganese	17276920
Thioredoxin	17285654
Thioredoxin reductase	17279611
Thioredoxin reductase	17250239



**Supplemental Table 4.2S.** Irradiance (% referred to sun) through the polyethylene mesocosm material (a) and mesocosm lids transmittance (% referred to lamp) measured with SMS-500 (Ocean Optics LLC, USA) between 200-800 nm. Lamp refers to a Qpanel lamp used for UVA and UVB control. MES refers to mesocosms lids.

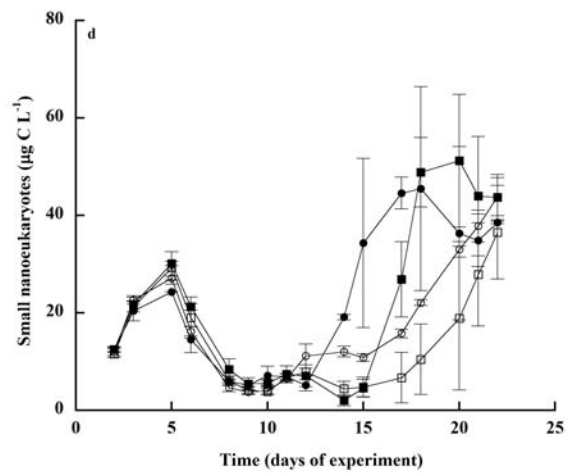
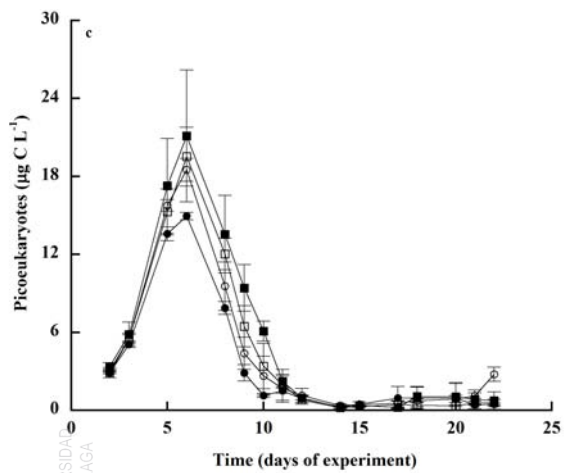
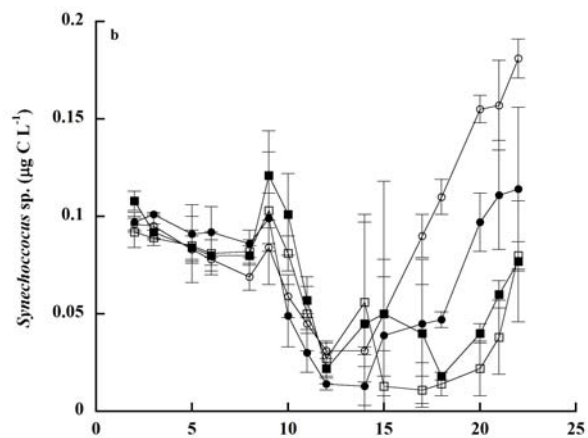
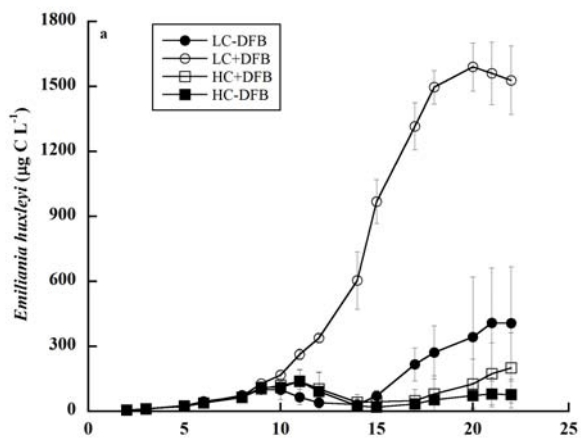
(a)

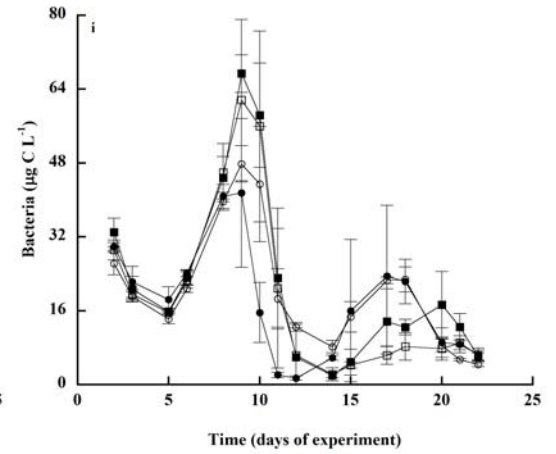
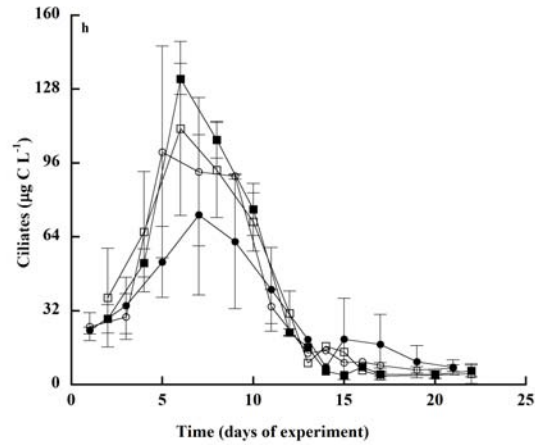
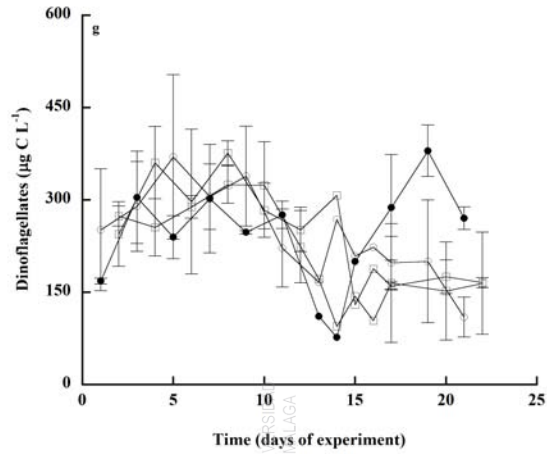
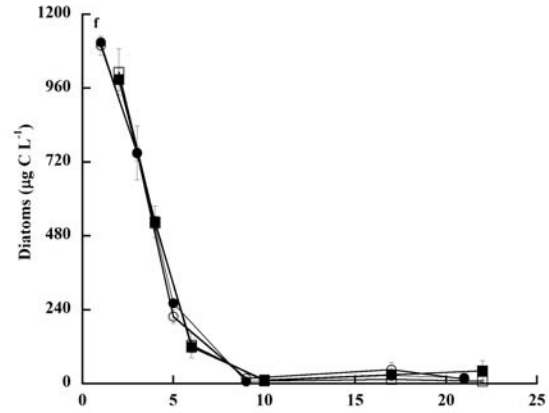
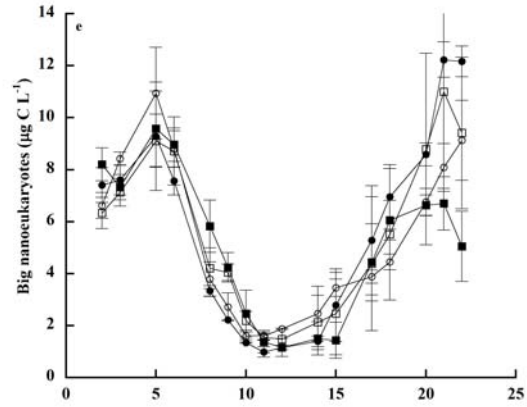
% Transmittance	Mesocosm
PAR	73.33
UVA (320-400 nm)	53.95
UVB (280-320 nm)	67.07

(b)

% Transmittance	Mesocosm lid
PAR	90.45
UVA (320-400 nm)	83.64
UVB (280-320 nm)	80.92

**Supplemental Figure 4.1S.** Temporal development of phytoplankton, microzooplankton and heterotrophic bacterioplankton biomasses ( $\mu\text{gC L}^{-1}$ ) in the mesocosms exposed to different CO<sub>2</sub> and dFe treatments. (a) *Emiliana huxleyi* (5-10  $\mu\text{m}$ ); (b) *Synechococcus* sp., (0.6-2  $\mu\text{m}$ ); (c) picoeukaryotes (0.1-2  $\mu\text{m}$ ); (d) small nanoeukaryotes (Prasinophytes, small Haptophytes, 2-7  $\mu\text{m}$ ); (e) big nanoeukaryotes (small single celled diatoms and flagellated forms, 6-20  $\mu\text{m}$ ); (f) Diatoms (chain forming *Skeletonema costatum*, 20->500 $\mu\text{m}$ ); (g) Dinoflagellates (20-200  $\mu\text{m}$ ); (h) Ciliates (20-200  $\mu\text{m}$ ); (i) heterotrophic bacterioplankton (0.2-0.7  $\mu\text{m}$ ). Symbols (as in Figure 2.1) indicate means of measurements in three independent mesocosms (n=3) except for LC-DFB where n=2. Error bars indicate standard deviations.





## Chapter 5

# **Particulate trace metal dynamics in response to increased CO<sub>2</sub> and iron availability in a coastal mesocosm experiment**

M Rosario Lorenzo\*, María Segovia, Maria T Maldonado

*Manuscript for submission*

## Abstract

Rising concentrations of atmospheric carbon dioxide are causing acidification of the oceans, which will undoubtedly influence marine processes and trace metal biogeochemistry. The importance of trace metals for marine ecosystem functioning has been reported, but the combined impacts of high CO<sub>2</sub> and changes in trace metal availability on plankton remain largely unknown. A mesocosm experiment was performed in the Raunefjord (Norway) to study changes in the trace metal concentrations of particles during a bloom dominated by the coccolithophore *Emiliana huxleyi* under different CO<sub>2</sub> and iron conditions. We employed a full-factorial design, comprising of all combinations of ambient and high pCO<sub>2</sub>, as well as dissolved iron (dFe). Particulate metal concentrations (Fe, Cu, Zn, Co, Mn, Cd, Mo, Ti and Pb) were determined by high-resolution inductively coupled plasma mass spectrometry (HR-ICPMS). This work also aimed to examine the source of particulate metals, either biogenic or lithogenic, and the evolution of both during the experiment. To estimate biogenic metal concentrations from bulk particle measurements we compared: i) the P-normalized quotas with published ratios, and ii) the concentrations of particulate trace metals in the presence and absence of an oxalate-EDTA wash. The two methods were in agreement. Our results also demonstrate that particulate Ti and Fe concentrations were dominated by lithogenic material in the fjord. In contrast, particulate Cu, Co, Mn, Zn, Mo and Cd concentrations were correlated with P concentrations and phytoplankton biomass, emphasizing their strong biogenic component. Furthermore, ocean acidification changed the relative concentrations of particulate metals; a result mainly driven by the effects of ocean acidification on the growth of different phytoplankton phyla. This study is the first to combine trace metal analyses of particles in a controlled mesocosm experiment with manipulation of CO<sub>2</sub> and Fe concentrations using natural assemblages of marine phytoplankton.





## Introduction

Marine phytoplankton contribute to half of the world's total primary productivity, sustaining marine food webs and driving the biogeochemical cycles of carbon and nutrients (Field et al. 1998). Annually, phytoplankton incorporates approximately 45 to 50 billion metric tons of inorganic carbon (Field et al. 1998), removing a quarter of CO<sub>2</sub> emitted to the atmosphere by anthropogenic activities (Canadell et al. 2007). Yet, as a result of anthropogenic CO<sub>2</sub> emissions, the atmospheric CO<sub>2</sub> concentration has increased by 40% since pre-industrial times, producing rapid changes in the global climate system (IPCC 2013). The dissolution of anthropogenic CO<sub>2</sub> in seawater, causes shifts in the carbonate chemical speciation, and leads to ocean acidification. Marine ecosystems are sensitive to changes in pH because pH strongly affects chemical and physiological reactions (Hoffman et al. 2012). Increased CO<sub>2</sub> in seawater is expected to enhance or diminish phytoplankton productivity (Mackey et al. 2015), to decline CaCO<sub>3</sub> production in most planktonic calcifiers (Riebsell & Tortell 2011), and/or to inhibit organic nitrogen and phosphorus acquisition (Hutchins et al. 2009). Thus, the biogeochemical cycling of nutrients is predicted to be greatly affected by ocean acidification (Hutchins et al. 2009). Variations in pH will also affect the distribution and speciation of trace metals in the ocean (Millero et al. 2009).

Trace metals, including Fe, Zn, Mn, Cu, Co, Cd and Mo, are essential for biological functions (e.g. photosynthesis, respiration and macronutrient assimilation). The availability of metals can influence phytoplankton growth and community structure (Morel & Price 2003). In turn, plankton may control the distribution, chemical speciation, and cycling of metals in the ocean (Sunda 2012). The effects of ocean acidification on inorganic metal speciation will be more pronounced for metals that form strong complexes with carbonates (e.g. copper) or hydroxides (e.g., iron and aluminium). In contrast, metals that are mainly in the free ionic form (e.g., manganese or cobalt) or those that form stable complexes with chlorides (e.g., copper and cadmium) will not be greatly affected. Thus, pH



mediated changes in trace metal concentrations and speciation could possibly affect the limitation and/or toxicity of metals to marine plankton (Millero et al. 2009).

Iron is the most essential trace metal for phytoplankton for crucial physiological processes, such as photosynthesis, respiration, and nitrate assimilation (Behrenfeld & Milligan 2013). The decrease in seawater pH has been suggested to promote higher Fe solubility (Millero et al. 2009), but may result in unchanged or lower Fe bioavailability, depending of the nature of strong organic Fe ligands (Shi et al. 2010). Consequently, changes in iron bioavailability due to ocean acidification may affect positively or negatively ocean productivity and CO<sub>2</sub> drawdown. Copper is an essential micronutrient but may be toxic at high concentrations. An increase in free cupric ion concentrations in coastal areas due to ocean acidification (Millero et al. 2009) could result in negative effects on marine phytoplankton. From the open-ocean to coastal areas, the concentration of metals differ, as well as the trace metal requirements of phytoplankton (Sunda & Huntsman 1995a), and the tolerance to metal toxicity. Thus, for example, changes in pH may promote an increase in Cu toxicity in coastal phytoplankton, or enhance Fe limitation in the open ocean. Given that trace metals are essential for phytoplankton productivity, and that are actively internalized during growth, it is important to study the impacts of ocean acidification in trace metal concentrations in ecologically significant plankton species.

A bloom of the coccolithophorid *Emiliana huxleyi* was induced in a mesocosm experiment to examine the interactive effects of increased CO<sub>2</sub> and/or dissolved iron in its growth and physiology. *Emiliana huxleyi* is the most cosmopolitan and abundant coccolithophore in the modern ocean (Paasche 2002). Coccolithophores play a key role in the global carbon cycle because they produce photosynthetically organic carbon, as well as particulate inorganic carbon through calcification. These two processes foster the sinking of particulate organic carbon to the deep ocean (carbon export). However, OA will affect the abundance of



coccolithophores and the rates of calcification and organic carbon fixation (Zondervan et al. 2007). The aim of the present study was to: i) analyse the changes in particulate trace metals concentrations during the bloom of *E. huxleyi*; ii) examine the effects of increased CO<sub>2</sub> and iron levels in particulate trace metals concentrations; and iii) estimate the origin (lithogenic or biotic) of the bloom particulate trace metals.

## Materials and methods

### Experimental set-up

The experimental work was carried out in June 2012 in the Raunefjord, off Bergen, Norway as described in Chapter 2. Twelve mesocosms (11 m<sup>3</sup> each) were set-up in a full-factorial design with all combinations of ambient and high pCO<sub>2</sub> and dFe in three independent replicate mesocosms. The mesocosms were covered by lids (both transparent to PAR and UVR) and filled with fjord water from 8 m depth. We achieved two CO<sub>2</sub> levels corresponding to present (390 µatm, LC) and those predicted for 2100 (900 µatm, HC) by adding different quantities of pure CO<sub>2</sub> gas (Schulz et al. 2009). The specific CO<sub>2</sub> concentration and the CO<sub>2</sub> inlet flows in the mesocosms were measured by non-dispersive infrared analysis by using a Li-Cor (LI-820) CO<sub>2</sub> gas analyser (Li-COR, Nebraska, USA) and CO<sub>2</sub> AirSense-310 sensors (Digital Control Systems, Inc, USA). CO<sub>2</sub> concentrations in the mesocosms were calculated from pH and total alkalinity measurements using the CO<sub>2</sub>SYS software (Robbins et al. 2010). Iron was also manipulated by addition of 70 nM of the siderophore desferrioxamine B (DFB) to half of the mesocosms on day 7, promoting two different iron conditions (+DFB, high dissolved iron; and -DFB, ambient dissolved iron). Dissolved iron concentration increased ~3-fold with respect to the control as a result of increased CO<sub>2</sub> and the addition of DFB. At the beginning of the experiment, nitrate (10 µM) and phosphate (0.3 µM final concentrations) were manipulated to induce a bloom of the coccolithophorid *Emiliania huxleyi*. The multifactorial, experimental design comprised of triplicate



mesocosms per treatment and the combinations of high and ambient pCO<sub>2</sub> and dFe levels, resulting in a total of 12 mesocosms: 3x LC-DFB (control), 3x LC+DFB, 3x HC+DFB and 3x HC-DFB. Water samples from each mesocosm were taken from 2 m depth by gentle vacuum pumping of 25 L volume into acid-washed carboys that were quickly transported to the onshore laboratory. The biological and chemical parameters analysed were cell abundance and composition, dissolved Fe and Cu concentrations, nutrient concentrations (nitrate, phosphate, silicic acid and ammonium) and particulate trace metal concentrations.

### **Dissolved copper**

Low density polyethylene (LDPE) bottles were cleaned using 1% alkaline soap solution for one week, then filled with 6 M trace metal grade HCl and submerged in a 2 M HCl bath for one month, after that they were filled with 1 M trace metal grade HCl (Fisher Chemicals) for one more month and then were kept double bagged. In between each acid treatment, the bottles were rinsed with Milli-Q water (Millipore; hereafter referred to as MQ). Before sampling, the bottles were rinsed three times with filtered seawater. Samples were collected from each mesocosm, filtered through 0.2 µm AcroPak Supor membrane capsule filters into the trace metal clean LDPE bottles, and acidified with ultra-clean HCl (Seastar) in a Class 100 laminar flow hood. Total dissolved Cu concentrations were measured following Zamzow et al. (1998) using a flow injection analysis chemiluminescence detection system (CL-FIA, Waterville Analytical).

### **Particulate metals**

*Sampling-* All equipment used during this study was rigorously acid-washed under trace metal clean conditions, including using dedicated clean areas. Filters were precleaned with 10% trace metal hydrochloric acid (Fisher, trace metal grade) at 60 °C overnight and were rinsed with Milli-Q H<sub>2</sub>O. Seawater samples (1-3.5 L) were filtered gently onto 0.45 µm acid washed Supor®-450 filters on days 12, 17



and 21 of the experiment. Four replicates were taken from each mesocosm. Two filters were analysed without manipulation and the other two were individually washed with oxalate reagent to remove extracellular Fe (Tang & Morel 2006). Following filtration the treated filters were soaked in an EDTA–oxalate solution, 20 mL of oxalate solution was added to the headspace of the Swinnex (Millipore) holders with an acid-washed polypropylene syringe immediately following filtration. After 10 min, vacuum was applied to remove the oxalate solution and 10 mL of 0.2 µM filtered chelexed synthetic oceanic water (SOW) solution was passed through the filter to rinse off any remaining oxalate solution. Replicate filters that were not treated with oxalate solution were transferred directly to centrifuge tubes for storage. The filters with particles were frozen in acid-washed 2 mL PP tubes and then, dried and stored until analysis.

*Analytical methods-* Filters were digested in 7-mL acid-washed Teflon (Teflon, Rochester, NY, USA) vials. Teflon vials were also precleaned using 10% trace metal HCl (Fisher, trace metal grade) during two days and then, with HNO<sub>3</sub> (Fisher, trace metal grade) at 70 °C during three days. In between each acid treatment, the bottles were rinsed with MQ. Samples were digested in 3 mL of HNO<sub>3</sub> and 0.5 mL of HF (Fisher, trace metal grade) with lids on for 1 h on a hot plate at 200 °C. After, the lids were removed to evaporate HF at 200 °C. After this, 1.5 mL of HNO<sub>3</sub> were added and the samples were heated with lids on overnight at 150 °C. Finally, 2.25 mL of HClO<sub>4</sub> (Fisher, Optima grade) were added and the samples were heated for 4 h at 200 °C. After complete digestion, the samples were dried on hot plates at 200°C. The dried samples were dissolved in 1% HNO<sub>3</sub> with 1 ppb In as internal standard. The analysis was performed using a high-resolution inductively coupled plasma-mass spectrometer (HR-ICPMS, Element XR, Thermo Scientific) and the described instrumental settings (Table 5.1). Filter blanks were collected and subjected to the same storage, digestion, dilution, and analysis processes, and these blank values were subtracted from sample measurements. Particulate samples for ICPMS analysis were processed in a trace metal-clean



laboratory under a trace metal-clean laminar flow fume hood.

**Table 5.1.** Instrumental conditions of ICP-MS and measurement parameters used during determination of trace elements concentrations.

<b>Instrument conditions</b>		
Instrument type	ELEMENT XR	
Torch	Fassel type	
Spray chamber	Glass cyclonic spray chamber	
Nebuliser	ESI microflow ST nebuliser (self aspirating)	
Cones	Standard Ni sampler and skimmer	
RF Power (W)	1120	
Cooling gas flow rate (L min <sup>-1</sup> )	16	
Auxiliary gas flow rate (L min <sup>-1</sup> )	0.9	
Sample gas flow rate (L min <sup>-1</sup> )	1.2	
Sample matrix	1% nitric acid	
<b>Method acquisition parameters</b>		
Scan type	E-scan	
Spectral resolution	Low (nominal $m/\Delta m \sim 300$ )	Medium (nominal $m/\Delta m \sim 3000$ )
Isotopes of interest	<sup>95</sup> Mo <sup>98</sup> Mo <sup>111</sup> Cd <sup>114</sup> Cd <sup>206</sup> Pb	<sup>27</sup> Al <sup>31</sup> P <sup>47</sup> Ti <sup>49</sup> Ti <sup>55</sup> Mn <sup>56</sup> Fe <sup>59</sup> Co
Internal standard	<sup>208</sup> Pb	<sup>63</sup> Cu <sup>65</sup> Cu <sup>66</sup> Zn <sup>68</sup> Zn
Mass window (%)	40	125
Samples/peak	10	20
Samples time (ms)	10	10
Runs	3	3
Passes	10	10

### Statistical analyses

Data were checked for normality (by Shapiro-Wilks' test), homoscedasticity (by Levene's test) and sphericity (by Mauchly's test). All data met the requirements to perform parametric tests. Statistical significance of treatment effects was carried out using Split-Plot ANOVA followed by post-hoc Sidak and Bonferroni tests (considering  $p < 0.05$  as significant). All analyses were performed using the General Linear Model (GLM) procedure. The correlation between variables was analysed by Pearson's product-moment multiple comparisons (considering  $p < 0.05$  as significant). Statistical analyses were carried out using SPSS v22 (IBM statistics).



## Results

### Biological and chemical characteristics during the bloom

All the biological and chemical variables measured during the experiment are presented in Table 5.2. At the beginning of the experiment (days 1-10, phase 1), a bloom of large chain diatoms was observed which declined by day 7. This diatom bloom was associated with a sharp decrease in nitrate and silicic acid concentrations. Picoeukaryotes, most likely *Micromonas*, dominated the phytoplankton community on day 8 (Chapter 2). During the first 10 days of the experiment, there were no significant differences in the variables measured between the treatments. On day 7, DFB was added to half of the mesocosms (+DFB treatments). An increase in dFe was observed in all treatments between day 6 and 12. This increase in dFe was sustained for the entire experiment in the DFB treatments (Table 5.2). Dissolved Cu concentrations were not affected by the different treatments (Table 5.2). After day 10, a bloom of the coccolithophore *E. huxleyi* developed under LC+DFB condition, outcompeting the rest of the plankton groups. This bloom was not observed either in the control treatment (LC-DFB) or in the HC treatments, although *E. huxleyi* was still the most abundant species in all treatments; the exception was the HC-DFB treatment.

### Particulate metal concentrations changed during the *Emiliania huxleyi* bloom

The particulate trace-metal concentrations (nmol L<sup>-1</sup>, mean of all treatments and dates) during the development of the bloom of *E. huxleyi* were highest for Al, Fe and Zn, and lowest for Cd, following this trend: Al ≈ Fe ≈ Zn > Ti > Cu ≈ Mn > Mo ≈ Pb > Co > Cd. Over time, significant changes in trace metals concentrations were observed for Fe, Cu, Co, Zn, Cd, Mn, Mo and Pb, while Ti and Al were unaffected (Table 5.3 and Table 5.5). The only metal that showed a decrease over time in its particulate concentration was Fe (Table 5.3, except for LC-DFB, d 17). In general, the treatments with the highest particulate metals concentrations also exhibited the highest particulate P, except for Al, Ti, Fe, and Pb (Table 5.3).



**Table 5.2.** Biological and chemical characteristics of the different treatments; LC: ambient CO<sub>2</sub> (390 µatm); HC: increased CO<sub>2</sub> (900 µatm); -DFB (ambient dFe); +DFB (increased dFe) during the development of a bloom of *Emiliana huxleyi*. All the data except dCu concentration were obtained from Chapter 2. Data are averages of replicate mesocosms and standard deviations are shown in brackets.

Treatment	CO <sub>2</sub> (µatm)	dFe (nM)	dCu (nM)	Nitrate (µM)	Phosphate (µM)	Silicate (µM)	Ammonium (µM)	Dominant size group	<i>E. huxleyi</i> abundance (cell/mL)
<i>Before Emiliana huxleyi bloom (d6)</i>									
LC-DFB	376 (9)	4.62 (0.33)	7.83 (0.83)	2.15 (0.48)	0.05 (0.03)	0.80 (0.20)	0.14 (0.07)	Picoeukaryotes	~1500
LC+DFB	388 (27)	4.45 (0.46)	7.75 (0.29)	2.16 (0.17)	0.05 (0.05)	0.78 (0.22)	0.06 (0.07)	Picoeukaryotes	~1500
HC+DFB	888 (38)	5.46 (0.98)	7.47 (0.45)	1.97 (0.54)	0.04 (0.03)	0.90 (0.08)	0.11 (0.04)	Picoeukaryotes	~1500
HC-DFB	930 (68)	5.27 (0.02)	7.30 (0.22)	2.47 (0.08)	0.04 (0.04)	0.71 (0.31)	0.08 (0.03)	Picoeukaryotes	~1500
<i>d12</i>									
LC-DFB	231 (27)	5.56 (1.85)	8.68 (0.45)	0.03 (0.06)	0.07 (0.06)	0.31 (0.03)	0.80 (0.19)	<i>Emiliana huxleyi</i>	~2000
LC+DFB	278 (33)	6.59 (0.29)	7.83 (0.31)	0.05 (0.04)	0.03 (0.03)	0.49 (0.07)	1.24 (0.13)	<i>Emiliana huxleyi</i>	~10000
HC+DFB	1112 (64)	8.66 (1.19)	7.44 (0.53)	0.02 (0.03)	0.03 (0.01)	0.40 (0.04)	0.61 (0.15)	<i>Emiliana huxleyi</i>	~5000
HC-DFB	1056 (21)	7.46 (0.57)	8.39 (0.23)	0.04 (0.04)	0.02 (0.01)	0.32 (0.03)	0.79 (0.14)	<i>Emiliana huxleyi</i>	~5000
<i>d17</i>									
LC-DFB	245 (31)	3.66 (0.52)	7.54 (0.79)	0.12 (0.11)	0.08 (0.04)	0.37 (0.01)	0.12 (0.06)	<i>Emiliana huxleyi</i>	~6000
LC+DFB	239 (8)	10.38 (1.31)	7.79 (0.35)	0.10 (0.08)	0.08 (0.08)	0.46 (0.03)	0.13 (0.19)	<i>Emiliana huxleyi</i>	~40000
HC+DFB	879 (16)	11.81 (0.30)	7.72 (0.14)	0.04 (0.06)	0.08 (0.06)	0.38 (0.07)	0.65 (0.07)	<i>Emiliana huxleyi</i>	~2000
HC-DFB	804 (29)	10.18 (1.15)	8.04 (0.09)	0.13 (0.07)	0.05 (0.06)	0.30 (0.09)	0.76 (0.33)	Small nanoeukaryotes	< 1000
<i>d21</i>									
LC-DFB	216 (32)	5.61 (0.20)	7.27 (0.11)	0.03 (0.05)	0.10 (0.02)	0.48 (0.02)	0.16 (0.11)	<i>Emiliana huxleyi</i>	~15000
LC+DFB	268 (24)	10.9 (1.25)	7.44 (0.13)	0.03 (0.05)	0.04 (0.03)	0.58 (0.06)	0.39 (0.24)	<i>Emiliana huxleyi</i>	~60000
HC+DFB	768 (49)	9.79 (1.69)	7.61 (0.40)	0.02 (0.05)	0.03 (0.04)	0.50 (0.08)	0.12 (0.10)	<i>Emiliana huxleyi</i>	~7000
HC-DFB	708 (38)	6.02 (0.69)	7.04 (0.34)	0.07 (0.00)	0.04 (0.04)	0.31 (0.01)	0.10 (0.09)	Small nanoeukaryotes	~3000

**Table 5.3.** The concentration of particulate metals in seawater (nmol L<sup>-1</sup>) in the different treatments; LC: ambient CO<sub>2</sub> (390 µatm); HC: increased CO<sub>2</sub> (900 µatm); - DFB (ambient dFe); +DFB (increased dFe) during the development of a bloom of *Emiliania huxleyi*. Data are averages of replicate mesocosms and standard deviations are shown in brackets.

Treatment	Al	Ti	P	Fe	Cu	Co (-10)	Zn	Cd (-100)	Mn	Mo	Pb (-10)
<i>d12</i>											
LC-DFB	9.16 (3.16)	1.30 (0.27)	131.8 (27.05)	13.5 (0.88)	0.24 (0.04)	0.10 (0.06)	3.24 (0.15)	0.28 (0.06)	0.24 (0.06)	0.08 (0.01)	0.25 (0.01)
LC+DFB	29.2 (6.00)	3.16 (0.52)	329.3 (107.8)	14.8 (1.78)	0.30 (0.01)	0.22 (0.05)	14.81 (2.69)	0.91 (0.22)	0.54 (0.14)	0.09 (0.02)	0.56 (0.05)
HC+DFB	11.0 (7.04)	1.23 (0.54)	120.1 (45.49)	7.29 (0.41)	0.32 (0.09)	0.07 (0.01)	3.13 (0.55)	0.26 (0.23)	0.17 (0.06)	0.04 (0.02)	0.12 (0.05)
HC-DFB	18.1 (8.53)	1.28 (0.53)	193.7 (66.43)	11.2 (4.43)	0.29 (0.08)	0.11 (0.07)	4.48 (0.38)	0.23 (0.03)	0.29 (0.13)	0.07 (0.01)	0.85 (0.51)
<i>d17</i>											
LC-DFB	27.1 (14.8)	0.27 (0.14)	171.6 (20.1)	17.1 (8.08)	0.10 (0.04)	0.07 (0.00)	2.87 (1.23)	0.45 (0.32)	0.20 (0.04)	0.08 (0.05)	0.28 (0.11)
LC+DFB	29.2 (19.2)	4.63 (2.84)	972.8 (563)	12.2 (9.14)	1.02 (0.56)	0.68 (0.42)	62.7 (38.2)	2.38 (0.87)	2.36 (1.49)	0.37 (0.08)	0.77 (0.41)
HC+DFB	5.94 (4.38)	0.59 (0.34)	134.1 (47.7)	1.98 (0.76)	0.13 (0.07)	0.05 (0.02)	2.53 (0.49)	0.19 (0.03)	0.14 (0.04)	0.06 (0.03)	0.14 (0.05)
HC-DFB	35.4 (17.9)	4.11 (1.86)	372.7 (253)	9.34 (7.29)	0.50 (0.06)	0.19 (0.02)	5.88 (3.78)	0.98 (0.65)	0.56 (0.42)	0.09 (0.06)	1.42 (0.37)
<i>d21</i>											
LC-DFB	19.2 (1.01)	2.95 (0.06)	341.9 (20.1)	5.83 (1.81)	0.48 (0.02)	0.35 (0.03)	15.5 (0.97)	1.13 (0.26)	0.66 (0.06)	0.10 (0.02)	2.07 (0.26)
LC+DFB	9.18 (5.35)	1.53 (0.55)	380.9 (45.3)	2.52 (0.35)	0.44 (0.06)	0.37 (0.07)	26.2 (2.96)	1.41 (0.25)	0.88 (0.09)	0.20 (0.05)	1.23 (0.75)
HC+DFB	2.64 (1.58)	0.49 (0.40)	95.9 (12.5)	0.53 (0.32)	0.15 (0.06)	0.09 (0.04)	3.24 (1.96)	0.30 (0.16)	0.14 (0.05)	0.05 (0.01)	0.19 (0.05)
HC-DFB	8.22 (2.05)	0.87 (0.20)	134.7 (22.1)	3.19 (1.21)	0.26 (0.05)	0.12 (0.02)	3.47 (0.97)	0.27 (0.13)	0.22 (0.08)	0.08 (0.03)	0.58 (0.18)

On day 12 and 17, the highest particulate metals concentrations were observed in the LC+DFB, while on day 21, they were observed in both LC treatments (Table 5.3).

#### **Increased CO<sub>2</sub> and DFB addition affected metal concentrations**

Increased CO<sub>2</sub> and DFB affected differently trace metals concentrations. Al, Cu, Ti and Pb were not affected by the different treatments. The addition of DFB did not influence the particulate concentrations of Al, Ti, Fe, Cu, Cd, and Pb. CO<sub>2</sub> levels had a negative impact on particulate Fe concentrations. Particulate Cd concentrations were also inversely affected by CO<sub>2</sub>, but mainly in the presence of DFB (CO<sub>2</sub>; and CO<sub>2</sub> x DFB effect, Table 5.5). All other elements (P, Co, Zn, Mn and Mo) exhibited significant effects by CO<sub>2</sub> and DFB, and an interaction between these two factors was clear (Table 5.5). For example, Zn concentrations were higher in the LC treatment, but only with the addition of DFB.

#### **Oxalate-wash reduced all particulate metal concentrations except for Al and Ti**

To better estimate the biogenic fraction of the particulate metals, the filters were washed with an oxalate-EDTA solution, which removes extracellular metals and oxyhydroxides (Tang & Morel 2006). The only two elements unaffected by the oxalate wash were Al and Ti. All other elements showed significantly lower concentrations in the oxalate-treated than untreated samples (Table 5.3 vs. 5.4). The quantity of metal remaining after the oxalate washed (ie. biogenic fraction) varied among elements. Biogenic concentrations of the most labile elements- Pb, Mo, Cd, Zn, Cu and Mn- comprised 30–60% of total particulate metals, while 70–80% of total particulate Co, Fe, and P remained in the biogenic fraction (Table 5.4). In general, after the oxalate wash, the elements showed the highest concentrations in the LC+DFB treatment at the beginning of the bloom (day 12). At the end of the experiment, the highest trace element concentrations were obtained in the LC treatments, except for Pb (Table 5.4).

**Table 5.4.** The concentration of particulate metals in seawater (nmol L<sup>-1</sup>) in the different treatments after oxalate-wash; LC: ambient CO<sub>2</sub> (390 µatm); HC: increased CO<sub>2</sub> (900 µatm); -DFB (ambient dFe); +DFB (increased dFe) during the development of a bloom of *Emiliania huxleyi*. Data are averages of replicate mesocosms and standard deviations are shown in brackets. The percentage (%) indicates the mean quantity of metal remaining after the oxalate wash. Statistically significant differences are indicated with asterisk (\* if p<0.05; \*\* if p<0.01 and \*\*\* if p<0.001; ns: not significant).

Treatment	Al	Ti	P	Fe	Cu	Co (-10)	Zn	Cd (-100)	Mn	Mo	Pb (-10)
<i>d12</i>											
LC-DFB	11.6 (2.8)	1.32 (0.34)	117 (3.27)	12.52 (0.78)	0.16 (0.03)	0.07 (0.00)	1.92 (0.86)	0.09 (0.06)	0.15 (0.02)	0.02 (0.00)	0.10 (0.00)
LC+DFB	28.3 (12)	4.49 (1.91)	258 (46.1)	14.67 (3.35)	0.23 (0.08)	0.19 (0.00)	7.16 (1.29)	0.51 (0.14)	0.41 (0.06)	0.03 (0.01)	0.20 (0.11)
HC+DFB	15.9 (2.3)	2.52 (0.66)	139 (14.2)	8.05 (1.08)	0.22 (0.06)	0.09 (0.01)	2.39 (0.93)	0.20 (0.09)	0.21 (0.07)	0.03 (0.01)	0.11 (0.06)
HC-DFB	11.6 (8.8)	1.66 (0.68)	178 (66.3)	9.79 (3.75)	0.19 (0.08)	0.08 (0.03)	2.84 (0.52)	0.22 (0.06)	0.28 (0.08)	0.02 (0.01)	0.19 (0.08)
<i>d17</i>											
LC-DFB	6.42 (2.9)	0.85 (0.35)	97 (41.6)	1.23 (0.56)	0.11 (0.07)	0.09 (0.05)	2.86 (1.45)	0.26 (0.09)	0.18 (0.07)	0.03 (0.00)	0.09 (0.05)
LC+DFB	7.53 (4.7)	1.85 (0.63)	245 (136)	1.28 (0.68)	0.24 (0.11)	0.22 (0.08)	12.1 (3.78)	1.20 (0.69)	0.54 (0.29)	0.05 (0.03)	0.18 (0.09)
HC+DFB	4.48 (0.2)	1.29 (0.01)	131 (5.31)	1.55 (0.19)	0.14 (0.01)	0.07 (0.00)	3.03 (0.90)	0.21 (0.06)	0.14 (0.02)	0.03 (0.00)	0.10 (0.05)
HC-DFB	12.8 (2.7)	1.98 (0.74)	233 (162)	5.31 (0.99)	0.29 (0.11)	0.18 (0.06)	5.03 (3.06)	0.35 (0.13)	0.43 (0.33)	0.06 (0.01)	0.24 (0.02)
<i>d21</i>											
LC-DFB	13.9 (3.2)	1.54 (0.48)	257 (20.9)	3.76 (0.75)	0.29 (0.06)	0.26 (0.01)	8.59 (0.69)	0.74 (0.31)	0.35 (0.04)	0.05 (0.02)	0.21 (0.08)
LC+DFB	4.36 (0.4)	1.01 (0.41)	253 (47.6)	2.04 (0.63)	0.23 (0.02)	0.20 (0.01)	14.3 (1.32)	0.67 (0.09)	0.43 (0.05)	0.05 (0.01)	0.09 (0.02)
HC+DFB	2.49 (0.9)	0.62 (0.17)	79 (19.6)	0.33 (0.07)	0.11 (0.02)	0.07 (0.03)	2.36 (1.38)	0.09 (0.06)	0.09 (0.03)	0.01 (0.00)	0.03 (0.01)
HC-DFB	2.56 (1.2)	0.98 (0.30)	74 (20.7)	1.03 (0.18)	0.12 (0.03)	0.05 (0.01)	1.01 (0.35)	0.05 (0.02)	0.07 (0.01)	0.02 (0.00)	0.13 (0.01)
%	ns	ns	80*	75*	60*	70*	55**	45***	55**	35***	30***

ns: not significant; \* p<0.05; \*\* p<0.01; \*\*\* p<0.001

**Table 5.5.** Statistical analyses (Split-plot ANOVA) of the effects of CO<sub>2</sub>, DFB, and their interaction, as well as the effect of time, on the concentrations of particulate metals in seawater (A) and on the oxalate-washed concentrations of particulate metals in seawater (B) in the different treatments LC: ambient CO<sub>2</sub> (390 µatm); HC: increased CO<sub>2</sub> (900 µatm); -DFB (ambient dFe); +DFB (increased dFe) during the development of a bloom of *Emiliania huxleyi*. Statistically significant differences are indicated with asterisk (\* if p<0.05; \*\* if p<0.01 and \*\*\* if p<0.001; ns: not significant).

(A)

Factor	Al	Ti	P	Fe	Cu	Co	Zn	Cd	Mn	Mo	Pb
Carbon	ns	ns	**	*	ns	**	***	***	**	***	ns
DFB	ns	ns	*	ns	ns	*	**	ns	*	*	ns
Carbon x DFB	ns	*	**	ns	ns	*	**	*	**	**	ns
Time	ns	ns	ns	***	*	***	***	***	***	***	**

(B)

Factor	Al	Ti	P	Fe	Cu	Co	Zn	Cd	Mn	Mo	Pb
Carbon	ns	ns	ns	ns	ns	***	***	***	*	*	ns
DFB	ns	*	ns	ns	ns	ns	*	ns	ns	ns	ns
Carbon x DFB	ns	ns	*	ns	*	ns	*	*	**	*	ns
Time	**	***	**	***	ns	*	*	*	ns	**	*

ns: not significant; \* p<0.05; \*\* p<0.01; \*\*\* p<0.001



### **After oxalate-wash P, Fe, Co, Zn Mn and Mo were less affected by increased CO<sub>2</sub> and DFB addition**

The effects of CO<sub>2</sub> and DFB on particulate metal concentrations were different for the oxalate-treated and untreated samples. All the elements, except Mn and Cu, showed significant differences over time (Table 5.5). Cobalt concentrations were negatively affected by high CO<sub>2</sub> levels. In contrast, DFB only induced changes in the particulate concentrations of Zn and Ti. Zinc concentrations showed a strong interaction between CO<sub>2</sub> and DFB, and the highest concentrations of this metal occurred in the LC+DFB treatment.

### **Fe and Ti were from abiotic origin**

The Fe:P and Ti:P ratios were relatively similar to crustal ratios. In addition, significant positive correlations were observed between Me:P and Al:P for Fe and Ti (Figure 5.1). These results suggest that particulate Fe and Ti were determined by lithogenic sources. Iron:P and Ti:P were not significantly affected by increased CO<sub>2</sub> and/or DFB addition, but showed significant differences over time (Table 5.7). Samples washed with oxalate-EDTA solution showed significant differences in Fe concentrations due to DFB addition. Furthermore, there was no significant relationship between particulate Fe and Ti concentrations (with or without oxalate wash) with either the total plankton (phytoplankton and microzooplankton) or *E. huxleyi* biomass (Table 5.6).



**Table 5.6.** The relationship (Pearson correlations,  $p < 0.05$ ) between particulate metals concentrations ( $\text{nmol L}^{-1}$ ) and the biomass ( $\mu\text{gC L}^{-1}$ ) of *Emiliana huxleyi* and total cells (phytoplankton and microzooplankton) obtained from Chapter 2 during the bloom.

		P	Fe	Cu	Co	Zn	Cd	Mn	Mo	Pb	Ti
<b>(A) Samples without treatment</b>											
<i>E. huxleyi</i>	Correlation coefficient	0.622	ns	0.614	0.756	0.747	0.818	0.686	0.825	ns	ns
	P-value	0.003		0.003	$7.35 \cdot 10^{-5}$	$1.01 \cdot 10^{-4}$	$6.02 \cdot 10^{-6}$	$5.93 \cdot 10^{-4}$	$4.20 \cdot 10^{-6}$		
Total cells	Correlation coefficient	0.641	ns	0.51	0.644	0.889	0.802	0.598	0.53	ns	ns
	P-value	0.002		0.02	$1.62 \cdot 10^{-3}$	$7.03 \cdot 10^{-8}$	$1.23 \cdot 10^{-5}$	$4.18 \cdot 10^{-3}$	$1.35 \cdot 10^{-2}$		
<b>(B) Oxalate-washed samples</b>											
<i>E. huxleyi</i>	Correlation coefficient	0.647	ns	0.637	0.770	0.758	0.826	0.702	0.819	ns	ns
	P-value	0.002		0.002	$4.52 \cdot 10^{-5}$	$6.79 \cdot 10^{-5}$	$3.92 \cdot 10^{-6}$	$3.86 \cdot 10^{-4}$	$5.68 \cdot 10^{-6}$		
Total cells	Correlation coefficient	0.513	ns	0.569	0.656	0.886	0.809	0.605	0.513	ns	ns
	P-value	0.02		0.009	$1.25 \cdot 10^{-3}$	$9.53 \cdot 10^{-8}$	$8.98 \cdot 10^{-6}$	$3.68 \cdot 10^{-3}$	0.0175		

**Table 5.7.** P-values for the effects of CO<sub>2</sub>, DFB, their interaction and time on the P-normalized metal quotes (A) and on the oxalate-washed concentrations of P-normalized metal quotes (B) during the development of the bloom of *Emiliania huxleyi*. Statistically significant differences are indicated with asterisk (\* if p<0.05; \*\* if p<0.01 and \*\*\* if p<0.001).

A)

Factor	Fe:P	Cu:P	Co:P	Zn:P	Cd:P	Mn:P	Mo:P	Pb:P	Ti:P
Carbon	ns	*	***	**	ns	*	ns	ns	ns
DFB	ns								
Carbon x DFB	ns								
Time	***	***	***	***	ns	ns	ns	ns	***

B)

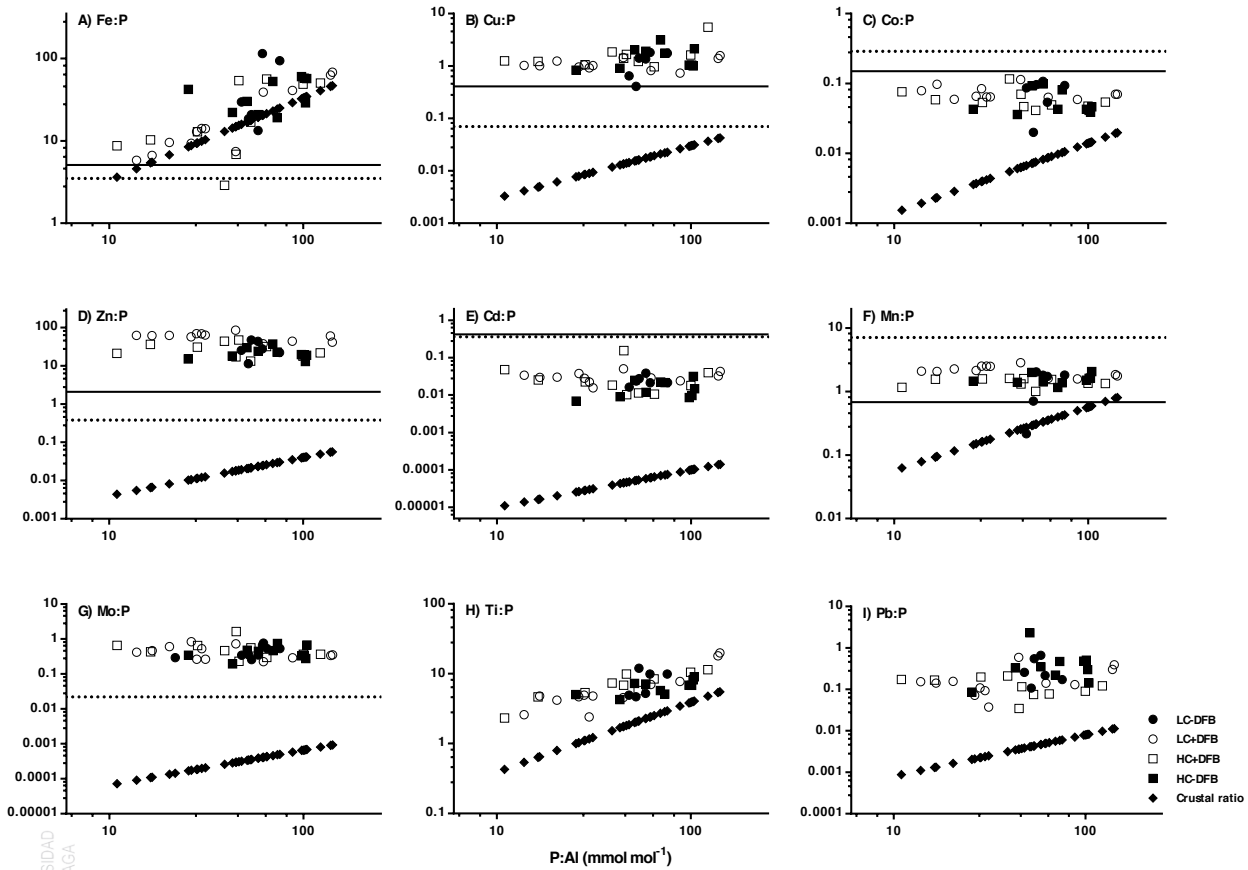
Factor	Fe:P	Cu:P	Co:P	Zn:P	Cd:P	Mn:P	Mo:P	Pb:P	Ti:P
Carbon	ns	**	***	**	***	**	ns	ns	ns
DFB	*	*	**	ns	**	**	ns	ns	ns
Carbon x DFB	ns	ns	ns	ns	*	**	ns	ns	ns
Time	***	*	***	***	***	ns	***	ns	**

ns: not significant; \* p<0.05; \*\* p<0.01; \*\*\* p<0.001

### Co, Cu, Zn, Cd, Mn and Mo were associated with phytoplankton

The comparison of the P-normalized quotas with Al:P showed no correlations with Co, Cu, Zn, Cd, Mn and Mo (Figure 5.1), indicating that these particulate metals were not from lithogenic origin. Compared to trace metal ratios in marine plankton assemblages (Me:P, Ho 2006), our measured ratios were similar for Cu, higher for Mn and Zn, and lower for Co and Cd (Figure 5.1). Furthermore, the metal ratios we measured (Me:P) were higher for Cu, Zn and Mo, and lower for Mn, Co and Cd, than the ratios published for *E. huxleyi* (Figure 5.1). Copper, Co and Zn:P ratios changed significantly over time (Table 5.7). Copper, Co, Zn and Mn:P ratios showed significant effects due to increased CO<sub>2</sub> (Table 5.7). DFB did not affect Me:P ratios of these elements. In contrast, the oxalate-EDTA washed metal ratios (Me:P) for Cu and Co were significantly influenced by DFB (Table 5.7). The oxalate washed samples also presented a significant effect of CO<sub>2</sub> on the Cu:P, Co:P, and Zn:P ratios. An interaction between the effects of CO<sub>2</sub> and DFB was detected in Cd:P and Mn:P ratios (Table 5.7). The concentrations of these metals also showed significant correlations with the biomass of *E. huxleyi* and that of total plankton cells ( $p < 0.05$ ) in both untreated or treated oxalate-washed samples (Table 5.6).

**Figure 5.1.** Comparison of P-normalized metal quotas (mmol:mol P) of particles from different treatments; LC: ambient CO<sub>2</sub> (390  $\mu$ atm); HC: increased CO<sub>2</sub> (900  $\mu$ atm); -DFB (ambient dFe); +DFB (increased dFe) during the development of a bloom of *Emiliana huxleyi*. The x-axis parallel solid and dotted lines represent the average metal quotas obtained from marine plankton assemblages (Ho 2006) and from cultures of *Emiliana huxleyi* (Ho et al. 2003) and, respectively. The symbol  $\blacklozenge$  denotes the average metal: Al in crustal material (Taylor 1964). (A) Fe:P, (B) Cu:P, (C) Co:P, (D) Zn:P, (E) Cd:P, (F) Mn:P, (G) Mo:P, (H) Ti:P, (I) Pb:P.



## Discussion

The purpose of this study was to investigate particulate trace metal concentrations in response to increased CO<sub>2</sub> and iron availability in a coastal mesocosm experiment dominated by a bloom of the coccolithophore *Emiliania huxleyi*. This work also aimed to examine the source of particulate metals, either biogenic or lithogenic, and the evolution of both fractions due to experimental increased iron and/or CO<sub>2</sub> levels. Furthermore, we compared two common approaches to estimate biogenic metal concentrations from bulk particle measurements: comparing the P-normalized quotas with the ratios published for natural assemblages and for *E. huxleyi* cultures (Ho et al. 2003, Ho 2006), as well as with crustal ratios (Taylor 1964). To assess the biogenic fraction of the particulate metals, we also compared the concentrations of particulate trace metals in the presence and absence of an oxalate-EDTA wash, which removes extracellular Fe and P (Sanudo-Wilhelmy et al. 2004, Tovar-Sanchez et al. 2003). The results of the two methods used to calculate biogenic metal concentrations from bulk particle measurements, were in agreement. This study is the first to combine trace metal analyses of particles in a controlled mesocosm experiment with manipulation of CO<sub>2</sub> and Fe levels using natural assemblages of marine phytoplankton. Our results demonstrate that in the studied fjord, particulate Ti and Fe concentrations were dominated by lithogenic material. In contrast, particulate Cu, Co, Mn, Zn, Mo and Cd concentrations were correlated with P concentrations, as well as phytoplankton biomass, suggesting their strong biogenic influence (Table 6). The concentrations of these biogenic metals in our *E. huxleyi* bloom were ranked as: Zn > Cu ≈ Mn > Mo > Co > Cd. The total particulate and biogenic metal concentrations were affected by CO<sub>2</sub> and/or Fe levels, but not all metals were equally affected. Changes in CO<sub>2</sub> had the most significant effect on particulate Fe concentrations. In contrast, the effects of CO<sub>2</sub> on the Me:P ratios were only measured in Co, Cu, Zn, and Mn.



### **Efficacy of the oxalate-EDTA wash removing lithogenic trace metals from particles**

The oxalate–EDTA reagent was developed to remove surface-adsorbed Fe prior to particulate trace metal analyses (Tovar-Sanchez et al. 2003). This reagent works primarily through ligand-promoted dissolution via complexation both to EDTA and oxalate (Tovar-Sanchez et al. 2003, Tang & Morel 2006). In this study, the oxalate wash significantly decreased the concentration of all particulate metals, with the exception of Al and Ti (Table 5.4), as observed by Rauschenberg & Twining (2015). In general, the concentrations of Fe and Co in the particles were decreased the least (by ~25%), while Mo and Pb concentrations were decreased the most (by ~70%) by the oxalate wash. The concentrations of particulate Cu, Zn, Cd and Mn were reduced by 50% by the oxalate wash. As shown previously (Sanudo-Wilhelmy et al. 2004), the oxalate reagent also removed extracellular P (by ~20%). Compared to Rauschenberg & Twining (2015), the estimates of the biogenic fraction, after the oxalate wash, were in agreement for Co, Cu and P, and lower for Fe, Mn, Zn and Cd concentrations. The efficacy of the oxalate wash to dissolve Fe, and other metals, from lithogenic particles is not well constrained (Frew et al. 2006, Rauschenberg & Twining 2015, King et al. 2012). Therefore, the results obtained after the oxalate-EDTA wash are hard to interpret because we do not know whether the removed metal fraction is a) only lithogenic; b) mainly lithogenic but some biogenic fraction is also removed, or c) whether metals absorbed onto particles are equally labile to the wash on biogenic and lithogenic particles. However, some of the trends we observed [eg. higher Me concentrations in the LC+DFB treatments (Table 5.4); or positive correlations between phytoplankton biomass and Me concentrations (Table 5.6)] were identical for the oxalate-EDTA washed and non-washed particles. Thus, below we focus our discussion on the non-oxalate wash results.



### **Particulate elements (P, Cu, Co, Zn, Cd, Mn and Mo) were mainly associated with phytoplankton**

Certain particulate elements (P, Cu, Co, Zn, Cd, Mn and Mo) were clearly biogenic. Three lines of evidence are presented in support of this. First, the total biomass of phytoplankton exhibited a significant positive correlation with particulate P (Table 5.6), showing that most particulate P was biogenic, as shown previously (Ho et al. 2007, Ho et al. 2009). The concentrations of Cu, Co, Zn, Cd, Mn and Mo also exhibited positive significant correlations with the biomass of total cells (phytoplankton and microzooplankton) or *E. huxleyi* (Table 5.6), indicating that these particulate metals were also associated with phytoplankton. Second, the Me:P ratios are not similar to crustal ratios. Third, the Me:P ratios we measured in the particles are similar to those of natural phytoplankton assemblages (Ho 2006) and of *Emiliana huxleyi* cultures (Ho et al. 2003).

The concentrations of biogenic metals in the *Emiliana huxleyi* bloom that we studied were ranked as: Zn > Cu ≈ Mn > Mo > Co > Cd (Table 5.3), similar to those reported in indigenous phytoplankton populations by Twining & Baines (2013; Fe ≈ Zn > Mn ≈ Ni ≈ Cu ≫ Co ≈ Cd). Particulate Zn concentrations were especially high in the LC+DFB treatment, where the highest *E. huxleyi* biomass was observed. The only treatment where *E. huxleyi* did not dominate the community was the HC-DFB. In this treatment, the particulate trace metal ranking was the same, but their concentrations were higher than those in HC+DFB on day 17. At the end of the experiment, the trace metal concentrations in both HC treatments were comparable and, similar effect of both factors (increased CO<sub>2</sub> and the addition of DFB) was observed (lower values in HC treatments, Table 5.3).

The coccolithophorid *Emiliana huxleyi* is well known for its high Zn cellular requirements (Sunda 2012). This essential metal serves as a cofactor in enzymes involved in biochemical processes, such as alkaline phosphatase, RNA polymerase, or superoxide dismutase (Cu/Zn-SOD). An increase in dissolved Zn levels can stimulate the growth of *E. huxleyi* in natural communities but its effect





is less pronounced than that of dissolved Fe (Crawford et al. 2003). The cellular concentrations of Zn, Co and Cd in marine microalgae are highly interdependent (Price & Morel 1990, Sunda & Huntsman 1995b, Jakuba et al. 2008) because these metals have similar size/charge ratios (Zn and Co) or chemical nature (Zn and Cd) and thus can substitute for each other in certain biochemical functions, as it has been demonstrated for *E. huxleyi* (Xu et al. 2007). However, if available, *E. huxleyi* has a preference for Zn (Sunda & Huntsman 1995b). Our results support these findings, showing significantly higher particulate concentrations of Zn, and Zn:P ratios than those of Co and Cd (Table 5.3, Figure 5.1).

Though, it is well known that *E. huxleyi* has higher Zn requirements relative to those of other phytoplankton, the unique physiological functions of Zn in *E. huxleyi* are still unresolved. Indeed, we currently know very little about the molecular mechanisms of zinc acquisition and homeostasis in eukaryotic phytoplankton, and in coccolithophores in particular. However, the presence of genes encoding for Zn-metalloproteins in the *Emiliania huxleyi* genome (Read et al. 2013) provide further evidence for the importance of Zn nutrition in this coccolithophore. For example, we have found  $\alpha$ ,  $\beta$ ,  $\gamma$  and  $\delta$ -carbonic anhydrases annotated genes encoding for enzymes involved in carbon concentrating mechanisms (CCMs). Interestingly, we also found a putative ZIP-transporter gene. ZIP-transporters are involved in Zn uptake, and are able to regulate Zn transport under high Zn to prevent intracellular Zn toxicity. Genes encoding for Zn fingers proteins are also present in the genome. The functions of these proteins are extremely diverse and include DNA recognition, RNA packaging, transcriptional activation, regulation of apoptosis, etc. We also found a putative DNAJ gene (also known as Hsp40 or DNAJ heat-shock proteins encoding gene). These heat-shock proteins protect other proteins from irreversible aggregation during synthesis or stress conditions. Genes encoding for  $\alpha$  and  $\beta$  chains of the RNA polymerase (needed for nucleic acid replication and transcription), alkaline phosphatase (involved in the assimilation of P from organic P compounds), and Cu-Zn



superoxide dismutase (Cu/Zn-SOD, involved in detoxification of reactive oxygen species) were also found in the genome. However, we did not find in the *E. huxleyi* genome other key common Zn-metalloproteins, such as tRNA synthetase, reverse transcriptase, metallo-carboxypeptidase, ABC-Zn-transporter and CDF-Zn-transporter. *Emiliana huxleyi* plays a major role in the global carbon cycle by regulating the exchange of CO<sub>2</sub> across the ocean-atmosphere interface through photosynthesis and calcium carbonate precipitation (Dymond & Lyle 1985). Thus, dissolved Zn could indirectly affect the global C pump by influencing the growth of coccolithophores.

The ratios (Me:P) obtained for Cu, Co, Cd and Mn in this study were similar to those obtained in a study in North Atlantic (Tovar-Sanchez 2006, Nuester et al. 2012). The Co:P and Mn:P were also close to published phytoplankton ratios (Figure 5.1). The dissolved and particulate Cu concentrations in our experiment were high, and similar to those measured in this fjord previously (Muller et al. 2005). The Cu:P ratios were mainly biogenic, but the values were relatively elevated compared to those of other phytoplankton (Ho et al. 2003, Ho 2006). Rain events in this fjord result in high dissolved Cu and the active production of strong organic ligands by *Synechococcus*—to lower the free Cu concentrations (Muller et al. 2005). Therefore, high Cu might be a general condition in this fjord, and indigenous plankton might have developed physiological mechanisms to deal with high Cu, such as the production of organic ligands to prevent uptake (Vraspir & Butler 2009), or of heavy-metal-binding peptides (phytochelatins) to lower Cu toxicity inside the cell (Ahner & Morel 1995, Ahner et al. 1995, Knauer et al. 1998). Given that we measured high particulate Cu in our experiment but comparable to previous studies (Muller et al. 2005), *E. huxleyi* might have been relying mainly on phytochelatins to buffer high intracellular Cu or on other detoxification mechanisms (Ahner et al. 2002). Indeed, in the genome of *E. huxleyi*, we found a gene encoding for a hypothetical protein with high homology to a phytochelatin synthase. Alternatively, Cu might be particularly important for





the growth of this coccolithophore, as indicated by a culture study with a coastal strain, which had high Cu requirements to maintain maximum growth rate regardless of Fe levels in the media (Guo et al. 2012). Therefore, the high concentrations of particulate Cu in the *E. huxleyi* bloom might be due to high dissolved Cu concentration in the fjord, unregulated uptake and/or high Cu requirements.

The Cd:P were significantly lower than those found in phytoplankton and *E. huxleyi*. This was surprising, because Cd quotas are normally higher in coccolithophores than in diatoms and chlorophytes (Sunda & Huntsman 2000, Ho et al. 2003). Ho et al. 2009 proposed that the high Cd quotas in coccolithophores could be caused by accidental uptake through Ca transporters and channels. The low Cd quotas here may be explained by the antagonistic interaction between Mn and Cd or Zn and Cd under high Mn and Zn, respectively (Sunda & Huntsman 1998, 2000, Cullen & Sherrell 2005). The high Zn:P ratios in this study indicate high bioavailability of Zn. Our Mn:P ratios were below those in cultures of *E. huxleyi* (Ho et al. 2003). However, in this published study, *E. huxleyi* was grown in the presence of high Mn concentrations (Ho et al. 2003), thus its Mn:P ratios are expected to be higher than those required, and may represent luxury Mn uptake. In addition, differences between the Me:P ratios in this experiment and those in previous studies could simply imply different growth conditions (e.g. light levels, macronutrient concentrations, etc.) and the dominance of a few algal species, such as *Emiliana huxleyi* (Ho et al. 2006).

### **Fe in bulk particles was mainly lithogenic**

Iron enrichment is common in coastal waters, due to sediment resuspension, rivers input, aeolian deposition and mixing or upwelling of deep water. The metal with the highest particulate concentrations in our study was Fe (Table 5.3). Furthermore, particulate Fe and Ti were the only metals with positive correlations



with Al and without correlation with phytoplankton biomass (Figure 5.1, Table 5.5), indicating a strong lithogenic component. The similarity between our values Fe:P values and that of the crustal ratio (Figure 5.1) also supports this finding. Indeed, the Fe:P ratios were significantly higher than those of indigenous plankton assemblages and phytoplankton cultures (Figure 5.1). We believe that the lithogenic fraction of Fe in the bulk particles in our experiment masked the biogenic signal, as proposed by King et al. 2012. Interestingly, the particulate Fe concentration ( $\text{nmol L}^{-1}$ ) decreased between days 12 and 21 (Table 5.3 and 5.5); this could be due to the solubilisation of particulate Fe to the dissolved phase, as demonstrated by the increase in dissolved Fe in treatments with high  $\text{CO}_2$  and/or the addition of DFB (Table 5.1). The sinking of pFe could have resulted in less pFe, as indicated by the lowering of the ratio between the concentration of Fe in particles and that in the dissolved phase (i.e. partition coefficient, Supplemental Figure 5.S2).

### **Effects of high $\text{CO}_2$ and dissolved Fe levels on particulate metal concentrations and Me:P ratios**

The concentrations of particulate Al, Ti, Pb and Cu, were unaffected by changes in  $\text{CO}_2$  and/or iron levels. However, high  $\text{CO}_2$  clearly decreased the concentration of particulate Fe (an increased dissolved Fe) as predicted by Millero et al. (2009). The decreased in particulate Fe might have been due to the abundance of Fe hydroxides in the fjord, and the enhanced solubility of these oxides at low pH. Finally, the concentration of the elements P, Co, Zn, Mn and Mo were influenced by  $\text{CO}_2$  and Fe levels, but the interaction between these factors was complex. In general, the highest Me ratios for P, Co, Zn, Mn and Mo were observed in the LC+DFB treatment, where the addition of DFB resulted in higher dissolved Fe, and optimal pH enhanced *E. huxleyi* growth. This promoted metal accumulation in biogenic particles. Elevated  $\text{CO}_2$  levels in the mesocosms had a significant effect



on the Me:P ratios of Cu, Co, Zn, and Mn. For example, while Zn:P and Mn:P ratios were higher under low CO<sub>2</sub>, those of Co:P were higher under high CO<sub>2</sub>. Thus, the CO<sub>2</sub> effects did not follow a clear trend and were sometimes positive and other times negative.

### Concluding remarks

Particulate trace metal ratios are especially useful for modelling plankton processes and nutrient cycling, as well as for estimating primary productivity after the supply of limiting nutrients. Likewise, knowledge of trace metal composition of marine phytoplankton may allow us to determine how microalgae can influence the relative distribution and vertical transport of trace metals in the ocean. The results presented here showed that except for Ti and Fe, the trace metal concentrations of marine particles during a bloom of *Emiliana huxleyi* are a) highly dynamic, b) positively correlated with plankton biomass, c) influenced by growth requirements, and d) strongly affected by changes in CO<sub>2</sub> and dissolved Fe. According to our results, ocean acidification will decrease *E. huxleyi* abundance, and as a result, the concentration of some particulate trace metals that are especially high in *E. huxleyi*, like Zn. Most importantly, OA is expected to change the relative concentrations of particulate metals, due to the differential effects of OA on the growth of marine phytoplankton species, and the contrasting metal requirements of phytoplankton phyla. Therefore, as suggested by Twining & Baine (2013), we require the development of ecophysiological models that link trace element composition of phytoplankton to physiological performance, as well as ecological models that determine effective strategies in changing environmental conditions.



### **Acknowledgments**

This work was funded by CTM/MAR 2010-17216 (PHYTOSTRESS) research grant from the Spanish Ministry for Science and Innovation (Spain) to MS. MRL was funded by a FPU grant from the Ministry for Education (Spain). MRL was also funded by fellowships associated to the above mentioned research grants to carry out a short-stay at MTM and JTC laboratories to analyse dissolved and particulate metals. We thank all the participants of the PHYTOSTRESS experiment for their collaboration.

## Supplemental Material

**Supplemental Table 5.1S.** P-values for the effects of CO<sub>2</sub>, DFB, their interaction and time on the Al-normalized metal quotes during the development of the bloom of *Emiliana huxleyi*. Statistically significant differences are indicated with asterisk (\* if p<0.05; \*\* if p<0.01 and \*\*\* if p<0.001). The comparison reflects if the filters treated with oxalate wash present more factors with statistically significant differences and blank values means that both treatments present the same significative factors.

A)

Factor	Fe:Al	Cu:Al	Co:Al	Zn:Al	Cd:Al	Mn:Al	Mo:Al	Pb:Al	Ti:Al
Carbon	ns	ns	ns	*	ns	ns	ns	ns	ns
DFB	*	ns	**	***	**	**	***	ns	*
Carbon x DFB	ns	ns	ns	*	ns	*	ns	ns	ns
Time	**	*	**	**	**	ns	*	*	*

B)

Factor	Fe:Al	Cu:Al	Co:Al	Zn:Al	Cd:Al	Mn:Al	Mo:Al	Pb:Al	Ti:Al
Carbon	*	ns	ns	**	***	ns	ns	ns	ns
DFB	*	*	**	***	***	**	**	ns	**
Carbon x DFB	ns	ns	ns	*	**	ns	*	ns	ns
Time	***	***	***	***	***	*	***	*	**
Compare with oxalate wash	Yes	Yes	-	-	Yes	No	Yes	-	-

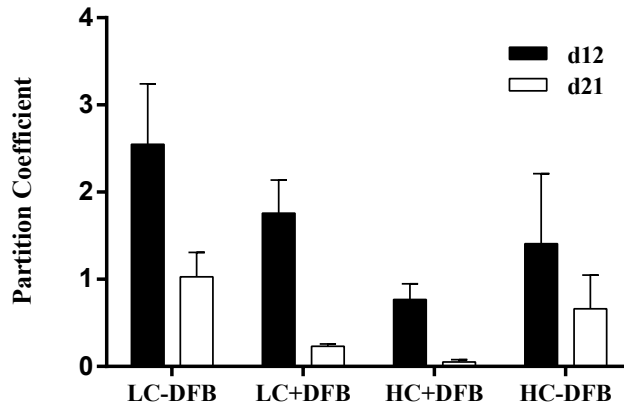
ns: not significant; \* p<0.05; \*\* p<0.01; \*\*\* p<0.001

**Supplemental Table 5.2S.** Identified Zn-Metalloproteins genes in the genome of *Emiliania huxleyi* (Read et al. 2013), encoding for the corresponding following proteins.

Gene name	ID
Alkaline phosphatase	17253330
Carbonic anhydrase	17257927
$\alpha$ carbonic anhydrase	17284926
$\alpha$ -type carbonic anhydrase	17277840
$\beta$ carbonic anhydrase	17269168
$\delta$ carbonic anhydrase	17265607
$\gamma$ carbonic anhydrase	17260688
$\gamma$ carbonic anhydrase	17282862
DNL zinc finger protein	17285443
DNL zinc finger protein	17254351
Mitochondrial RNA polymerase	17251597
NAD(P)H dehydrogenase	19046606
NADPH-cytochrome P450 reductase	17280251
Phytochelatin synthase	
Putative alkaline phosphatase	17271603
Putative DNAJ	17273860
Putative DNAJ	17263200
Putative zinc transporter	17276740
Superoxide dismutase, Cu-Zn	17260763
Zinc finger-containing protein	17280277
Zinc finger-containing protein	17272883
Zinc finger-containing protein	17282784
Zinc finger-containing protein	17262888

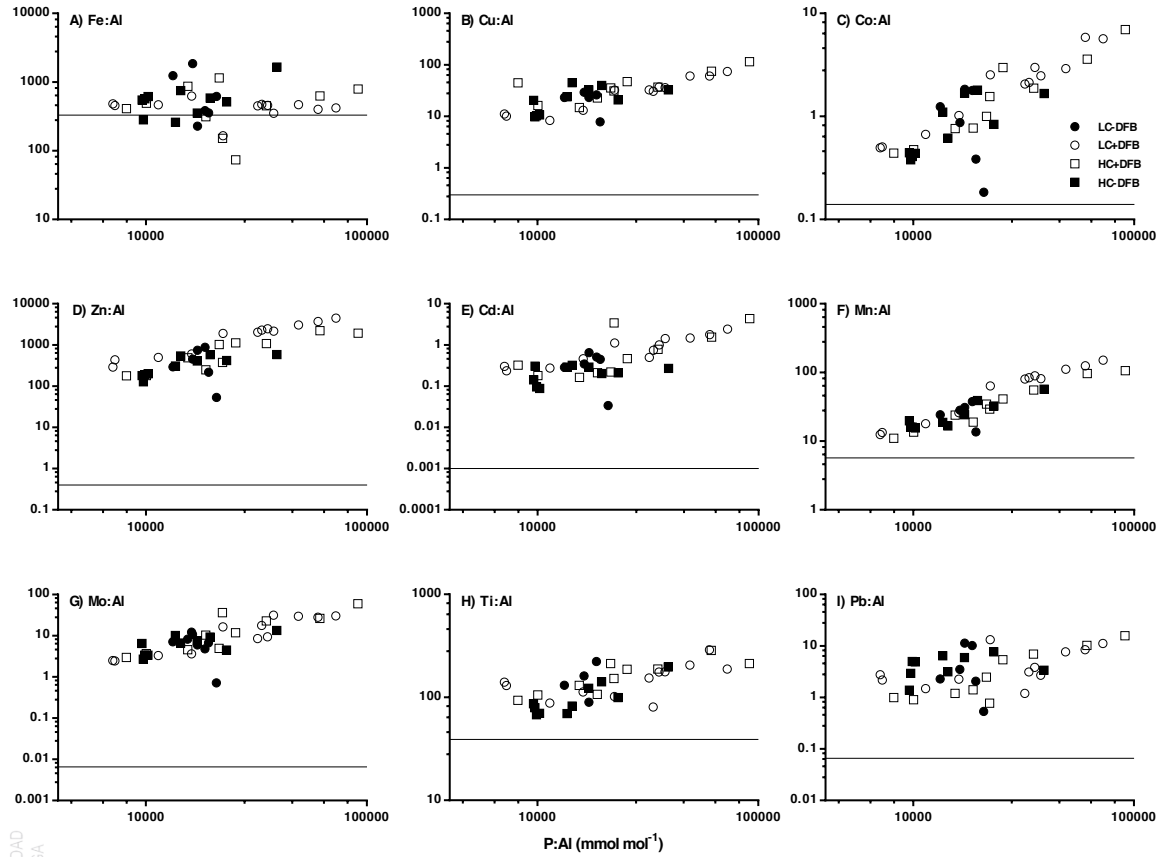


**Supplemental Figure 5.1S.** The partition coefficients in the different treatments; LC: ambient CO<sub>2</sub> (390 μatm); HC: increased CO<sub>2</sub> (900 μatm); -DFB (ambient dFe); +DFB (increased dFe) at the beginning and the end of the bloom.



**Supplemental Figure 5.2S.** Comparison of Al-normalized metal quotas (mmol:mol Al) of particles from different treatments; LC: ambient CO<sub>2</sub> (390 μatm); HC: increased CO<sub>2</sub> (900 μatm); -DFB (ambient dFe); +DFB (increased dFe) during the development of a bloom of *Emiliania huxleyi*. The x-axis parallel solid lines represent the crustal ratio (Taylor, 1964) (A) Fe:Al, (B) Cu:Al, (C) Co:Al, (D) Zn:Al, (E) Cd:Al, (F) Mn:Al, (G) Mo:Al, (H) Ti:Al, (I) Pb:Al.





## Chapter 6

# ***In vitro* physiological response of *Emiliana huxleyi* to increased CO<sub>2</sub>, Fe limitation and UV radiation:**

### **6.1. Effects of elevated CO<sub>2</sub> in the coccolithophore *Emiliana huxleyi*: Effects on growth, photosynthesis, calcification and spectral sensitivity of photoinhibition**

M Rosario Lorenzo\*, Patrick J Neale, María Segovia

*Manuscript for submission*

### **Abstract**

We studied the effects of elevated CO<sub>2</sub> concentrations on cell growth, photosynthesis, calcification and susceptibility of photosynthesis to ultraviolet radiation (UVR) in the coccolithophore *Emiliana huxleyi*. The susceptibility of photosynthesis to UVR was estimated by using biological weighting functions (BWFs) for the inhibition of photosynthesis and a model that predicts primary productivity under photosynthetically active radiation (PAR) and UVR exposures. The photosynthetic response vs. weighted exposure revealed that there is a threshold above which photosynthesis is inhibited because of the repair rate is limited during exposure to high radiation (“*T* model”). However, the mechanisms that limit the repair rate are still unknown. Our results indicate that the sensitivity to UVR will be the same at ambient and high CO<sub>2</sub> (future predicted) conditions in the strain of *Emiliana huxleyi* used. We propose that there is a downregulation of the mechanisms of incorporation of inorganic carbon and the formation of the coccoliths, saving this energy for other mechanisms such photosynthesis without altering the mechanisms for UVR defense. Finally, it is important to consider the wide range of different responses to ocean acidification of *Emiliana huxleyi*, due to the differences presented between strains or to different experimental conditions including temperature, levels of CO<sub>2</sub>, irradiance and nutrients availability.



## Introduction

The atmospheric concentration of carbon dioxide (CO<sub>2</sub>) has increased by 40% since pre-industrial times due to anthropogenic activities. The 5<sup>th</sup> IPCC report (2013) predicts an increase in the atmospheric CO<sub>2</sub> concentration above 900 μatm by the end of this century for the worst-case scenario (Representative Concentration Pathway (RCP) 8.5). Unfortunately the values predicted by RCP 8.5 match the measured concentrations in the atmosphere to date. The oceans are absorbing most of the anthropogenic emissions of CO<sub>2</sub>, which not only affects the quantity and speciation of the dissolved inorganic carbon (DIC) in the ocean, but also decreases the pH of the seawater (Doney et al. 2009). These changes in pH affect the biogeochemical and physiological processes in marine ecosystems (Hoffman et al. 2012). Thus, increased CO<sub>2</sub> is expected to have direct impacts on the physiological responses of primary producers such as phytoplankton among other organisms (Riebesell & Tortell 2011, Mackey et al. 2015). Phytoplankton play a key role in determining the effects of environmental change on the ocean surface since it is responsible for around 50% of the net amount of carbon assimilated annually by photoautotrophs (Field et al. 1998). Apart from acidification, global warming enhances stratification, which reduces nutrient availability in the euphotic layer by strengthening and shoaling of the thermocline (Boyd & Doney 2002, Polovina et al. 2008). Depth of the surface mixed layer, on the other hand, is determined by the balance between surface forces causing vertical mixing vs stratification (both affected by global warming), future shifts in this balance are expected to be regionally dependent (Boyd & Doney 2002). Accordingly, phytoplankton in the open ocean would be exposed to increasing CO<sub>2</sub> concentrations, low nutrient concentrations and regionally variable changes in average surface layer irradiance.

Global change also affects exposure of phytoplankton in surface waters to solar ultraviolet B (UVB, 280–320 nm) and ultraviolet A (UVA, 320–400 nm) penetration in surface waters through changes in the stratospheric ozone



concentration, cloud cover and levels of dissolved organic matter (Zepp et al. 2007). Although the production and use of CFCs has been curtailed since the Montreal Protocol (Bancroft et al. 2007), UV radiation (UVR) is still considered a global change stressor. This is due to the long time required for ozone recovery (McKenzie et al. 2011, Shanklin 2010) and the interactive effects with other global change drivers are also affecting stratospheric dynamics and temperature, delaying the ozone layer recovery (Weatherhead & Andersen 2006).

UVR causes deleterious effects on the physiological performance and growth of marine phytoplankton and other organisms (Häder et al. 2011). The estimation of the sensitivity to UVR exposure in relation to wavelength can be quantified by biological weighting functions (BWFs) (reviewed by Neale 2000). They allow comparison between responses to different wavelengths of UVR as well as photosynthetically available radiation (PAR, 400-700 nm) and can be utilized to predict effects given an appropriate exposure response model.

Change in several variables may not result in a simple additive response relative to that occurring by a given variable alone (Boyd & Hutchins 2012), they can produce either synergistic or antagonistic effects (Folt et al. 1999). Accordingly, it has been observed that the effects of UVR are modulated by other environmental factors such as light availability, nutrient limitation and levels of dissolved CO<sub>2</sub> (Beardall et al. 2009, 2014). Some studies have shown that the increase in CO<sub>2</sub> concentrations affected the sensitivity of phytoplankton photosynthesis to inhibition by solar irradiance (Sobrino et al. 2005, 2008, 2009, Gao et al 2009, 2012). These studies did not show a unique pattern of the interactive effects of UVR and increased CO<sub>2</sub>, but confirmed that they depend on the species suggesting that the interactions between elevated CO<sub>2</sub> and UVR may produce changes in the taxonomic composition of phytoplankton assemblages (Beardall et al. 2009).



Coccolithophores (Haptophyta) play a major role in the global carbon cycle by contributing ca. 1–10% to total organic carbon fixation (Poulton et al. 2007) and approximately 50% to pelagic deep ocean CaCO<sub>3</sub> sediments (Broecker & Clark 2009). In particular, *Emiliana huxleyi* is the most common bloom forming species (Brand 1994) and the most abundant and widespread coccolithophore in the world ocean (Paasche 2002). It is expected that ocean acidification will affect the abundance of coccolithophores and the rates of calcification and organic carbon fixation (Zondervan et al. 2007).

The objective of this study was to analyse the effects of elevated CO<sub>2</sub> conditions on the physiological response of *Emiliana huxleyi*. The response was focused on the effects on growth, photosynthesis and calcification under non-photoinhibitory exposures but also under damaging conditions through the assessment of exposure response curves and spectral dependence weighting functions (BWFs) for UV and PAR inhibition of photosynthesis.

## Material and methods

Cultures of *Emiliana huxleyi* (RCC #1226) were provided by the Roscoff Culture Collection and grown at constant aeration in two different treatments: (1) ambient CO<sub>2</sub> (400 ppm CO<sub>2</sub>) and (2) high CO<sub>2</sub> (800 ppm CO<sub>2</sub>) (CO<sub>2</sub> provided by Air products). Aeration with 800 ppm CO<sub>2</sub> changed the pH of the media from 8.14 to 7.84. The two CO<sub>2</sub>-conditions were verified by measuring the pH in the seawater and determining dissolved inorganic carbon (DIC) by using the standard inorganic carbon protocol for the Shimadzu TOC-V analyser. Growth irradiance was provided by cool white fluorescent lamps on a 14 h light:10 h dark photoperiod at an irradiance of 170–180  $\mu\text{mol photons m}^{-2} \text{s}^{-1}$ . Growth PAR was measured with a 4- $\pi$  probe immersed in water inside the culture flasks. The growth medium consisted of filtered seawater from the Sargasso Sea enriched with f/2 nutrients with Fe concentration reduced by half (Guillard & Ryther 1962). The experiments were carried out in the middle of exponential growth phase and repeated at least three



times with independently grown cultures for each treatment. Cell numbers were counted every day with a Neubauer hemacytometer. The growth rate ( $\mu$ ,  $d^{-1}$ ) was calculated as  $\ln(N_2/N_1)/t$ , where  $N_1$  and  $N_2$  are the cell concentrations, and  $t$  is the time between samples (d).

### **Maximum photosynthetic efficiency of PSII**

A pulse amplitude-modulated fluorometer Diving PAM/B (Walz) with blue light-emitting-diode (LED; 470 nm) excitation was used to assess the maximum photosynthetic efficiency of the cultures at different times during the experiment. The data are expressed as the photosystem II (PSII) quantum yield measured in low light acclimated samples,  $F_v:F_m = (F_m - F_0):F_m$ , which has been correlated with the maximum quantum yield of photosynthesis (Genty et al. 1989).  $F_0$  is the steady-state yield of *in vivo* chlorophyll fluorescence of phytoplankton under low light acclimated conditions, and  $F_m$  is the maximum yield of fluorescence obtained from an illuminated sample after a saturating light pulse (400-ms pulse duration) has been applied.

### **Chlorophyll concentration and cellular absorbance**

Chlorophyll concentration was measured on aliquots concentrated on glass-fiber filters (GF/F, Whatman Inc.) and extracted with 90% acetone overnight at  $-20\text{ }^{\circ}\text{C}$ . After extraction, fluorescence was measured before and after acidification on a Turner 10-AU fluorometer. Cellular pigment absorbance ( $a_p(\lambda)$ ,  $\text{m}^2 \text{mg Chl } a^{-1}$ ) was measured using the quantitative filter technique (QFT) as described in Cleveland & Weidemann (1993). Cells concentrated on the filters were scanned from 280 to 750 nm in a Cary 4 dual-beam spectrophotometer, using a blank filter wetted with filtrate as a reference. The filter was extracted with 100% methanol, washed with filtrate, and rescanned using a similar procedure as for the non-extracted filter.



### Photosynthesis measurements

The photosynthetic response to UVR was performed using a polychromatic UV+ PAR incubator that uses a 2.5 kW xenon lamp (“photoinhibitron”), based on the design of Cullen et al. (1992) with modified block construction similar to that described by Smyth et al. (2012).

Photosynthesis was measured as total incorporation of acid stable  $^{14}\text{C-HCO}_3^-$  during 1 h of incubation. Details of the photoinhibitron are given in Neale et al. (2014). The incubator emits PAR, UVA and UVB in similar proportions as solar irradiance, allowing the assessment of realistic responses. Long-pass filters were used to define a total of 12 spectral treatments per incubation, which were combined with neutral density screens to produce ten irradiances for a total of 120 treatments of varying spectral composition and irradiance. The filter combinations are listed in Table 6.1.1. Spectral irradiance ( $\text{mW m}^{-2} \text{nm}^{-1}$ ) for each position in the photoinhibitron was measured with a custom-built fiber-optic radiometer as described by Neale & Fritz (2001).

Data were fit to BWF/P-E functions:

$$P^B = P_s^B \cdot (1 - e^{-E_{\text{PAR}}/E_s}) \cdot \text{ERC} (E_{\text{inh}}^*)$$

$$E_{\text{inh}}^* = \sum_{265\text{nm}}^{400\text{nm}} \epsilon(\lambda) \cdot E(\lambda) \cdot \Delta\lambda + \epsilon_{\text{PAR}} \cdot E_{\text{PAR}}$$

where  $P^B$  is photosynthetic rate per unit chlorophyll ( $\text{mg C mg Chl}^{-1} \text{h}^{-1}$ ),  $P_s^B$  is the light-saturated rate of photosynthesis, ERC is the exposure response curve for inhibition of photosynthesis,  $E_{\text{inh}}^*$  is a dimensionless index for biologically effective or weighted irradiance,  $\epsilon(\lambda)$  is biological weight of inhibitory effect of UV ( $\text{m}^2 \text{mW}^{-1}$ ) at  $\lambda$  and  $\epsilon_{\text{PAR}}$  is biological weight of inhibitory effect of PAR ( $\text{m}^2 \text{mW}^{-1}$ ).  $E(\lambda)$  is spectral irradiance ( $\text{mW m}^{-2} \text{nm}^{-1}$ ) at  $\lambda$  (265-400 nm) and  $E_{\text{PAR}}$  is PAR irradiance (400-700 nm).



**Table 6.1.1.** Filter configuration for the 12 spectral treatment groups of the photoinhibitor as used in this study. Table taken from Neale et al. 2014.

	Nominal cutoff		Components
	% of PAR T		
	1%	50%	
A	268	291	WG280
B	285	300	WG280 x 2 <sup>a,b</sup>
C	290	300	WG280 + Cellulose Acetate <sup>b</sup>
D	283	303	WG305
E	290	309	WG305 x 2
F	291	306	WG305 + Cellulose Acetate
G	302	312	WG320
H	308	325	WG320 x 2
I	320	335	WG335
J	312	346	WG295 + LG350 <sup>c</sup>
K	358	375	WG295 + LG370
L	386	408	GG395 + Coutergard <sup>d</sup> x 2

<sup>a</sup> All Schott filters were 3 mm thick; “x 2” denotes that two pieces of filter glass or film were combined, doubling the effective pathlength (thus red-shifting the cutoff wavelength, especially for 1 % T).

<sup>b</sup> All filter combinations (either two pieces of filter glass or filter glass + film as indicated) were assembled with a high-purity silicone optical grease. This decreased variation in the index of refraction along the optical path and minimized scattering. Filter–filter or filter–film combinations had the same transmittance in the visible as single layer elements.

<sup>c</sup> LG filters are manufactured by Corion and contain a polymer film sandwiched between two glass layers. The WG295 “prefilter” protected the polymer film from solarization by the short-wavelength irradiance from the xenon arc lamp.

<sup>d</sup> Courtgard, a film manufactured by Solutia, Inc, blocks UV below 400 nm.



BWF were estimated from the measured rates of photosynthesis using non-linear regression and principal component analysis (PCA). Details of the principal-component-based estimation procedure and error assessment are given in Cullen & Neale (1997). Standard error for the parameter means over-replicate experiments ( $n \geq 3$ ) are the root mean square (rms, quadrature) of the estimation standard errors (propagated from regression standard errors) and the standard error due to between-replicate variability. The BWF fits were performed using three different response models (ERCs) to determine the proper exposure – response model at high exposure. The “ $E$  model” is used to model responses to UV as measured in the photoinhibitor (Cullen et al. 1992) and the response (“repair”) is proportional to inhibition (“damage”) at all exposures.

$$\frac{P^B}{P_{pot}^B} = \frac{1}{1 + E_{inh}^*}$$

The “ $T$  model” determines the presence of a threshold ( $E_{inh}^* = 1$ ) above which, by definition, photosynthesis is inhibited. Compared to the  $E$  model, this model was significantly better at fitting observations at high  $E_{inh}^*$  in several studies of cultures and natural assemblages (Sobrino et al. 2005, 2008, 2009). However, the imposition of a threshold in the  $T$  model has the disadvantage of ignoring the effects of UV and PAR at low exposures.

$$\frac{P^B}{P_{pot}^B} = \begin{cases} 1 & E_{inh}^* \leq 1 \\ \frac{1}{E_{inh}^*} & E_{inh}^* > 1 \end{cases}$$

And finally, the “ $E_{max}$  model” uses a combination of the  $E$  model at low exposures and  $T$  model at high exposures. The new  $E_{max}$  parameter defines the transition between the exposure range over which repair rate increases with damage and



higher exposures for which repair rate is constant (i.e., operating at some maximum rate).

$$\frac{P^B}{P_{pot}^B} = \begin{cases} \frac{1}{1 + E_{inh}^*} & E_{inh}^* \leq E_{max}^* \\ \frac{1}{C E_{inh}^*} & E_{inh}^* > E_{max}^* \end{cases}$$

$$C = \frac{1 + E_{max}^*}{E_{max}^*}$$

The relation between repair and damage of each of the models is represented in Figure 6.1.1. The  $E_{max}$  model has an additional parameter compared to the  $E$  and  $T$  model. Whether sufficient increase in explained variance is gained to justify the incorporation of an additional parameter was assessed by evaluation of the Akaike information criterion (AIC; Andersen et al. 2005) for each of the fits using the Matlab NonLinearModel function (Statistics toolbox).

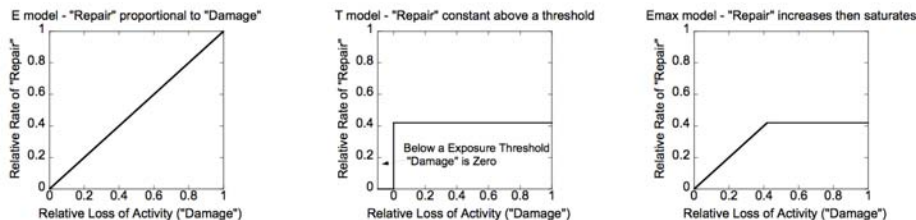


**Figure 6.1.1.** Graphical illustrations of the implied dependence of repair and damage rates for the  $E$ ,  $T$  and  $E_{max}$  models. Figures taken from Neale et al. 2014.

### Elemental composition

For elemental composition analyses, cells were filtered onto precombusted GF/F filters (Whatman). To determine cellular particulate organic carbon (POC) quotas, respective filters were fumed with pure HCl overnight to remove calcite. Cellular particulate inorganic carbon (PIC) quotas were assessed as the difference in carbon content between the HCl-treated (POC) and untreated filters (total particulate C, TPC). Particulate organic nitrogen (PON) was also measured in all filters.



### Primary productivity and calcification

The POC and PIC production, primary productivity and calcification respectively, were determined by following the microdiffusion technique (Paasche & Brubak 1994; Poulton et al. 2010). Samples (20 mL) of each independent culture ( $n=3$ ) were inoculated with  $\text{H}^{14}\text{CO}_3^-$  (approximately  $1 \mu\text{Ci mL}^{-1}$  final concentration) and incubated in triplicates at the same culture conditions. Incubations were ended after 2 hours by filtration under low-vacuum pressure through polycarbonate filters (25-mm diameter,  $0.2\text{-}\mu\text{m}$  pore size), which were then rinsed with  $0.2\text{-}\mu\text{m}$  filtered seawater to remove the non-incorporated  $^{14}\text{C}$ -labelled DIC. Filters were then placed in 20- mL scintillation vials with a glass-fiber Whatman filters (GF/F) soaked with 0.2 mL  $\beta$ -phenylethylamine (Sigma) located in the screw cap. Phosphoric acid (1 mL, 1%) was added into the bottom of the vial to convert  $^{14}\text{C}$ -labeled calcite into  $^{14}\text{CO}_2$ , which was then sequestered by the  $\beta$ -phenylethylamine–soaked GF/F filter. After 20–24 h, the GF/F filters were removed and placed in fresh scintillation vials. Primary production rates were determined by measurements of acid stable  $^{14}\text{C}$  retained on the polycarbonate filter, calcification by the  $^{14}\text{C}$ - $\text{CO}_2$  adsorbed on to the GF/F filter. In each case, measurement occurred after the addition of the scintillation cocktail (Insta-gel, Perkin Elmer), by using a scintillation counter LS-6599 (Beckman), and referred to the total inorganic carbon content of the incubation media used. Activity spike was checked by removal of 20  $\mu\text{L}$  from each replicate after the spike addition, mixing with 0.2 mL of  $\beta$ -phenylethylamine and liquid scintillation cocktail, and counting on the scintillation counter. Capture efficiency was 93% and it was assessed by adding the  $^{14}\text{C}$  spike to seawater samples, acidifying the samples with 1% phosphoric acid, and determining the  $^{14}\text{C}$  activity on the Whatman GF/F filter relative to the spike activity. The average relative standard deviation (SD divided by mean  $\times$  100) of triplicate measurements was 7.6% for POC production and 7.9 % for PIC production.



### Biometric analysis

For scanning electron microscopy (SEM) analyses, 1 ml of sample was concentrated onto a polycarbonate filter (0.8  $\mu\text{m}$  pore-size). The filters were fitted onto glass microscope slides with conductive glue and then sputter-coated with gold (Quorum Q150T ES, Quorum Technologies Ltd., East Grinstead, UK). Digital images of coccospheres were acquired using a Carl Zeiss Evo<sup>®</sup> MA10 SEM. All the measurements of the coccoliths were done in the distal shield and the measured parameters on the coccoliths of *E. huxleyi* were the distal shield length (DL), distal shield width (DW), central area length (CAL), central area width (CAW) and the number of slits (shown in Figure 6.1.2) using Fiji-ImageJ 1.47v (National Institutes of Health, USA) analysis program. The surface area of the distal shield (DSA) was estimated with the values of DSL and DSW as Bach et al. 2012:

$$\text{DSA} = \pi \times \frac{\text{DL} \times \text{DW}}{4}$$

The outer shield length (OSL) was calculated assuming an elliptical shape of the coccolith as:

$$\text{OSL} = \frac{\text{DL} - \text{CAL} + \text{DW} - \text{CAW}}{4}$$

In addition, the length and the width of the coccospheres were also measured. The mean values of the measured parameters were constant when counting more than 20 coccospheres / coccoliths per sample, so this number can be considered as statistically significant as proposed Triantaphyllou et al. 2010.

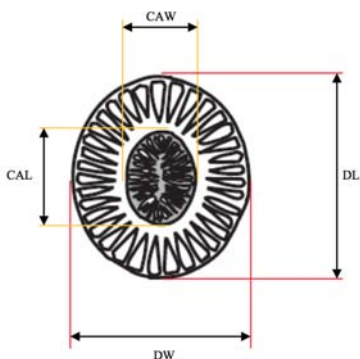


**Figure 6.1.2.** Measured parameters on coccoliths DL: distal shield length, DW: distal shield width, CAL: central area length and CAW: central area width. Figure modified from Hagino et al. 2005.



## Statistical analyses

Significant differences between treatments were analysed using a t-test considering significant if  $p < 0.05$ . BWFs were estimated for each experiment, and the mean BWF was calculated for each treatment ( $n = 3-4$ ), with confidence limits for the mean derived from individual error estimates by propagation of errors.

## Results

### Physiological measurements were not affected by high CO<sub>2</sub>

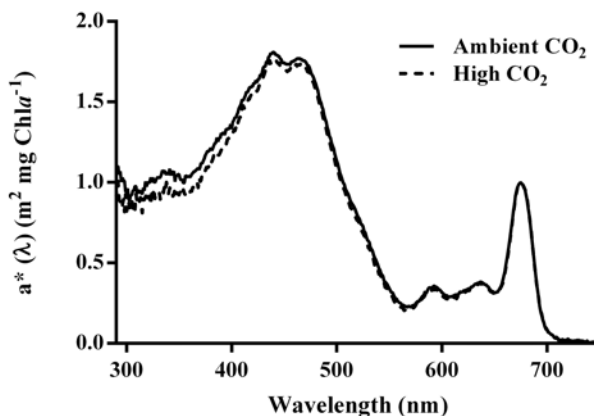
Physiological variables of *E. huxleyi* cultures maintained in ambient and high CO<sub>2</sub> concentrations are shown in Table 6.1.2. The average of  $F_v/F_m$  was the same ( $0.60 \pm 0.01$ ) for both conditions, showing that high CO<sub>2</sub> concentrations did not decrease the physiological performance of *E. huxleyi* and that cultures were in a good physiological state under the experimental conditions. No significant differences in growth rates, Chl *a* concentration, or Chl *a* cell<sup>-1</sup> were observed between treatments. Cellular absorbance normalized to Chl *a*, shown in Figure 6.1.3, was similar between treatments. The profile of spectral absorbance did not reveal presence of any UV-absorbing compounds.

**Table 6.1.2.** Physiological variables of *Emiliana huxleyi* grown under ambient CO<sub>2</sub> (400 ppm) and high CO<sub>2</sub> (800 ppm). Mean  $\pm$  standard deviation ( $n=3-4$ ). Statistically significant differences are indicated with asterisk (\*) if  $p < 0.05$ .

	Ambient CO <sub>2</sub>	High CO <sub>2</sub>
Specific growth rate (d <sup>-1</sup> )	0.60 $\pm$ 0.06	0.58 $\pm$ 0.03
POC quota ( $\mu\text{g } \mu\text{g Chl } a^{-1}$ )	57.7 $\pm$ 0.38*	68.0 $\pm$ 0.89*
PIC quota ( $\mu\text{g } \mu\text{g Chl } a^{-1}$ )	21.27 $\pm$ 1.35	22.55 $\pm$ 1.83
PON quota ( $\mu\text{g } \mu\text{g Chl } a^{-1}$ )	9.93 $\pm$ 0.24*	10.56 $\pm$ 0.30*
PIC:POC (mol mol <sup>-1</sup> )	0.37 $\pm$ 0.02	0.33 $\pm$ 0.03
POC:PON (mol mol <sup>-1</sup> )	7.48 $\pm$ 0.22*	8.17 $\pm$ 0.31*
Chl <i>a</i> quota (pg cell <sup>-1</sup> )	0.23 $\pm$ 0.04	0.25 $\pm$ 0.05
Chl <i>a</i> :POC (pg pg <sup>-1</sup> )	0.02 $\pm$ 0.00*	0.01 $\pm$ 0.00*



**Figure 6.1.3.** Cellular absorbance of UVR and PAR measured as Chl *a* specific absorption ( $a^*[\lambda]$   $\text{m}^2 \text{mg Chl } a^{-1}$ ) of *Emiliania huxleyi* under ambient and high  $\text{CO}_2$  concentrations ( $n=3$ ). The solid line corresponds to ambient  $\text{CO}_2$  concentration and the dashed line corresponds to increased  $\text{CO}_2$  cultures.



### UV sensitivity was the same in high $\text{CO}_2$ conditions

Exposure of *E. huxleyi* to simulated solar exposures using the photoinhibitor allowed the estimation of biological weighting functions (BWFs) for the inhibition of photosynthesis in cells grown at ambient and high  $\text{CO}_2$  conditions. We tested the three possible ERCs fittings (model  $E$ , model  $T$  and model  $E_{max}$ ) to the response of *E. huxleyi* to UV and PAR exposure. The Figure 6.1.4 shows an example of the observed photosynthetic rates and the predicted values for one incubation using the estimates for each of the three BWF/P-E models, where photosynthesis ( $P^B$ ,  $\text{mg C mg Chl } a^{-1} \text{h}^{-1}$ ) is plotted versus weighted irradiance ( $E^*_{inh}$ , dimensionless). All three models provided good estimates of the overall response with  $R^2 > 0.89$  ( $n = 120$ ), but there were differences between the ERCs fittings. The  $E$  model tends to underestimate observed rates at moderate exposures while overestimating rates at high exposures (Figure 6.1.4a) and showed the lowest value of  $R^2$ . In comparison, the predicted photosynthesis rates from the BWF/P-E using the  $T$  model were similar to the predictions using  $E_{max}$  model and there were no



differences between  $R^2$  and RMSE (Figure 6.1.4). The  $E_{max}$  model requires the use of an additional parameter, thus, to assess the predictions with this model it has to improve significantly the fit. We calculated the AIC for each fit (Table 6.1.3). The AIC takes into account both the prediction performance and number of model parameters and the best model is the one providing the lowest AIC (Andersen et al. 2005). There were no differences between  $T$  and  $E_{max}$  model. So statistically, there was not justification to use the  $E_{max}$  model, as the addition of an extra parameter did not improve the model fit. Consequently, the model used in the predictions was the  $T$  model.

The BWFs demonstrated that sensitivity of photosynthesis to UVR was not significantly different between cells grown under elevated and ambient  $\text{CO}_2$ . For *E. huxleyi* cultures grown in either condition, the average specific weights for inhibition of photosynthesis ( $\epsilon$  [ $\lambda$ ], [ $\text{mW m}^{-2}$ ] $^{-1}$ ) were not significantly different over the full wavelength range (i.e. differences were less than the standard error of the average weight) (Figure 6.1.5). The overall shape of the BWF is a decrease in weights from 270 to 345 nm with an exponential slope of about  $7\% \text{ nm}^{-1}$  and a relatively constant weight at longer wavelengths. The sensitivity to inhibition by PAR ( $\epsilon_{\text{PAR}}$ , ( $\text{W m}^{-2}$ ) $^{-1}$ ) was low and also not significantly different between growth conditions (Table 6.1.4). At the average  $\epsilon_{\text{PAR}}$ , PAR inhibition would only become significant at exposures  $> 380 \text{ W m}^{-2}$  (ca  $1580 \mu\text{mol photons m}^{-2} \text{ s}^{-1}$ ). The average between both treatments of the fitted parameters for the  $T$  model were 2.08 for the maximum rates of uninhibited photosynthesis ( $P_s^B$ ), 16.72 for the saturation irradiance parameter ( $E_s$ ) and  $2.79 \cdot 10^{-3}$  for the  $\epsilon_{\text{PAR}}$  (Table 6.1.4).

**Table 6.1.3.** Difference in AICs calculated for  $E$ ,  $T$  and  $E_{max}$  model fits to experimental data on the response of *E. huxleyi* photosynthesis to UV + PAR exposure.

	$\Delta\text{AIC}$ (T vs. E)	High $\text{CO}_2$ (T vs. $E_{max}$ )
Average	101.7	-0.01
SD	15.5	0.71



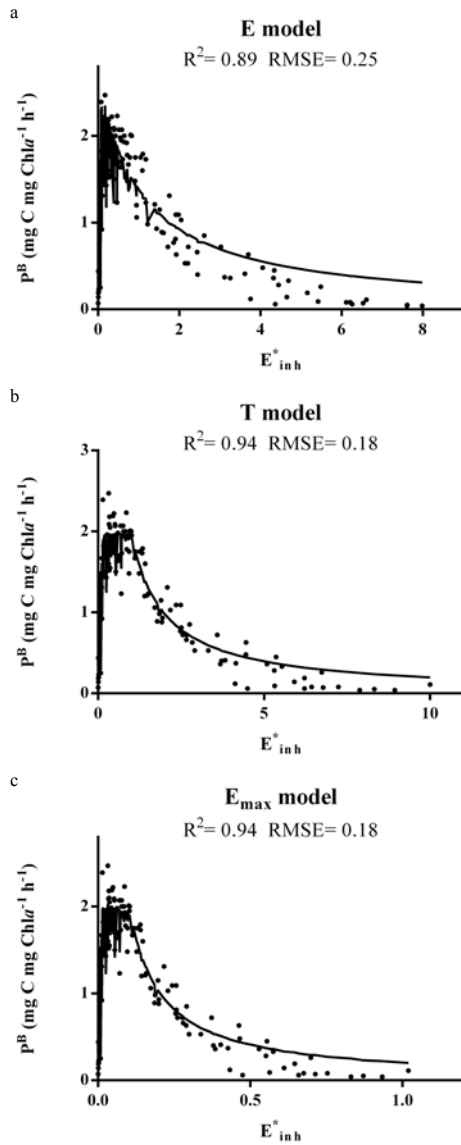


**Figure 6.1.4.** The panels illustrate the observed (points) vs. fitted (lines) results for three BWF/P-E models, the  $E$  (a),  $T$  (b) and  $E_{max}$  (c) models. Observed (points) and fitted (lines) biomass-specific photosynthesis (mgC mg Chl  $a^{-1}h^{-1}$ ) as a function of UV+PAR exposure weighted by a spectral biological weighting function for inhibition,  $E_{inh}^*$  (dimensionless). RMSE is in mg C mg Chl  $a^{-1}h^{-1}$ .



**Table 6.1.4.** Fitted parameters for the *T* model, mean  $\pm$  standard errors for  $n \geq 3$  experiments under each condition ambient and high  $\text{CO}_2$  concentration.

	Ambient $\text{CO}_2$	High $\text{CO}_2$
$P_s^B$	$2.17 \pm 0.22$	$2.01 \pm 0.21$
$E_s$	$16.1 \pm 0.98$	$17.2 \pm 0.96$
$\epsilon_{\text{PAR}} \times 10^{-3}$	$2.77 \pm 0.28$	$2.81 \pm 0.22$

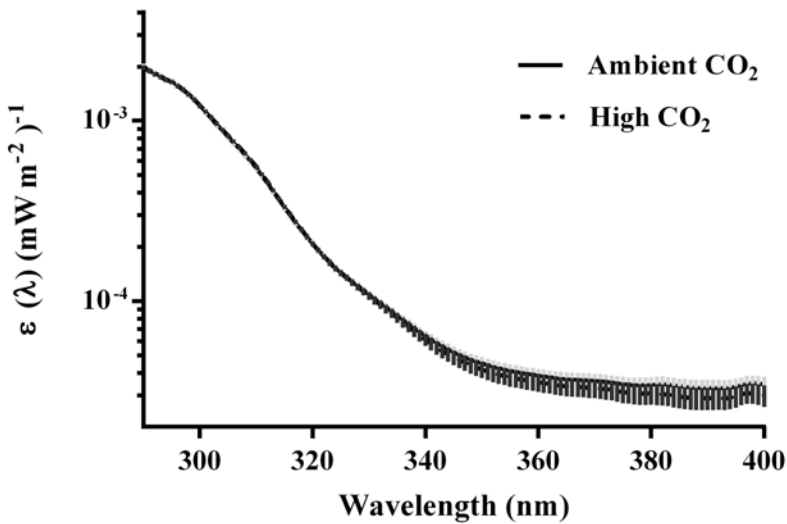


**Figure 6.1.5.** BWFs for the inhibition of photosynthesis by UVR ( $\epsilon[\lambda]$ ,  $[\text{mW m}^{-2}]^{-1}$ ) of *E. huxleyi* under ambient and increased  $\text{CO}_2$  concentrations. Curves are the average BWF ( $n=3-4$ ) for each treatment. The solid line corresponds to ambient  $\text{CO}_2$  concentration and the dashed line corresponds to high  $\text{CO}_2$  cultures. The grey and the black shading represents the standard error of the mean (SEM) of ambient and high  $\text{CO}_2$  respectively calculated from the standard error estimate of the individual BWFs.

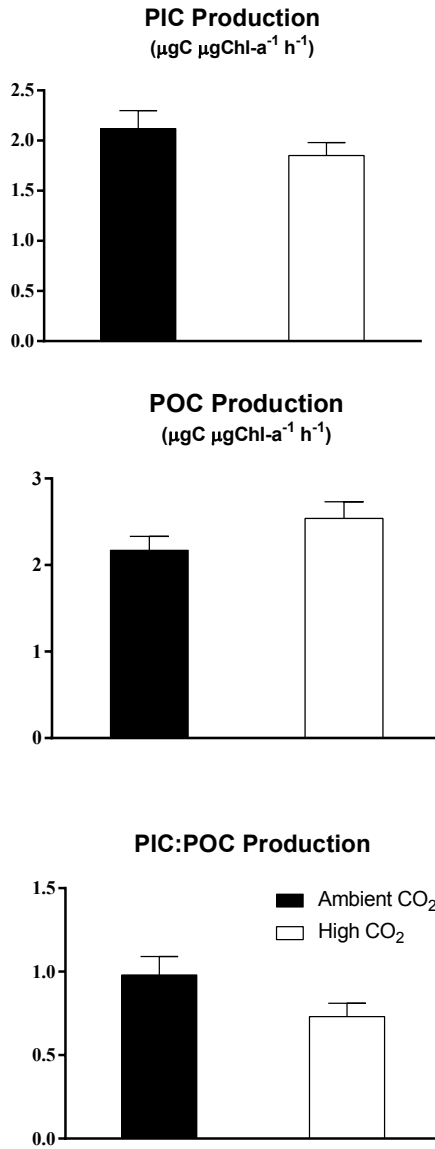


**Figure 6.1.6.** PIC production rate (a), POC production rate (b) and PIC:POC productivity ratio (c) during the exponential phase of the batch culture experiments. Bars represent the mean of the triplicate cultures and the error bars denote the standard deviation.



### Carbon productions and calcification showed opposite responses to high CO<sub>2</sub>

The results showed that high CO<sub>2</sub> concentration increased *E. huxleyi* POC content relative to Chl *a* by 15% ( $p < 0.001$ ) (Table 6.1.2). For the same samples, PIC content did not show significant differences between treatments. The PIC:POC ratio also presented similar values in both CO<sub>2</sub> conditions but the POC:PON ratio was 9% higher in the elevated CO<sub>2</sub> conditions showing significant differences between treatments ( $p = 0.035$ ). Unlike PIC bulk ratios, PIC production rates (mean  $\pm$  SD) significantly decreased (13%, Figure 6.1.6A) from  $2.12 \pm 0.18 \mu\text{g C } \mu\text{g Chl } a^{-1} \text{ h}^{-1}$  in ambient CO<sub>2</sub> cultures to  $1.85 \pm 0.13 \mu\text{g C } \mu\text{g Chl } a^{-1} \text{ h}^{-1}$  in high CO<sub>2</sub> cultures ( $p = 0.002$ ). However, the opposite response occurred in POC production. In accordance to POC bulk content, POC fixation rates increased by 15% ( $p < 0.001$ ), changing from  $2.17 \pm 0.16$  to  $2.54 \pm 0.19 \mu\text{g C } \mu\text{g Chl } a^{-1} \text{ h}^{-1}$  in the high CO<sub>2</sub> cultures (Figure 6.1.6B). The PIC:POC production rates showed a significant 25 % decrease in high CO<sub>2</sub> cultures ( $p < 0.001$ , Figure 6.1.6C).

### Coccoliths were affected by high CO<sub>2</sub> conditions

The selected morphometric parameters measured in coccoliths and coccospheres are presented in Table 6.1.5. The coccoliths only showed significant differences due to the treatments in the central area width (CAW). The distal shield length (DL), distal shield width (DW) and central area length (CAL) did not show significant differences between both CO<sub>2</sub> conditions. The coccosphere diameter was significantly different in the length ( $p < 0.05$ ), decreasing the size of the coccosphere under elevated CO<sub>2</sub> conditions.



**Figure 6.1.7.** Representative scanning electron microscope (SEM) images of *Emiliania huxleyi* cells grown at: (A) ambient CO<sub>2</sub> and (B) high CO<sub>2</sub> conditions at 16°C under PAR illumination of 200  $\mu\text{mol m}^{-2} \text{s}^{-1}$  and free coccoliths from (C) ambient and (D) high CO<sub>2</sub> conditions.

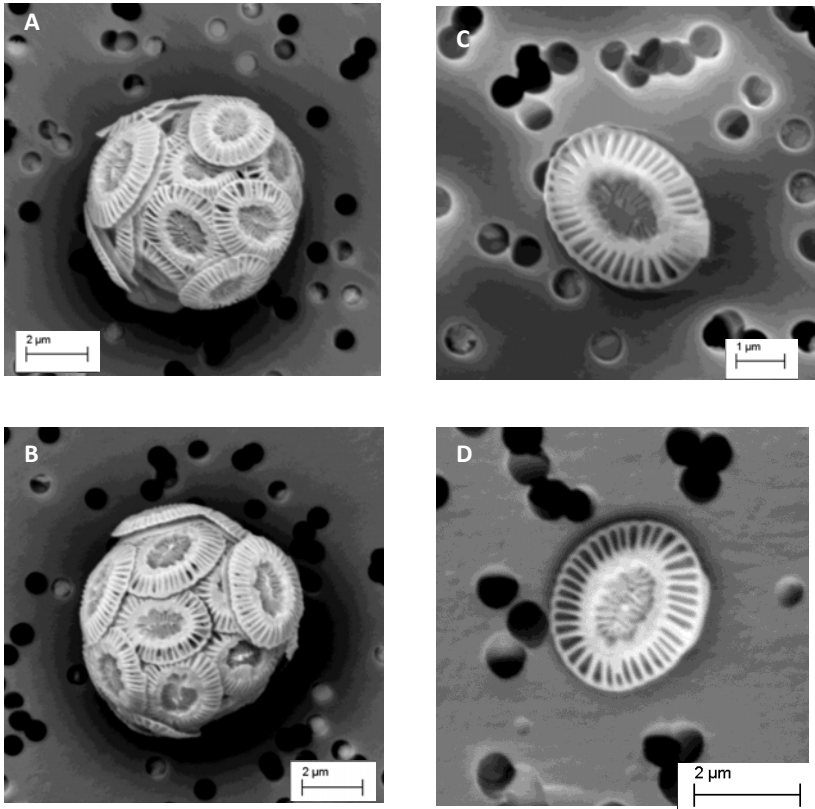




**Table 6.1.5.** Morphometric analysis of detached coccoliths and coccospheres of *Emiliana huxleyi* grown under ambient CO<sub>2</sub> (400 ppm) and high CO<sub>2</sub> (800 ppm). Mean ± standard deviation (n=3-4). Statistically significant differences are indicated with asterisk (*P* <0.05). Measured parameters on coccoliths DL: distal shield length; DW: distal shield width; DSA: distal shield area; CAL: central area length; CAW: central area width and OSL: outer shield length.

	Ambient CO <sub>2</sub>	High CO <sub>2</sub>
<i>Coccoliths</i>		
DL	3.17 ± 0.27	3.17 ± 0.28
DW	2.54 ± 0.27	2.55 ± 0.33
DSA	6.39 ± 1.21	6.40 ± 1.28
CAL	1.42 ± 0.20	1.48 ± 0.19
CAW	0.83 ± 0.14*	0.94 ± 0.17*
OSL	0.87 ± 0.11	0.83 ± 0.09
Number of slits	30.72 ± 3.40*	34.16 ± 3.37*
n	30	30
<i>Coccospheres</i>		
Length	6.88 ± 0.52*	6.44 ± 0.61*
Width	6.47 ± 0.47	6.22 ± 0.59
n	25	30

## Discussion

This study demonstrates that photosynthesis in *Emiliana huxleyi* under saturating light and nutrient conditions showed the same sensitivity to UVR exposure under present atmospheric CO<sub>2</sub> levels (400 ppm) and to the levels predicted for the end of the century (800 ppm) (IPCC 2013). Although elevated CO<sub>2</sub> concentrations did not affect the growth rate, the particulate carbon production was altered under high-CO<sub>2</sub> conditions. We observed two opposite responses: on one hand the particulate organic carbon production rates and content increased under elevated CO<sub>2</sub> concentrations and, on the other hand, the particulate inorganic carbon production rates decreased under high CO<sub>2</sub>.



The sensitivity of each phytoplankton species to UVR is determined by the capability for protection and repair to counteract UVR damage and the influence of the environmental factors on this capability in different ways, increasing damage, decreasing efficiency of repair and indirectly promoting repair and protection mechanisms (Litchman et al. 2002, Neale 2001). The susceptibility of photosynthesis to UVR was estimated using biological weighting functions (BWFs) for the inhibition of photosynthesis, and a model that predicts primary productivity behaviour under PAR and UVR exposures. The  $T$  model (the model used in this article) provided the best prediction for inhibition of photosynthesis. Together with previous studies using the same model (Sobrinho et al. 2005, 2008, 2009), these results suggest that there is an exposure threshold above which inhibition of photosynthesis is more severe because repair rate is limited. While inhibition is absent below this exposure threshold in the  $T$  model, more recent studies indicate that inhibition is still present but much less severe since repair rate increases with exposure (Neale et al. 2014). This below-threshold response is quantified in the  $E_{\max}$  model through introduction of an additional parameter (Neale et al. 2014). Unfortunately in the case of *E. huxleyi*, rates were too variable to resolve the below-threshold response. Therefore, the  $E_{\max}$  and  $T$  models gave equivalent AIC values and the additional parameter was not justified. However, the  $T$  model tends to underestimate the maximum rate of uninhibited photosynthesis ( $P_s^B$ ) since it ignores any inhibition below the threshold. For this reason, the  $E_{\max}$  model is more appropriate for modelling primary productivity in the ocean (more details in Neale et al. 2014). It could be also the reason why the  $T$  model  $P_s^B$  estimates were lower than primary productivity measured under culture conditions (no UV at saturating PAR). However, differences due to methodological issues should be also taken into account since  $P_s^B$  estimates include the particulate and dissolved fraction of the assimilated carbon while primary production measured in the filter excludes the dissolved fraction. Further experiments should be performed with *E. huxleyi* to better define inhibition at lower exposures to





enable fitting of the  $E_{\max}$  model and the role of DOC in the calculations. Nevertheless, the  $T$  model provides a good basis for comparing responses to UV of *E. huxleyi* growing at different  $\text{CO}_2$  concentrations.

*Emiliana huxleyi* showed the same sensitivity of photosynthesis to UVR in cells grown both under ambient and under high  $\text{CO}_2$  concentrations. This is not surprising, since the responses to UVR at increased  $\text{CO}_2$  levels vary between phytoplankton species (Gao et al. 2009, 2012, García-Gómez et al. 2014, Sobrino et al. 2005, 2008, 2009, Wu et al. 2012). But, one of the main questions is why there is such a diversity of responses. Raven (1991) proposed theoretically that a downregulation of the photosynthetic machinery in phytoplankton under high  $\text{CO}_2$  conditions could increase the resource use efficiency. Sobrino et al. (2008, 2009) observed a higher productivity in *Thalassiosira pseudonana* and natural assemblages under high  $\text{CO}_2$  levels related to decreases in cellular chlorophyll content, suggesting that elevated  $\text{CO}_2$  might increase passive diffusion rates and decrease the amount of energy and metabolites necessary to drive the active transport of carbon to Rubisco. As a consequence, the photosynthetic rate per cell was the same between ambient and elevated  $\text{CO}_2$  despite the lower chlorophyll content. This “downregulated” metabolism under high  $\text{CO}_2$  acclimated conditions was also demonstrated to have relatively lower enzymatic activity and a lower activation state of the general defence mechanism in natural waters assemblages (Sobrino et al. 2014) which might affect the repair process of UVR-caused damage. Decreases in cellular metabolite content as observed for important photosynthetic metabolites as Chl or Rubisco (Sobrino et al. 2008, Loss et al. 2012) can also indicate lower concentrations of repair enzymes related to UVR damage such as superoxide dismutase and ascorbate peroxidase (Lesser 1996).

Reduced amount or activity of the enzymes involved in cellular repair of the photosynthesis apparatus would increase susceptibility to UVR, resulting in more photoinhibition when UVR stress is imposed than would occur in cells with normal metabolic activity (Sobrino et al. 2008, 2009, 2014, Gao et al. 2009, 2012).



Following recent calculations from diatoms, a doubling of ambient CO<sub>2</sub> could save about 20% of the CCM expenditure (Hopkinson et al. 2011). This value is related to the energy saved by the CCM downregulation under high CO<sub>2</sub> conditions in terms of ATP investment, however higher values are expected if the catalytic machinery costs are added to the operating machinery expense (Raven et al. 2014). Downregulation to decrease the catalytic costs of photosynthesis is expected if growth is not energy (light) limited as it was in studies showing increases in sensitivity to UVR under enhanced CO<sub>2</sub> (Sobrino et al. 2008, 2009, 2014, Gao et al 2009, 2012). However, if concomitant with energy savings due to less CCM activity there is increased energy demand for other processes, for example changes in calcification rates due to the CO<sub>2</sub> increase as in this study, downregulation does not occur and increases in sensitivity to UVR are not observed.

The opposite reaction, i.e. less sensitivity to UVR, has been shown in *Nannochloropsis gaditana* (Sobrino et al. 2005) and in *Dunaliella tertiolecta* at elevated CO<sub>2</sub> cultures (García-Gómez et al. 2014, 2016). In the latter, the response has been related to an enhancement of the antioxidant systems and the upregulation of a cyclobutane pyrimidine dimer photolyase gene (CPD-PL) at elevated CO<sub>2</sub> conditions (García-Gómez et al. 2014), as well as the differential expression of a plethora of other genes involved in UV repair and in the maintenance of the cell's metabolism (García-Gómez et al. 2016). On the other hand, and in accordance with the results obtained in this study, *Nannochloris atomus* did not show differences in the susceptibility to UVR between high and ambient CO<sub>2</sub> treatments (Sobrino et al. 2005). Responses to CO<sub>2</sub> of both *N. gaditana* and *N. atomus* were tested after only 4 days since the start of CO<sub>2</sub> aeration. It is possible that under that short period of time cells were not acclimated since at least 4 days are necessary for species with similar growth rates, and grown under similar growth conditions, to reach the steady state (Sobrino et al. 2008). On top of that *N. gaditana* showed lower growth rates and lack of





differences in primary production under high CO<sub>2</sub> conditions, while in *N. atomus* high CO<sub>2</sub> increased growth and carbon fixation rates (Sobrino et al. 2005).

As in *N. atomus*, the absence of differences between the BWFs was accompanied with an increase in primary production in *E. huxleyi*. The increase in primary production in *E. huxleyi* could be due because photosynthesis is not saturated at normal DIC levels. Previous studies with photosynthetic O<sub>2</sub> evolution curves and <sup>14</sup>C incorporation studies have indicated that photosynthesis in *E. huxleyi* is not saturated at ambient CO<sub>2</sub> (Paasche 1964, Herfort et al. 2002, Rost et al. 2003). Such increase in primary production could be also related to the inorganic carbon source used, that could be CO<sub>2</sub> and/or HCO<sub>3</sub><sup>-</sup> depending on the strain used and /or the cultures conditions (Chapter 3, Rost et al. 2003, Rokkita & Rost 2012, Kottmeier et al. 2014, Schulz et al. 2007, Stojkovic et al. 2013). Moreover, the carbon concentrating mechanisms (CCMs) likely varied the threshold of DIC concentration that the regulation occurred. These changes in thresholds could result from strain-specific differences between *E. huxleyi* clones (Langer et al. 2009) and/or could be altered by culture conditions (Rokkita & Rost, 2012). The strain we have used for this study corresponds to a moderate- heavily calcified Type A strain isolated from the North Sea but the main inorganic carbon source used by this strain is still unknown. Rokkita & Rost (2012) hypothesized that there was a reallocation of the acquired resources from PIC toward POC production due to the inorganic carbon acquisition appeared unaltered in the assays. The same pattern could well occur in our cultures suggesting in addition that if it was due to a downregulation of the photosynthetic machinery, the UV radiation-defence mechanisms of the cell were not affected.

The capacity of withstand excess irradiance and the absence of photoinhibition in this phytoplankton species (Paasche 2000) could be due to the photoprotective role played by the coccoliths in mitigating excess PAR and UV stress in *E. huxleyi*. These findings could suggest that coccolithophores may have an advantage compared to other phytoplankton groups regarding stressful



irradiance management (Raven & Crawford 2012). The comparison with the other species showed that *E. huxleyi* showed similar BWFs as other species at ambient CO<sub>2</sub> concentration. In particular, the sensitivity of *E. huxleyi* seems to be similar to *T. pseudonana*. In the same way, cells acclimated to high CO<sub>2</sub> concentrations showed similar susceptibility to UV comparing *E. huxleyi* with the other species studied (Figure 6.1.8).

Similarly to the sensitivity to UV, growth rates of *E. huxleyi* did not change under both CO<sub>2</sub> concentrations used in this experiment (Table 6.1.2). Most studies on coccolithophores show no change or a slight decrease in cell division rates in response to elevated CO<sub>2</sub>, although there were some exceptions (reviewed in Riebesell & Tortell 2011). Furthermore, the growth rates were also unaffected under limited or saturated conditions of nutrients and light at high CO<sub>2</sub> levels (Sciandra et al. 2003, Engel et al. 2005, Gao et al. 2009). As mentioned above, the POC production significantly increased by 15 % in cells acclimated to high CO<sub>2</sub> concentrations (Figure 6.1.6). Likewise, the POC content also increased by 15% under high CO<sub>2</sub> (Table 6.1.2). Previous studies are in concordance with this result (Riebesell & Tortell 2011). Alternatively, the calcification rate was affected significantly and the coccoliths morphology only slightly under increased CO<sub>2</sub> concentrations. The cellular PIC production rates decreased significantly with increasing pCO<sub>2</sub> as confirmed by a 12% difference in production between the present and the future CO<sub>2</sub> treatment. De Bodt et al. (2010) proposed that the decrease in cellular PIC production rates at high pCO<sub>2</sub> could be explained by: a lower calcite content per coccolith, a decrease in coccoliths number per cell or, a decrease in the coccolith production rate, being all of them not mutually exclusive. Riebesell et al. 2000 showed that the number of attached or free coccoliths per coccusphere might not be affected by lowering the pH. In this work, the PIC content ( $\mu\text{g C } \mu\text{g Chl } a^{-1}$ ) did not show significant differences of this decrease between treatments, although the mean content of high CO<sub>2</sub> was higher.

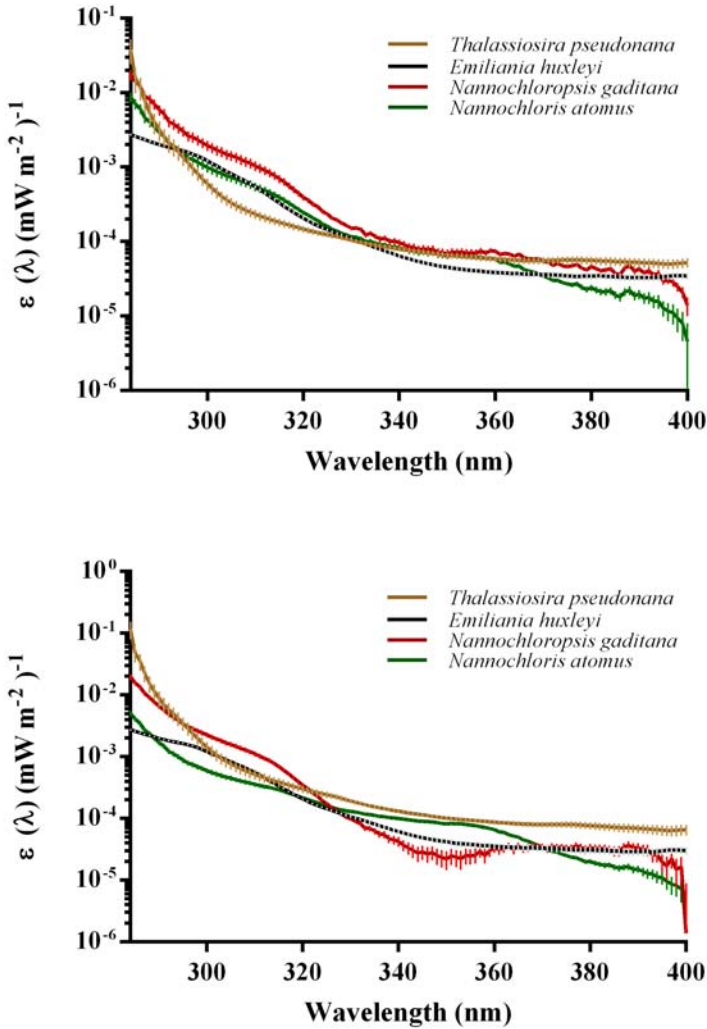


**Figure 6.1.8.** Biological weighting functions for the inhibition of photosynthesis by UV ( $\epsilon(\lambda)$ ,  $[\text{mW m}^{-2}]^{-1}$ ) estimated by statistical analysis of data from different phytoplanktonic species. The solid line is the average biological weight for *E. huxleyi*, the brown line is for *Thalassiosira pseudonana* (Sobrino et al. 2008), the green line is for *Nannochloris atomus* (Sobrino et al. 2005) and the red line is for *Nannochloropsis gaditana* (Sobrino et al. 2005) at ambient  $\text{CO}_2$  conditions (A) and high  $\text{CO}_2$  conditions (B).

This lack of differences could be related to the presence of free coccoliths in the culture that could affect the mean value of the cell content. These changes in PIC production have already been associated with alterations of coccolith morphology (Langer et al. 2006). Riebesell et al. (2000) have also documented *E. huxleyi* cells with malformed coccoliths or incomplete coccospheres in high  $p\text{CO}_2$  cultures. Decreased calcification at lowered pH may be due to a lower saturating state of calcite in the coccolith vesicles and subsequently disturbed nucleation and formation of the crystallization (Zondervan et al. 2002). The morphometric analyses of coccoliths and coccospheres of *E. huxleyi* in both  $\text{CO}_2$  conditions (Figure 6.5) revealed that the coccosphere-sized particles showed a reduction trend with increasing  $p\text{CO}_2$  as already shown (De Bodt et al. 2010). The area of calcification is the region between the slits and the central area and, an increase in the central area is reflected as a decreased in the region of calcification. The central area showed significant increase in the width and a slight difference in the length in cells acclimated to high  $\text{CO}_2$  concentrations (Figure 6.1.7b,d). Thus, the cells showed that the coccoliths and the coccospheres were affected by high  $\text{CO}_2$  concentrations although these alterations did not contribute to increase the susceptibility of *E. huxleyi* to UVR, as opposed to studies describing an increase in inhibition of photosynthesis under the same scenario (Gao et al. 2009).

During the past years there is a growing body of studies focusing on the effects of ocean acidification on coccolithophores (Riebesell & Tortell 2011). However, the interaction with other factors still needs further investigation, thus, the role of UVR in combination with the increase in  $\text{CO}_2$  needs to be considered. Our results indicate that the sensitivity to UV will be the same at high  $\text{CO}_2$  conditions in this strain of *E. huxleyi*. We have proposed that there is a downregulation of the mechanisms of incorporation of inorganic carbon and a decrease in the production of the inorganic carbon of the cells, leaving this energy for other mechanisms like photosynthesis but the mechanisms to UV defences are





still active. Finally, it is important to consider the wide range of different responses to ocean acidification of *E. huxleyi*, due to the differences presented between strains (Langer et al. 2006, 2009, Riebesell & Tortell 2011) or to different experimental conditions including temperature, levels of CO<sub>2</sub>, irradiance and nutrients availability.





## Chapter 6

# ***In vitro* physiological response of *Emiliana huxleyi* to increased CO<sub>2</sub>, Fe limitation and UV radiation:**

## **6.2. Short-term response to the effects of Fe availability, increased CO<sub>2</sub> and UV radiation of *Emiliana huxleyi***

M. Rosario Lorenzo\*, María Segovia

*Manuscript for submission*

## Abstract

We report in this study the interactive effects of changes in iron concentration and CO<sub>2</sub> levels predicted by the end of this century on the physiology of the coccolithophore *Emiliana huxleyi* exposed to UV radiation (UVR). We assessed the impact on growth, cell viability, photosynthesis and calcification due to UVR stress under the different Fe and CO<sub>2</sub> scenarios. The effect of UVR at ambient CO<sub>2</sub> conditions was compared with cultures only exposed to photosynthetically active radiation (PAR). Iron concentration played a key role in controlling the response of all physiological processes. When Fe-depleted cultures were exposed to UVR, *E. huxleyi* cells showed a reduction on their capacity to cope with the generated stress and the growth rate, cell viability, photosynthesis and calcification were inhibited. However, such inhibition was mitigated under increased CO<sub>2</sub> conditions, suggesting a possible CO<sub>2</sub>-mediated-signalling role in photoprotective mechanisms. This response was less evident in Fe-depleted cultures as previously demonstrated other studies, showing only differences in the processes related to photosynthesis.



## Introduction

The oceans have absorbed more than 30% of the emitted anthropogenic CO<sub>2</sub> provoking that the surface of the ocean is acidified (the so called ocean acidification, OA) (Caldeira & Wickett 2003). The worst-case scenario predicted is an increase in atmospheric CO<sub>2</sub> concentration higher than 900 ppm and a maximum decrease in seawater pH of 0.32 by the year 2100 (IPCC 2013). Annually, phytoplankton incorporates approximately 45 to 50 billion metric tons of inorganic carbon (Field et al. 1998), removing a quarter of CO<sub>2</sub> emitted to the atmosphere by anthropogenic activities (Canadell et al. 2007). Thus, the response of phytoplankton to OA is key for understanding future changes in marine ecosystems (Doney et al. 2009).

Concomitant with OA, the distribution and speciation of trace metals in the ocean will be also affected by changes in the seawater pH and it could possibly modify the limitation and/or toxicity of metals to marine plankton (Millero et al. 2009). Iron is the most essential trace metal for phytoplankton because it is a key nutrient for biochemical pathways including photosynthesis (Behrenfeld & Milligan 2013). The decrease in seawater pH has been suggested to promote higher Fe solubility (Millero et al. 2009), but may result in unchanged or lower Fe bioavailability, depending of the nature of strong organic Fe ligands present (Shi et al. 2010). Consequently, changes in iron bioavailability due to OA may affect positively or negatively ocean productivity and CO<sub>2</sub> drawdown. The effects of changes in iron availability with changes in CO<sub>2</sub> conditions could differ depending on the nature of the iron requirement of each phytoplankton species. Such requirement is generally higher in coastal phytoplankton species than in oceanic species, probably due to the environmental conditions (Sunda & Huntsman 1995a).

Global change also affects exposure of phytoplankton to ultraviolet B (UVB, 280–320 nm) and ultraviolet A (UVA, 320–400 nm) radiation penetration due to changes in the stratospheric ozone concentration, cloud cover and the levels of dissolved organic matter (Zepp et al. 2007). Despite that the Montreal Protocol



curtailed the release of harmful chlorofluorocarbons (CFCs) into the atmosphere, ozone levels have not recovered in all latitudes (McKenzie et al. 2011), and in some regions they are still rising due to interactions with other global change drivers (Weatherhead & Andersen 2006). It is widely known that UVR has deleterious effects on phytoplankton's physiology, including the inhibition of nutrient uptake, DNA damage, injuries to antennas (i.e. to light transduction) and decreased carbon assimilation mechanisms (Häder et al. 2011). However, the effects of UVR may be modulated by other environmental changes that govern the overall impacts of global change (Beardall et al. 2014). In fact, as a consequence of atmospheric CO<sub>2</sub> elevation, not only the ocean will be more acid, it will also be warmer. This will have a direct consequence on shoaling of the permanent thermocline. Thus, phytoplankton will be exposed to increased solar radiation, temperature and nutrient stress.

Previous studies have focused on manipulation experiments that only perturb one environmental property (Gattuso & Hansson 2011). But, natural environments are characterized by the presence of continuous interactions of multiple environmental factors (Boyd & Hutchins 2012). Thus, it is necessary to carry out experiments with associated-changes in several environmental factors, such as temperature, macronutrients, trace metals, oxygen content, stratification, mixing, and irradiance (Boyd & Hutchins 2012, Riebesell & Gattuso 2015), that could influence the effects of OA to understand the responses of planktonic communities to the interactive effects of these factors on phytoplankton physiology in a rapidly changing environment.

The aim of this study was to examine the effect to UVR exposure of the coccolithophore *Emiliania huxleyi* depending on Fe concentration at ambient and increased CO<sub>2</sub> conditions to discriminate the response due to UVR stress. We investigated how the treatments affected the growth rates, cell viability, photosynthesis and calcification in a short-term experiment in controlled laboratory conditions. We also compared the results with cultures exposed to





only-PAR in ambient CO<sub>2</sub> conditions. *Emiliana huxleyi* is the most abundant coccolithophore in the world's oceans (Paasche 2002). It plays a major role in the global carbon cycle by contributing ca. 1–10% to total organic carbon fixation (Poulton et al. 2007) and approximately 50% to pelagic deep ocean CaCO<sub>3</sub> sediments (Broecker & Clark 2009), thus changes in the physiology of this paramount significant species due to global stress factors, warrant further considerations on how this might affect C-cycling in the ocean.

## Material and methods

### Experimental design and culture conditions

Cultures of *Emiliana huxleyi* (RCC#1226) provided by Roscoff Culture Collection were cultured in 28 mL polycarbonate tubes in artificial seawater medium-AQUIL (Price et al. 1989) with different Fe concentrations: low (12.5 nM, pFe21) and no addition (1 nM, pFe22.3). The AQUIL medium was prepared as described by Maldonado et al. (2006). Cultures were kept in exponential growth phase using semicontinuous cultures with 200- $\mu\text{mol photons m}^{-2} \text{s}^{-1}$  saturating light intensity at 16 °C. Cultures were considered acclimated to each specific Fe concentration when growth rates varied <15% (Brand et al. 1981) in five successive dilutions. Prior to the experiments, cultures in log phase of growth were transferred to sterile acrylic cylinders (Plexiglas XT<sup>®</sup> 29080) transparent to UVR for preacclimation and were maintained under a 20:4 h light:dark photoperiod at 200  $\mu\text{mol photons m}^{-2} \text{s}^{-1}$  for 48 h. After preacclimation, and 24 h before the beginning of the experiment, cultures were diluted to 50000 cells/mL as starting cell abundance. Initial samples were taken (T<sub>0</sub>), and immediately after, cultures were exposed to PAR and UVR (PAB) and to the different pCO<sub>2</sub> conditions. Cultures of each Fe condition were maintained with only PAR at ambient CO<sub>2</sub> conditions as controls. In total, duplicate cultures were exposed to 6 different treatments as shown in Table 6.2.1.



**Table 6.2.1.** Nomenclature of the different treatments used.

Light		Carbon		Fe		Treatments
Treatment	Nomenclature	Conc.	Nom.	Concentration	pFe <sup>*</sup>	Nomenclature
Only PAR	PAR	380 ppm	LC	Low (12.5 nM)	21	PAR-LC21
Only PAR	PAR	380 ppm	LC	No addition (1-2 nM)	22.3	PAR-LC22
PAR+UVA+UVB	PAB	380 ppm	LC	Low (12.5 nM)	21	PAB-LC21
PAR+UVA+UVB	PAB	380 ppm	LC	No addition (1-2 nM)	22.3	PAB-LC22
PAR+UVA+UVB	PAB	1000 ppm	HC	Low (12.5 nM)	21	PAB-HC21
PAR+UVA+UVB	PAB	1000 ppm	HC	No addition (1-2 nM)	22.3	PAB-HC22

*pFe<sup>\*</sup> indicates the concentration of inorganic iron*

The two different CO<sub>2</sub> levels corresponding to the present pCO<sub>2</sub> conditions (390 ppmv) and high pCO<sub>2</sub> conditions (1000 ppmv) (henceforth “LC” for 390 ppmv, and “HC” for CO<sub>2</sub> enriched cultures at 1000 ppmv) were achieved by manipulating the seawater carbonate chemistry. CO<sub>2</sub> enrichment conditions were carried out by mixing atmospheric air with pure CO<sub>2</sub> (Biogon, Linde, Germany) in the aeration system. The specific pCO<sub>2</sub> in the enriched mixture, as well as pCO<sub>2</sub> inlet flows in the culture cylinders, were measured by non-dispersive infrared analysis by using a Li-Cor (LI-820) CO<sub>2</sub> gas analyser (Li-COR, Nebraska, USA) and CO<sub>2</sub> AirSense-310 sensors (Digital Control Systems, Inc, USA). Partial pressure of CO<sub>2</sub> in the cultures (pCO<sub>2</sub>) was calculated from pH and total alkalinity (TA) measurements using the CO2Calc software (Robbins et al. 2010) as shown in Table 6.2.1S in supplemental material. The light treatments were: only PAR radiation (PAR) for the controls (PAR- LC and PAR-HC) and PAR and UVR (PAB) for both CO<sub>2</sub> conditions (PAB-LC and PAB-HC). The different irradiance conditions were achieved by covering the experimental cylinders with cut-off filters. Ultraphan UBT 395 (Digefra, München, Germany) transmitted only PAR (P treatment), and low-density polyethylene (LDPE) filter transmitted PAR, UVA and UVB (PAB treatment). PAR was obtained by using Optimarc 250W lamps (DuroTest, USA) and measured using an Ocean Optics



SMS 500 spectroradiometer (Sphaerooptics, Contoocook, New Hampshire, USA) calibrated after NPL standards with a cosine-corrected sensor. UV fluence rates were provided by Qpanel-340 lamps ( $2.8 \text{ Wm}^{-2}$  UVA and  $0.21 \text{ Wm}^{-2}$  UVB, unweighted) and measured with a MACAM UV203 radiometer (MACAM Photometrics Ltd, Livingston, UK) and with the Ocean Optics SMS 500 spectroradiometer mentioned above. Spectra were measured in the range 250–800 nm. All light measurements were carried out inside the cylinders once they were wrapped with the appropriate cut-off filters.

All the variables were analysed by means of comparing two conditions: LC treatments and PAB treatments. In LC conditions the comparison was between light (PAR vs. PAB) and Fe concentrations (pFe21 vs. pFe22.3) and in PAB conditions, between CO<sub>2</sub> levels (LC vs. HC) and Fe concentrations (pFe21 vs. pFe22.3). The treatment pFe22.3 was showed in the figures and tables as “22”.

### Cell density

Cell numbers were counted every day with a Neubauer hemacytometer. Specific growth rates ( $\mu$ ) were calculated by fitting the logarithmic phase of the growth to the exponential growth model:

$$N_t = N_0 e^{-\mu t}$$

where  $N_0$  is the initial number of cells, and  $N_t$  is the daily number of cells up to 4 days.

### Cell death

Cell death was assessed using the nucleic acid stain SYTOX Green (Invitrogen, Oregon, USA) according to Segovia & Berges (2009). SYTOX Green only stains the nucleic acid of cells that have compromised plasma membranes. Green staining of the cell nucleus indicates a dead cell, before the cell loses its integrity and lyses (Veldhuis et al. 2001). Briefly, 50  $\mu\text{l}$  of a 100  $\mu\text{M}$  working stock of SYTOX Green was added to 1 ml samples (5  $\mu\text{M}$  final concentration). Samples were taken at 0, 24, 48



y 96 h and incubated at 16 °C in darkness for 30 min. Fluorescence was quantified using the epifluorescence microscope (Leitz, Wetzlar, Germany) at an excitation of 490 nm and an emission of 525 nm. About 250 cells per sample were analysed. Positive controls consisting of 100% killed cells were run in parallel and obtained by pre-treating the samples with 1% glutaraldehyde (final concentration) for 2 h at 4 °C.

### **Cell viability**

Non-specific cell esterase activity of cells was analysed by using fluorescein diacetate (FDA, Invitrogen, Carlsbad, CA, USA) to measure cell viability as described by Segovia & Berges (2009). Samples were taken at 0, 24, 48 y 96 h. FDA was added to 1 mL samples at 20 µM final concentration and incubated at 16 °C in darkness for 60 min. Fluorescence was quantified using the epifluorescence microscope (Leitz, Wetzlar, Germany) at an excitation of 490 nm and an emission of 525 nm and 250 cells per sample were analysed.

### ***In vivo* Chlorophyll *a* fluorescence**

Optimal quantum yield of photosystem II (PSII) fluorescence ( $F_v/F_m$ ) was measured every day by means of a pulse amplitude modulated fluorometer (Water-PAM, Walz, Effeltrich, Germany) after 20 min of incubation in darkness, as described by Schreiber et al. (1986). Immediately after, rapid light curves were measured, estimating the effective quantum yield of PSII ( $\Phi_{PSII} = \Delta F/F_m'$ ) for 12 different white light irradiances provided by the internal halogen lamp.  $F_v$  is the maximal variable fluorescence of a dark-adapted sample,  $F_m$  the fluorescence intensity with all PSII reaction centres closed,  $F$  the fluorescence at any time during induction and  $F_m'$  the light-saturated fluorescence (Genty et al. 1989). Relative electron transport rate between PSII and PSI (ETR) was calculated as:

$$rETR = \Phi_{PSII} \cdot E_{PAR} \cdot 0.5$$





where  $E_{PAR}$  is the incident PAR irradiance and 0.5 stands for the assumption of equal contribution of excitons from PSI and PSII.

ETR vs. irradiance curves were fitted to the non-linear least-squares regression model by Eilers & Peeters (1988) using the Solver function of Excel (Microsoft, Redmond, U.S.A.) in order to obtain the photosynthetic parameters: maximum electron transport rate ( $rETR_{max}$ ), the initial slope of the curve related to the photosynthetic light-harvesting efficiency ( $\alpha$ ), the light requirement for saturating photosynthetic rate ( $E_k$ ), and the irradiance at which chronic photoinhibition begins ( $E_{opt}$ ).

### Photosynthesis and calcification

Parallel incubations were carried out to measure the photosynthetic production of particulate and dissolved organic carbon (POC and DOC, respectively) at 0, 24, 48 and 96 h. Samples (20 mL) of each independent culture were inoculated with  $H^{14}CO_3^-$  (approximately  $1 \mu Ci mL^{-1}$  final concentration) and incubated at the same culture conditions and in the dark for 2 hours. For POC production, incubations were ended by filtration of 5-10 mL under low-vacuum pressure through polycarbonate filters (25-mm diameter, 0.7- $\mu m$  pore size), which were then rinsed with 0.2- $\mu m$  filtered seawater to remove the non-incorporated  $^{14}C$ -labelled DIC. For the determination of particulate inorganic carbon (PIC) production (referred as calcification) at the end of the experiment (96 h), a parallel sample (5 mL) was also filtered but not exposed to HCl fumes. The filter was rinsed 3-4 times with filtered seawater. The photosynthetic carbon fixation was estimated according to the radioactivity of HCl-fumed filters and the rate of calcification was determined as the difference between the total particulate carbon (non-fumed filter) and the photosynthetic carbon fixation (fumed filter). For the dissolved organic carbon (DOC) production, 5 mL were filtered (25-mm diameter, 0.7- $\mu m$  pore size) and the filtrate was collected in scintillation vials to assess  $^{14}C$  activity in the dissolved



fraction. Non-assimilated  $^{14}\text{C}$  was released by exposing the filters to acid fumes (50% HCl) or by adding 200  $\mu\text{l}$  of 10% HCl to the filtrates and shaking overnight. The carbon fixation rates were determined by measurements of acid stable  $^{14}\text{C}$  fixation after the addition of scintillation cocktail (Instagel, Perkin Elmer), using a scintillation counter LS-6599 (Beckman), and referred to the total inorganic carbon content of the incubation media used. The spike activity was checked by removal of 20  $\mu\text{L}$  from each replicate after its addition by mixing it with 0.2 mL of  $\beta$ -phenylethylamine (PEA) and liquid scintillation cocktail, and counting it on the scintillation counter. The percentage of  $\text{DO}^{14}\text{C}$  extracellular release (PER) was calculated as the ratio  $\text{DOC}/\text{DOC}+\text{POC}$  ( $\text{DOC}+\text{POC}$  correspond to the total organic carbon fixed, TOC).

### Statistical analyses

Data were checked for normality (by Shapiro-Wilks' test), homoscedasticity (by Levene's test) and sphericity (by Mauchly's test). All data met the requirements to perform parametric tests therefore statistical significance of treatment effects on the variables was performed by using Split-Plot ANOVA (also called SPANOVA or mixed-model ANOVA) followed by post-hoc Sidak or Tukey and Bonferroni tests, respectively (considering  $p < 0.05$ ). All analyses were performed using the general linear model (GLM) procedure with main effects, time (repeated measure) and interaction terms. When appropriate, data were specifically tested for significant differences ( $p < 0.05$ ) induced by the treatments by using 2-Way ANOVAs. Statistical analyses were performed by using the software SPSS v22 (IBM statistics) and Statistica v7 (Statsoft, Inc.).



## Results

### Effect of Fe with UVR or increased CO<sub>2</sub> on the specific growth rates

Growth rates were higher in pFe21 (Fe concentration= 16 nM) than in pFe22.3 (concentration without addition of Fe= 1-2 nM) in LC conditions (Figure 6.2.1,  $p < 0.05$ ). Under PAR, the growth rate of pFe22.3 decreased by 30% compared to pFe21 and the same inhibition rate took place between LC treatments under UVR exposure (PAB-LC21 vs. PAB-LC22). The LC treatments exposed to UVR also showed lower growth rates compared with the treatments only exposed to PAR ( $p < 0.05$ ). The HC treatments showed different responses. HC-pFe21 did not change with respect to the control (PAR-LC21) and was higher than PAB-LC. However, there were not significant differences between both CO<sub>2</sub> conditions with pFe22.3 under PAB (Figure 6.2.1).

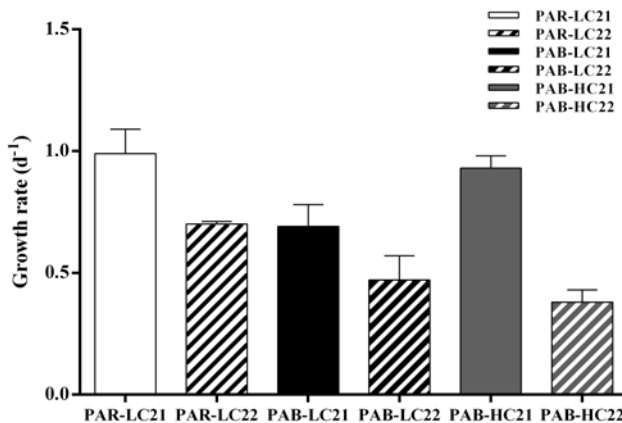


**Figure 6.2.1.** Specific growth rates of *Emiliana huxleyi* cultures exposed to different irradiance, CO<sub>2</sub> and Fe treatments. Cells were exposed to the following 6 different treatments: only PAR, ambient CO<sub>2</sub> and pFe21 (PAR-LC-21); only PAR, ambient CO<sub>2</sub> and pFe22.3 (PAR-LC-22); PAR+UVA+UVB, ambient CO<sub>2</sub> and pFe21 (PAB-LC-21); PAR+UVA+UVB, ambient CO<sub>2</sub> and pFe22.3 (PAB-LC-22); PAR+UVA+UVB, high CO<sub>2</sub> and pFe21 (PAB-HC-21) and PAR+UVA+UVB, high CO<sub>2</sub> and pFe22.3 (PAB-HC-22). Data are means of duplicate independent cultures. Error bars indicate standard deviations.

### Cell death and cell viability

The percentage of SYTOX-positive *E. huxleyi* cells was ca. 15% in all of the treatments without significant differences at 24 h (Figure 6.2.2). After 48 h, the percentage of dead cells in pFe22.3 treatments exposed to UVR (PAB-22) increased significantly up to 25% in both LC and HC ( $p < 0.01$ ). At the end of the experiment, these treatments (PAB-22) reached ca. 40% of positive-dead cells after 96 h of UVR exposure. The other treatments showed a 15% threshold of dead cells.

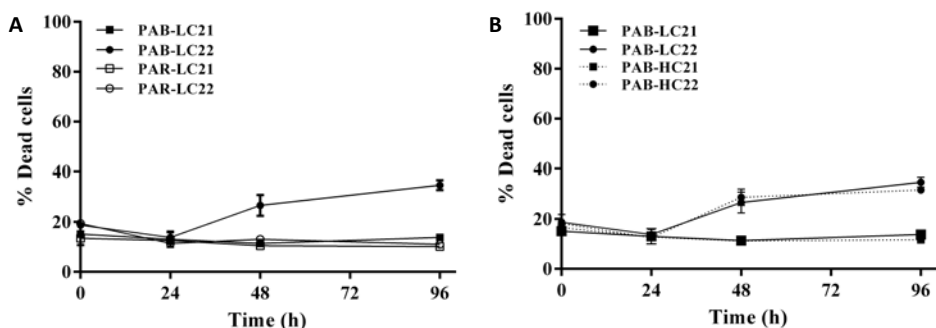


**Figure 6.2.2.** Percentage of dead cells based on SYTOX Green staining of *Emiliana huxleyi* cultures exposed to different irradiance, CO<sub>2</sub> and Fe treatments. (A) Cells in ambient CO<sub>2</sub> conditions were exposed to the different treatments, only PAR, ambient CO<sub>2</sub> and pFe21 (PAR-LC-21); only PAR, ambient CO<sub>2</sub> and pFe22.3 (PAR-LC-22); PAR+UVA+UVB, ambient CO<sub>2</sub> and low Fe (PAB-LC-21) PAR+UVA+UVB, ambient CO<sub>2</sub> and pFe22.3 (PAB-LC-22). (B) Cells in PAB conditions were exposed to the different treatments: PAB-LC-21; PAB-LC-22; PAR+UVA+UVB, high CO<sub>2</sub> and pFe21 (PAB-HC-21) and PAR+UVA+UVB, high CO<sub>2</sub> and pFe22.3 (PAB-HC-22). Symbols are means of measurements in two independent replicate cultures and error bars indicate standard deviations.

The percentage of FDA-positive cells (i.e viable cells) was in accordance with the results obtained for dead cells (Figure 6.2.3). All the treatments with the exception of the pFe22.3 under UVR (PAB22) showed a constant value of 85% of viable cells without differences over time. A decrease in cell viability in PAB22 was observed



at 48 and 96 h. Both CO<sub>2</sub> conditions (LC and HC) presented 70% of viable cells at 48 h and 65% at 96 h (Figure 6.2.3).

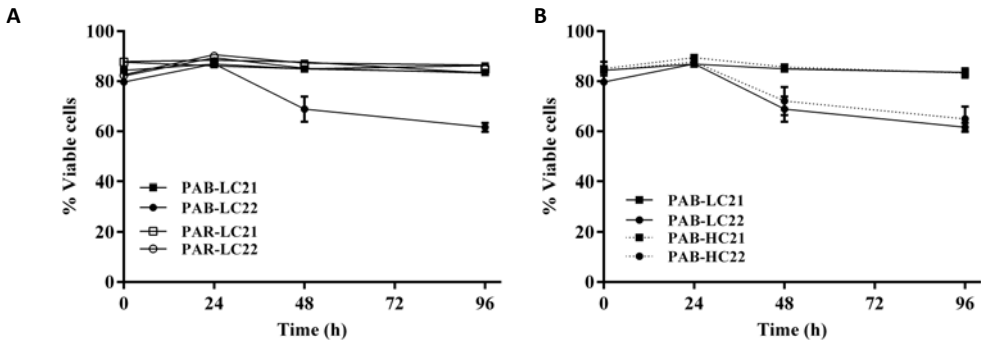


**Figure 6.2.3.** Percentage of cell viability based on FDA green fluorescence emission of *Emiliania huxleyi* cultures exposed to different irradiance, CO<sub>2</sub> and Fe treatments. (A) Cells in ambient CO<sub>2</sub> conditions were exposed to the different treatments, only PAR, ambient CO<sub>2</sub> and pFe21 (PAR-LC-21); only PAR, ambient CO<sub>2</sub> and pFe22.3 (PAR-LC-22); PAR+UVA+UVB, ambient CO<sub>2</sub> and low Fe (PAB-LC-21) PAR+UVA+UVB, ambient CO<sub>2</sub> and pFe22.3 (PAB-LC-22). (B) Cells in PAB conditions were exposed to the different treatments: PAB-LC-21; PAB-LC-22; PAR+UVA+UVB, high CO<sub>2</sub> and pFe21 (PAB-HC-21) and PAR+UVA+UVB, high CO<sub>2</sub> and pFe22.3 (PAB-HC-22). Symbols are means of measurements in two independent replicate cultures and error bars indicate standard deviations.

### In vivo chlorophyll *a* fluorescence

The optimum quantum yield of PSII ( $F_v/F_m$ ) was used as an indicator of stress and photoinhibition (Figure 6.2.4). Initial values ( $T_0$ ) corresponded to values typically shown by healthy cells (around 0.6-0.7). In LC, there were differences between PAR treatments at 24 and 48 h, but, at the end of the experiment, both treatments showed the same values, indicating that cells were always healthy (Figure 6.2.4A). In contrast, PAB treatments caused a drop in both Fe conditions, decreasing  $F_v/F_m$  by 65% after 96 h of exposure to UVR (Figure 6.2.4A). There were significant differences due to the light treatment ( $p < 0.001$ ) but not due to Fe

concentration ( $p>0.05$ ). In PAB, the lowest values were found in LC treatments without differences between Fe concentrations (pFe21 vs. pFe22.3). Furthermore,  $F_v/F_m$  values in HC were higher with respect to LC treatments. The Fe effect was observed between HC treatments showing significant higher values with pFe21 concentration ( $p<0.001$ , Figure 6.2.4B).

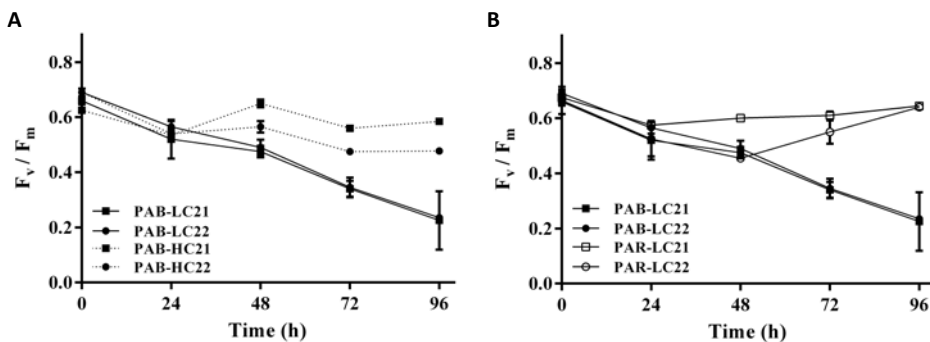


**Figure 6.2.4.** Changes in the optimum quantum yield ( $F_v/F_m$ ) in cultures of *Emiliana huxleyi* exposed to different irradiance, CO<sub>2</sub> and Fe treatments. (A) Cells in ambient CO<sub>2</sub> conditions were exposed to the different treatments, only PAR, ambient CO<sub>2</sub> and pFe21 (PAR-LC-21); only PAR, ambient CO<sub>2</sub> and pFe22.3 (PAR-LC-22); PAR+UVA+UVB, ambient CO<sub>2</sub> and low Fe (PAB-LC-21) PAR+UVA+UVB, ambient CO<sub>2</sub> and pFe22.3 (PAB-LC-22). (B) Cells in PAB conditions were exposed to the different treatments: PAB-LC-21; PAB-LC-22; PAR+UVA+UVB, high CO<sub>2</sub> and pFe21 (PAB-HC-21) and PAR+UVA+UVB, high CO<sub>2</sub> and pFe22.3 (PAB-HC-22). Symbols are means of measurements in two independent replicate cultures and error bars indicate standard deviations.

Photosynthetic parameters (Table 6.2.2) indicated that that the  $E_k$  and  $E_{opt}$  did not show any differences between treatments.  $rETR_{max}$  presented minimum values in LC treatments under PAB without differences due to Fe (PAB-LC treatments). There were no differences between treatments under only PAR and also, compared to HC at the higher Fe concentration (PAB-HC21). However, pFe22.3 had significant lowest values in HC treatments. The  $rETR$  at 200  $\mu\text{mol photons m}^{-2}$



$s^{-1}$ , the irradiance of the culture, and the photosynthetic efficiency ( $\alpha$ ) showed the same patterns described in  $rETR_{max}$  (Table 6.2.2).

**Table 6.2.2.** Photosynthetic parameters of *Emiliana huxleyi* calculated from chlorophyll *a* fluorescence measurements after 4 days of cultures at different conditions: PAR-LC-21 (only PAR, ambient  $CO_2$  and pFe21); PAR-LC-22 (only PAR, ambient  $CO_2$  and pFe22.3); PAB-LC-21 (PAR+UVA+UVB, ambient  $CO_2$  and pFe21); PAB-LC-22 (PAR+UVA+UVB, ambient  $CO_2$  and pFe22.3); PAB-HC-21 (PAR+UVA+UVB, high  $CO_2$  and pFe21) and PAB-HC-22 (PAR+UVA+UVB, high  $CO_2$  and pFe22.3). Data correspond to the mean  $\pm$  standard deviation ( $n=2-3$ ).  $rETR_{200}$  represents the electron transport rate at an irradiance of  $200 \mu mol e^{-} m^{-2} s^{-1}$  similar to culture conditions.

	PAR-LC21	PAR-LC22	PAB-LC21	PAB-LC22	PAB-HC21	PAB-HC22
$rETR_{200}$ ( $\mu mol e^{-} m^{-2} s^{-1}$ )	$38.0 \pm 1.6$	$36.3 \pm 0.3$	$14.2 \pm 5.5$	$15.5 \pm 3.0$	$34.8 \pm 0.6$	$28.8 \pm 0.1$
$rETR_{max}$ ( $\mu mol e^{-} m^{-2} s^{-1}$ )	$40.5 \pm 8.6$	$41.9 \pm 0.1$	$16.8 \pm 6.2$	$20.3 \pm 8.7$	$40.5 \pm 1.9$	$33.4 \pm 0.8$
$\alpha$ ( $e^{-} photons^{-1}$ )	$0.31 \pm 0.03$	$0.29 \pm 0.00$	$0.11 \pm 0.04$	$0.11 \pm 0.00$	$0.26 \pm 0.00$	$0.22 \pm 0.01$
$E_k$ ( $\mu mol photons m^{-2} s^{-1}$ )	$132 \pm 42$	$146 \pm 0.6$	$158 \pm 1.6$	$177 \pm 78$	$156 \pm 7.5$	$152 \pm 10$
$E_{opt}$ ( $\mu mol photons m^{-2} s^{-1}$ )	$263 \pm 84$	$293 \pm 1.6$	$316 \pm 3.2$	$355 \pm 156$	$311 \pm 15$	$303 \pm 20$

### Photosynthetic production of POC and DOC

The cell-normalised photosynthetic production of POC was affected by light,  $CO_2$  and Fe treatments ( $p < 0.05$ ). The pFe21 control showed the highest values increasing over time (Figure 6.2.5A). At the beginning of the experiment, there were significant differences between the two Fe concentrations ( $p < 0.05$ ). After exposure of the other two treatments (light and  $CO_2$  conditions) the trends changed between all conditions. The control for pFe21 (PAR-LC21) showed the highest POC productions (Figure 6.2.5A). The concentrations in LC21 under UVR exposure decreased significantly although the rates increased at the end of the experiment ( $p < 0.05$ ; 96 h). At this time, UVR inhibited 75% POC production in LC21



treatments (Figure 6.2.5A). In PAB conditions, the rate of POC production showed the highest values in HC21, with the same trend and values as the pFe21 control (PAR21). The treatments with pFe22.3 concentrations under UV exposure (PAB-22) showed higher values in the HC compared to the LC treatment during the experiment (Figure 6.2.5B).

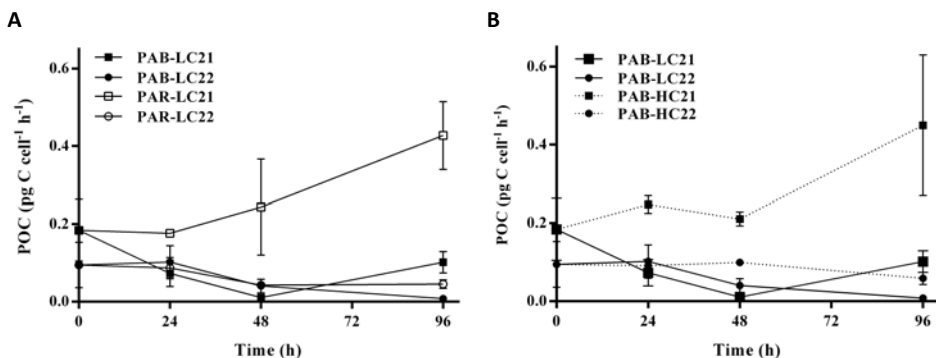


**Figure 6.2.5.** Changes in photosynthetic production of particulate organic carbon (POC) of *Emiliana huxleyi* cultures exposed to different irradiance, CO<sub>2</sub> and Fe treatments. (A) Cells in ambient CO<sub>2</sub> conditions were exposed to the different treatments, only PAR, ambient CO<sub>2</sub> and pFe21 (PAR-LC-21); only PAR, ambient CO<sub>2</sub> and pFe22.3 (PAR-LC-22); PAR+UVA+UVB, ambient CO<sub>2</sub> and low Fe (PAB-LC-21) PAR+UVA+UVB, ambient CO<sub>2</sub> and pFe22.3 (PAB-LC-22). (B) Cells in PAB conditions were exposed to the different treatments: PAB-LC-21; PAB-LC-22; PAR+UVA+UVB, high CO<sub>2</sub> and pFe21 (PAB-HC-21) and PAR+UVA+UVB, high CO<sub>2</sub> and pFe22.3 (PAB-HC-22). Symbols are means of measurements in two independent replicate cultures and error bars indicate standard deviations.

The fraction of fixed C released as DOC responded in a different way than POC production rates. In LC treatments, PAB-LC22 presented the highest values after 24 h of UVR exposure, but this rate dropped and remained steady until the end of the experiment (Figure 6.2.6A). DOC production rates increased significantly after 24 h of the exposure to UV and HC in PAB conditions. The rates decreased in all of the PAB treatments except in PAB-LC21 that showed the lowest values and the same trend during the experiment (Figure 6.2.6B).

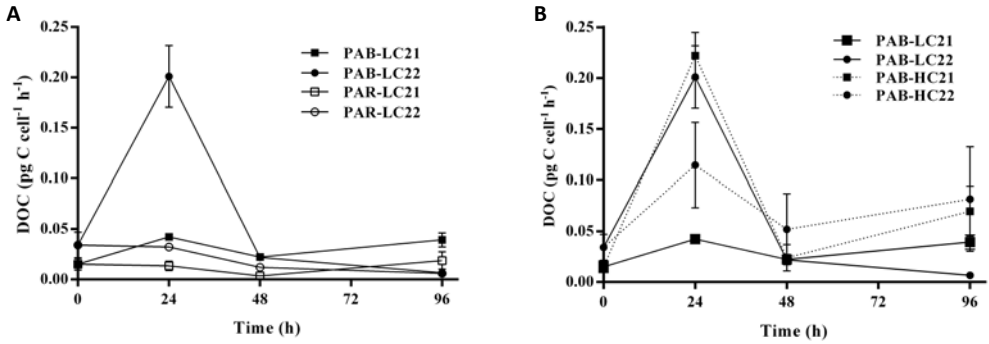


**Figure 6.2.6.** Changes in photosynthetic production of dissolved organic carbon (DOC) of *Emiliana huxleyi* cultures exposed to different irradiance, CO<sub>2</sub> and Fe treatments. (A) Cells in ambient CO<sub>2</sub> conditions were exposed to the different treatments, only PAR, ambient CO<sub>2</sub> and pFe21 (PAR-LC-21); only PAR, ambient CO<sub>2</sub> and pFe22.3 (PAR-LC-22); PAR+UVA+UVB, ambient CO<sub>2</sub> and low Fe (PAB-LC-21) PAR+UVA+UVB, ambient CO<sub>2</sub> and pFe22.3 (PAB-LC-22). (B) Cells in PAB conditions were exposed to the different treatments: PAB-LC-21; PAB-LC-22; PAR+UVA+UVB, high CO<sub>2</sub> and pFe21 (PAB-HC-21) and PAR+UVA+UVB, high CO<sub>2</sub> and pFe22.3 (PAB-HC-22). Symbols are means of measurements in two independent replicate cultures and error bars indicate standard deviations.

The percentage of DO<sup>14</sup>C extracellular release (PER) increased after 24 h of UV exposure ranging from 38 to 66% in the PAB treatments. The values in the different controls (PAR treatments) varied from 2 to 7% in pFe21 and from 12 to 28 % in pFe22 (Table 6.2.3). In general, the pFe22.3 treatments presented the highest PER compared to pFe21 treatments. At the end of the experiment, the controls (PAR treatments) showed the lowest percentage and LC-PAB treatments the highest. In PAB conditions, the treatments with pFe22.3 concentrations showed the highest percentages in comparison with the pFe21 treatments without differences between both CO<sub>2</sub> conditions (LC and HC). The percentage of the PAB-LC21 was 2-fold higher than PAB-HC21 treatment at the end of the experiment (Table 6.2.3).

**Table 6.2.3.** Percentage of DO<sup>14</sup>C extracellular release (PER) of dissolved organic carbon of *Emiliania huxleyi* at different conditions: PAR-LC-21 (only PAR, ambient CO<sub>2</sub> and pFe21); PAR-LC-22 (only PAR, ambient CO<sub>2</sub> and pFe22.3); PAB-LC-21 (PAR+UVA+UVB, ambient CO<sub>2</sub> and pFe21); PAB-LC-22 (PAR+UVA+UVB, ambient CO<sub>2</sub> and pFe22.3); PAB-HC-21 (PAR+UVA+UVB, high CO<sub>2</sub> and pFe21) and PAB-HC-22 (PAR+UVA+UVB, high CO<sub>2</sub> and pFe22.3). Data correspond to the mean  $\pm$  standard deviation (n=2).

	PAR-LC21	PAR-LC22	PAB-LC21	PAB-LC22	PAB-HC21	PAB-HC22
T0	7.5 $\pm$ 0.2	28.2 $\pm$ 5.8	-	-	-	-
T24	7.0 $\pm$ 1.9	27.5 $\pm$ 4.4	38.3 $\pm$ 11	66.5 $\pm$ 12.7	47.3 $\pm$ 0.3	54.9 $\pm$ 9.1
T48	1.8 $\pm$ 1.5	22.3 $\pm$ 4.2	25.9 $\pm$ 6.5	36.4 $\pm$ 8.1	10.3 $\pm$ 5.8	32.7 $\pm$ 17
T96	4.4 $\pm$ 2.7	11.9 $\pm$ 4.1	28.5 $\pm$ 9.2	45.8 $\pm$ 2.9	13.5 $\pm$ 0.6	55.8 $\pm$ 9.9

### PIC production

The PIC production was only measured at the end of the experiment (Figure 6.2.7). In LC, the PAR treatments showed significant differences between both Fe conditions, the calcification was inhibited by 80% ( $p < 0.05$ ) in the lower Fe concentration. PAB showed lower values compared to PAR conditions between LC treatments (Figure 6.2.7A). There was 90% inhibition of PIC production in pFe21 and 50% in pFe22.3. The LC treatments showed no differences due to the Fe concentrations in PAB. HC presented higher values compared with LC in PAB (CO<sub>2</sub> treatment,  $p < 0.001$ ). Comparing the controls (PAR treatments) with HC (PAB conditions), there was 20% inhibition in pFe21 concentration, whereas a decrease of 25% was observed in pFe22.3.

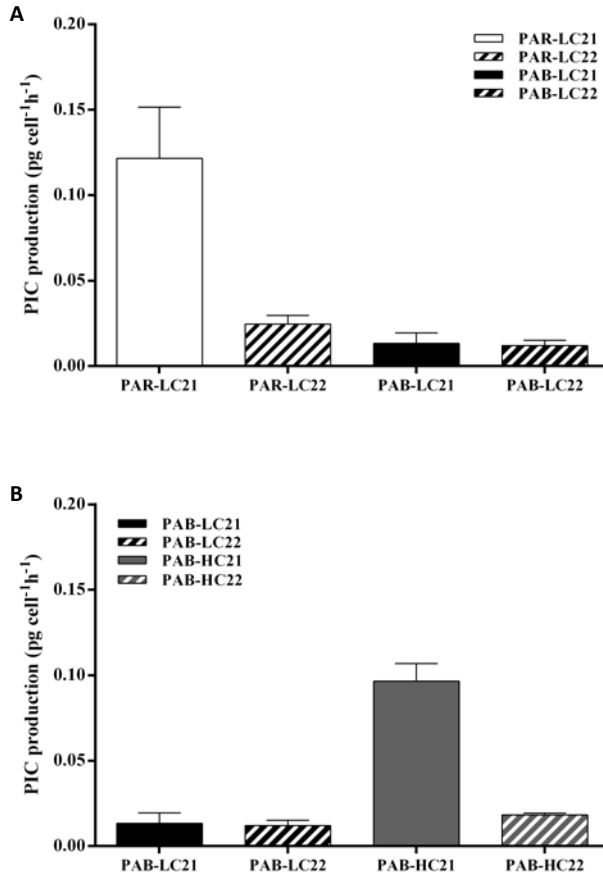


**Figure 6.2.7.** Calcification rates of *Emiliania huxleyi* after 4 days of cultures exposed to different irradiance, CO<sub>2</sub> and Fe treatments. (A) Cells in ambient CO<sub>2</sub> conditions were exposed to the different treatments, only PAR, ambient CO<sub>2</sub> and pFe21 (PAR-LC-21); only PAR, ambient CO<sub>2</sub> and pFe22.3 (PAR-LC-22); PAR+UVA+UVB, ambient CO<sub>2</sub> and low Fe (PAB-LC-21) PAR+UVA+UVB, ambient CO<sub>2</sub> and pFe22.3 (PAB-LC-22). (B) Cells in PAB conditions were exposed to the different treatments: PAB-LC-21; PAB-LC-22; PAR+UVA+UVB, high CO<sub>2</sub> and pFe21 (PAB-HC-21) and PAR+UVA+UVB, high CO<sub>2</sub> and pFe22.3 (PAB-HC-22). Data are mean means of measurements in two independent replicate cultures and error bars indicate standard deviations.

## Discussion

This study shows that the physiological processes in *Emiliania huxleyi* were affected with both separate and simultaneous changes in Fe availability and carbonate chemistry, including the negative stress generated by UV radiation exposure. Reduced Fe concentration constrained the capacity of this species to cope with UVR-induced stress. Such cell stress was alleviated under increased CO<sub>2</sub> respect to ambient CO<sub>2</sub> conditions even in Fe-depleted cultures (pFe22.3), as evidenced by increasing photosynthetic production of POC, electron transport rates and calcification. Furthermore, this response was also evident in the specific growth rates and cell viability in Fe-replete conditions (pFe21).

### *Emiliania huxleyi*'s physiology was controlled by Fe levels

*Emiliania huxleyi* showed a significant reduction in growth (ca. 25%) without Fe addition in only PAR although the growth rate was still high in this Fe condition ( $\mu = 0.7 \text{ d}^{-1}$ ). It is known that coastal strains of this species are able to maintain similar growth rates under different Fe concentrations, even in the absence of Fe additions (Guo et al. 2012), or that oceanic strains show higher rates in absence of Fe in comparison with cultures with the metal added (Muggli & Harrison 1997). The POC production results obtained in the in pFe21 conditions are in agreement with former data obtained with the same strain under high Fe concentrations (Chapter 6.1). Schulz et al. 2007 demonstrated that the reduction of photosynthetic carbon fixation in Fe-depleted scenarios compared to Fe-replete conditions were the result of decreased active CO<sub>2</sub> and HCO<sub>3</sub><sup>-</sup> uptake fluxes, and decreased activity of CCMs and carbon fixation efficiency. In line with this, the photosynthetic production of POC was also reduced in pFe22.3 cultures and decreased over time (Figure 6.2.5A). This reduction was also observed in the diatom *Chaetoceros simplex* under low iron concentrations in parallel with decreased of the photosynthetic parameters (Petrou et al. 2014). Similarly, Hoppe et al. 2013 determined significant differences in  $F_v/F_m$  and rETR<sub>s</sub> in a natural





community dominated by diatoms with different iron levels, such combination of symptoms has been proposed to be typical of Fe deficient algae (Behrenfeld & Milligan 2013). Our results showed that the photochemical performance of the coccolithophore was unaffected by Fe concentration, including  $F_v/F_m$ , which indicates the efficiency of PSII and it is used as a marker for stress (Table 6.2.2 and Figure 6.2.4). Iron is required for photosystems functioning, the cytochrome *b6f* complex, and ferredoxin (Raven 1990). Given the substantial requirement of iron within the photosynthetic electron transport chain, Fe-limitation strongly influences electron transport kinetics. Thus, our strain could maintain the photosynthetic electron transport chain practically unaltered, in spite of the low concentration of Fe presented in pFe22.3 cultures.

The production of POC via photosynthetic production is accompanied by the extracellular release (ER) of various amounts of dissolved DOC. Dissolved organic carbon release has been proposed as a regulatory mechanism able to respond to the environment (Fogg 1983, Sobrino et al. 2014), which would maintain the metabolic integrity of the cell and would protect the photosynthetic apparatus from an overload of products that cannot be used in growth or stored (Wood & Van Valen 1990). Furthermore, it has been related to stress conditions (Fogg 1983, Wood & Van Valen 1990, Berman-Frank & Dubinsky 1999). Our results indicated low levels of DOC production without differences between both Fe conditions. The Fe-depleted cultures showed higher percentages of extracellular release (PER) indicating stressful conditions in comparison with pFe21. Yet, the PIC production, (i.e. calcification), was also reduced with lower Fe concentrations as previously demonstrated by Schulz et al. (2007).

### **UVR inhibited cells growth at lower Fe concentration**

UVR has been shown to have inhibitory effects in the physiology of phytoplankton, such as increased membrane permeability, changes in cell elemental composition, DNA damage, impairment of light transduction and carbon assimilation



mechanisms, and reduced growth (Buma et al. 1996, Häder et al. 2007). The growth of *E. huxleyi* is sensitive to UVR (Buma et al. 2000, Van Rijssel & Buma 2002, Guan & Gao 2010). The growth rates decreased ca. 30% in *E. huxleyi* in the presence of UVR in both Fe levels under ambient CO<sub>2</sub> conditions (Figure 6.2.1). The pFe22.3 treatments under UVR showed higher sensitivity to UVR, decreasing viability after by the end of the experiment (Figure 6.2.2A & 6.2.3A). The detrimental effects of UV exposure were also shown by the decrease of the photosynthetic production of POC in both Fe conditions but especially in the Fe-depleted cultures. This was also in agreement with the diminished photosynthetic parameters in both Fe conditions under UVR (Table 6.2.2). The inhibition of photosynthesis could be mostly due to decreased photochemical efficiency and repair rates, which can be attributed to UV-induced damage of the D1 protein (Bouchard et al. 2005). The damage produced on PSII cause photoinhibition, decreasing photosynthetic activity and growth (Häder 2011) as observed in our results.  $F_w/F_m$  decreased over time without differences between both Fe concentrations indicating the UVR-induced stress.

The production of DOC has been related to stress conditions including nutrient limitation, photoinhibition by PAR and UVR and cell death (Sharp 1977, Mague et al. 1980, Carrillo et al. 2002, Agustí & Duarte 2013). *Emiliania huxleyi* increased DOC production when the cells were acclimating to stress conditions (i.e exposure to UVR in Fe-depleted cultures). Thus, LC-PAB22 showed a sharply increase at 24 h. After that, DOC production decreased, but the cultures maintained higher values (Figure 6.2.6A). Other reports describe the relation between DOC production and UV exposure (Carrillo et al. 2002, Panzenböck 2007, Fuentes-Lema et al. 2015). In this study, the highest percentages of DOC release (PER) were obtained in Fe-depleted cultures under UV exposure. Although these percentages showed higher values in the cultures exposed to UVR and/or Fe-depleted (Table 6.2.3) compared to the control of Fe-replete cultures. The





percentages showed in this treatment (PAR-21) indicated that the cells seemed healthy (PER < 10%, Sharp 1977).

The molecular mechanisms for calcification in *E. huxleyi* must have been negatively affected by UVR. Inhibition of calcification by UVR was ca. 90% in pFe21 cultures to ca. 50% in Fe-depleted cultures. UV stress might have further stimulated such strategy for much less calcification in both Fe conditions. The inhibition of Fe-depleted cultures was lower than pFe21 cultures probably because there was a previous inhibition under low Fe concentration. This inhibition in calcification due to UVR has been previously documented (Raven & Crawford 2012). It is known that nutrient limitation enhances UV-induced inhibition due to the reduced capacity of algae to screen out UVB and/or impairment of their capacity to repair damage (Beardall et al. 2014). The major differences in all processes were due to Fe deficiency although UVR exposure augmented this inhibition.

### **Increased CO<sub>2</sub> allows cells to cope better with photoinhibition**

The responses to UVR at high CO<sub>2</sub> levels vary between phytoplankton species (Gao et al. 2009, 2012, García-Gómez 2014, Sobrino et al. 2005, 2008, 2009, Wu et al. 2012). The downregulation of the photosynthetic machinery in phytoplankton under high CO<sub>2</sub> conditions increasing the resource use efficiency (Raven 1991) has been proposed as a possible response. High CO<sub>2</sub> concentrations elevate passive diffusion and reduce the amount of energy and metabolites necessary to drive the active transport of carbon to Rubisco, leaving this energy for other mechanisms. Such energy would be diverted to other physiological processes in cells including mechanisms to minimise or repair damage (García-Gómez et al. 2014, Sobrino et al. 2005). In the diatom *Phaeodactylum tricoratum*, increased CO<sub>2</sub> and UVB exposure showed antagonistic effects, resulting in fast photochemical recovery and a higher repair/damage ratio in the cells grown in higher CO<sub>2</sub> conditions (Li et al. 2012). Another possibility is that the sensitivity of phytoplankton is increased



under high solar radiation (Sobrino et al. 2008, 2009, Gao et al. 2009, 2012, Wu et al. 2012). Our results showed a significant increase in cell's efficiency in those cultures acclimated to high CO<sub>2</sub> when compared to cells in ambient conditions under PAB, in agreement with the observed response in the unicellular chlorophyte *Dunaliella tertiolecta* (García-Gómez et al. 2014). The growth rates, the photophysiology, and the POC and PIC production rates were higher in HC than in ambient CO<sub>2</sub> and UVR exposed cells. The response of POC production in *E. huxleyi* is strain-specific (Langer et al. 2006, 2009), showing decreases, increases or no response in cultures grown in high CO<sub>2</sub> concentrations (Riebesell & Tortell 2011). The strain used in this study also showed an increase in POC production with high CO<sub>2</sub> conditions under only PAR exposure (Chapter 6.1). A contradictory result was observed with *E. huxleyi*, showing an inhibition of POC production with high CO<sub>2</sub> concentrations under PAB conditions (Gao et al. 2009). The response of PIC production was different and calcification was also more inhibited with the exposure to UVR (Gao et al. 2009). These differences could be due to different responses between strains under same conditions as mentioned above, given the high within-strain genomic variability existing in this species (Read et al. 2013). Van de Poll et al. 2009 showed an increase in ROS scavengers in Fe-limited cells, because Fe-limited cultures were less sensitive to high levels of PAR and UVR than Fe-replete cultures. We suggest that a similar response of antioxidant activity could be present in HC cultures maybe as a result of a direct CO<sub>2</sub> signalling – mediated response, reducing the inhibition produced by UVR. A possible antioxidant system could be the DMSP and its breakdown products (DMS, acrylate, dimethylsulphoxide, and methane sulphonic acid) (Sunda et al. 2002) although the general response to elevated CO<sub>2</sub> is a decrease in DMS production (Hopkinson et al. 2011) but this response could change with interactive effects between two variables (Arnold et al. 2013).

This positive response was more evident in pFe21 than in Fe-depleted cultures. The response of the Fe-depleted cultures only showed significant





differences between both CO<sub>2</sub> conditions in the photophysiology and POC production. These minimal effects of high CO<sub>2</sub> conditions under iron-depleted conditions compared with iron-replete conditions have been observed previously in natural phytoplankton communities (Hoppe et al. 2013) and in laboratory experiments (Sugie & Yoshimura 2016).

### Concluding remarks

In this study, we analysed the effects of Fe concentrations and increased CO<sub>2</sub> in the physiology of the coccolithophorid *Emiliana huxleyi* with UVR. The concentration of Fe played the major role in control the response of all processes, reducing the capacity of the *E. huxleyi* cells to cope the stress with Fe-depletion. The exposure to UV radiation inhibited the physiological processes as growth rate, photosynthesis and calcification of *E. huxleyi*, but the interaction with increased CO<sub>2</sub> reduced the negative effects under UV exposure. The results obtained in this short-term experiment contribute to a better understanding of first-order responses of the physiological processes, but the progress of ocean acidification in nature is a much slower process. Thus the extrapolation of laboratory data shall take in account that long-term adaptive responses could differ from short-term results (Lohbeck et al. 2012, Collins et al. 2014). However, the plastic responses showed in this study could provide relevant information for the future acidified ocean ecosystem because phenotypic plasticity may be important for the subsequent adaptation of organisms (Collins et al. 2014). Little is known about the interactive effects of Fe concentrations, increased CO<sub>2</sub> conditions and UVR exposure in phytoplankton. Thus, we will need more studies both in the short and long-term effect on these conditions to be able to understand phytoplankton ecophysiology under a changing ocean.



### **Acknowledgments**

Chapter 6.1: This work was funded by CTM/MAR 2010-17216 research grant from the Spanish Ministry for Science and Innovation (Spain) to MS. MRL was funded by a FPU grant from the Ministry for Education and Plan Propio grant from University of Malaga (Spain). We thank Patrick J Neale for hosting MRL at his laboratory for the BWFs study, Eileen Bresnan, Pablo Leon and Víctor M Vazquez for SEM analysis. We also thank Cristina Sobrino for discussions and suggestions.

Chapter 6.2: This work was funded by CTM/MAR 2010-17216 (PHYTOSTRESS) research grant from the Spanish Ministry for Science and Innovation (MICINN) (Spain) to MS. MRL was funded by FPU grant from the Ministry for Education. We also thank Pavel Rychtecky for his help during the experiment.



## Supplemental Material

**Supplemental Figure 6.2.1S.** Seawater carbonate system during the experiment. The  $\text{CO}_2$  speciation was calculated using the  $\text{CO}_2$ -calc Package (Robbins et al. 2010) with the  $\text{CO}_2$  acidity constants of Mehrbach et al. (1973). Values are the mean  $\pm$  standard deviation (SD).

Treatment	$\text{pH}_{\text{NBS}}$	$\text{pCO}_2$ ( $\mu\text{atm}$ )	$\text{CO}_2$ ( $\mu\text{mol kg SW}^{-1}$ )	$\text{HCO}_3^-$ ( $\mu\text{mol kg SW}^{-1}$ )	$\text{CO}_3^{2-}$ ( $\mu\text{mol kg SW}^{-1}$ )
PAR-LC-21	$8.38 \pm 0.10$	$267 \pm 27$	$9.4 \pm 0.9$	$283 \pm 18$	$283 \pm 18$
PAR-LC-22	$8.29 \pm 0.02$	$333 \pm 13$	$11.5 \pm 0.7$	$239 \pm 5.7$	$239 \pm 5.7$
PAB-LC-21	$8.23 \pm 0.04$	$407 \pm 40$	$14 \pm 1.4$	$216 \pm 14.1$	$216 \pm 14.1$
PAB-LC-22	$8.20 \pm 0.03$	$432 \pm 39$	$15 \pm 1.5$	$204 \pm 8.5$	$204 \pm 8.5$
PAB-HC-21	$7.88 \pm 0.08$	$1002 \pm 89$	$35.5 \pm 3.5$	$106 \pm 8.5$	$106 \pm 8.5$
PAB-HC-22	$7.85 \pm 0.05$	$1100 \pm 19$	$41 \pm 2.8$	$102 \pm 1.4$	$102 \pm 1.4$



## Chapter 7

# General Discussion and Conclusions





## General Discussion

Previous studies have focused on unravelling the effect of ocean acidification as the unique stressor to elucidate the physiological, ecological and biogeochemical consequences of this stressor in nature. Although all this information has helped to get a deeper knowledge, there are increasing evidences that this traditional reductive approach cannot capture a truly prognostic view of future ecosystem changes. Ocean acidification has profound and diverse consequences for marine organisms and ecosystems but will not occur in isolation. Concurrent shifts in many other environmental factors could all potentially influence the biological effects of increased CO<sub>2</sub> concentration, including temperature, macronutrients, trace metals, oxygen content, stratification, mixing, and irradiance (Boyd et al. 2010, Boyd & Hutchins 2012). The interactive effects of CO<sub>2</sub> and Fe observed in our mesocosm study highlight the importance of examining multiple stressors simultaneously combined in natural communities.

Manipulative experiments can be performed on various scales ranging from cultures controlled in a laboratory to whole ecosystem perturbation studies. The controlled laboratory experiments let us to study the physiological mechanisms involved in organism responses, but the analysis of this response to community and ecosystem level requires larger scale community level experiments (Riebesell et al. 2008). Thus, mesocosm experiments allow directly analysis of the interactive effects of multiple stressors across multiple trophic levels (Riebesell et al. 2010, Stewart et al. 2013, Riebesell & Gattuso 2015). Mesocosms show a high degree of realism compared to controlled laboratory experiments, and lack the limitations of large-scale ocean acidification experiments in the natural system (Stewart et al. 2013). Recent mesocosm experiments have provided a wealth of information on the sensitivities of natural assemblages to ocean changes (Riebesell et al. 2008).



In this work, we investigated the interactive effects of CO<sub>2</sub> and iron availability on functional plankton groups within predicted future scenarios using mesocosms and employing a full-factorial design, comprising all combinations of ambient and increased pCO<sub>2</sub> and dFe. The dissolved Fe levels were enhanced at increased CO<sub>2</sub> conditions due to pH lower as previously observed in a mesocosm experiment in the same fjord (Breithbarth et al. 2010). Furthermore, the addition of DFB enhanced dFe levels, likely due to an increase in Fe solubility with a decrease in particulate Fe concomitant to an increase in dissolved Fe. Thus, the manipulation of both factors increased the dissolved Fe levels in this fjord. This work demonstrates that ocean acidification can enhance Fe bioavailability, contrary to the idea that Fe is rarely limited in fjord and/or estuarine environments, and that ocean acidification might decrease or does not change Fe availability depending on the organic ligands.

These conditions promoted the development of two clearly differentiated phases. During phase 1 (days 1-10), a phytoplankton bloom succession (Paulino et al. 2008) occurred without differences due to the factors (Fe and CO<sub>2</sub>). But a strong community response was evident in phase 2 (days 11-22), where the coccolithophore *Emiliania huxleyi* biomass massively increased at ambient CO<sub>2</sub> and high dFe. However, the rest of planktonic groups with the exception of *Synechococcus* sp. did not show any effect during this phase. The effects of increased pCO<sub>2</sub> in *E. huxleyi* are in agreement with former mesocosms studies (Riebesell et al. 2007), showing that elevated pCO<sub>2</sub> had a detrimental impact on the net growth and biomass of the coccolithophore. However, the results obtained in the control condition of our experiment, revealed that the cells were most likely experiencing Fe limitation (i.e. the rate of dFe supply is slower than that of iron demand by the coccolithophore), which was affecting their growth rates and consequently biomass increase.



The bloom of *Emiliana huxleyi* was promoted by an observed increase in carbon assimilation processes although the mechanisms of inorganic carbon acquisition were unaffected by the different conditions. We observed the presence of pigments with light-harvesting functions that seemed to be highly efficient transferring energy to chlorophylls, hence leading to a better functioning of the electron transport chains. Furthermore, DNA lesions accumulated to excess irradiance measured in the fjord (cyclobutane pyrimidine dimers, CPDs) were minimised by high dFe showing that Fe is needed for DNA repair and to overcome oxidative stress in *E. huxleyi* because every aspect of thylakoid electron transport and accessory pigments is also iron dependent.

The availability of metals can influence phytoplankton growth and community structure (Morel & Price 2003). In turn, plankton may control the distribution, chemical speciation, and cycling of metals in the ocean (Sunda 2012). Therefore, we analysed the origin (lithogenic and biogenic) and the evolution of different trace metals (Fe, Cu, Zn, Mn, Co, Cd and Mo) concentrations during the bloom of *E. huxleyi*. This study is the first to combine trace metal analyses of particles in a controlled mesocosm experiment with simultaneous manipulation of CO<sub>2</sub> and Fe levels using natural assemblages of marine phytoplankton. Our results demonstrate that in the studied fjord, particulate Ti and Fe concentrations were dominated by lithogenic material. We think that the lithogenic fraction of Fe in the bulk particles in our experiment masked the biogenic signal, as proposed by King et al. 2012. In contrast, particulate Cu, Co, Mn, Zn, Mo and Cd concentrations showed a strong biogenic influence. Specially, particulate Zn and Cu concentrations were especially high in the LC+DFB treatment, where the highest *E. huxleyi* biomass was observed. This coccolithophorid showed high Zn cellular requirements to other phytoplankton (Sunda 2012) but the unique physiological functions of Zn are still unresolved. However, the genome of *E. huxleyi* provides evidences for the importance of Zn nutrition in this coccolithophore. Considering that the concentration of dissolved Zn could indirectly affect the global C pump by



influencing the growth of coccolithophores due to the importance of this group in the global carbon cycle. Likewise, the particulate Cu concentrations were high probably due to the high dissolved Cu concentration measured in this fjord, the presence of phytochelatins or other detoxification mechanisms (Ahner et al. 2002) to buffer high intracellular Cu due to unregulated uptake and/or the high Cu requirements to maintain maximum growth rate as previously reported (Guo et al. 2012). According to our results, ocean acidification is expected to change the relative concentrations of particulate metals, due to the differential effects of ocean acidification on the growth of marine phytoplankton species, and the contrasting metal requirements of phytoplankton phyla. Therefore, as suggested by Twining & Baine (2013), we require the development of ecophysiological models that link trace element composition of phytoplankton to physiological performance considering the changing environmental conditions.

The importance of metals could be related with the limitation of Fe that cells experienced in the control treatment (ambient CO<sub>2</sub> and Fe conditions). These cells showed the combination of symptoms typical of Fe deficient algae: slower net growth rates, reduced Chl *a* and lower F<sub>v</sub>/F<sub>m</sub> (Behrenfeld & Milligan 2013). Furthermore, it is demonstrated that dFe levels in the control were insufficient because they were below the cell's iron demand to sustain the biomass achieved during the peak of the bloom at ambient CO<sub>2</sub> and increased dFe. The processes of carbon assimilation also pinpointed this limitation, and the carbon fixation rates were similar to the rates of high CO<sub>2</sub> treatments (affected by ocean acidification). This indicates that *E. huxleyi* cells may down-regulate their maximum carbon fixation capacity due a constrained metabolism because iron was limiting.

The net growth rate, biomass and calcification of *E. huxleyi* were affected by ocean acidification due to the changes in the pH. The intracellular pH in coccolithophores is particularly sensitive to changes in external pH (Suffrian et al. 2011) and maintaining a constant intracellular pH is energetically costly, affecting



ocean acidification the cellular energy demands (Flynn et al. 2012, Taylor et al. 2012). Our results suggest that *E. huxleyi* is able to utilise DFB-bound Fe (FeDFB) as previously demonstrated (Shaked & Lis 2012, Lis et al. 2015). Thus, increased dFe may have helped the cells to meet the extra metabolic demands imposed by the decrease in pH during the experiment, allowing them to cope better with the unfavourable effects of ocean acidification and to sustain the growth rates. The physiological stress response of the community and in particular that of *Emiliania huxleyi* was affected by the changes in CO<sub>2</sub> and Fe concentrations. The protective mechanisms (i.e. pigmentary response) were negatively affected by CO<sub>2</sub> levels but, most of them positively by dFe, highlighting that cells under low Fe concentration showed a high susceptibility to photooxidation, pointing out to a constrained physiological status of these cells that was amended when Fe was available. The same applies for the thylakoidal electron transport chain that showed how dFe positively modulated the effect of increased CO<sub>2</sub>. The most probable reason for the negative effect caused by high CO<sub>2</sub> is that cell homeostasis is lost because of intracellular changes in pH and the difficulty of maintaining them (Flynn et al. 2012, Taylor et al. 2012). DNA lesions and oxidative stress were minimised by high dFe. Thus, Fe is needed for DNA repair and to overcome oxidative stress in *E. huxleyi*, ensuring cellular viability and growth. Fe might be indirectly needed to fulfil the energy requirements imposed by the proteins involved in these processes, and that is not supplied under ambient dFe due to limitation, or that is diminished due to the negative effect of OA on cell's physiology.

This study demonstrates that the detrimental effects of increased pCO<sub>2</sub> on these strains can be partially mitigated by enhanced dFe in areas with high total Fe concentrations (particulate and dissolved Fe), possibly having cascading effects on food web dynamics, carbon export, and the rain ratio, finally affecting the exchange of CO<sub>2</sub> across the ocean-atmosphere interface.



### Future perspectives

These results highlighted that it is necessary to assess the combined effects of global environmental factors to understand the future responses of the ecosystem to ocean acidification. Thus, we initiated some approaches to understand the effect of the light (UV radiation) in the interaction between Fe and CO<sub>2</sub> availability. The experiments were performed under controlled laboratory cultures with a strain of *Emiliana huxleyi* from coastal waters from the Roscosff Culture Collection. Firstly, we estimated the sensitivity to UVR exposure in relation to wavelength by biological weighting functions (BWFs) (reviewed by Neale 2000). We proposed an appropriate model for the estimation the inhibition of photosynthesis under PAR and UVR exposures in ambient and future CO<sub>2</sub> conditions. Our results indicate that the sensitivity to UVR will be the same at ambient and high CO<sub>2</sub> conditions (future prediction) for the strain of *Emiliana huxleyi* used. After this, we studied the effect of the Fe concentration in the physiological processes of *Emiliana huxleyi* in both CO<sub>2</sub> conditions (ambient and future) under UV exposure. We analysed the inhibition of the exposure to UV radiation in comparison with the exposure to only PAR. The results showed that reduced concentrations of Fe restricted the capacity to manage stress conditions generated by the exposure to UVR in this specie. Furthermore, the stress was alleviated in increased CO<sub>2</sub> under UVR exposure as evidenced by increasing photosynthetic production of POC, electron transport rates and calcification even in Fe-depleted cultures. This demonstrates that *E. huxleyi* coped better with the stress generated by the exposure to UVR in increased CO<sub>2</sub>, and that Fe concentration played a major role in controlling the response of all processes.



## Conclusions

1. *Emiliana huxleyi* was iron limited at ambient CO<sub>2</sub> and ambient dissolved Fe concentrations in the studied fjord and in the control treatment.
2. The siderophore desferrioxamine B (DFB) and high CO<sub>2</sub> increased the concentration of dissolved Fe in the fjord.
3. Increased CO<sub>2</sub> negatively affected *Emiliana huxleyi* and *Synechococcus* sp while the rest of the plankton community was unaffected.
4. Increased dissolved Fe enhanced *Emiliana huxleyi* growth and its biomass at ambient CO<sub>2</sub> and mitigated the negative effect of high CO<sub>2</sub>.
5. *Emiliana huxleyi* seems to have bicarbonate transporters due to the low activity of the external carbonic anhydrase and the use of bicarbonate as inorganic carbon source.
6. Carbon assimilation was always higher under increased dissolved Fe and it was negatively impacted by elevated CO<sub>2</sub> concentration.
7. Calcification was reduced at increased CO<sub>2</sub> and it was unaffected by Fe. As a consequence, the rain ratio decreased in high CO<sub>2</sub> regardless of Fe, directly affecting the biological C-pump.
8. Elevated CO<sub>2</sub> concentration had a negative effect in the pigmentary concentration and thylakoidal electron transport chain that was counterbalanced by increased Fe levels.



9. Iron is needed for DNA repair and for reactive oxygen species (ROS) scavenging.
10. All the particulate trace metals analysed were from biogenic origin except Fe and Ti.
11. Increased CO<sub>2</sub> changed the relative quotas of particulate metals due to its effect on the growth of the different phytoplankton taxa. Therefore, such quotas were modulated by dissolved Fe concentration.
12. Exposure of *E. huxleyi* cultures to UV radiation (UVR) showed the same effect in photosynthesis in both elevated and ambient CO<sub>2</sub> conditions.
13. The ultraviolet radiation (UVR) sensitivity of *Emiliana huxleyi* cultures to different CO<sub>2</sub> conditions is dependent on Fe levels.
14. High CO<sub>2</sub> induced a lower UV radiation sensitivity in *Emiliana huxleyi* cultures regardless of Fe levels.

## References

- Agusti S, Duarte CM** (2013) Phytoplankton lysis predicts dissolved organic carbon release in marine plankton communities. *Biogeosciences* 10: 1259–1264
- Ahner BA, Liping W, Oleson JR, Ogura N** (2002) Glutathione and other low molecular weight thiols in marine phytoplankton under metal stress. *Mar Ecol Prog Ser* 232:93-103
- Andersen RA, Berges JA, Harrison PJ, Watanabe M** (2005) Recipes for Freshwater and Seawater Media, in: *Algal Culturing Techniques*, edited by: Andersen, RA, Elsevier Academic Press, Hong Kong, 429–538
- Andreasson KIM, Wängberg S-A** (2006) Biological weighting functions as a tool for evaluating two ways to measure UVB radiation inhibition on photosynthesis. *J Photochem Photobiol B* 84:111–8
- Arnold HE, Kerrison P, Steinke M** (2013) Interacting effects of ocean acidification and warming on growth and DMS-production in the haptophyte coccolithophore *Emiliana huxleyi*. *Glob Chang Biol* 19:1007–1016
- Baar de HJW, Boyd PW** (2000) The role of iron in plankton ecology and carbon dioxide transfer of the global oceans. In Hanson RB, Ducklow HW, Field JG (eds) *The changing ocean carbon cycle*. Cambridge University Press, p 61-140
- Bach LT, Riebesell U, Schulz KG** (2011) Distinguishing between the effects of ocean acidification and ocean carbonation in the coccolithophore *Emiliana huxleyi*. *Limnol Oceanogr* 56:2040–2050
- Bach LT, Bauke C, Meier KJS, Riebesell U, Schulz KG** (2012) Influence of changing carbonate chemistry on morphology and weight of coccoliths formed by *Emiliana huxleyi*. *Biogeosciences* 9:3449–3463
- Bach LT, MacKinder LCM, Schulz KG, Wheeler G, Schroeder DC, Brownlee C, Riebesell U** (2013) Dissecting the impact of CO<sub>2</sub> and pH on the mechanisms of photosynthesis and calcification in the coccolithophore *Emiliana huxleyi*. *New Phytol* 199:121–134
- Barbeau K, Rue EL, Trick CG, Bruland KT, Butler A** (2003). Photochemical reactivity of siderophores produced by marine heterotrophic bacteria and cyanobacteria based on characteristic Fe(III) binding groups. *Limnol Oceanogr* 48, 1069–1078
- Beardall J, Giordano M** (2002) Ecological implications of microalgal and cyanobacterial CO<sub>2</sub> concentrating mechanisms, and their regulation. *Funct Plant Biol* 29:335–334
- Beardall J, Raven J** (2004) The potential effects of global climate change on microalgae photosynthesis, growth and ecology. *Phycologia* 43:26–40
- Beardall J, Stojkovic S, Larsen S** (2009) Living in a high CO<sub>2</sub> world: impacts of global climate change on marine phytoplankton. *Plant Ecol Divers* 2:191–205

- Beardall J, Stojkovic S, Gao K** (2014) Interactive effects of nutrient supply and other environmental factors on the sensitivity of marine primary producers to ultraviolet radiation: Implications for the impacts of global change. *Aquat Biol* 22:5–23
- Beaufort L, Probert I, Garidel-Thoron T de, Bendif EM, Ruiz-Pino D, Metzl N, Goyet C, Buchet N, Coupel P, Grelaud M, Rost B, Rickaby REM, de Vargas C** (2011) Sensitivity of coccolithophores to carbonate chemistry and ocean acidification. *Nature* 476:80–83
- Behrenfeld MJ, Milligan AJ** (2013) Photophysiological expressions of iron stress in phytoplankton. *Ann Rev Mar Sci* 5:217–246
- Bellerby RGJ, Schulz KG, Riebesell U, Neill C, Nondal G, Heegaard E, Johannessen T, Brown KR** (2008) Marine ecosystem community carbon and nutrient uptake stoichiometry under varying ocean acidification during the PeECE III experiment. *Biogeosciences* 5:1517–1527
- Berge T, Daugbjerg N, Andersen BB, Hansen PJ** (2010) Effect of lowered pH on marine phytoplankton growth rates. *Mar Ecol Prog Ser* 416:79–91
- Berman-Frank I, Dubinsky Z** (1999) Balanced growth in aquatic plants: myth or reality? *Bioscience* 49: 29–37
- Billard C** (1994) Life cycles. In Green JC. & Leadbeater BSC (Eds.) *The Haptophyte Algae*. Clarendon Press, Oxford, UK p 167–186
- Bodt C De, Oostende N Van, Harlay J, Sabbe K, Chou L** (2010) Individual and interacting effects of pCO<sub>2</sub> and temperature on *Emiliana huxleyi* calcification: Study of the calcite production, the coccolith morphology and the coccosphere size. *Biogeosciences* 7:1401–1412
- Boelen P, Veldhuis M, Buma A** (2001) Accumulation and removal of UVBR-induced DNA damage in marine tropical plankton subjected to mixed and simulated non-mixed conditions. *Aquat Microb Ecol* 24:265–274
- Bouchard JN, Campbell DA, Roy S** (2005) Effects of UV-B radiation on the D1 protein repair cycle of natural phytoplankton communities from three latitudes (Canada, Brazil, and Argentina). *J Phycol* 41:273–286
- Bouchard JN, García-Gómez C, Lorenzo MR, Segovia M** (2013) Differential effect of ultraviolet exposure (UVR) in the stress response of the Dinophyceae *Gymnodinium* sp. and the Chlorophyta *Dunaliella tertiolecta*: mortality versus survival. *Mar Biol* 160:2547–2560
- Boyd PW, Doney SC** (2002) Modelling regional responses by marine pelagic ecosystems to global climate change. *Geophys Res Lett* 29:53–1–53–4
- Boyd P, Hutchins D** (2012) Understanding the responses of ocean biota to a complex matrix of cumulative anthropogenic change. *Mar Ecol Prog Ser* 470:125–135



- Boyd PW, Dillingham PW, McGraw CM, Armstrong EA, Cornwall CE, Feng Y -Y., Hurd CL, Gault-Ringold M, Roleda MY, Timmins-Schiffman E, Nunn BL** (2016) Physiological responses of a Southern Ocean diatom to complex future ocean conditions. *Nat Clim Change* 6:207-213
- Boye M, van den Berg CMG** (2000) Iron availability and the release of iron-complexing ligands by *Emiliana huxleyi*. *Mar Chem* 70:277-287
- Brand LE, Guillard RRL, Murphy LS** (1981) A method for the rapid and precise determination of acclimated phytoplankton reproduction rates. *J Plankton Res* 3:193-201
- Brand LE** (1994) Physiological ecology of marine coccolithophores. In: Winter A, Siesser WG (eds) *Coccolithophores*. Cambridge University Press, Cambridge, pp 39-49
- Brazard J, Ley C, Lacombat F, Plaza P, Mony L, Heijde M, Zabulon G, Bowler C** (2012) Photoantenna in two cryptochrome-photolyase proteins from *O. tauri*: Presence, nature and ultrafast photoinduced dynamics. *J Photochem Photobiol A Chem* 234:135-145
- Breitbarth E, Bellerby RJ, Neill CC, Ardelan M V, Meyerh M** (2010) Ocean acidification affects iron speciation during a coastal seawater mesocosm experiment. *Biogeosciences* 7:1065-1073
- Britt AB** (2004) Repair of DNA damage induced by solar UV. *Photosynth Res* 81:105-112
- Broecker W, Clark E** (2009) Ratio of coccolith  $\text{CaCO}_3$  to foraminifera  $\text{CaCO}_3$  in late Holocene deep sea sediments. *Paleoceanography* 24
- Bruland KW** (2001) Chapter 6: Iron: Analytical methods for the determination of concentrations and speciation. SCOR - IUPAC Working Group on Iron in the Oceans
- Buma AGJ, VanHannen EJ, Veldhuis MJW, Gieskes WWC** (1996) UV-B induces DNA damage and DNA synthesis delay in the marine diatom *Cyclotella* sp. *Sci Mar* 60:101-106
- Buma AG, Oijen T Van, Poll W Van De, Veldhuis MJW, Gieskes WWC** (2000) The sensitivity of *Emiliana huxleyi* (Prymnesiophyceae) to ultraviolet-B radiation. *J Phycol* 36:296-303
- Caldeira K, Wickett ME** (2003) Anthropogenic carbon and ocean pH. *Nature* 425:365
- Caldwell M** (1971) Solar UV irradiance and the growth and development on higher plants. *Photophysiology* 4:131-177
- Canadell JG, Quéré C Le, Raupach MR, Field CB, Buitenhuis ET, Ciais P, Conway TJ, Gillett NP, Houghton RA, Marland G** (2007) Contributions to accelerating atmospheric  $\text{CO}_2$  growth from economic activity, carbon intensity, and efficiency of natural sinks. *Proc Natl Acad Sci U S A* 104:18866-18870
- Caron DA, Hutchins DA** (2013) The effects of changing climate on microzooplankton grazing and community structure: Drivers, predictions and knowledge gaps. *J Plankton Res* 35:235-252



- Carrillo P, Medina-Sánchez JM, Villar-Argaiz M** (2002) The interaction of phytoplankton and bacteria in a high mountain lake: importance of the spectral composition of solar radiation. *Limnol Oceanogr* 47:1294–1306
- Cassar N, Laws EA, Bidigare RR, Popp BN** (2004) Bicarbonate uptake by Southern Ocean phytoplankton. *Global Biogeochem Cycles* 18:1–10
- Ciais P, Sabine C, Bala G, Bopp L, Brovkin V, Canadell J, Chhabra A, DeFries R, Galloway J, Heimann M, Jones C, Le Quééré C, Myneni RB, Piao S, Thornton P** (2013) Carbon and Other Biogeochemical Cycles. In: *Climate Change 2013: The Physical Science Basis. Contribution of Working Group I to the Fifth Assessment Report of the Intergovernmental Panel on Climate Change* (Stocker TF, Qin D, Plattner G-K, Tignor M, Allen SK, Boschung J, Nauels A, Xia Y, Bex V, Midgley PM (eds.)). Cambridge University Press, Cambridge, United Kingdom and New York, NY, USA
- Cleveland JS, Weidemann AD** (1993) Quantifying absorption by aquatic particles. A multiple scattering correction for glass-fiber filters. *Limnol Oceanogr* 38:1321–1327
- Collins S, Rost B, Rynearson TA** (2014) Evolutionary potential of marine phytoplankton under ocean acidification. *Evolutionary Applications* 7:140–155
- Colman B, Huertas IE, Bhatti S, Dason JS** (2002) The diversity of inorganic carbon acquisition mechanisms in eukaryotic microalgae. *Funct Plant Biol* 29:261–270
- Czerny J, Schulz KG, Boxhammer T, Bellerby RGJ, Büdenbender J, Engel A, Krug SA, Ludwig A, Nachtigall K, Nondal G, Niehoff B, Silyakova A, Riebesell U** (2013) Implications of elevated CO<sub>2</sub> on pelagic carbon fluxes in an arctic mesocosm study- an elemental mass balance approach. *Biogeosciences* 10:3109–3125
- Crawford DW, Lipsen MS, Purdie DA, Lohan MC, Statham PJ, Whitney FA, Putland JN, Johnson WK, Sutherland N, Peterson TD, Harrison PJ, Wong CS** (2003) Influence of zinc and iron enrichments on phytoplankton growth in the northeastern subarctic Pacific. *Limnol Oceanogr* 48:1583–1600
- Cullen JJ, Neale PJ, Lesser MP** (1992) Biological weighting function for the inhibition of phytoplankton photosynthesis by ultraviolet radiation. *Science* (80) 258:646–650
- Cullen J, Neale P** (1997) Biological weighting functions for describing the effects of ultraviolet radiation on aquatic systems. In: Häder D-P (ed) *The effects of ozone depletion on aquatic ecosystems.*, RG Landes . Austin, p 97–118
- Cullen JT, Sherrell RM** (2005) Effects of dissolved carbon dioxide, zinc, and manganese on the cadmium to phosphorus ratio in natural phytoplankton assemblages *Limnol Oceanogr* 50: 1193–1204
- Delille B, Harlay J, Zondervan I, Jacquet S, Chou L, Wollast R, Bellerby RGJ, Frankignoulle M, Borges AV, Riebesell U, Gattuso J-P** (2005) Response of primary production and calcification to changes of pCO<sub>2</sub> during experimental blooms of the coccolithophorid *Emiliania huxleyi*. *Global Biogeochem Cycles* 19:1–14



- Dell AI, Pawar S, Savage SM** (2011) Systematic variation in the temperature dependence of physiological and ecological traits. *Proc Natl Acad Sci USA* 108:10591–10596
- Demmig-Adams B, Adams WW** (1996) Xanthophyll cycle and light stress in nature: uniform response to excess direct sunlight among higher plant species. *Planta* 198:460–470
- Desai DK, Desai FD, Laroche J** (2012) Factors influencing the diversity of iron uptake systems in aquatic microorganisms. *Front Microbiol* 3:362
- Doney SC, Fabry VJ, Feely RA, Kleypas JA** (2009) Ocean acidification: The other CO<sub>2</sub> problem. *Ann Rev Mar Sci* 1:169–192
- Egge JK, Heimdal BR** (1994) Blooms of phytoplankton including *Emiliania huxleyi* (Haptophyta). Effect of nutrient supply in different N:P ratios. *Sarsia* 79:333–348
- Egge JK, Thingstad TF, Engel A, Bellerby RGJ, Riebesell U, Larsen A, Engel A, Wohlers J, Bellerby RGJ, Riebesell U** (2009) Primary production during nutrient-induced blooms at elevated CO<sub>2</sub> concentrations. *Biogeosciences* 6:877–885
- Eileers PHC, Peeters JCH** (1988) A model for the relationship between light intensity and the rate of photosynthesis in phytoplankton. *Ecol Modell* 42:199–215
- Elzenga JTM, Prins HBA, Stefels J** (2000) The role of extracellular carbonic anhydrase activity in inorganic carbon utilization of *Phaeocystis globosa* (Prymnesiophyceae): A comparison with other marine algae using the isotopic disequilibrium technique. *Limnol Oceanogr* 45:372–380
- Endres S, Galgani L, Riebesell U, Schulz KG, Engel A** (2014) Stimulated bacterial growth under elevated pCO<sub>2</sub>: Results from an off-shore mesocosm study. *PLoS One* 9, 1–8
- Engel A, Goldthwait S, Passow U, Alldredge A** (2002) Temporal decoupling of carbon and nitrogen dynamics in a mesocosm diatom bloom. *Limnol Oceanogr* 47:753–761
- Engel A, Schulz KG, Riebesell U, Bellerby R, Delille B, Schartau M** (2008) Effects of CO<sub>2</sub> on particle size distribution and phytoplankton abundance during a mesocosm bloom experiment (PeECE II). *Biogeosciences* 5:509–521
- Engel A, Zondervan I, Aerts K, Beaufort L, Benthien A, Chou L, Delille B, Gattuso J-P, Harlay J, Heemann C, Villefranche D, Harlay J, Heemann C, Hoffmann L, Nejtgaard J, Rochelle-newall E, Schneider U, Terbrueggen A** (2005) Testing the direct effect of CO<sub>2</sub> concentration on a bloom of the coccolithophorid *Emiliania huxleyi* in mesocosm experiments. *Limnol Oceanogr* 50:493–507
- Feng Y, Hare CE, Rose JM, Handy SM, DiTullio GR, Lee PA, Smith WO, Peloquin J, Tozzi S, Sun J, Zhang Y, Dunbar RB, Long MC, Sohst B, Lohan M, Hutchins DA** (2010) Interactive effects of iron, irradiance and CO<sub>2</sub> on Ross Sea phytoplankton. *Deep Res Part I Oceanogr Res Pap* 57:368–383
- Field CB** (1998) Primary production of the biosphere: Integrating terrestrial and oceanic components. *Science* 281:237–240



- Field CB, Barros V, Stocker TF, Dahe Q, Mach KJ, Plattner G-K, Mastrandrea MD, Tignor M, Ebi KL** (2011) Workshop report of the Intergovernmental Panel on Climate Change workshop on impacts of ocean acidification on marine biology and ecosystems. Stanford, California, United States of America
- Figueroa FL, Korbee N, Carrillo P, Medina-Sánchez JM, Mata MT, Bonomi J, Sánchez-Castillo PM** (2009) The effects of UV radiation on photosynthesis estimated as chlorophyll fluorescence in *Zygnemopsis decussata* (Chlorophyta) growing in a high mountain lake (Sierra Nevada, Southern Spain). *J Limnol* 68:206–216
- Flynn KJ, Blackford JC, Baird ME, Raven JA, Clark DR, Beardall J, Brownlee C, Fabian H, Wheeler GL** (2012) Changes in pH at the exterior surface of plankton with ocean acidification. *Nat Clim Chang* 2:510–513
- Fogg GE** (1983) The ecological significance of extracellular products of phytoplankton photosynthesis. *Bot Mar* 26: 3–14
- Folt CL, Chen CY, Moore MV, Burnaford J** (1999) Synergism and antagonism among multiple stressors. *Limnol Ocean* 44:864–877
- Foyer CH, Lelandais M, Kunert KJ** (1994) Photooxidative stress in plants. *Physiol Plant* 92:696–717
- Frew RD, Hutchins DA, Nodder S, Sanudo-Wilhelmy S, Tovar-Sanchez A, Leblanc K, Hare CE, Boyd PW** (2006) Particulate iron dynamics during FeCycle in subantarctic waters southeast of New Zealand. *Glob. Biogeochem. Cycles* 20, GB1S93. <http://dx.doi.org/10.1029/2005GB002558>.
- Fuentes-Lema A, Sobrino C, González N, Estrada M, Neale P** (2015) Effect of solar UVR on the production of particulate and dissolved organic carbon from phytoplankton assemblages in the Indian Ocean. *Mar Ecol Prog Ser* 535:47–61
- Gao K, Ruan Z, Villafañe VE, Gattuso J-P, Helbling EW** (2009) Ocean acidification exacerbates the effect of UV radiation on the calcifying phytoplankter *Emiliania huxleyi*. *Limnol Oceanogr* 54:1855–1862
- Gao K, Xu J, Gao G, Li Y, Hutchins DA, Huang B, Wang L, Zheng Y, Jin P, Cai X, Häder D-P, Li W, Xu K, Liu N, Riebesell U** (2012) Rising CO<sub>2</sub> and increased light exposure synergistically reduce marine primary productivity. *Nat Clim Chang* 2:519–523
- García-Gómez C, Parages ML, Jimenez C, Palma A, Mata MT, Segovia M** (2012) Cell survival after UV radiation stress in the unicellular chlorophyte *Dunaliella tertiolecta* is mediated by DNA repair and MAPK phosphorylation. *J Exp Bot* 63:695–709
- García-Gómez C, Gordillo FJL, Palma A, Lorenzo MR, Segovia M** (2014) Elevated CO<sub>2</sub> alleviates high PAR and UV stress in the unicellular chlorophyte *Dunaliella tertiolecta*. *Photochem Photobiol Sci* 13:1347–1358



- García-Gómez C, Mata MT, Van Breusegem F, Segovia M** (2016) Low-steady-state metabolim induced by elevated CO<sub>2</sub> increases resilience to UV radiation in the unicellular green-algae *Dunaliella tertiolecta*. *Environ Exp Bot* 132:163-174
- Gattuso JP, Hansson L** (2011) Ocean acidification. Oxford University Press, Oxford
- Genty B, Briantais J-M, Baker NR** (1989) The relationship between the quantum yield of photosynthetic electron transport and quenching of chlorophyll fluorescence. *Biochim Biophys Acta* 990:87-92
- Giordano M, Beardall J, Raven JA** (2005) CO<sub>2</sub> concentrating mechanisms in algae: mechanisms, environmental modulation, and evolution. *Annu Rev Plant Biol* 56:99-131
- Gledhill M, van den Berg CMG** (1994) Determination of complexation of iron (III) with natural organic complexing ligands in seawater using cathodic stripping voltammetry. *Marine Chemistry* 47(1): 41-54
- Gran G** (1952) Determination of the equivalence point in potentiometric titrations of seawater with hydrochlorid acid. *Oceanol Acta* 5:209-218
- Green JC, Course PA, Tarran GA** (1996) The life-cycle of *Emiliana huxleyi*: a brief review and a study of relative ploidy levels using flow cytometry. *J Mar Syst* 9:33-44
- Guan W, Gao K** (2010) Enhanced calcification ameliorates the negative effects of UV radiation on photosynthesis in the calcifying phytoplankton *Emiliana huxleyi*. *Chinese Sci Bull* 55:588-593
- Guo J, Lapi S, Ruth TJ, Maldonado MT** (2012) The effects of iron and copper availability on the copper stoichiometry of marine phytoplankton. *J Phycol* 48:312-325
- Häder D-P, Kumar HD, Smith RC, Worrest RC** (2007) Effects of solar UV radiation on aquatic ecosystems and interactions with climate change. *Photochem Photobiol Sci* 6:267-85
- Häder D-P** (2011) Does enhanced solar UV-B radiation affect marine primary producers in their natural habitats? *Photochem Photobiol* 87:263-266
- Hartnett A, Böttger LH, Matzanke BF, Carrano CJ** (2012) Iron transport and storage in the coccolithophore: *Emiliana huxleyi*. *Metallomics* 4, 1127-1227
- Hassler CS, Schoemann V** (2009) Bioavailability of organically bound Fe to model phytoplankton of the Southern Ocean. *Biogeosciences* 6:2281-2296
- Heijde M, Zabulon G, Corellou F, Ishikawa T, Brazard J, Usman A, Sanchez F, Plaza P, Martin M, Falcitore A, Todo T, Bouget F-Y, Bowler C** (2010) Characterization of two members of the cryptochrome/photolyase family from *Ostreococcus tauri* provides insights into the origin and evolution of cryptochromes. *Plant Cell Environ* 33:1614-1626
- Herfort L, Thake B, Roberts J** (2003) Acquisition and use of bicarbonate by *Emiliana huxleyi*. *New Phytol* 156:427-436



- Ho T-Y** (2006) The trace metal composition of marine microalgae in cultures and natural assemblages. In: Rao S (ed) *Algal cultures, analogues of blooms and applications*. Science Publishers, New Hampshire, p 271–299
- Ho T, Quigg A, Zoe V, Milligan AJ, Falkowski PG, Morel MM** (2003) The elemental composition of some marine phytoplankton. *J Appl Phycol* 1159:1145–1159
- Ho T-Y, Wen L-S, You C-F, Lee D-C** (2007) The trace metal composition of size-fractionated plankton in the South China Sea: Biotic versus abiotic sources. *Limnol Oceanogr* 52:1776–1788
- Ho T-Y, You CF, Chou W-C, Pai S-C, Wen L-S, Sheu DD** (2009) Cadmium and phosphorus cycling in the water column of the South China Sea: The roles of biotic and abiotic particles. *Mar. Chem.* 115:125–133.
- Hoegh-Guldberg O, Bruno JF** (2010) The impact of climate change on the world's marine ecosystems. *Science* 328:1523–1528
- Hoffmann LJ, Breitbarth E, Boyd PW, Hunter KA** (2012) Influence of ocean warming and acidification on trace metal biogeochemistry. *Mar Ecol Prog Ser* 470:191–205
- Hofmann M, Schellnhuber H** (2009) Oceanic acidification affects marine carbon pump and triggers extended marine oxygen holes. *Proc Natl Acad Sci U S A* 106:3017–3022
- Holligan PM, Fernández E, Aiken J, Balch WM, Boyd P, Burkill PH, Finch M, Groom SB, Malin G, Muller K, Purdie DA, Robinson C, Trees CC, Turner SM, Wal Pvd** (1993) A biogeochemical study of the coccolithophore, *Emiliana huxleyi*, in the North Atlantic. *Global Biogeochem Cycles* 7:879–900
- Holtz L-M, Wolf-Gladrow D, Thoms S** (2015) Numerical cell model investigating cellular carbon fluxes in *Emiliana huxleyi*. *J Theor Biol* 364:305–315
- Honey DJ, Gledhill M, Bibby TS, Legiret F-E, Pratt NJ, Hickman AE, Lawson T, Achterberg EP** (2013) Heme *b* in marine phytoplankton and particulate material from North Atlantic Ocean. *Mar Ecol Prog Ser*. 483:1–17
- Hopkinson BM, Xu Y, Shi D, McGinn PJ, Morel FMM** (2010) The effect of CO<sub>2</sub> on the photosynthetic physiology of phytoplankton in the Gulf of Alaska. *Limnol Oceanogr* 55:2011–2024
- Hoppe CJM, Hassler CS, Payne CD, Tortell PD, Rost BR, Trimborn S** (2013) Iron limitation modulates ocean acidification effects on Southern Ocean phytoplankton communities. *PLoS One* 8
- Hutchins D, Mulholland M, Fu F** (2009) Nutrient cycles and marine microbes in a CO<sub>2</sub>-enriched ocean. *Oceanography* 22:128–145
- Iglesias-Rodriguez MD, Halloran PR, Rickaby REM, Hall IR, Colmenero-Hidalgo E, Gittins JR, Green DRH, Tyrrell T, Gibbs SJ, von Dassow P, Rehm E, Armbrust EV, Boessenkool KP** (2008) Phytoplankton calcification in a high-CO<sub>2</sub> world. *Science* 320:336–340



- Iglesias-Rodriguez MD, Fabricius KE, McElhany P** (2016) Ecological effects of ocean acidification. Chapter 11. pp 195-212. In: Solan M, Whiteley N (Eds) Stressors in the Marine Environment. Oxford University Press, UK
- IPCC, 2013.** In: **Stocker TF, Qin D, Plattner G-K, Tignor M, Allen SK, Boschung J, Nauels A, Xia Y, Bex V, Midgley PM** (Eds) Climate Change 2013: The Physical Science Basis. Contribution of Working Group I to the Fifth Assessment Report of the Intergovernmental Panel on Climate Change. Cambridge University Press, Cambridge, United Kingdom and New York, NY, USA
- Jakobsen H, Carstensen J** (2011) FlowCAM: Sizing cells and understanding the impact of size distributions on biovolume of -planktonic community structure. *Aquat Microb Ecol* 65:75–87
- Jakuba RW, Moffett JW, Dyhrman ST** (2008) Evidence for the linked biogeochemical cycling of zinc, cobalt, and phosphorus in the western North Atlantic Ocean. *Global Biogeochem. Cycles* 22, GB4012
- Jones L, Kok B** (1966) Photoinhibition of chloroplast reactions. I. Kinetics and action spectra. *Plant Physiol* 41:1037–1043
- Jong de JT, den Das J, Bathmann U, Stoll MH, Kattner G, Nolting R, de Baar HJ** (1998) Dissolved iron at subnanomolar levels in the Southern Ocean as determined by ship-board analysis. *Anal Chim Acta* 377:113–124
- Kana TM, Glibert PM** (1987) Effect of irradiances up to 2000  $\mu\text{Em}^{-2}\text{s}^{-1}$  on marine *Synechococcus* WH7803-I. Growth, pigmentation and cell composition. *Deep-Sea Res* 34:479-495
- Kim J-M, Lee K, Shin K, Kang J-H, Lee H-W, Kim M, Jang P-G, Jang M-C** (2006) The effect of seawater  $\text{CO}_2$  concentration on growth of a natural phytoplankton assemblage in a controlled mesocosm experiment. *Limnol Oceanogr* 51:1629–1636
- King AL, Sanudo-Wilhelmy SA, Boyd PW, Twining BS, Wilhelm SW, Breene C, Ellwood MJ, Hutchins DA** (2012) A comparison of biogenic iron quotas during a diatom spring bloom using multiple approaches. *Biogeosciences* 9:667–687
- Klaas C, Archer DE** (2002) Association of sinking organic matter with various types of mineral ballast in the deep sea: Implications for the rain ratio. *Global Biogeochem Cycle* 10.1029/2001GB001765
- Klaveness D** (1972) *Coccolithus huxleyi* (Lohm.) Kamptn. II. The flagellate cell, aberrant cell types, vegetative propagation and life cycles. *Br Phycol J* 7:309–318
- Kottmeier DM, Rokitta SD, Tortell PD, Rost B** (2014) Strong shift from  $\text{HCO}_3^-$  to  $\text{CO}_2$  uptake in *Emiliania huxleyi* with acidification: New approach unravels acclimation versus short-term pH effects. *Photosynth Res* 121:265–275

- Kranz SA, Levitan O, Richter K-U, Prásil O, Berman-Frank I, Rost B** (2010) Combined effects of CO<sub>2</sub> and light on the N<sub>2</sub>-fixing cyanobacterium *Trichodesmium* IMS101: physiological responses. *Plant Physiol* 154:334–345
- Kuma K, Nishioka J, Matsunaga K** (1996) Controls on iron(III) hydroxide solubility in seawater: The influence of pH and natural organic chelators. *Limnol Oceanogr* 41:396–407
- Langer G, Geisen M, Baumann K-H, Kläs J, Riebesell U, Thoms S, Young JR** (2006) Species-specific responses of calcifying algae to changing seawater carbonate chemistry. *Geochemistry, Geophys Geosystems* 7
- Langer G, Nehrke G, Probert I, Ly J, Ziveri P** (2009) Strain-specific responses of *Emiliana huxleyi* to changing seawater carbonate chemistry. *Biogeosciences*, 6, 2637-2646
- Langer G** (2011) CO<sub>2</sub> mediation of adverse effects of seawater acidification in *Calcidiscus leptoporus*. *Geochemistry, Geophys Geosystems* 12, Q05001
- Larsen A, Castberg T, Sandaa RA, Brussaard CPD, Egge JK, Heldal M, Paulino A, Thyraug R, Hannen EJ van, Grøtbak G** (2001) Population dynamics and diversity of viruses, bacteria and phytoplankton in a shallow eutrophic lake. *Microb Ecol* 221:47–57
- Larsen JB, Larsen A, Thyraug R, Bratbak G, Sandaa RA** (2008) Response of marine viral populations to a nutrient induced phytoplankton bloom at different pCO<sub>2</sub> levels. *Biogeosciences* 5:523–533
- Lee S, Fuhrman JA** (1987) Relationships between biovolume and biomass of naturally derived marine bacterioplankton. *Appl Environ Microbiol* 53:1298–1303
- Lefebvre SC, Benner I, Stillman JH, Parker AE, Drake MK, Rossignol PE, Okimura KM, Komada T, Carpenter EJ** (2012) Nitrogen source and pCO<sub>2</sub> synergistically affect carbon allocation, growth and morphology of the coccolithophore *Emiliana huxleyi*: Potential implications of ocean acidification for the carbon cycle. *Glob Chang Biol* 18:493–503
- Lesser MP** (2006) Oxidative stress in marine environments: biochemistry and physiological ecology. *Annu Rev Physiol* 68:253–278
- Li Y, Gao K, Villafañe VE, Helbling EW** (2012) Ocean acidification mediates photosynthetic response to UV radiation and temperature increase in the diatom *Phaeodactylum tricorutum*. *Biogeosciences* 9: 3931-3942
- Lis H, Shaked Y, Kranzler C, Keren N, Morel FMM** (2015) Iron bioavailability to phytoplankton: an empirical approach. *Isme J* 9:1003–1013
- Litchman E, Neale PJ, Banaszak AT** (2002) Increased sensitivity to ultraviolet radiation in nitrogen-limited dinoflagellates: Photoprotection and repair. *Limnol Oceanogr* 47:86–94

- Litchman E, Edwards KF, Klausmeier CA, Thomas MK** (2012) Phytoplankton niches, traits and eco-evolutionary responses to global environmental change. *Mar Ecol Prog Ser* 470:235–248
- Lohbeck KT, Riebesell U, Reusch TBH** (2012) Adaptive evolution of a key phytoplankton species to ocean acidification. *Nature Geoscience* 5: 346–351
- Losh JL, Morel FMM, Hopkinson BM** (2012) Modest increase in the C:N ratio of N-limited phytoplankton in the California Current in response to high CO<sub>2</sub>. *Mar Ecol Prog Ser* 468:31–42
- Lubian LM, Montero O** (1998) Excess light-induced violaxanthin cycle activity in *Nannochloropsis gaditana* (Eustigmatophyceae): effects of exposure time and temperature. *Phycologia* 37:16–23
- Lukianova OA, David SS** (2005) A role for iron-sulfur clusters in DNA repair. *Curr Opin Chem Biol* 9:145–151
- Mackey KRM, Morris JJ, Morel FMM** (2015) Response of photosynthesis to ocean acidification. *Oceanography* 28:74–91
- Mague TH, Friberg E, Hughes DJ, Morris I** (1980) Extracellular release of carbon by marine-phytoplankton; a physiological approach. *Limnol Oceanogr* 25:262–279
- Maldonado MT, Price NM** (2001) Reduction and transport of organically bound iron by *Thalassiosira oceanica* (Bacillariophyceae). *J Phycol* 37:298–309
- Maldonado MTM, Allen AAE, Chong JJS, Lin K, Leus D, Karpenko N, Harris SL** (2006) Copper-dependent iron transport in coastal and oceanic diatoms. *Limnol Oceanogr* 51:1729–1743
- Marchetti A, Maldonado MT** (2016) Iron. In: Borowitzka MA, Beardall J, Raven JA (eds) *The Physiology of Microalgae*. Springer International Publishing, Switzerland. DOI 10.1007/978-3-319-24945-2\_11
- Marie D, Brussaard CPD, Thyrrhaug R, Bratbak G, Vaulot D** (1999) Enumeration of marine viruses in culture and natural samples by flow cytometry. *Appl Environ Microbiol* 65:45–52
- Martin C, Tortell P** (2006) Bicarbonate transport and extracellular carbonic anhydrase activity in Bering Sea phytoplankton assemblages: Results from isotope disequilibrium experiments. *Limnol Oceanogr* 51:2111–2121
- Mckenzie RL, Aucamp PJ, Bais AF, Ilyas M, Madronich S, Norval M, Lucas RM, Cullen AP, Gruijl FR De, Longstreth J, Takizawa Y, Leun JC Van Der, Caldwell MM, Flint SD, Robinson SA, Bornman JF, Helbling EW, Williamson CE, Worrest RC, Zepp RG, Paul ND, Sulzberger B, Tang X, Wilson SR, Solomon KR, Shao M, Andradý AL, Hamid H, Torikai A, Lucas R** (2011) Ozone depletion and climate change : impacts on UV radiation. *Photochem Photobiol Sci* 10:182–198



- Menden-Deuer S, Lessard EJ** (2000) Carbon to volume relationships for dinoflagellates, diatoms, and other protist plankton. *Limnol Oceanogr* 45:569–579
- Meyer J, Riebesell U** (2015) Reviews and Syntheses: Responses of coccolithophores to ocean acidification: a meta-analysis. *Biogeosciences* 12:1671–1682
- Millero FJ, Woosley R, Ditrolio B, Waters J** (2009) Effect of ocean acidification on the speciation of metals in seawater. *Oceanography* 22:72–85
- Mizoguchi T, Kimura Y, Yoshitomi T, Tamiaki H** (2011) The stereochemistry of chlorophyll- c 3 from the haptophyte *Emiliana huxleyi*: The (132R)-enantiomers of chlorophylls- c are exclusively selected as the photosynthetically active pigments in chromophyte algae *Several st.* *Biochim Biophys Acta* 1807:1467–1473
- Mohan R, Mergulhao LP, Guptha MVS, Rajakumar A, Thamban M, Kumar N, Sudhakar M, Ravindra R** (2008) Ecology of coccolithophores in the Indian sector of the Southern Ocean. *Mar Micropaleontol* 67:30–45
- Morel FM, Price NM** (2003) The biogeochemical cycles of trace metals in the oceans. *Science* 300:944–947
- Morita R, Nakane S, Shimada A, Inoue M, Iino H, Wakamatsu T, Fukui K, Nakagawa N, Masui R, Kuramitsu S** (2010) Molecular mechanisms of the whole dna repair system: a comparison of bacterial and eukaryotic systems. *J Nucleic Acids* 2010:1–32
- Muggli DL, Harrison PJ** (1996) Effects of nitrogen source on the physiology and metal nutrition of *Emiliana huxleyi* grown under different iron and light conditions. *Mar Ecol Prog Ser* 130:255–267
- Muggli DL, Harrison PJ** (1997) Effects of iron on two oceanic phytoplankters grown in natural NE subarctic pacific seawater with no artificial chelators present. *J Exp Mar Bio Ecol* 212:225–237
- Muller FL, Larsen A, Stedmon CA, Søndergaard M** (2005) Interactions between algal – bacterial populations and trace metals in fjord surface waters during a nutrient-stimulated summer bloom. *Limnol Oceanogr* 50:1855–1871
- Muller EB, Nisbet RM** (2014) Dynamic energy budget modeling reveals the potential of future growth and calcification for the coccolithophore *Emiliana huxleyi* in an acidified ocean. *Glob Chang Biol* 20:2031–2038
- Nanninga HJ, Tyrrell T** (1996) Importance of light for the formation of algal blooms by *Emiliana huxleyi*. *Mar Ecol Prog Ser* 136(1–3): 195–203
- Neale PJ** (2001) Modeling the effects of ultraviolet radiation on estuarine phytoplankton production: impact of variations in exposure and sensitivity to inhibition. *J Photochem Photobio B: Biol* 62: 1–8



- Neale PJ, Pritchard AL, Ihnacik R** (2014) UV effects on the primary productivity of picophytoplankton: biological weighting functions and exposure response curves of *Synechococcus*. *Biogeosciences* 11:2883–2895
- Nejstgaard JC, Naustvoll LJ, Sazhin A** (2001) Correcting for underestimation of microzooplankton grazing in bottle incubation experiments with mesozooplankton. *Mar Ecol Prog Ser* 221:59–75
- Nejstgaard JC, Frischer ME, Verity PG, Anderson JT, Jacobsen A, Zirbel MJ, Larsen A, Martínez-Martínez J, Sazhin AF, Walters T, Bronk DA, Borrett SR, Pattern BC, Long JD** (2006) Plankton development and trophic transfer in seawater enclosures with nutrients and *Phaeocystis pouchetii* added. *Mar Ecol Prog Ser* 321:99–121
- Niehoff B, Schmithüsen T, Knüppel N, Daase M, Czerny J, Boxhammer T** (2013) Mesozooplankton community development at elevated CO<sub>2</sub> concentrations: results from a mesocosm experiment in an Arctic fjord. *Biogeosciences* 10:1391–1406
- Norman L, Cabanes DJ, Blanco-Ameijeiras S, Moisset SA, Hassler CS** (2014) Iron biogeochemistry in aquatic systems: from source to bioavailability. *Chimia* 68:764–771
- Nuester J, Vogt S, Newville M, Kustka AB, Twining BS** (2012) The unique biogeochemical signature of the marine diazotroph *Trichodesmium*. *Front Microbiol Chem* 3:150
- Olenina I, Hajdu S, Edler L, Wasmund N, Busch S, Göbel J, Gromisz S, Huseby S, Huttunen M, Jaanus A, Kokkonen P, Ledaine I, Niemkiewicz E** (2006) Biovolumes and size-classes of phytoplankton in the Baltic Sea. *HELCOM BaltSea Environ Proc* 106, pp 144
- Paasche E, Brubak S** (1994) Enhanced calcification in the coccolithophorid *Emiliana huxleyi* (Haptophyceae) under phosphorus limitation. *Phycologia* 33:324–330
- Paasche E** (2002) A review of the coccolithophorid *Emiliana huxleyi* (Pymnesiophyceae), with particular reference to growth, coccolith formation, and calcification-photosynthesis interactions. *Phycologia* 40:503–529
- Panzenböck M** (2007) Effect of solar radiation on photo - synthetic extracellular carbon release and its microbial utilization in alpine and Arctic lakes. *Aquat Microb Ecol* 48:155–168
- Paulino AI, Heldal M, Norland S, Egge JK** (2013) Elemental stoichiometry of marine particulate matter measured by wavelength dispersive X-ray fluorescence (WDXRF) spectroscopy. *J Mar Biol Assoc United Kingdom* 93:2003–2014
- Pelletier H, Gieskes WWC, Buma AGJ** (1996) Ultraviolet-B radiation resistance of benthic diatoms isolated from tidal flats in the Dutch Wadden Sea. *Mar Ecol Prog Ser* 135:163–168
- Petrou K, Trimborn S, Rost B, Ralph PJ, Hassler CS** (2014) The impact of iron limitation on the physiology of the Antarctic diatom *Chaetoceros simplex*. *Mar Biol* 161:925–937



- Platt T, Gallegos C** (1980) Modelling primary production. In: Primary Productivity in the Sea. Brookhaven Symposia in Biology, New York, USA. Plenum Press.p 31:339–362
- Polimene L, Brunet C, Allen JI, Butenschon M, White DA, Llewellyn CA** (2012) Modelling xanthophyll photoprotective activity in phytoplankton. *J Plankton Res* 34:196–207
- Poll WH van de, Janknegt PJ, Leeuwe MA van, Visser RJW, Buma AGJ** (2009) Excessive irradiance and antioxidant responses of an Antarctic marine diatom exposed to iron limitation and to dynamic irradiance. *J Photochem Photobiol B Biol* 94:32–37
- Polovina JJ, Howell EA, Abecassis M** (2008) Ocean's least productive waters are expanding. *Geophys Res Lett* 35
- Poulton AJ, Adey TR, Balch WM, Holligan PM** (2007) Relating coccolithophore calcification rates to phytoplankton community dynamics: Regional differences and implications for carbon export. *Deep Sea Res Part II Top Stud Oceanogr* 54:538–557
- Poulton AJ, Charalampopoulou A, Young JR, Tarran GA, Lucas MI, Quartly GD** (2010) Coccolithophore dynamics in non-bloom conditions during late summer in the central Iceland Basin (July-August 2007). *Limnol Oceanogr* 55:1601–1613
- Price NM, Harrison GI, Hering JG, Hudson RJ, Nirel PMV, Palenik B, Morel FMM** (1989) Preparation and chemistry of the artificial algal culture medium Aquil *Biol Oceanogr* 6:443–61
- Price NM, Morel FMM** (1990) Cadmium and cobalt substitution for zinc in a marine diatom. *Nature* 344:658–660
- Quigg A, Finkel ZV, Irwin AJ, Rosenthal Y, Ho T-Y, Reinfelder JR, Schofield O, Morel FMM, Falkowski PG** (2003) The evolutionary inheritance of elemental stoichiometry in marine phytoplankton. *Nature* 425:291–294
- Rauschenberg S, Twining BS** (2015) Evaluation of approaches to estimate biogenic particulate trace metals in the ocean. *Mar Chem* 171:67-77
- Raven JA** (1990) Predictions of Mn and Fe use efficiencies of phototrophic growth as a function of light availability for growth and of C assimilation pathway. *New Phytol* 116:1–18
- Raven JA** (1991) Physiology of inorganic C acquisition and implications for resource use efficiency by marine phytoplankton: relation to increased CO<sub>2</sub> and temperature. *Plant, Cell Environ* 14:779–794
- Raven JA, Evans MCW, Korb RE** (1999) The role of trace metals in photosynthetic electron transport in O<sub>2</sub> evolving organisms. *Photosynth Res* 60(2-3):111-149
- Raven J, Caldeira K, Elderfield H, Hoegh-Guldberg O, Liss P, Riebsell U, Shepherd J, Turley C, Watson A** (eds.) (2005) Ocean acidification due to increasing atmospheric carbon dioxide. The Royal Society, UK
- Raven JA, Crawford K** (2012) Environmental controls on coccolithophore calcification. *Mar Ecol Prog Ser* 470:137–166



- Read B A, Kegel J, Klute MJ, Kuo A, Lefebvre SC, Maumus F, Mayer C, Miller J, Monier A, Salamov A, Young J, Aguilar M, Claverie J-M, Frickenhaus S, Gonzalez K, Herman EK, Lin Y-C, Napier J, Ogata H, Sarno AF, Shmutz J, Schroeder D, Vargas C de, Verret F, Dassow P von, Valentin K, Peer Y Van de, Wheeler G, Dacks JB, Delwiche CF, Dyhrman ST, Glöckner G, John U, Richards T, Worden AZ, Zhang X, Grigoriev IV** (2013) Pan genome of the phytoplankton *Emiliana* underpins its global distribution. *Nature* 499:209–213
- Richier S, Fiorini S, Kerros ME, von Dassow P, Gattuso J-P** (2011) Response of the calcifying coccolithophore *Emiliana huxleyi* to low pH/high pCO<sub>2</sub>: From physiology to molecular level. *Mar Biol* 158:551–560
- Richier S, Achterberg EP, Dumousseaud C, Poulton AJ, Suggett DJ, Tyrrell T, Zubkov M V., Moore CM** (2014) Phytoplankton responses and associated carbon cycling during shipboard carbonate chemistry manipulation experiments conducted around Northwest European shelf seas. *Biogeosciences* 11:4733–4752
- Rickaby REM, Henderiks J, Young JN** (2010) Perturbing phytoplankton: Response and isotopic fractionation with changing carbonate chemistry in two coccolithophore species. *Clim Past* 6:771–785
- Ridgwell A, Hargreaves JC, Edwards NR, Annan JD, Lenton TM, Marsh R, Yool A, Watson A** (2007) Marine geochemical data assimilation in an efficient Earth System Model of global biogeochemical cycling. *Biogeosciences* 4:87–104
- Riebesell U, Zondervan I, Rost B, Tortell PD, Zeebe RE, Morel FMM** (2000) Reduced calcification of marine plankton in response to increased atmospheric CO<sub>2</sub>. *Nature* 407:2–5
- Riebesell U** (2004) Effects of CO<sub>2</sub> enrichment on marine phytoplankton. *J Oceanogr* 60:719–729
- Riebesell U, Schulz KG, Bellerby RGJ, Botros M, Fritsche P, Meyerhöfer M, Neill C, Nondal G, Oschlies A, Wohlers J, Zöllner E** (2007) Enhanced biological carbon consumption in a high CO<sub>2</sub> ocean. *Nature* 450:545–548
- Riebesell U, Bellerby RGJ, Engel A, Fabry VJ, Hutchins DA, Reusch TBH, Schulz KG, Morel FMM** (2008) Comment on “Phytoplankton calcification in a high-CO<sub>2</sub> world”. *Science* 322:1466; author reply 1466
- Riebesell U, Lee K, Nejtgaard JC** (2010) Pelagic mesocosms. In: Riebesell U, Fabry VJ, Hansson L, Gattuso J-P (eds) Guide to best practices for ocean acidification research and data reporting. Office for Official Publications of the European Union, p 95–112
- Riebesell U, Tortell PD** (2011) Effects of ocean acidification on pelagic organisms and ecosystems. In: Gattuso J-P, Lansson L (eds) *Ocean Acidification*. Oxford University Press., Oxford, p 99–121

- Riebesell U, Gattuso JP, Thingstad TF, Middelburg JJ** (2013) Arctic ocean acidification : pelagic ecosystem and biogeochemical Dynamics responses during a mesocosm study. *Biogeosciences* 10:5619–5626
- Riebesell U, Gattuso J-P** (2015) Lessons learned from ocean acidification research. *Nat Clim Change* 5:12–14
- Rijssel M van, Buma AGJ** (2002) UV radiation induced stress does not affect DMSP synthesis in the marine prymnesiophyte *Emiliana huxleyi*. *Aquat Microb Ecol* 28:167–174
- Robbins LL, Hansen ME, Kleypas JA, Meylan SC** (2010) CO<sub>2</sub>calc: A User Friendly Carbon Calculator foe Windows, Mac OS X and iOS (iPhone) Open File Rep. 2010-1280
- Rokitta SD, John U, Rost B** (2012) Ocean acidification affects redox-balance and ion-homeostasis in the life-cycle stages of *Emiliana huxleyi*. *PLoS One* 7:e52212
- Rokitta SD, Rost B** (2012) Effects of CO<sub>2</sub> and their modulation by light in the life-cycle stages of the coccolithophore *Emiliana huxleyi*. *Limnol Oceanogr* 57:607–618
- Rost B, Burkhardt S, Sültemeyer D, Riebesell U** (2003) Carbon acquisition of bloom-forming marine phytoplankton. *Limnol Oceanogr* 48:55–67
- Rost B, Riebesell U** (2004) Coccolithophores and the biological pump: responses to environmental changes. In: Thierstein HR, Young JR (eds) *Coccolithophores: from molecular process to global impact*. Springer, Berlin, p 99–125
- Rost B, Sültemeyer D** (2006) Carbon acquisition of marine phytoplankton: Effect of photoperiod length. *Limnol. Oceanogr.* 51: 12–20
- Rue EL, Bruland KW** (1995) Complexation of iron(III) by natural organic-ligands in the Central North Pacific as determined by a new competitive ligand equilibration adsorptive cathodic stripping voltammetric method. *Marine Chemistry* 50(1-4):117-138
- Sabine CL, Feely RA, Gruber N, Key RM, Kitack L, Bullister JL, Wanninkhof R, Wong CS, Wallace DWR, Tilbrook B, Millero FJ, Peng T, Kozyr A, Ono T, Rios AF** (2004) The oceanic sink for anthropogenic CO<sub>2</sub>. *Science* (80-) 305:367–371
- Saito MA, Goepfert TJ, Ritt JT** (2008) Some thoughts on the concept of colimitation: Three definitions and the importance of bioavailability. *Limnol Oceanogr* 53:276–290
- Sancar A** (1994) Structure and function of DNA photolyase. *Biochemistry* 33:2–9
- Sanders R, Morris PJ, Poulton AJ, Stinchcombe MC, Charalampopoulou A, Lucas MI, Thomalla SJ** (2010) Does a ballast effect occur in the surface ocean? *Geophys Res Lett* 37 L08602, doi :10.1029/ 2010GL042574. 1
- Sanudo-Wilhelmy SA, Tovar-Sanchez A, Fu FX, Capone DG, Carpenter EJ, Hutchins DA** (2004) The impact of surface-adsorbed phosphorus on phytoplankton Redfield stoichiometry. *Nature* 432:897–901



- Sarthou G, Timmermans KR, Blain S, Tréguer P** (2005) Growth physiology and fate of diatoms in the ocean: a review. *J Sea Res* 53:25–42
- Schartau M, Engel A, Schröter J, Thoms S, Völker C, Wolf-Gladrow D** (2007) Modelling carbon overconsumption and the formation of extracellular particulate organic carbon. *Biogeosciences* 4:433–454
- Schreiber U, Schliwa U, Bilger W** (1986) Continuous recording of photochemical and non-photochemical chlorophyll fluorescence quenching with a new type of modulation fluorometer. *Photosynth Res* 10:51–62
- Schulz KG, Zondervan I, Gerringa LJA, Timmermans KR, Veldhuis MJW, Riebesell U** (2004) Effect of trace metal availability on coccolithophorid calcification. *Nature* 430:673–676
- Schulz KG, Rost B, Burkhardt S, Riebesell U, Thoms S, Wolf-Gladrow DA** (2007) The effect of iron availability on the regulation of inorganic carbon acquisition in the coccolithophore *Emiliania huxleyi* and the significance of cellular compartmentation for stable carbon isotope fractionation. *Geochim Cosmochim Acta* 71:5301–5312
- Schulz KG, Ramos JB, Zeebe RE, Riebesell U** (2009) CO<sub>2</sub> perturbation experiments: similarities and differences between dissolved inorganic carbon and total alkalinity manipulations. *Biogeosciences* 6:2145–2153
- Sciandra A, Harlay J, Lefèvre D, Lemée R, Rimmelin P, Denis M, Gattuso J-P** (2003) Response of coccolithophorid *Emiliania huxleyi* to elevated partial pressure of CO<sub>2</sub> under nitrogen limitation. *Mar Ecol Prog Ser* 261: 111–122
- Segovia M, Berges JA** (2009) Inhibition of caspase-like activities prevents the appearance of reactive oxygen species and dark-induced apoptosis in the unicellular chlorophyte *Dunaliella tertiolecta*. *J Phycol* 45:1116–1126
- Setlow RB** (1974) The wavelengths in sunlight effective in producing skin cancer: a theoretical analysis. *Proc Natl Acad Sci U S A* 71:3363–3366
- Shaked Y, Lis H** (2012) Disassembling iron availability to phytoplankton. *Front Microbiol* 3:123
- Shanklin J** (2010) Reflections on the ozone hole. *Nature* 465: 34–35
- Sharp JH** (1977) Excretion of organic matter by marine phytoplankton: Do healthy cells do it? *Limnol Oceanogr* 22:381–399
- Shi D, Xu Y, Hopkinson BM, Morel FMM** (2010) Effect of ocean acidification on iron availability to marine phytoplankton. *Science* 327:676–679
- Smyth RL, Sobrino C, Phillips-Kress J, Kim H-C, Neale PJ** (2012) Phytoplankton photosynthetic response to solar ultraviolet irradiance in the Ross Sea Polynya: Development and evaluation of a time-dependent model with limited repair. *Limnol Oceanogr* 57:1602–1618

- Sobrinho C, Neale PJ, Lubián LM** (2005) Interaction of UV radiation and inorganic carbon supply in the inhibition of photosynthesis: spectral and temporal responses of two marine picoplankters. *Photochem Photobiol* 81:384–393
- Sobrinho C, Ward ML, Neale PJ** (2008) Acclimation to elevated carbon dioxide and ultraviolet radiation in the diatom *Thalassiosira pseudonana*: Effects on growth, photosynthesis, and spectral sensitivity of photoinhibition. *Limnol Oceanogr* 53:494–505
- Sobrinho C, Neale PJ, Phillips-Kress JD, Moeller RE, Porter JA** (2009) Elevated CO<sub>2</sub> increases sensitivity to ultraviolet radiation in lacustrine phytoplankton assemblages. *Limnol Oceanogr* 54:2448–2459
- Sobrinho C, Segovia M, Neale PJ, Mercado JM, García-Gómez C, Kulk G, Lorenzo MR, Camarena T, Poll WH Van De, Spilling K, Ruan Z** (2014) Effect of CO<sub>2</sub>, nutrients and light on coastal plankton. IV. Physiological responses. *Aquat Biol* 22:77–93
- Solomon S, Qin D, Manning M, Chen Z, Marquis M, Averyt KB, Tignor M, Miller HL** (eds.) *Climate Change 2007: The Physical Science Basis. Contribution of Working Group I to the Fourth Assessment Report of the Intergovernmental Panel on Climate Change.* Cambridge (UK): Cambridge University
- Steedmann Nielsen E** (1952) The use of radioactive (<sup>14</sup>C) for measuring organic production in the sea. *J du Cons / Cons Perm Int pour l'Exploration la Mer* 18:117–140
- Stewart RIA, Dossena M, Bohan DA, Jeppesen E, Kordas RL, Ledger ME, Meerhoff M, Moss B, Mulder C, Shurin JB, Suttle B, Thompson R, Trimmer M, Woodward G** (2013) Mesocosm experiments as a tool for ecological climate change. *Adv Ecol Res* 48:71–181
- Stojkovic S, Beardall J, Matear R** (2013) CO<sub>2</sub>-concentrating mechanisms in three southern hemisphere strains of *Emiliana huxleyi* (S Lin, Ed.). *J Phycol* 49:670–679
- Stolte W, Kraay GW, Noordeloos AAM, Riegman R** (2000) Genetic and physiological variation in pigment composition of *Emiliana huxleyi* (Prymnesiophyceae) and the potential use of its pigment ratios as a quantitative physiological marker. *J Phycol* 36:529–539
- Striebel M, Kirchmaier L, Hingsamer P** (2013) Different mixing techniques in experimental mesocosms- does mixing affect plankton biomass and community composition? *Limnol Oceanogr Methods* 11:176–186
- Suffrian K, Simonelli P, Nejtgaard JC, Putzeys S, Carotenuto Y, Antia AN** (2008) Microzooplankton grazing and phytoplankton growth in marine mesocosms with increased CO<sub>2</sub> levels. *Biogeosciences* 5:1145–1156
- Suffrian K, Schulz KG, Gutowska MA, Riebesell U, Bleich M** (2011) Cellular pH measurements in *Emiliana huxleyi* reveal pronounced membrane proton permeability. *New Phytologist* 190:595–608



- Sugie K, Endo H, Suzuki K, Nishioka J, Kiyosawa H, Yoshimura T** (2013) Synergistic effects of pCO<sub>2</sub> and iron availability on nutrient consumption ratio of the Bering Sea phytoplankton community. *Biogeosciences* 10:6309–6321
- Sugie K, Yoshimura T** (2013) Effects of pCO<sub>2</sub> and iron on the elemental composition and cell geometry of the marine diatom *Pseudo-nitzschia pseudodelicatissima* (Bacillariophyceae). *J Phycol* 49:475–488
- Sugie K, Yoshimura T** (2016) Effects of high CO<sub>2</sub> levels on the ecophysiology of the diatom *Thalassiosira weissflogii* differ depending on the iron nutritional status. *ICES J Mar Sci* 73:529–536
- Sunda WG, Huntsman, SA** (1995a) Iron uptake and growth limitation in oceanic and coastal phytoplankton. *Mar Chem* 50:189–206
- Sunda WG, and Huntsman SA** (1995b) Cobalt and zinc interreplacement in marine phytoplankton: biological and geochemical implications. *Limnol Oceanogr* 40:1404–1417
- Sunda WG, Huntsman SA** (1998) Control of Cd concentrations in a coastal diatom by interactions among free ionic Cd, Zn, and Mn in seawater. *Environ Sci Technol* 32:2961–2968
- Sunda WG, Huntsman SA** (2000) Effect of Zn, Mn, and Fe on Cd accumulation in phytoplankton: implications for oceanic Cd cycling. *Limnol. Oceanogr.* 45, 1501–1516
- Sunda W, Kieber DJ, Kiene RP, Huntsman S** (2002) An antioxidant function for DMSP and DMS in marine algae. *Nature* 418:317–320
- Sunda WG** (2010) Oceans. Iron and the carbon pump. *Science* 327:654–655
- Sunda WG** (2012) Feedback interactions between trace metal nutrients and phytoplankton in the ocean. *Front Microbiol* 3:204
- Takaichi S** (2011) Distributions, biosyntheses and functions of carotenoids in algae. *Agro Food Ind Hi Tech* 24:55–58
- Tang DG, Morel FMM** (2006) Distinguishing between cellular and Fe-oxide-associated trace elements in phytoplankton. *Mar Chem* 98:18–30
- Tans P, Keeling RF** (2014) Trends in atmospheric carbon dioxide, National Oceanic & Atmospheric Administration, Earth System Research Laboratory (NOAA/ESRL) & Scripps Institution of Oceanography, available at: <http://www.esrl.noaa.gov/gmd/ccgg/trends/> and <http://scrippsco2.ucsd.edu/>
- Taylor S** (1964) Abundance of chemical elements in the continental crust: a new table. *Geochim Cosmochim Acta* 28:1273–1285
- Taylor AR, Brownlee C, Wheeler GL** (2012) Proton channels in algae: Reasons to be excited. *Trends Plant Sci* 17:675–684

- Taucher J, Schulz KG, Dittmar T, Sommer U, Oschlies A, Riebesell U** (2012) Enhanced carbon overconsumption in response to increasing temperatures during a mesocosm experiment. *Biogeosciences* 9:3531–3545
- Timmermans KR, van der Wagt B, Veldhuis MJW, A. Maatman A, de Baar HJW** (2005) Physiological responses of three species of marine picophytoplankton to ammonium, phosphate, iron and light limitation. *J Sea Res* 53:109–120
- Toggweiler JR** (1993) Carbon overconsumption. *Nature* 363:210–211
- Tortell PD, Mills MM, Payne CD, Maldonado MT, Chierici M, Fransson A, Alderkamp AC, Arrigo KR** (2013) Inorganic C utilization and C isotope fractionation by pelagic and sea ice algal assemblages along the antarctic continental shelf. *Mar Ecol Prog Ser* 483:47–66
- Tortell PD, Payne CD, Li Y, Trimborn S, Rost B, Smith WO, Riesselman C, Dunbar RB, Sedwick P, DiTullio GR** (2008) CO<sub>2</sub> sensitivity of Southern Ocean phytoplankton. *Geophys Res Lett* 35:L04605
- Tortell PD, Trimborn S, Li Y, Rost B, Payne CD** (2010) Inorganic carbon utilization by Ross sea phytoplankton across natural and experimental CO<sub>2</sub> gradients. *J Phycol* 46:433–443
- Tovar-Sanchez A, Sanudo-Wilhelmy SA, Garcia-Vargas M, Weaver RS, Popels LC, Hutchins DA** (2003) A trace metal clean reagent to remove surface-bound iron from marine phytoplankton. *Mar Chem* 82:91–99
- Tovar-Sanchez A, Sañudo-Wilhelmy SA, Kustka AB, Agustí S, Dachs J, Hutchins DA, Capone DG, Duarte CM** (2006) Effects of dust deposition and river discharges on trace metal composition of *Trichodesmium* spp. in the tropical and subtropical North Atlantic Ocean. *Limnol Oceanogr* 51:1755–1761
- Triantaphyllou M, Dimiza M, Krasakopoulou E, Malinverno E, Lianou V, Souvermezoglou E** (2010) Seasonal variation in *Emiliania huxleyi* coccolith morphology and calcification in the Aegean Sea (Eastern Mediterranean). *Geobios* 43:99–110
- Trimborn S, Wolf-Gladrow D, Richter K-U, Rost B** (2009) The effect of pCO<sub>2</sub> on carbon acquisition and intracellular assimilation in four marine diatoms. *J Exp Mar Bio Ecol* 376:26–36
- Twining BS, Baines SB** (2013) The trace metal composition of marine phytoplankton. *Ann Rev Mar Sci* 5:191–215
- Tyrrill T, Taylor AH** (1996) A modelling study of *Emiliania huxleyi* in the NE Atlantic. *J Mar Syst* 9:83–112
- Veldhuis M, Kraay G, Timmermans K** (2001) Cell death in phytoplankton: correlation between changes in membrane permeability, photosynthetic activity, pigmentation and growth. *Eur J Phycol* 36:167–177



- Vrede K, Heldal M, Norland S, Bratbak G** (2002) Elemental composition (C, N, P) and cell volume of exponentially growing and nutrient-limited bacterioplankton. *Appl Environ Microbiol* 68:2965–2971
- Weatherhead EC, Andersen SB** (2006) The search for signs of recovery of the ozone layer. *Nature* 441:39–45
- Wellburn AR** (1994) The Spectral determination of chlorophylls *a* and *b*, as well as total carotenoids, using various solvents with spectrophotometers of different resolution. *J Plant Physiol* 144:307–313
- Wells ML** (1999) Manipulating iron availability in nearshore waters. *Limnol Oceanogr* 44:1002–1008
- Wood AM, Van Valen LM** (1990) Paradox lost? On the release of energy-rich compounds by phytoplankton. *Mar Microb Food Webs* 4:103–116
- Xing T, Gao K, Beardall J** (2015) Response of growth and photosynthesis of *Emiliana huxleyi* to visible and UV irradiances under different light regimes. *Photochem Photobiol* 91:343–349
- Xu Y, Tang D, Shaked Y, Morel FMM** (2007) Zinc, cadmium, and cobalt interreplacement and relative use efficiencies in the coccolithophore *Emiliana huxleyi*. *Limnol Oceanogr* 52:2294–2305
- Xu K, Gao K, Villafañe VE, Helbling EW** (2011) Photosynthetic responses of *Emiliana huxleyi* to UV radiation and elevated temperature: Roles of calcified coccoliths. *Biogeosciences* 8:1441–1452
- Xu J, Bach LT, Schulz KG, Zhao W, Gao K, Riebesell U** (2016) The role of coccoliths in protecting *Emiliana huxleyi* against stressful light and UV radiation. *Biogeosciences Discuss*:1–26
- Yi Y, Yi C, Qian L, Min L, Long C, Linhan B, Zhirong Y, Dairong Q** (2006) Cloning and sequence analysis of the gene encoding (6-4)photolyase from *Dunaliella salina*. *Biotechnol Lett* 28:309–314
- Yoshimura T, Suzuki K, Kiyosawa H, Ono T, Hattori H, Kuma K, Nishioka J** (2013) Impacts of elevated CO<sub>2</sub> on particulate and dissolved organic matter production: Microcosm experiments using iron-deficient plankton communities in open subarctic waters. *J Oceanogr* 69:601–618
- Yoshimura T, Sugie K, Endo H, Suzuki K, Nishioka J, Ono T** (2014) Organic matter production response to CO<sub>2</sub> increase in open subarctic plankton communities: Comparison of six microcosm experiments under iron-limited and -enriched bloom conditions. *Deep Res Part I Oceanogr Res Pap* 94:1–14
- Zamzow H, Coale KH, Johnson KS, Sakamoto CM** (1998) Determination of copper complexation in seawater using flow injection analysis with chemiluminescence detection. *Anal Chim Acta* 377:133–144



- Zepp RG, Erickson DJ, Paul ND, Sulzberger B** (2007) Interactive effects of solar UV radiation and climate change on biogeochemical cycling. *Photochem Photobiol Sci* 6:286–300
- Zickfeld K, Eby M, Alexander K, Weaver AJ, Crespin E, Fichetef T,; Goosse H, Philippon-Berthier G, Edwards NR, Holden PB, Eliseev AV, Mokhov II, Feulner G, Kienert H, Perrette M, Schneider von Deimling T, Forest CE, Friedlingstein P, Joos F, Spahni R, Steinacher M, Kawamiya M, Tachiiri K, Kicklighter D, Monier E, Schlosser A, Sokolov A, Matsumoto K, Tokos KS, Olsen SM, Pedersen JOP, Ridgwell A, Shaffer G, Yoshimori M, Zeng N and Zhao F** (2013) Long-term climate change commitment and reversibility: an EMIC intercomparison. *Journal of Climate* 26(6):5782–5809
- Zondervan I, Zeebe RE, Rost B, Riebesell U** (2001) Decreasing marine biogenic calcification: A negative feedback on rising atmospheric pCO<sub>2</sub>. *Global Biogeochem Cycles* 15:507–516
- Zondervan I, Rost B, Riebesell U** (2002) Effect of CO<sub>2</sub> concentration on the PIC/POC ratio in the coccolithophore *Emiliana huxleyi* grown under light-limiting conditions and different daylengths, *J Exp Mar Biol Ecol* 272:55–70
- Zondervan I** (2007) The effects of light, macronutrients, trace metals and CO<sub>2</sub> on the production of calcium carbonate and organic carbon in coccolithophores—A review. *Deep Sea Res Part II Top Stud Oceanogr* 54:521–537

---

**CHAPTER 1** **1**


---

- Figure 1.1.** Atmospheric CO<sub>2</sub> simulated for the four Representative Concentration Pathways (RCP) up to year 2300 4
- Figure 1.2.** Diagram of the effects on biochemistry, the response of the organism and the ecological responses as a consequence of the ocean acidification and the changes in seawater carbon chemistry. 7

---

**CHAPTER 2** **17**


---

- Figure 2.1.** Temporal development of CO<sub>2</sub> partial pressures (pCO<sub>2</sub>) and dissolved iron (dFe) 29
- Table 2.1.** Measured pH, total alkalinity (TA, μmol L<sup>-1</sup>), calculated dissolved inorganic carbon (DIC, μmol L<sup>-1</sup>) and calcite saturation estate ( $\Omega_{\text{calcite}}$ ) 30
- Figure 2.2.** Temporal development of total Chl *a* concentration and optimal quantum yield of Chl *a* associated to photosystem II 31
- Figure 2.3.** Temporal development of phytoplankton, microzooplankton and heterotrophic bacterioplankton biomasses (μgC L<sup>-1</sup>) 33
- Table 2.2.** Net growth rates (μ in d<sup>-1</sup>) of the different groups calculated with the logistic model under the different treatments 36
- Figure 2.4.** Total mesozooplankton biomass and calanoid copepods ) at the beginning and at the end of the experiment 37
- Figure 2.5.** SEM photographs with the decline of *Skeletonema* sp and during the bloom of *Emiliana huxleyi* (day 18) 40
- Table 1.1S.** Fe demand was calculated for each group to meet their Fe quotas at the highest cell numbers reached during the experiment and transformed into biomass 47
- Table 1.2S.** Fold change in particulate and dissolved iron between days 12 and 21 under the different treatments 48
- Figure 2.1S.** Temporal development of phytoplankton, microzooplankton and heterotrophic bacterioplankton (cells mL<sup>-1</sup>) within the mesocosms 49
- Figure 2.2S.** Temporal development of total iron (tFe) concentrations within the mesocosms in the different treatments 51
- Figure 2.3S.** Temporal development of major nutrient concentrations within the mesocosms in the different treatments 51

---

**CHAPTER 3** **53**


---

- Table 3.1.** Carbon uptake parameters derived from isotope disequilibrium results in all treatments 63
- Figure 3.1.** Results of isotope disequilibrium experiments from the different treatments at the end of the experiment 64
- Figure 3.2.** Instantaneous <sup>14</sup>C uptake curves for phytoplankton in LC+DFB treatment on day 3 65
- Figure 3.3.** Temporal development of carbon fixation per volume (μg C μg Chl *a*<sup>-1</sup> h<sup>-1</sup>) and carbon fixation per Chl *a* (μg C L<sup>-1</sup> h<sup>-1</sup>) 66
- Table 3.2.** Elemental ratio of particulate organic carbon to nitrogen (POC:PON in mol:mol) 67
- Figure 3.4.** Temporal development of particulate organic nitrogen, particulate organic carbon and inorganic carbon concentrations (μmol L<sup>-1</sup>) 68
- Figure 3.5.** Temporal development of molar inorganic C:organic C and molar Ca:organic C ratios 70

<b>Table 3.3.</b> Statistical analyses of the effects of CO <sub>2</sub> , DFB, and their interaction on the variables analysed in the different treatments	71
<b>Figure 3.6.</b> Total particulate carbon (TPC) production, organic carbon (POC) production and particulate calcium (Ca) production	72
<b>Figure 3.1S.</b> Temporal development of phytoplankton and microplankton abundances (cells mL <sup>-1</sup> )	81
<b>Figure 3.2S.</b> Temporal development of molar Ca in all the treatments during the experiment	82

---

## CHAPTER 4 85

---

<b>Figure 4.1.</b> Experimental irradiances (PAR, UVA and UVB radiation) in the control mesocosms in day 6 (just before the addition of DFB on day 7)	95
<b>Table 4.1.</b> Experimental irradiances, corresponding weighted irradiances (BEI) and the biological effective dose (BED)	96
<b>Figure 4.2.</b> Temporal development of pigments concentrations within the mesocosms	97
<b>Figure 4.3.</b> Ratios of diatoxanthin and diadinoxantin to total fucoxanthins and hexanoyloxyfucoxanthin to total fucoxanthins	101
<b>Figure 4.4.</b> Temporal development of the photosynthetic parameters: $F_v/F_m$ , $\alpha$ , $rETR_{max}$ and $E_k$	102
<b>Figure 4.5.</b> Temporal development of percentage of cells SYTOX-Green labelled and percentage of cells c-H2DFFDA-green labelled	104
<b>Figure 4.6.</b> Temporal development of cyclobutane pyrimidine dymers (CPDs) within the mesocosms	105
<b>Table 4.2.</b> Statistical analyses of the effects of CO <sub>2</sub> , DFB, and their interaction, as well as the effect of time, on the variables analysed in the different treatments	106
<b>Table 4.1S.</b> Identified Fe-Metalloproteins genes in the genome of <i>Emiliana huxleyi</i>	116
<b>Table 4.2S.</b> Irradiance through the polyethylene mesocosm material and mesocosm lids transmittance	118
<b>Figure 4.2S.</b> Temporal development of phytoplankton, microzooplankton and heterotrophic bacterioplankton biomasses	118

---

## CHAPTER 5 121

---

<b>Table 5.1.</b> Instrumental conditions of ICP-MS and measurement parameters used during determination of trace elements concentrations.	128
<b>Table 5.2.</b> Biological and chemical characteristics of the different treatments during the development of a bloom of <i>Emiliana huxleyi</i>	130
<b>Table 5.3.</b> The concentration of particulate metals in seawater (nmol L <sup>-1</sup> ) during the development of a bloom of <i>Emiliana huxleyi</i>	131
<b>Table 5.4.</b> The concentration of particulate metals in seawater (nmol L <sup>-1</sup> ) in the different treatments after oxalate-wash	133
<b>Table 5.5.</b> Statistical analyses of the effects of CO <sub>2</sub> , DFB, and their interaction, as well as the effect of time, on the concentrations of particulate metals in seawater	134
<b>Table 5.6.</b> The relationship between particulate metales concentrations and the biomass of <i>Emiliana huxleyi</i> and total cells (phytoplankton and microzooplankton)	136
<b>Table 5.7.</b> P-values for the effects of CO <sub>2</sub> , DFB, their interaction and time on the P-normalized metal quotes and on the oxalate-washed concentrations	137
<b>Figure 5.1.</b> Comparison of P-normalized metal quotas (mmol:mol P) of particles from different treatments	138



<b>Table 5.1S.</b> <i>P</i> -values for the effects of CO <sub>2</sub> , DFB, their interaction and time on the Al-normalized metal	149
<b>Table 5.2S.</b> Identified Zn-Metalloproteins genes in the genome of <i>Emiliana huxleyi</i> (Read et al. 2013), encoding for the corresponding following proteins	150
<b>Figure 5.1S.</b> The partition coefficients in the different treatments at the beginning and the end of the bloom	151
<b>Figure 5.2S.</b> Comparison of Al-normalized metal quotas (mmol:mol Al) of particles from different treatments	151

---

## CHAPTER 6.1 153

---

<b>Table 6.1.1.</b> Filter configuration for the 12 spectral treatment groups of the photoinhibitor	160
<b>Figure 6.1.1.</b> Graphical illustrations of the implied dependence of repair and damage rates for the E, T and E <sub>max</sub> models	162
<b>Figure 6.1.2.</b> Measured parameters on coccoliths DL: distal shield length, DW: distal shield width, CAL: central area length and CAW: central area width	164
<b>Table 6.1.2.</b> Physiological variables of <i>Emiliana huxleyi</i> grown under ambient CO <sub>2</sub> (400 ppm) and high CO <sub>2</sub> (800 ppm)	165
<b>Figure 6.1.3.</b> Cellular absorbance of UVR and PAR measured as Chl <i>a</i> specific absorption ( $a^*[\lambda] \text{ m}^2 \text{ mg Chl a}^{-1}$ )	166
<b>Table 6.1.3.</b> Difference in AICs calculated for E, T and E <sub>max</sub> model fits to experimental data on the response of <i>E. huxleyi</i> photosynthesis to UV + PAR exposure	167
<b>Figure 6.1.4.</b> The panels illustrate the observed (points) vs. fitted (lines) results for three BWF/P-E models, the E, T and E <sub>max</sub> models	169
<b>Table 6.1.4.</b> Fitted parameters for the T model, mean $\pm$ standard errors for $n \geq 3$ experiments under each condition ambient and high CO <sub>2</sub> concentration	169
<b>Figure 6.1.5.</b> BWFs for the inhibition of photosynthesis by UVR ( $\epsilon [\lambda], [\text{mW m}^{-2}]^{-1}$ ) of <i>E. huxleyi</i> under ambient and increased CO <sub>2</sub> concentrations	169
<b>Figure 6.1.6.</b> PIC production rate, POC production rate and PIC:POC productivity ratio during the exponential phase	170
<b>Figure 6.1.7.</b> Representative scanning electron microscope (SEM) images of <i>Emiliana huxleyi</i> cells and free coccoliths	172
<b>Table 6.1.5.</b> Morphometric analysis of detached coccoliths and coccospheres of <i>Emiliana huxleyi</i> grown under ambient CO <sub>2</sub> (400 ppm) and high CO <sub>2</sub> (800 ppm)	173
<b>Figure 6.1.8.</b> Biological weighting functions for the inhibition of photosynthesis by UV ( $(\epsilon[\lambda], [\text{mW m}^{-2}]^{-1})$ data from different phytoplanktonic species	179

---

## CHAPTER 6.2 183

---

<b>Table 6.2.1.</b> Nomenclature of the different treatments used in the experiment	189
<b>Figure 6.2.1.</b> Specific growth rates of <i>Emiliana huxleyi</i> cultures exposed to the different irradiance, CO <sub>2</sub> and Fe treatments	193
<b>Figure 6.2.2.</b> Percentage of dead cells based on SYTOX Green staining of <i>Emiliana huxleyi</i> cultures exposed to the different irradiance, CO <sub>2</sub> and Fe treatments	194
<b>Figure 6.2.3.</b> Percentage of cell viability based on FDA green fluorescence emission of <i>Emiliana huxleyi</i> cultures exposed to the different irradiance, CO <sub>2</sub> and Fe treatments	195
<b>Figure 6.2.4.</b> Changes in the optimum quantum yield ( $F_v/F_m$ ) in cultures of <i>Emiliana huxleyi</i> exposed to the different irradiance, CO <sub>2</sub> and Fe treatments	196
<b>Table 6.2.2.</b> Photosynthetic parameters of <i>Emiliana huxleyi</i> calculated from chlorophyll <i>a</i> fluorescence measurements after 4 days of cultures at different conditions	197

<b>Figure 6.2.5.</b> Changes in photosynthetic production of particulate organic carbon (POC) of <i>Emiliana huxleyi</i> cultures exposed to the different irradiance, CO <sub>2</sub> and Fe treatments	198
<b>Figure 6.2.6.</b> Changes in photosynthetic production of dissolved organic carbon (DOC) of <i>Emiliana huxleyi</i> cultures exposed to the different irradiance, CO <sub>2</sub> and Fe treatments	199
<b>Table 6.2.3.</b> Percentage of DO <sup>14</sup> C extracellular release (PER) of dissolved organic carbon of <i>Emiliana huxleyi</i>	200
<b>Figure 6.2.7.</b> Calcification rates of <i>Emiliana huxleyi</i> after 4 days of cultures exposed to the different irradiance, CO <sub>2</sub> and Fe treatments	201
<b>Figure 6.2.1S.</b> Seawater carbonate system during the experiment	209

# Resumen



## Resumen

Las emisiones de dióxido de carbono ( $\text{CO}_2$ ) producidas por las actividades humanas derivadas del uso de combustibles fósiles y los distintos usos de la Tierra han causado un considerable aumento de la concentración de  $\text{CO}_2$  atmosférico desde el inicio de la revolución industrial. La concentración ha aumentado de 280 a 400  $\mu\text{atm}$ . Los océanos han absorbido aproximadamente un 30% de las emisiones de carbono antropogénicas durante los últimos 200 años. Además, las predicciones establecen que la concentración de  $\text{CO}_2$  se duplicará con respecto a la concentración actual en el peor de los escenarios posibles hacia finales de este siglo. Como consecuencia de la disolución del  $\text{CO}_2$  en el agua de mar, el pH disminuirá. Este proceso se denomina acidificación oceánica. Cuando el  $\text{CO}_2$  se disuelve en el agua, éste reacciona con el agua y se forma ácido carbónico ( $\text{H}_2\text{CO}_3$ ) que es una forma inestable y rápidamente se disocia en bicarbonato ( $\text{HCO}_3^-$ ) y en iones libres de hidrógeno ( $\text{H}^+$ ). El aumento de  $\text{H}^+$  conlleva una disminución del pH, aumentando la acidez de los sistemas acuáticos. Los modelos que se han propuesto establecen un aumento adicional a dicha disminución, que de hecho, ya se ha producido desde el comienzo de la era industrial. Este aumento sería de 0.06 a 0.32 unidades de pH en la disminución global, y la variación final dependerá de las futuras emisiones. Además, la incorporación de  $\text{CO}_2$  en los océanos conllevará una disminución de los iones carbonato ( $\text{CO}_3^{2-}$ ) y de los niveles de saturación del carbonato cálcico ( $\text{CaCO}_3$ ) en los minerales calcita y aragonito. La acidificación de los océanos potencialmente afectará de forma severa los organismos marinos. El fitoplancton marino contribuye con la mitad de la producción primaria global, siendo la base de las redes tróficas marinas y de los ciclos biogeoquímicos, especialmente del carbono y otros nutrientes. Además, dicho fitoplancton marino incorpora aproximadamente de 45 a 50 billones de toneladas métricas de carbono inorgánico de forma anual, retirando un cuarto del  $\text{CO}_2$  emitido a la atmósfera derivado de las actividades de origen humano. Por ello, la respuesta



del fitoplancton a la acidificación de los océanos es clave para comprender los futuros cambios globales en los ecosistemas marinos.

La posible respuesta del fitoplancton al incremento de la concentración de  $\text{CO}_2$  en los océanos y con ello, a la disminución del pH, es dependiente de los mecanismos fisiológicos de incorporación de carbono inorgánico y su asimilación dentro de la célula. Durante la fotosíntesis, el  $\text{CO}_2$  es fijado por la enzima rubisco (Ribulosa-1,5-bifosfato carboxilasa-oxigenasa). La enzima Rubisco con las concentraciones actuales de  $\text{CO}_2$  presenta una saturación inferior a la mitad en la mayoría de las especies. Por otra parte, esta enzima presenta tanto actividad enzimática carboxilasa para la fijación de carbono como actividad oxigenasa. La actividad oxigenasa produce una disminución significativa de la fijación de  $\text{CO}_2$  por parte de la enzima Rubisco. Esta limitación de la fijación de  $\text{CO}_2$  junto con la baja afinidad de la Rubisco por el  $\text{CO}_2$  es compensada por la actividad de mecanismos concentradores de carbono (CCMs). Los CCMs aumentan la concentración de  $\text{CO}_2$  alrededor de la enzima. De este modo, se suprime la actividad oxigenasa y aumenta la actividad carboxilasa de la Rubisco. La mayoría de las especies de fitoplancton marino en principio presentarían poco efecto en sus tasas de fotosíntesis, porque ésta ya estaría saturada de  $\text{CO}_2$  gracias a la actividad de los CCMs que activamente incorporan carbono inorgánico,  $\text{CO}_2$ , bicarbonato o incluso ambos. El aumento de la concentración de  $\text{CO}_2$  debería beneficiar directamente a la producción de biomasa por el aumento de la reacción carboxilasa en la enzima rubisco y por la reducción de las pérdidas de  $\text{CO}_2$  debido a las diferencias de concentración entre los medios. Además, con el aumento de la concentración de  $\text{CO}_2$  se produciría una reducción de la actividad de los CCMs que consumen mucha energía. Se ha propuesto que una disminución en la regulación de la maquinaria fotosintética al disminuir la actividad de los CCMs podría aumentar el uso eficiente de la energía del fitoplancton. Por otra parte, la bajada de pH que se ha predicho representa un



aumento en las concentraciones de los iones de hidrógeno libres ( $H^+$ ) que pueden afectar el pH del interior de las células, el potencial de membrana y la actividad de las enzimas. Debido al efecto de la disminución del pH en las células, la acidificación de los océanos podría reducir el crecimiento del fitoplancton marino. Por ello, el efecto de la acidificación de los océanos presenta un doble rol. Por una parte, el aumento de la concentración de  $CO_2$  favorecería la fotosíntesis y por otra parte, la disminución de pH que afectaría a los organismos reduciendo la producción primaria.

La disminución de pH producida por el aumento de la concentración de  $CO_2$  también podría afectar las tasas de calcificación de los organismos. La calcita es uno de los materiales más comunes que se utiliza en la formación de esqueletos, conchas y otras estructuras protectoras de organismos. La calcificación es facilitada por un aumento en pH y un aumento en la concentración de carbonato. Estas condiciones se alcanzan en las zonas de calcificación mediante procesos de transporte de iones que consumen energía como puede ser la incorporación de fosfato. El coste energético de la calcificación aumentaría debido a la disminución del pH y de las concentraciones de carbonato. Esta energía necesaria extra se utilizaría para compensar los cambios químicos que se producirían en el agua de mar y dependería del proceso de calcificación de cada grupo taxonómico.

Con respecto a lo anteriormente dicho, los cocolitofóridos son especialmente importantes. Pertenecen a un grupo de microalgas unicelulares que habitan en la capa superficial de los océanos y que son los organismos que tienen mayores tasas de calcificación. El pH intracelular de los cocolitofóridos es muy sensible a cualquier cambio externo de pH. Por ello, la mayoría de los cocolitofóridos reducen sus tasas de calcificación cuando se realizan simulaciones de las concentraciones de  $CO_2$  que se alcanzarán a final de siglo. El aumento de la concentración de  $CO_2$  alterará las relaciones de competencia



entre especies produciendo cambios en la composición fitoplanctónica de las comunidades, debido a que la sensibilidad al aumento de  $\text{CO}_2$  varía entre especies. Todos estos cambios alterarán los procesos fisiológicos afectando a la dinámica de las poblaciones y de este modo, a todo el ecosistema.

Según los procesos biológicos de incorporación de  $\text{CO}_2$  se definen dos tipos de bombas biológicas de carbono. Por un lado está la bomba de carbono inorgánico basada en la fotosíntesis, y por otro lado, la bomba de carbonato, generada por la formación de carbonato cálcico en las estructuras externas del plancton que calcifica. Mientras que la fotosíntesis fija  $\text{CO}_2$  en carbono orgánico (la llamada "*carbon pump*"), actuando como un sumidero de  $\text{CO}_2$  atmosférico, la calcificación convierte 2 aniones bicarbonato en una molécula de carbonato cálcico y en otra molécula de  $\text{CO}_2$ , actuando como una fuente de  $\text{CO}_2$  de los océanos (denominada "*carbonate counter-pump*"). Son por lo tanto, dos bombas relacionadas entre sí en términos de alteración del carbono inorgánico disuelto (DIC), que además se contrarrestan la una a la otra alterando el impacto de cambios en concentración de  $\text{CO}_2$  entre el mar y la atmósfera. La relación entre las dos bombas se denomina "*rain ratio*", que es el ratio entre el carbono particulado inorgánico (PIC) y el carbono particulado orgánico (POC). Este ratio determina el flujo de  $\text{CO}_2$  entre la atmósfera y el océano. Los estudios existentes del flujo global de carbono orgánico, indican que la bomba de carbono es superior a la bomba de carbonato, pero el aumento de la concentración de  $\text{CO}_2$  y su efecto en la fotosíntesis y en la calcificación podría alterar el "*rain ratio*". Una reducción en la calcificación produce una retroalimentación negativa al aumento de la concentración de  $\text{CO}_2$ , es decir, se reduciría la concentración de  $\text{CO}_2$  liberada a la atmósfera. Pero se sabe que hay una fuerte relación entre el carbono orgánico particulado que migra al fondo de los océanos con el carbono inorgánico que se produce por la calcificación. Este proceso se denomina "*ballast effect*". Si se altera la producción de carbonato cálcico, afectaría a la migración de carbono orgánico





que se retira de las capas altas. El POC se quedaría en las capas altas, reduciéndose y aumentando de este modo la concentración de  $\text{CO}_2$ . El efecto global sería negativo debido al aumento de la concentración de  $\text{CO}_2$ , que pasaría a la atmosfera disminuyendo la capacidad de los océanos de retirar  $\text{CO}_2$ . Por otra parte, los cambios de pH debido a la acidificación oceánica pueden afectar a los metales trazas. Concretamente, se afectaría a la concentración y el tipo de especie predominante debido a la sensibilidad a los cambios de pH. El efecto final sería que los cambios originados por la disminución de pH afectarían a la disponibilidad de los metales y a los niveles de toxicidad de los distintos organismos marinos.

Los metales traza (Mn, Fe, Co, Cu, Zn, y Cd) son necesarios para numerosos procesos en fitoplancton y pueden influenciar el crecimiento y la estructura de la comunidad planctónica. Además, los metales traza son necesarios para el crecimiento y la supervivencia de los organismos fotosintéticos. El contenido celular de los metales en el fitoplancton reflejan la demanda bioquímica/fisiológica de las células además de la disponibilidad en el ambiente de los mismos. Esto altera la distribución de los metales en el océano. Entre todos los metales traza, el hierro (Fe) es el más importante porque es requerido para procesos fisiológicos y moleculares esenciales. El Fe es un cofactor de metaloenzimas y proteínas que son esenciales para la fotosíntesis, respiración, transporte de electrones, metabolismo del nitrato, la detoxificación de especies reactivas de oxígeno y la reparación del ADN. Aunque sea el cuarto elemento más abundante de la Tierra, su solubilidad es muy baja en agua tan oxigenadas, lo que produce que se presenten bajas concentraciones de Fe en la mayoría de los sistemas acuáticos. El fitoplancton presenta distintos mecanismos para incorporar el Fe y para que su uso no sea excesivo. El Fe existe en 2 estados de oxidación: Fe(II) que es muy soluble y Fe (III) que es menos soluble. Generalmente, la forma predominante que es la más estable es la de Fe(III). Además el Fe se clasifica en 2 tipos de fracciones



basado en los sistemas de filtración: Fe particulado ( $>0.2 \mu\text{m}$ ) y Fe disuelto ( $<0.2 \mu\text{m}$ ). Además, la fracción de Fe disuelto se divide en coloidal y soluble. Distintos estudios han demostrado que la mayoría de la fracción disuelta ( $>99\%$ ) está formando parte de compuestos orgánicos con metales. El Fe se une a moléculas orgánicas denominadas ligandos orgánicos que pueden ser fuertes o débiles en función de la constante de estabilidad (constante de asociación para el equilibrio que existe entre el metal y el ligando orgánico). Los complejos de coordinación orgánicos formados son importantes debido a que influyen en la solubilidad y controlan la disponibilidad del Fe por parte del fitoplancton. Los compuestos formados con las distintas especies del Fe pueden resultar en condiciones de limitación de Fe, porque el Fe disponible para los organismos es inferior a las necesidades que presentan los organismos. La biodisponibilidad de un metal se define como el grado al que cierto compuesto, en este caso el Fe, es accesible y lo puede utilizar un organismo. Por ello, las condiciones de estrés debido a la concentración baja de Fe son muy extendidas tanto en océanos como en ciertas zonas costeras, afectando al crecimiento, fisiología y producción de materia orgánica por parte del fitoplancton. La acidificación oceánica afectará la termodinámica y cinética de los metales, además de la especiación de los distintos metales. La disminución de la concentración de  $\text{OH}^-$  debido a la disminución del pH y de el ion carbonato debido a todos los cambios del sistema carbónico-carbonato afectarán tanto a la solubilidad como a la adsorción, toxicidad y las reacciones de oxidación y reducción de los metales. Todos estos cambios posiblemente afectarán a la concentración y a la química de especiación del Fe y con ello, a la disponibilidad del Fe para las distintas especies de fitoplancton. La acidificación oceánica puede aumentar la solubilidad del Fe aumentando la concentración del mismo, pero como el Fe disuelto mayoritariamente está unido a ligandos orgánicos, el resultado final de la concentración biodisponible dependerá de la naturaleza del ligando.



Solo unos pocos estudios se han centrado en el estudio de los efectos interactivos entre la acidificación oceánica y la concentración del Fe. Además, las respuestas obtenidas han dependido en parte de las características de la comunidad fitoplanctónica. Las necesidades de Fe por parte de una comunidad determinada están relacionadas con las condiciones ambientales de dicha comunidad. De forma general, las especies costeras de fitoplancton tienen necesidades superiores de ciertos metales que las especies oceánicas. Por ello, el efecto de los cambios en la disponibilidad de Fe debido a los cambios en la concentración del CO<sub>2</sub> dependerán de las demandas de Fe de las distintas especies de fitoplancton.

La interacción de los efectos de la acidificación oceánica y de la concentración de Fe han mostrado que influyen en la fisiología del fitoplancton y que producen cambios en la comunidad fitoplanctónica. Las respuestas obtenidas han sido diferentes en función de la región (en experimentos en condiciones naturales) y de la especie que se haya estudiado (en experimentos de laboratorio). Además influye la concentración del Fe, la especiación del Fe y la composición de la comunidad fitoplanctónica. En un futuro escenario de cambio global, los distintos factores variarán simultáneamente. Considerando la importancia del fitoplancton como base de las cadenas tróficas y en los ciclos biogeoquímicos de los distintos nutrientes, es necesario entender todas las posibles respuestas por parte de las distintas especies como consecuencia del cambio climático. El ciclo biogeoquímico más importante es el del carbono y el grupo de fitoplancton compuesto por los cocolitofóridos, se caracterizan por contribuir con aproximadamente entre 1-10 % del carbono total fijado y con la mitad de la calcita producida que migra hacia los sedimentos. En particular, la especie *Emiliana huxleyi* se caracteriza por ser la especie de los cocolitofóridos que se distribuye de forma más amplia y que además, es la más estudiada. Se caracteriza por ser una especie formadora de "blooms". Los resultados obtenidos con esta especie, *E. huxleyi*, son dependientes de la zona



estudiada en experimentos en condiciones naturales y de las condiciones de cultivo en experimentos en condiciones controladas de cultivos en laboratorios. Aunque la respuesta general obtenida es que *E. huxleyi* está afectada por la acidificación oceánica, hay una falta de conocimiento en la respuesta de distintos factores del cambio global, específicamente, en cambios producidos por la acidificación oceánica y los cambios en la concentración de Fe de forma simultánea.

El **objetivo de esta tesis** ha sido profundizar en el estudio de la respuesta fisiológica de *Emiliana huxleyi* a condiciones de aumento de la concentración de CO<sub>2</sub> y de la disponibilidad de Fe dentro de la red trófica planctónica utilizando mesocosmos y en cultivos.

Los experimentos se pueden realizar en distintas escalas de complejidad desde las condiciones controladas de los cultivos en el laboratorio a estudios del ecosistema completo en condiciones naturales. Las condiciones controladas de experimentos de laboratorio nos permiten estudiar los mecanismos fisiológicos relacionados con la respuesta de los organismos de forma individual, pero el análisis de esta respuesta en el contexto de la comunidad y el ecosistema necesitan experimentos que abarquen todos los niveles tróficos, siendo necesarios los experimentos de gran escala. Por ello, los mesocosmos son esenciales debido a que nos permiten directamente analizar los efectos interactivos de múltiples factores del cambio climático en los distintos niveles tróficos. Además, los mesocosmos presentan un alto grado de realismo comparado con las condiciones controladas de laboratorio y tienen menos limitaciones para realizar experimentos de sistemas naturales a gran escala. Tienen por lo tanto, valor predictivo.

En este trabajo se ha investigado los efectos interactivos del aumento de la concentración de CO<sub>2</sub> y de la variación de la disponibilidad de Fe en los distintos grupos que forman el plancton utilizando mesocosmos en un fiordo





de la costa noruega (Raunefjord, Bergen). Se empleó un diseño factorial con todas las combinaciones posibles de condiciones ambientales y elevadas de las concentraciones de CO<sub>2</sub> y Fe. Las concentraciones de Fe aumentaron a causa del aumento de la concentración de CO<sub>2</sub> en la mitad de los mesocosmos debido a la disminución del pH. Este resultado ya se había observado previamente en el mismo fiordo en estudios anteriores. Además para crear los distintos niveles de concentración de Fe, se añadió el quelante deferoxamina B (DFB) a la mitad de los mesocosmos. La adición del quelante contribuyó en el aumento de la solubilidad del Fe y con ello, a la disminución de la concentración de Fe particulado del fiordo. Por ello, la manipulación de ambos factores aumentó la concentración del Fe disuelto en este fiordo. Este trabajo demuestra que la acidificación oceánica puede aumentar la disponibilidad de Fe.

Las condiciones desarrolladas por el efecto de los dos factores (Fe y CO<sub>2</sub>) promovieron el desarrollo de dos fases claramente diferenciadas. Durante la primera fase (del día 1 al 10 del experimento), una sucesión normal de fitoplancton ocurrió sin diferencias debido a los 2 factores (Fe y CO<sub>2</sub>). En cambio, durante la segunda fase se obtuvo una fuerte respuesta por parte de la comunidad, donde la biomasa del cocolitofórido *E. huxleyi* aumentó de forma masiva a condiciones ambientales de la concentración de CO<sub>2</sub> y aumentadas de la concentración del Fe disuelto debido a la adición del quelante (DFB). Sin embargo, el resto de la comunidad planctónica con excepción de *Synechococcus* sp., no presentó ningún cambio debido a los factores (Fe y CO<sub>2</sub>) y su interacción. El efecto negativo del aumento de la concentración de CO<sub>2</sub> en *E. huxleyi* se había observado previamente en otros estudios, y al igual que en este se observa que el aumento de la concentración de CO<sub>2</sub> tiene un efecto dañino en el crecimiento y la biomasa del cocolitofórido.



Sin embargo, los resultados obtenidos en la condición control de nuestro experimento, demuestran que las células de este tratamiento estaban en condiciones de limitación de Fe. Este resultado es contradictorio a lo observado previamente ya que la concentración de Fe en los sistemas costeros y fiordos no se consideraba limitante. Las razones para establecer que en el tratamiento control *E. huxleyi* estaba en limitación de Fe han sido que estimando la concentración de Fe necesaria para que se formara un bloom con la concentración de *E. huxleyi* como en el otro la concentración de Fe era inferior del tratamiento control.

El bloom de *E. huxleyi* fue promovido por un aumento de los procesos de asimilación de carbono aunque los mecanismos de incorporación de carbono inorgánico no se vieron afectados por las distintas condiciones. Se observó que la presencia de pigmentos con funciones recolectoras de luz (que son altamente eficientes con la transferencia de energía a las clorofilas), conducían a un mejor funcionamiento de las cadenas transportadoras de electrones. Además, los daños producidos en el ADN por el exceso de irradiancia medido en este fiordo son minimizados por el aumento de la concentración del Fe disuelto, los daños que se producen en el ADN se denominan dímeros de pirimidina ciclobutano (CPDs). Estos resultados muestran que la concentración del Fe disuelto es necesaria para disminuir el daño del ADN y para sobrellevar el estrés oxidativo en *E. huxleyi*, debido a que la cadena transportadora de electrones y los pigmentos son dependientes de la concentración de Fe disuelto.

La disponibilidad de los metales puede influenciar el crecimiento del fitoplancton y la estructura de la comunidad. Además, el fitoplancton controla la distribución, la especiación química y el ciclado de los metales en el océano. Por ello, se ha analizado el origen de dichos metales, que puede ser litogénico o biótico y la evolución de las concentraciones de dichos metales traza (Fe, Cu,





Zn, Mn, Co, Cd and Mo) durante el bloom del cocolitofórido *E. huxleyi*. Este estudio es el primero en combinar los análisis de los metales traza de las partículas en un experimento controlado utilizando mesocosmos con una manipulación simultánea de las concentraciones de CO<sub>2</sub> y Fe utilizando una comunidad fitoplanctónica natural. Nuestros resultados demuestran que en el fiordo estudiado, las concentraciones de Fe y titanio (Ti) fueron principalmente de origen litogénico. Por el contrario, las concentraciones de los otros metales particulados (Cu, Zn, Mn, Co, Cd and Mo) mostraron una fuerte influencia biótica. Para el estudio del origen de los distintos metales trazas particulados se llevaron a cabo dos tipos de análisis. En primer lugar, se realizaron ratios considerando la concentración de aluminio y fósforo que son indicadores de la fracción abiótica y biótica respectivamente. Estos ratios se compararon con ratios de estudios previos en sistemas naturales y en cultivos con el cocolitofórido *E. huxleyi* para determinar si el contenido era biótico. Además se realizaron correlaciones con la biomasa del cocolitofórido y con la concentración de fósforo (como indicador biótico) del medio con las concentraciones de los distintos metales particulados. Los metales que presentaron correlación positiva fueron cobre (Cu), cinc (Zn), manganeso (Mn), cobalto (Co), cadmio (Cd) y molibdeno (Mo). Para determinar la fracción abiótica se llevó a cabo una comparación con estudios previos de la corteza terrestre, presentando valores similares el Fe y el Ti. Especialmente, las concentraciones de los metales particulados de Zn y Cu que fueron especialmente elevadas en el tratamiento con condiciones ambientales de CO<sub>2</sub> y con el aumento de la concentración de Fe disuelto, siendo los mesocosmos donde se observó el bloom de *E. huxleyi*. Los cocolitofóridos suelen presentar un mayor requerimiento de concentraciones de Zn en comparación con otras especies de fitoplancton. Aunque el análisis del genoma de *E. huxleyi* nos ha permitido observar la importancia del Zn en este cocolitofórido, el uso de estas elevadas concentraciones de Zn es aún desconocido. Por ello, se puede



establecer que las concentraciones de Zn disuelto al ser tan importante para el crecimiento de los cocolitóforos y la importancia de este grupo para el ciclo global del carbono, pueden influir de forma indirecta en la bomba biológica de carbono. Del mismo modo, las concentraciones de Cu particulado en nuestro experimento fueron más altas de lo habitual probablemente debido a las altas concentraciones de Cu disuelto que se midieron durante el experimento y que ya se habían observado previamente en otros estudios. Las concentraciones tan elevadas del cobre particulado, indicando una elevada concentración de Cu en el contenido celular pueden ser debido a la presencia de fitoquelatinas o de otros mecanismos detoxificantes que previamente se han observado en este cocolitofórido para amortiguar las elevadas concentraciones en el interior celular debido a una incorporación elevada de Cu. También, puede ser debido a que este cocolitofórido presente unos requerimientos de cobre más elevados para el mantenimiento del crecimiento óptimo y que se había observado previamente en otros estudios con esta especie en cepas costeras y oceánicas. De acuerdo con nuestros resultados, la acidificación de los océanos se espera que cambie las concentraciones de los distintos metales particulados, debido a los distintos efectos de la acidificación de los océanos en el crecimiento de las distintas especies del fitoplancton marino considerando los distintos requerimientos de los distintos grupos de fitoplancton.

La importancia de los metales traza se pueden relacionar con la limitación al Fe que las células experimentan en el tratamiento control (condiciones ambientales de CO<sub>2</sub> y Fe disuelto). Las células presentaron una combinación de síntomas característicos de limitación por Fe. Estos síntomas son una disminución de las tasas de crecimiento, la reducción del contenido en clorofila *a* y una disminución del  $F_v/F_m$ , un valor derivado del análisis del fotosistema II que nos indica si las células presentan estrés en unas condiciones determinadas. Además, se ha demostrado que los niveles de Fe disuelto en el control no fueron suficientes porque eran inferiores a la



concentración de Fe que necesitan las células para mantener las concentraciones de biomasa alcanzadas durante la fase del bloom donde se presentan las concentraciones más elevadas del cocolitifórido a condiciones ambientales de CO<sub>2</sub> y aumentadas de Fe disuelto. Además, los procesos de asimilación de carbono mostraban la limitación en Fe en *E. huxleyi* en el tratamiento control. Las tasas de fijación de carbono fueron similares tanto en condiciones futuras de la concentración de CO<sub>2</sub> como en el tratamiento control. Esto indicaría que las células pueden disminuir la capacidad máxima de su fijación de carbono debido a que presentan un metabolismo limitado a causa de la limitación por Fe. En cambio, no se observó en las concentraciones de materia orgánica particulada, específicamente, en el carbono particulado, donde los mesocosmos del tratamiento control presentaron concentraciones más elevadas que los de tratamientos que simulan las condiciones futuras de acidificación de los océanos. La posible causa de las diferencias de los resultados medidos es que las tasas de fijación serían tasas brutas de fotosíntesis. En cambio, con la acumulación de carbono orgánico particulado observamos el resultado tras la fijación de carbono y otros procesos donde puede disminuir la concentración final de carbono fijado como puede ser la respiración o la liberación de carbono orgánico disuelto (un mecanismo que se ha observado en otros estudios debido a condiciones de estrés).

La tasa de crecimiento, la biomasa y la tasa de calcificación del cocolitifórido *E. huxleyi* se afectaron en los tratamientos que simulan las condiciones futuras de la concentración de CO<sub>2</sub>, debido a los cambios derivados del pH. El pH del interior de las células en los cocolitifóridos, como se mencionó anteriormente, es muy sensible a los cambios del pH externos, es decir, del ambiente. Además, el mantenimiento del pH interno de las células es un proceso muy costoso energéticamente y la acidificación de los océanos se caracteriza por afectar en los organismos a la demanda de energía celular. Por otra parte, nuestros resultados sugieren que *E. huxleyi* es capaz de utilizar el Fe



unido al quelante DFB (FeDFB) como se había observado previamente en otros estudios. Por ello, las células del tratamiento de concentraciones elevadas de CO<sub>2</sub> con la adición del quelante DFB presentaron una mayor facilidad para sobrellevar el gasto energético metabólico extra debido a la disminución del pH, en comparación con el otro tratamiento de concentraciones elevadas de CO<sub>2</sub> que no presentan la adición del quelante. Esto le permitió también sobrellevar mejor los efectos negativos de la acidificación oceánica y mantener las tasas de crecimiento. La respuesta al estrés fisiológico de la comunidad y en particular, de *E. huxleyi* fue afectado por las condiciones de CO<sub>2</sub> y Fe disuelto. Los mecanismos protectores (la composición y concentración de los pigmentos) se afectaron de forma negativa por el incremento en la concentración de CO<sub>2</sub> pero el efecto negativo fue contrarrestado por el aumento de la concentración de Fe disuelto. Este resultado destaca que las células en condiciones de baja concentración de Fe muestran una mayor susceptibilidad a la fotoinhibición, destacando que el estado fisiológico de estas células limitadas fueron mejoradas con el aumento de la concentración de Fe disuelto. Los mismos resultados se observaron en la cadena transportadora de electrones donde se destaca el efecto positivo del aumento de la concentración de Fe modulando el efecto negativo del aumento de la concentración de CO<sub>2</sub>. La razón más probable de esta disminución en la capacidad de los mecanismos protectores de las células, al igual que en los procesos anteriores, sería como se ha mencionado anteriormente por la disminución del pH. Además, el estrés oxidativo y el daño en el ADN fueron minimizados también debido a el aumento de la concentración del Fe disuelto. Por ello, el Fe sería necesario para la reparación del ADN por daños derivados del exceso de irradiancia y para superar el estrés oxidativo generado por los factores de estudio (CO<sub>2</sub> y Fe), asegurando la viabilidad celular y el crecimiento de *E. huxleyi*. El Fe sería necesario para mantener los requerimientos energéticos impuestos por las proteínas relacionadas en estos procesos, y que



la concentración de Fe necesaria no es suplida en condiciones ambientales o la energía se invierte en sobrellevar el efecto negativo de la acidificación oceánica en la fisiología celular.

Este estudio demuestra que los efectos negativos del aumento de la concentración de CO<sub>2</sub> en estas cepas de *E. huxleyi* pueden ser parcialmente mitigadas por el aumento de la concentración de Fe disuelto en áreas con concentraciones totales de Fe elevadas (tanto la concentración particulada como disuelta), posiblemente teniendo efectos derivados en la dinámica de las redes tróficas, en la exportación del carbono al fondo de los océanos, en el *rain ratio* que relaciona el carbono particulado inorgánico y orgánico y finalmente afectaría al intercambio de la concentración de CO<sub>2</sub> entre el océano y la atmosfera.

Estos resultados establecen que son necesarios los estudios que consideran los efectos combinados de distintos factores derivados del cambio global para poder entender las futuras respuestas de los ecosistemas. Por esta razón, además del estudio en condiciones naturales utilizando mesocosmos se realizaron una serie de experimentos en condiciones controladas de cultivo con una cepa costera de *E. huxleyi*, aislada en Noruega. En estos estudios, además de considerar variaciones de la concentración de CO<sub>2</sub> y Fe disuelto se consideró un tercer factor que sería la exposición a radiación ultravioleta (RUV). Además, se analizó la interacción de la exposición a la RUV con distintos niveles de los otros factores (CO<sub>2</sub> y Fe). En primer lugar, se estimó la sensibilidad a la exposición de la RUV de los cultivos en dos condiciones de CO<sub>2</sub>, ambiental y a una concentración elevada de CO<sub>2</sub>. La concentración fue de 800 ppm, el doble de la concentración actual. Se estableció mediante modelos matemáticos la sensibilidad de la tasa de fotosíntesis de la cepa en ambas condiciones de CO<sub>2</sub> analizando el efecto de la RUV en cada longitud de onda. Se analizaron distintos modelos posibles que analizan la inhibición de la fotosíntesis por la RUV y se estableció el modelo más adecuado en función del



ajuste estadístico entre lo observado y lo que se predice. Este modelo está caracterizado porque hay un umbral a partir cual se produce la inhibición de la fotosíntesis pero que por debajo de este umbral no hay un efecto negativo en la tasa de fotosíntesis. Nuestros resultados indicaron que no hay diferencias en la sensibilidad a la exposición de la RUV en la tasa de fotosíntesis en las distintas condiciones de CO<sub>2</sub> estudiadas (400 y 800 ppm) para esta cepa de *E. huxleyi*. Por otra parte, se realizó otro experimento donde se estudiaba el efecto de la concentración del hierro disuelto en los procesos fisiológicos de *E. huxleyi* en las dos condiciones de CO<sub>2</sub>. Se estudió la inhibición de los procesos fisiológicos a la exposición de RUV en comparación con cultivos expuestos únicamente a la radiación PAR en condiciones ambientales de CO<sub>2</sub>. Los resultados mostraron que las concentraciones de Fe reducidas presentan restricciones en la capacidad de sobrellevar las condiciones de estrés por la exposición a la RUV en esta especie. Además, el estrés fue disminuido en las condiciones de CO<sub>2</sub> para finales de este siglo bajo la exposición de RUV como se observa incluso en los cultivos con la menor concentración de Fe disuelto; observándose un aumento de la producción de carbono orgánico particulado, de las tasas de transporte de electrones y las tasas de calcificación. Esto demuestra que *E. huxleyi* es capaz de sobrellevar mejor el estrés generado por la exposición de la RUV en condiciones de CO<sub>2</sub> futuras, y que el Fe presenta es el factor principal en controlar la respuesta en todos los procesos fisiológicos.



## Conclusiones

1. *Emiliana huxleyi* estaba limitada por hierro en condiciones ambientales de CO<sub>2</sub> y de hierro disuelto en el fiordo estudiado y en el tratamiento control.
2. El sideróforo deferoxamina B (DFB) y una elevada concentración de CO<sub>2</sub> aumentó la concentración de hierro disuelto en el fiordo.
3. El aumento de CO<sub>2</sub> afectó negativamente a *Emiliana huxleyi* y a *Synechococcus* sp. mientras que no afectó al resto de la comunidad planctónica.
4. El aumento del hierro disuelto aumento el crecimiento y la biomasa de *E. huxleyi* a condiciones ambientales, mitigando el efecto negativo del alto CO<sub>2</sub>.
5. *Emiliana huxleyi* presenta transportadores de bicarbonato debido a la baja actividad de la enzima anhidrasa carbónica externa y el uso del bicarbonato como fuente de carbono inorgánico.
6. Los procesos de asimilación de carbono aumentaron a altas concentraciones de hierro disuelto y a concentraciones ambientales de CO<sub>2</sub> y por el contrario, fueron afectados negativamente por las concentraciones de CO<sub>2</sub> elevadas.
7. La calcificación disminuyó en concentraciones de CO<sub>2</sub> elevadas y no se vio afectada por la concentración de hierro. Como consecuencia, el "rain ratio" disminuyó en condiciones de elevado CO<sub>2</sub>



independientemente del nivel de Fe, afectando directamente la bomba biológica de carbono.

8. El aumento de CO<sub>2</sub> tuvo efectos negativos en la concentración de pigmentos y en la cadena transportadora de electrones tilacoidal, siendo contrarrestado por el aumento de la concentración de hierro.
9. El hierro es necesario para la reparación de ADN y para controlar la formación de especies reactivas de oxígeno (ROS).
10. Todos los metales trazas particulados analizados son de procedencia biótica con la excepción del hierro y titanio.
11. El aumento de la concentración de CO<sub>2</sub> cambió las concentraciones celulares de los metales traza particulados debido a su efecto en el crecimiento de los distintos grupos de fitoplancton. Además, dichas concentraciones fueron moduladas por la concentración de hierro disuelto.
12. La exposición a la radiación ultravioleta (RUV) de *Emiliana huxleyi* tuvo el mismo efecto en la fotosíntesis en las distintas concentraciones de CO<sub>2</sub>.
13. La sensibilidad de *Emiliana huxleyi* a la radiación ultravioleta (RUV) en las distintas condiciones de CO<sub>2</sub> es dependiente de los niveles de hierro.



14. Las altas concentraciones de CO<sub>2</sub> inducen a una menor sensibilidad de *Emiliana huxleyi* a la radiación ultravioleta independientemente de los distintos niveles de hierro.





Después de más de 4 años de trabajo, llega el momento de dar las gracias a todas las personas que me han ayudado y apoyado durante este camino. A pesar de todo el esfuerzo, me siento muy afortunada y orgullosa de haber podido realizar la tesis doctoral por todo el conocimiento y todas las experiencias que he vivido, pero sobre todo por las personas que me han acompañado en esta andadura.

En primer lugar, me gustaría darle las gracias a mi directora de tesis, Prof. Dra. María Segovia, por todo el conocimiento que ha compartido conmigo durante estos años, por su apoyo pero especialmente por su confianza desde el principio. Además, gracias por darme la oportunidad de trabajar con investigadores de otros sitios que tanto me ha enriquecido como científica y tantos lugares me ha permitido conocer. Si tuviera un *giratiempo* volvería a comenzar esta aventura.

Gracias a todos los miembros del Área de Ecología por la disponibilidad a ayudarme en todo momento. En especial, al Prof. Dr. Francisco J. L. Gordillo por todas sus aportaciones a mi trabajo y por brindarme la oportunidad de colaborar en su investigación.

Sin duda, este trabajo no hubiera sido posible sin todos los integrantes de "*Phytostress*". Muchísimas gracias por vuestra colaboración y entrega durante el experimento pero también por los momentos de diversión compartidos en el fiordo. Gracias Prof. Dra. Jorun Egge por tu ayuda.

Muchísimas gracias Prof. Dra. Maria T. Maldonado por todo lo que me has enseñado a lo largo de estos años tanto en España como en Canadá, por la hospitalidad cuando trabajé en tu laboratorio y sobre todo, por hacerme sentir en casa a pesar de estar tan lejos de la mía.

No hay dos sin tres estancias, así que por último, gracias Dr. Patrick J. Neale por enseñarme tanto en tan sólo dos meses y porque a pesar de todos los problemas siempre me mostrabas el camino para encontrar la solución. Gracias Dra. Cristina Sobrino por ser mi guía de la producción primaria desde que nos conocimos.

Gracias a mis dos evaluadoras externas, Prof. Angela Wulff y Dra. Paraskevi Pitta, por vuestras aportaciones de forma desinteresada a esta tesis y por todas las molestias burocráticas que hemos tenido que pasar.

De lo mejor de trabajar en Ecología es compartir este proceso con mis compañeros de la sala de becarios que me han ayudado tanto. Gracias a todos los que habéis formado y aún formáis parte de ella por hacerlo todo tan especial. Gracias a mis compañeras a las que he pasado a llamar amigas por quererme tanto y demostrármelo siempre, por vuestra ayuda a cualquier hora, en cualquier lugar y por cualquier medio y por ser imprescindibles en mi vida.



En especial, gracias a Candela por todos los experimentos compartidos, por todos tus consejos a lo largo de este tiempo y por tu ayuda desinteresada con la tesis. Gracias Conchi porque tu amistad es un regalo, gracias por todo lo que hemos vivido juntas en nuestras estancias noruegas pero sobre todo por lo que nos queda por compartir. *¿Podemos buscar ya al oso?*

Desde hace muchos años tengo la suerte de tener como amiga a Raquel y etapa tras etapa siempre seguimos juntas. Gracias por formar parte de mi vida y por permitirme formar parte de la tuya desde hace tanto.

Es un privilegio tener tantos amigos para compartir los buenos y malos momentos, sin ellos hubiera sido difícil llegar hasta el final. Gracias Laura por todo tu apoyo y amistad ya que la distancia no es un impedimento para nosotras y gracias por todo lo que compartes conmigo. Gracias a *La Orden* por las escapadas por tierras inglesas, por las vivencias compartidas y por las que quedan por compartir. A mis *mamuchis* porque con vosotros la vida es más divertida, gracias por vuestro apoyo y por tener siempre un brindis pendiente que haga que nos reunamos. Por último, gracias a mis nuevos amigos que me han adoptado en estos últimos años, por darme siempre ánimos y por las barbacoas compartidas. En especial, a los nuevos papis y a Carla por todo vuestro cariño.

Dejando lo más importante para el final, me gustaría agradecer a mi familia todo el apoyo que he recibido durante este tiempo. Gracias por perdonarme las ausencias y por todos los ánimos durante este tiempo. Gracias abuela por ser un ejemplo de vida, ojalá la sigamos compartiendo muchos años juntas. Gracias tita Inés por todo tu cariño de forma tan desinteresada y gracias Marta por ser más hermana que prima. Gracias a mis padres por ser los pilares de mi vida, por toda vuestra confianza y apoyo pero sobre todo por vuestro amor incondicional. Sin vosotros esto no hubiera sido posible. Gracias a mis hermanos, Edu y Mariló, por quererme y enseñarme tanto desde que tengo uso de razón. Gracias por compartir nuestras vidas, me siento afortunada de saber que siempre os tendré. También gracias a mis cuñados y a mi nueva familia por acompañarme y animarme durante todo este tiempo.

Por último, gracias Noel por quererme tanto y ayudarme siempre, por darme la calma en los momentos más difíciles y por hacerme reír cada día. Me faltan palabras para agradecerte todo lo que haces por mí cada día pero sé que tengo todo una vida para decírtelas. Gracias por ser mi compañero de vida.

*Esta tesis está dedicada a mis padres, a mis hermanos y a Noel*



UNIVERSIDAD  
DE MÁLAGA

**UNIVERSITY OF MALAGA  
FACULTY OF SCIENCES**

PhD Programme in  
Cell and Molecular Biology

Department of Ecology 2016

**Response of the coccolithophore  
*Emiliana huxleyi* to increased CO<sub>2</sub> and Fe  
availability within the plankton food web**

**Doctoral Thesis**

*Maria del Rosario Lorenzo Garrido*